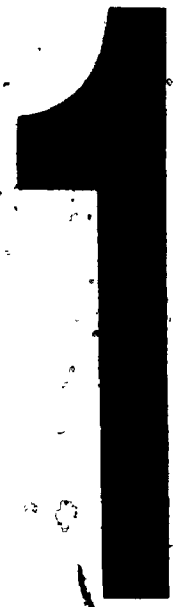

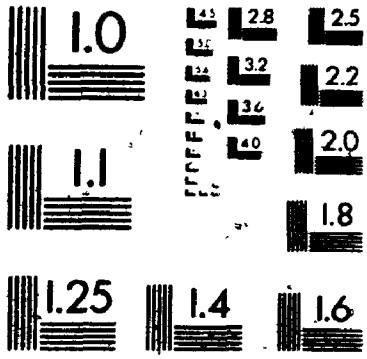
1.0
1.1
1.25
1.4
1.6
1.8
2.0
2.2
2.5
2.8
3.2
3.6
4.0

MicroD

National Library of Canada
Bibliothèque nationale du Canada

Canadian Theses Service
Service des thèses canadiennes

Ottawa, Canada
K1A 0N4

NOTICE

The quality of this microform is heavily dependent upon the quality of the original thesis submitted for microfilming. Every effort has been made to ensure the highest quality of reproduction possible.

If pages are missing, contact the university which granted the degree.

Some pages may have indistinct print especially if the original pages were typed with a poor typewriter ribbon or if the university sent us an inferior photocopy.

Previously copyrighted materials (journal articles, published tests, etc.) are not filmed.

Reproduction in full or in part of this microform is governed by the Canadian Copyright Act, R.S.C. 1970, c. C-30.

AVIS

La qualité de cette microforme dépend grandement de la qualité de la thèse soumise au microfilmage. Nous avons tout fait pour assurer une qualité supérieure de reproduction.

S'il manque des pages, veuillez communiquer avec l'université qui a conféré le grade.

La qualité d'impression de certaines pages peut laisser à désirer, surtout si les pages originales ont été dactylographiées à l'aide d'un ruban usé ou si l'université nous a fait parvenir une photocopie de qualité inférieure.

Les documents qui font déjà l'objet d'un droit d'auteur (articles de revue, tests publiés, etc.) ne sont pas microfilmés.

La reproduction, même partielle, de cette microforme est soumise à la Loi canadienne sur le droit d'auteur, SRC 1970, c. C-30.

NL-339 (r. 88/04)

Canada

INTERNAL PRESSURES IN FREEZING SOILS

by

JOHN ANDERSON WOOD, B.Sc.

A thesis submited to

the Faculty of Graduate Studies and Research

in partial fulfilment of

the requirements for the degree of

Doctor of Philosophy

Department of Geology

Carleton University

Ottawa, Ontario

November 29, 1985

© copyright

1985, John Anderson Wood

Permission has been granted to the National Library of Canada to microfilm this thesis and to lend or sell copies of the film.

The author (copyright owner) has reserved other publication rights, and neither the thesis nor extensive extracts from it may be printed or otherwise reproduced without his/her written permission.

L'autorisation a été accordée à la Bibliothèque nationale du Canada de microfilmer cette thèse et de prêter ou de vendre des exemplaires du film.

L'auteur (titulaire du droit d'auteur) se réserve les autres droits de publication; ni la thèse ni de longs extraits de celle-ci ne doivent être imprimés ou autrement reproduits sans son autorisation écrite.

ISBN 0-315-39358-0

The undersigned hereby recommend to

The Faculty of Graduate Studies and Research

acceptance of the thesis,

"INTERNAL PRESSURES IN FREEZING SOILS"

submitted by

JOHN ANDERSON WOOD, B.Sc.

in partial fulfilment of the requirements

for the degree of Doctor of Philosophy

Chairman, Department of Geology

Thesis Supervisor

External Examiner

Carleton University

December 18, 1985

ABSTRACT

Existing theories of frost heaving do not take into consideration the effect of the soil rheological properties on the growth of ice lenses and the heaving pressures established. The expansive work of heaving must take place against the resistance offered by the frozen soil itself. A thermo-rheological model of frost heaving is proposed for a confined soil in which there is a thermal gradient. The heaving pressures and their internal distribution are described in terms of the soil temperature, the unfrozen water pressure and the rheological properties of the soil. The latter limit the ability of the system to reach thermodynamic equilibrium, which imposes a constraint on the heaving pressures that can develop. The soil continuously attempts to reach an equilibrium ice pressure distribution which is determined by the thermodynamic conditions (temperature and unfrozen water pressure). However, stress relaxation tends to dissipate any ice pressure gradient which develops. Stress relaxation is attributed to a slow creep of the ice in the soil, on the molecular scale, toward warmer temperatures where the ice pressure is lower. The system attempts to restore the thermodynamic equilibrium condition by melting in the warmer regions of the soil and freezing in the colder regions. The departure from local equilibrium depends upon the rate of stress relaxation.

A series of prolonged experiments was carried out where the ice pressures were measured internally in freezing soils in which there was a thermal gradient. The values obtained can be explained in accordance with the thermo-rheological hypothesis of frost heaving. Differences in pressure up to 210 kPa were observed in a normally

consolidated saturated silt and a clay, associated with a temperature difference of 0.20°C. When the temperature gradient was reversed after the pressure difference was established, the pressures rapidly equalized and then slowly began to diverge again in accordance with the new direction of the thermal gradient.

Differences in the observed pressures were very sensitive to small changes in soil density. Results are explained by changes in the amount of pore ice formed in the soil which affects its resistance to stress relaxation. In normally consolidated soils, the observed gradient in ice pressure was close to the gradient required for thermodynamic equilibrium according to the Clausius-Clapeyron equation. In this case the soil behaved in a 'semi-rigid' manner with a significant resistance to stress relaxation. The establishment of perfect equilibrium was prevented by a very slow movement of the ice toward warmer temperatures.

In compacted soils and slurries, the soil behaved in a 'quasi-viscous' fashion. The observed pressures tended toward a uniform distribution. This was attributed to a substantial reduction in the resistance to stress relaxation of these materials, as a result of changes in the soil porosity and ice content.

Acknowledgements

I would like to express my thanks and appreciation to my thesis committee supervisor Dr. Peter Williams for the guidance and support given during my term at Carleton. His expertise on permafrost and frozen soils and many stimulating discussions over the years were essential in all aspects of the study. Thanks are also extended to Dr. Ken Torrance and Dr. Mike Smith who served on my thesis committee. Their suggestions and criticism are appreciated. Larry Boyle and Alan Pendlington also deserve special thanks for technical assistance in the design and construction of the apparatus. Larry Boyle's expertise was invaluable to the success of the experiment. Discussions with my colleagues, especially Scott Dallimore are also appreciated. My father A.D. Wood deserves mention for his advice on certain aspects of the experiment.

Thanks are also extended to Dr. Alan Judge for providing financial support for the project over the years. The work was carried out under contract to the Earth Physics Branch, Dept. of Energy, Mines and Resources, Ottawa, Canada. The experiments were conducted in the Geotechnical Science Laboratories at Carleton.

Finally, I would like to express my gratitude to Dr. John Moore for his assistance in admitting me to the Ph.D. (geology) program at the Ottawa-Carleton Geoscience Centre.

TABLE OF CONTENTS

Abstract iii

Acknowledgements v

Table of Contents vi

List of Tables ix

List of Illustrations x

List of Plates xiv

List of Appendices xv

Nomenclature xvi

I INTRODUCTION

1.1 Frost Heaving: Definition and General Description 1

1.2 Hypothesis and Objectives of the Research 3

II LITERATURE REVIEW

2.1 Freezing-Point Depression In Soils 7

2.2 Glausius-Clapeyron Equation 9

2.3 Significance of Anisotropic Ice and Water Pressures 11

2.4 Ice and Water Pressures In Different Freezing Scenarios 14

2.5 Investigations of Frost Heaving Pressures in Soils 18

2.6 Current Physical Theory of Frost Heaving 20

2.7 Permeable Nature of Frozen soils 27

2.8 Series-Parallel Transport 31

2.9 Irreversible Thermodynamics of Coupled Transport Phenomena In Frozen Soils 35

III EXPERIMENTAL INVESTIGATION OF REGELATION TRANSPORT IN AN ICE-SANDWICH PERMEAMETER

3.1 Background 40

3.2 Apparatus and Procedure 41

3.3 Results 42

3.4 Effects of Specimen Dimensions 47

3.5 Threshold Pressures 48

	3.6	Osmotically-Induced Regelation	51
	3.7	Effect of Secondary Thermal Gradients On The Rates of Flow	56
	3.8	Conclusions and Discussion	60
IV		A THERMO-RHEOLOGICAL MODEL OF THE FROST HEAVE PRESSURES IN SOILS	
	4.1	Rheological Behaviour of Frozen Soils: Review	62
	4.2	Distribution of Frost Heave Pressures In Confined Soils	72
V		EXPERIMENTAL APPARATUS AND PROCEDURE	
	5.1	Frost Pressure Cell	81
	5.2	Pressure Transducers	87
	5.3	Temperature Control and Measurement	88
	5.4	Water Supply	89
	5.5	Data Record	90
	5.6	Soil Specimens	91
	5.7	Soil Preparation	96
	5.8	Saturation of Soil Specimens	97
	5.9	Nucleation and Freezing	98
	5.10	Final Measurements	99
VI		RESULTS AND INTERPRETATION	
	6.1	Flows and Internal Pressures: General Observations	100
	6.2	Ice Contents and Ice Saturation	108
	6.3	Observations of Segregation Ice	113
	6.4	Graphical Presentation of Results	115
	6.5	Analysis of Pressure Differences In Normally Consolidated Soil Specimens	117
	6.6	Stress Relaxation and Consolidation During Transient Thermal Conditions	131
	6.7	Pressure Changes and Flows During Quasi-Steady-State Conditions	137
	6.8	Water Pressures and Hydraulic Gradients During Freezing	141
	6.9	Significance of Frost Line Temperature to the Pressures Established	142
	6.10	Reversal of Thermal Gradient	145
	6.11	Effect of Changes in Soil Density	151

6.12 Significance of Soil Strength to the Pressure Distribution 158
6.13 Externally Effective Frost Heaving Pressures 167
6.14 Frost Heave Pressures in Unconfined Soils 171
6.15 Location of Ice with Respect to the Bladders 171
6.16 Stress Concentrations 174
6.17 Wall Friction 176
6.18 Compressibility of the System 177
6.19 Flows at the Cold End 179

VII ADDITIONAL RESULTS AND ANALYSIS

7.1 Reproducibility 180
7.2 Effect of a Positive Pore Water Pressure on the Heaving Pressure 183
7.3 Experiments With Increased Thermal Gradients 187
7.4 Effect of Changes in the End Temperatures 192
7.5 Effect of Repeated Freezing 195
7.6 Significance of Frost Susceptibility Classification to the Pressures Established 196
7.7 Hydraulic conductivity of Caen Silt 196

VIII SUMMARY AND CONCLUSIONS 201

BIBLIOGRAPHY 205

LIST OF TABLES

Table		
2.1	Temperature Dependence of Heat of Fusion of Water and Fusion of Water and Specific Volume of Ice and Water	10
4.1	Instantaneous and Long-Term Strengths of Some Frozen Soils at Various Temperatures	68
5.1	Properties of Soils Used in the Experiments	92
6.1	Pressure and Flow Data for Experiments with Normally Consolidated Soil Specimens	101
6.2	Pressure and Flow Data for Experiments with Varying Densities and Thermal Gradients	104
6.3	Freezing Data	109
6.4	Observed Pressures and Equilibrium Ice Pressures for Normally Consolidated Soils	118
6.5	Creep Properties of Snec Sand and Caen Silt	129
6.6	Internal Pressure-Melting Data for Several Experiments	139
6.7	Observed Pressures and Equilibrium Ice Pressures for Incompressible (Compacted) Soils and for Slurries	152
6.8	Observed Pressures and Equilibrium Ice Pressures with Decrements in the Cold-End Temperature, Exp. 44	162
7.1	Observed Pressures and Equilibrium Ice Pressures with a Positive Pore Water Pressure and a Larger Thermal Gradient	186
7.2	Effect of Charges in End Temperature to the Internal Pressures	193

LIST OF FIGURES

Figure		
1.1	Frost Pressure Cell Designs	5
2.1	Enlargement of Soil Pore Showing Configuration of Ice and Unfrozen Water	8
2.2	Effect of Changes in Ice and Unfrozen Water Pressure on Equilibrium Freezing Temperature According to Clausius-Clapeyron Equation	15
2.3	Hydrodynamic Model of Frost Heaving Assuming a Linear Temperature Gradient	23
2.4	Ice Lens Distribution in a Freezing Soil Column Following a Step-Wise Decrease in Temperature at One End	24
2.5	Stress and Pressure Profiles in the Frozen Fringe During Ice Segregation as Proposed by Miller (1980)	28
2.6	Hydraulic Conductivities of Several Silts and Clays as a Function of Temperature	30
2.7	Series - Parallel Transport of Water in a Frozen soil	32
2.8	Flow of Water To and From a Frozen Soil Permeameter Induced by Gradients in Osmotic Potential Between the Reservoirs and the Soil, -0.30°C, Allendale Clay	37
3.1	Cross-Section of Ice Sandwich Permeameter	43
3.2	Outflow versus Time for Experiment A4	44
3.3	Flux versus Hydraulic Gradient for Experiment A4 at Various Temperatures	45
3.4	Hydraulic Transport Coefficient versus Temperature, Experiment A4 and A8	46
3.5	Threshold Pressures Required to Initiate Flow Through the Ice Sandwich, Experiment A4 and A8	49
3.6	Outflow versus Time for Experiment A2 and A3	50
3.7	Flow Through Ice Sandwich Induced by an Osmotic Gradient, Experiment A9, -0.110°C	53
3.8	Flow Through Ice Sandwich Induced by an Osmotic Gradient, Experiment A10, -0.300°C	54

3.9(a)	Cross-Section of Ice Sandwich for Measuring Effect of Secondary Thermal Gradients on Mass Flow Rates	58
3.9(b)	Circuit Diagram of Bridge Used to Detect Very Small Resistance Changes to Thermistors	58
4.1	Stress-Strain Curve and Creep Curves (a,b,c) for a Frozen Silty Clay at Different Temperatures	65
4.2	Stress-Strain Curve for Snèc Sand at Different Strain Rates, -2°C	66
4.3	Long-Term and Instantaneous Compressive Strengths of Two Frozen Sands at Various Temperatures	67
4.4	Example of Change in Short-Term Compressive Strength with Ice Content (Fine Sand)	69
4.5	Linarized Plot of Secondary Creep Rate versus Applied Stress	70
4.6	Idealized Model Showing Distribution of Frost Heave (Ice) Pressures in a Confined Soil with Different Rheological Properties	75
5.1	Cross-Section of Frost Pressure Cell	82
5.2	Experimental Lay-Out	83
5.3	Volume Displacement Due to Deflection of Perforated Aluminum Plates Under Pressure	86
5.4	Granulometry	94
5.5	Soil Freezing Characteristic Curves	95
6.1	Flows and Internal Pressures, Experiment 32A, Caen Silt ..	119
6.2	Temperature Profile During Freezing, Experiment 32A, Caen Silt	120
6.3	Flows and Internal Pressures, Experiment 30, Caen Silt ...	121
6.4	Temperature Profile During Freezing, Experiment 30, Alledale Clay	122
6.5	Flows and Internal Pressures, Experiment 33, Caen Silt ...	123
6.6	Temperature Profile During Freezing, Experiment 33, Caen Silt	124
6.7	Creep Curves for Caen Silt at Various Applied Stresses, -2°C	127

6.8	Creep Curves for Snec Sand at Various Applied Stresses, -2°C	128
6.9	Pressure as a Function of Bladder Temperature, Experiment 32A, Caen Silt	132
6.10	Pressure as a Function of Bladder Temperature, Experiment 30, Allendale Clay	133
6.11	Pressure as a Function of Bladder Temperature, Experiment 33, Caen Silt	134
6.12	Advance of Frost Line and Outflow from Warm end During Freezing	143
6.13	Flows and Internal Pressures, Experiment 39B, Caen Silt, Temperature Gradient Reversed	146
6.14	Temperature Profile During Freezing, Experiment 39B, Caen Silt	147
6.15	Reversal of Thermal Gradient, Experiment 39B, Caen Silt	148
6.16	Flows and Internal Pressures, Snec Sand, Experiment 36	153
6.17	Flows and Internal Pressures, Compacted Caen Silt, Experiment 31	154
6.18	Flows and Internal Pressures, Experiment 43A, Caen Silt Prepared as a Slurry	155
6.19	Flows and Internal Pressures, Experiment 29, Allendale Clary Prepared as a Slurry	156
6.20	Flows and Internal Pressures During Step-Wise Decreases in Temperature at the Cold End, Experiment 44, Caen Silt	163
6.21	Thermal Profile During Freezing, Experiment 44, Caen Silt	164
6.22	Stress-Strain Curve for Caen Silt at Different Strain Rates, -2°C	165
6.23	Modified Cell for Measuring Externally-Effective Frost Heave Pressures at the Cold End	169
6.24	Flows, Internal Pressures and Cold End Reservoir Pressure, Experiment 35, Caen Silt	170

7.1	Flows and Internal Pressures, Experiment 42A, Caen Silt ..	181
7.2	Flows and Internal Pressures, Experiment 34, Caen Silt ...	182
7.3	Flows and Internal Pressures with a Positive Hydrostatic Pressure, Experiment 44A, Caen Silt	185
7.4	Flows and Internal Pressures, Experiment 44B, Caen Silt ..	188
7.5	Flows and Internal Pressures, Experiment 40, Caen Silt ...	189
7.6	Hydraulic Conductivity of Frozen Caen silt as a Function of Temperature	198
K.1	Temperature Profile During Freezing, Experiment 29, Allendale Clay	250
K.2	Temperature Profile During Freezing, Experiment 31, Caen Silt	251
K.3	Temperature Profile During Freezing, Experiment 35, Caen Silt	252
K.4	Temperature Profile During Freezing, Experiment 36, Snec Sand	253
K.5	Temperature Profile During Freezing, Experiment 40, Caen Silt	254
K.6	Temperature Profile During Freezing, Experiment 42A, Caen Silt	255
K.7	Temperature Profile During Freezing, Experiment 43A, Caen Silt	256
K.8	Temperature Profile During Freezing, Experiment 44A, Caen Silt	257
K.9	Temperature Profile During Freezing, Experiment 44B, Caen Silt	258

LIST OF PLATES

Plate		
5.1	Exploded View of Frost Pressure Cell	84
5.2	Vertical View of Perspex Cell Showing Pressure Transducer Assemblies	85
6.1	Ice Lenses in a Frozen Soil Specimen	114
L.1	Test Set-Up for Measuring Wall Friction of Frost Pressure Cell	261

LIST OF APPENDICES

Appendix		
A	Design Specifications of Frost Pressure Cell	217
B	List of Equipment Used in the Experiment	221
C	Calibration Reports for Pressure Transducers	223
D	Fabrication and Installation of Rubber Bladders	229
E	Freezing Temperature of Lactose Solution as a Function of Lactose Concentration	232
F	Calibration Reports for Thermistors	236
G	Procedure for Developing Panatomic-X Black and White Film	239
H	Adjustment Procedure for Chart Recorder	241
I	Procedure for Determining Rheological Properties of Frozen Caen Silt and Snec Sand	244
J	Compaction Procedure for Caen Silt and Snec Sand	246
K	Thermal Profiles for Several Experiments	249
L	Procedure for Measuring Wall Friction	259

NOMENCLATURE

P_i	ice pressure
P_w	unfrozen pore water pressure
v_i	specific volume of ice
v_w	specific volume of water
L	latent heat of fusion of water
T	temperature
T*	frost line temperature
π	osmotic pressure
J	flux (flow rate)
i	hydraulic gradient
k	hydraulic conductivity (permeability coefficient)
K	overall hydraulic conductivity
z	distance
t	time
L_i	ice transport coefficient (ice sandwich)
L_m	mass transport coefficient (ice sandwich)
L_q	heat transport coefficient (ice sandwich)
L_{mq}, L_{qm}	coupled (mass-heat) transport coefficient (ice sandwich)
σ	stress
σ	strength
ε	strain
$\dot{\varepsilon}$	strain rate
σ_c, n	creep parameters
σ_k, k	instantaneous strain parameters
V	volume
κ	compressibility

I. INTRODUCTION

1.1 Frost Heaving: Definition and General Description

Frost heaving is the increase in pressure and/or volume displacement when a soil is frozen. The work of heaving can be manifested as either change, or a combination of both changes, depending upon the confining stress imposed upon the soil skeleton.[1] If the soil is unconfined, it typically exhibits a highly segregated structure with discrete layers of ice called 'ice lenses' alternating with layers of frozen soil. Volume increases greater than 40% are common (Williams, 1982).[2] This is a result of the migration of water from the unfrozen regions in the soil toward the frost line.

Recent theories suggest that ice lenses actually form in the frozen zone behind the frost line. This has been confirmed in x-ray tests on silts and clays by Penner and Goodrich (1980) and also, with a gamma-ray scanning technique, by Loch and Kay (1978). The relatively narrow zone between the warmest ice lens and the frost line has been dubbed the 'frozen fringe' by Miller (1978). Phukan et al. (1978) report frozen fringe thicknesses ranging from less than a millimeter up to several centimeters, depending upon the temperature gradient, overburden pressure and soil composition. Water is able to move through

---

[1] A 'confined' soil is one in which the soil skeleton is restrained from movement but water is allowed to move freely between the soil and the surroundings. This is different to a 'closed' system where both the soil skeleton and the pore water are restrained.

[2] The explanation of the pore fluid during freezing is not a requirement for heave to occur, as shown in the classic work by Taber (1930). He observed heave in soils saturated with fluids such as benzene and nitrobenzene which contract upon freezing rather than expand.

the frozen fringe by means of thin interconnected films of liquid water which envelop each mineral particle.

Ice lenses range in thickness from barely visible (and smaller) right up to 4m in extreme cases (French, 1976). Thicker ice lenses are associated with relatively slow rates of freezing. The heaving stresses are developed primarily in the direction of crystal growth, which is parallel to the direction of heat flow.

Miller et al. (1975) suggest the possibility that pore ice may actually be moving through the soil in addition to liquid film water. They propose a model in which water moves across the pores in the solid phase and around the particles in the liquid phase, with phase changes at the upstream and downstream ice-water interfaces in each pore. Although the ice is actually moving, its boundaries within the pores remain stationary. The phenomenon is known as 'regelation'. Although it is now widely accepted as a legitimate mechanism of water transport, it has never been proved to occur in the soil in practice. However, an experiment devised by Horiguchi and Miller (1980), which they call an 'ice sandwich', demonstrates that regelation transport actually does occur, at least with bulk water. The device allows investigation of the laws governing its behaviour.

The permeable nature of frozen soils, by whatever mechanism (liquid and/or simultaneous regelation transport), accounts for observations of the continued enlargement of ice lenses located well behind the frost line where the temperature is several degrees below freezing (Smith, 1985, Geotechnical Science Laboratories, 1984). The phenomenon is commonly known as 'secondary frost heaving'. If this continues over very long periods of time (years or even decades), the

pressures established and/or the associated volume displacements could be very large. Miller (1977) suggests that "Monotonic freezing will result in heaving of any load, no matter how large, at some rate which may be vanishingly small, if one waits long enough and if the surface temperature is cold enough. The theoretical upper limit of pressure is fixed only by the temperature at which the liquid phase ceases to be mobile." Anderson and Tice (1971) have detected unfrozen film water at temperatures as low as -50°C.

1.2 Hypothesis and Objectives of the Research

Existing theories of frost heave describe the heaving pressures as a function of the soil temperature and the potential of the water available to the ice lenses, in accordance with thermodynamic theory. This ignores the effect of the soil rheological properties, including creep, consolidation and multidimensional deformation. The central hypothesis of this thesis is that the frozen soil itself resists the expansive work of heaving. Frost heaving can be regarded as a thermo-rheological phenomenon in which the ice pressures established are a result of a complex interplay of the rheological properties of the soil, the soil temperature and the pressure of the unfrozen water available to the lenses. The ice pressures required for thermodynamic equilibrium increase with colder temperatures and higher unfrozen water pressures in accordance with the Clausius-Clapeyron equation. However, any tendency for the heaving (ice) pressure to approach an equilibrium condition depends upon the mechanical resistance of the soil to stress relaxation and, therefore, its rheological properties.

The rheological properties of the soil also have implications with regard to the distribution of pressures generated by the ice

lenses. In the existing theories of frost heaving, it is tacitly assumed that the heaving pressure is uniform and equal to the pressure of the coldest ice lens. This would occur only if the soil behaved as a fluid and could not sustain any shear stress. Since frozen soil is a 'semi-rigid' material, it would be reasonable to expect a gradient in ice pressure where there is a temperature gradient. If the soil was perfectly rigid, the pressure of the ice should increase with colder temperatures in accordance with the Clausius-Clapeyron equation (assuming the unfrozen water pressure = atmosphere pressure). In other words, perfect local equilibrium would be maintained interally by the soil, at each ice-water interface. The rheological behaviour of frozen soils suggests that perfect equilibrium is not maintained locally because the ice creeps slowly, at the molecular level, in the direction of lower pressures (warmer temperatures). However, the soil will attempt to restore the ice pressure gradient toward thermodynamic equilibrium by continuous melting in the warmer regions of the soil and freezing in the colder regions. The system should eventually stabilize at a steady-state condition where the departure from local equilibrium depends upon the rate of movement of the ice.

To investigate this possibility, experiments were carried out with a specially designed frost pressure cell. Pressures were measured internally at different locations within the soil, rather than externally at a single location, as with conventional techniques (Fig. 1.1). The findings are discussed in relation to the concept of combined rheological and thermodynamic constraints on frost heaving. The concept is of practical importance to the prediction of short-term and long-term (secondary) heaving pressures and volume displacements.

FIGURE 1.1

FROST PRESSURE CELL DESIGNS

(a)

Convential Methods

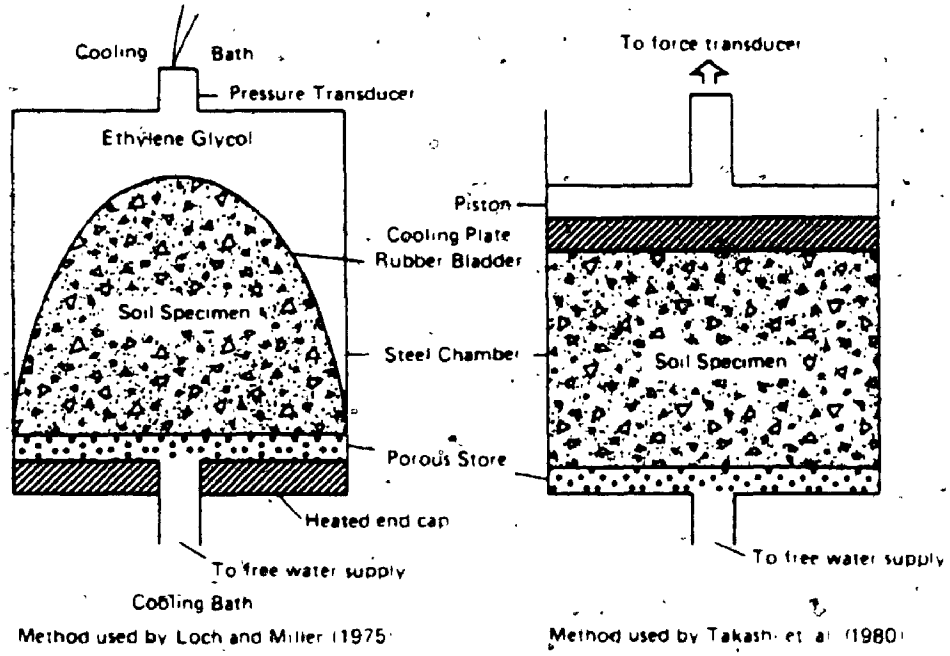

Method used by Loch and Miller (1975)

Method used by Takashi et al (1980)

(b)

Method of Measuring Pressures Internally, Used In This Investigation

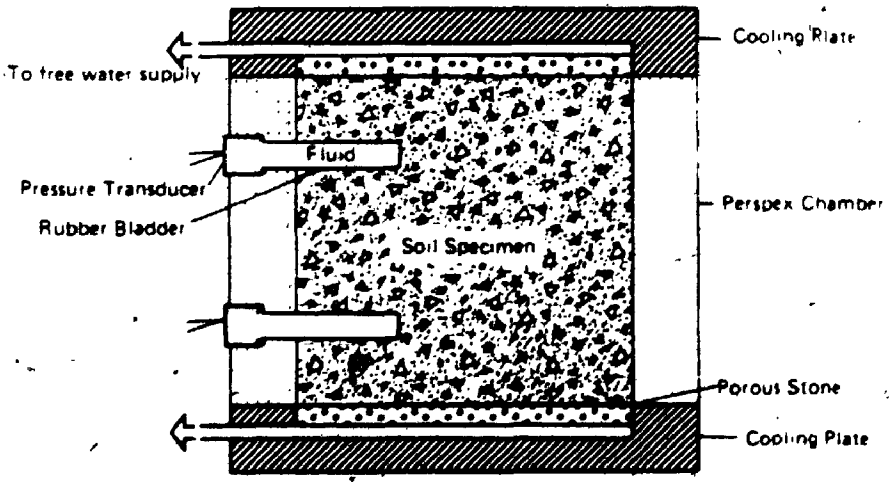

In addition to this work, an experimental investigation was also carried out into the regelation flow phenomenon, to confirm the findings of Horiguchi and Miller (1980) and to carry the work on the irreversible thermodynamics of the process a stage further. Results are of practical significance, not only to the understanding of the hydraulic properties of frozen soils but also to the rheological behaviour of the ice in the soil.

The literature is reviewed in the second chapter of the thesis with particular attention being given to the thermodynamics of freezing soils and the pressures established. Results from the 'ice-sandwich' experiment are discussed in chapter three. The fourth chapter reviews briefly the rheological properties of frozen soils and elaborates upon the hypothesis described above. The remainder of the thesis presents an analysis and discussion of the results from experiments carried out with the frost pressure apparatus.

II. LITERATURE REVIEW

2.1 Freezing-Point Depression in Soils

The presence of liquid films of water surrounding the soil particles in frozen soils implies that the chemical potential of the water is somehow lowered by the interaction with the mineral surfaces, thereby lowering its freezing temperature (Fig. 2.1). The phenomenon is generally attributed to a combination of factors including: (1) adsorptive forces originating in the double layer associated with the mineral surfaces, (2) the presence of 'free' solutes in the bulk (neutral) soil solution, and (3) capillary effects produced by the confining nature of the soil pores.

The configuration of ice in frozen soils is generally regarded as being similar to that of air in unsaturated soils. Ice first appears in the middle of the pores forming spherical interfaces with the unfrozen water.[1] Capillary effects are the dominant reason for freezing-point depression at temperatures within a few hundredths or tenths of a degree below freezing. As the temperature is lowered, the liquid water progressively freezes. Liquid layers form relatively thin films above the particle surfaces and thick wedges at the contacts between the particles (Fig. 2.1). At colder temperatures, only the water in the double layers remains unfrozen. This is confined to a relatively narrow zone within a few tens or hundreds of Angstrom units from the mineral surfaces.

Miller (1980a) points out that double layers are not a unique feature of clays and colloidal particles, as is sometimes assumed, but

---

[1] The Thompson equation relates freezing-point depression of a negatively curved (concave) ice-water interface to the radius of curvature.

FIGURE 2.1

ENLARGEMENT OF SOIL PORE SHOWING CONFIGURATION OF ICE AND UNFROZEN WATER

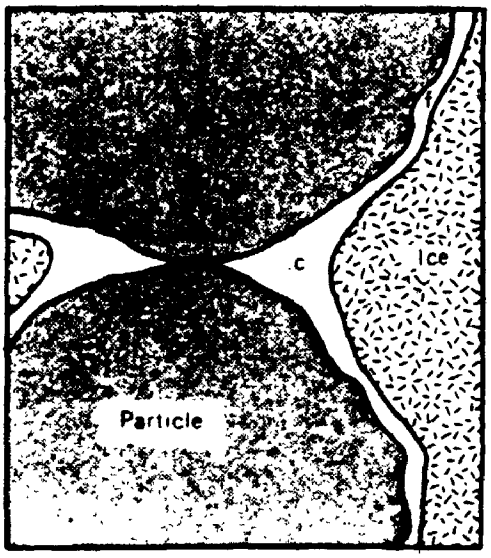

c capillary water

f adsorbed water

tend to form spontaneously on particles of all sizes. Liquid films, therefore, are a feature of sands and silts although the unfrozen water is present in smaller quantities (especially in sands) because of the relatively low specific surface area of these materials.

2.2 Clausius-Clapeyron Equation

Thermodynamics tells us that ice and water are unable to coexist in equilibrium at the same pressure. For equilibrium to occur, the ice pressure must exceed that of the water. This applies to the pore contents of frozen soils as well. The Clausius-Clapeyron equation (eqn.) relates the difference in pressure, at which the ice and water are able to coexist in thermodynamic equilibrium, to the temperature (Defay and Prigogine, 1951):[2]

$$v_i dP_i - v_w dP_w = - L \frac{dT}{T} \qquad 2.1$$

where dP_i and dP_w = change in the ice and water pressure, respectively, kPa

$v_i = 1.091 \times 10^{-3}$ m^3 Kg^{-1}, specific volume of ice,

$v_w = 1.000 \times 10^{-3}$ m^3 Kg^{-1}, specific volume of water,

$L = 3.336 \times 10^5$ J Kg^{-1}, specific latent heat of fusion of water,

T = 273.15 K, freezing temperature of pure free water at 1 atm. presssure (101.3 kPa),

dT = freezing-point depression, °C.

---

[2] If solutes are present $P_w = P_s - \Pi$, where P_w = partial pressure of the pore water, P_s = total pressure of the soil solution, Π = osmotic pressure.

Table 2.1

Temperature Dependence of Heat of Fusion of Water and Specific Volume of Ice and Water

T °C	L J Kg^{-1}	v_i m^3 Kg^{-1}	v_w m^3 Kg^{-1}
0	333.6×10^3	1.0908×10^{-3}	1.0008×10^{-3}
-5	308.5 "	1.0756 "	0.9740 "
-10	284.8 "	1.0642 "	0.9520 "
-15	261.6 "	1.0589 "	0.9371 "
-20	241.4 "	1.0547 "	0.9234 "
-22	234.8 "	1.0545 "	0.9193 "

Dorsey, 1968.

Equation 2.1 indicates that the difference in pressure between the ice and water increases linearly with lower temperatures. dT is the difference between the actual temperature of the system and the freezing temperature of pure water. The difference is normally expressed in degrees Celsius rather than Kelvin. Since v_i, v_w and L are temperature dependent (Table 2.1), the Clausius-Clapeyron equation is generally only applicable, in the form shown above, at temperatures within a few degrees of freezing.

Experiments by Buil and Aguirre-Puente (1981) and Biermans et al. (1978), in which an ice lens was equilibrated with supercooled water (separated by a fine-pored filter), verify this relationship between 0°C and -0.5°C. At lower temperatures, tests of this nature are generally limited by the tendency for supercooled water to freeze.

2.3 Significance of Anisotropic Ice and Water Pressures

The validity of the Clausius-Clapeyron eqn. where P_i and P_w are anisotropic is of particular concern to frost heaving and the pressures established because the state of stress in the ice lenses and the unfrozen water is complex. The ice and unfrozen water in the soil cannot be viewed as having an isotropic state of stress akin to a hydrostatic pressure. Because of this, it is sometimes argued that the Clausius-Clapeyron eqn. requires further modifications to allow for anisotropic stresses. Some researchers, notably Takagi (1980), speculate that adsorbed film water is 'solid-like' because it appears capable of sustaining large normal stresses (i.e. the weight of the overburden), while at the same time it retains the characteristics of a fluid (low viscosity). The solid-like stress is highest at the mineral

surface and diminishes with distance away from the surface, in accordance with the intensity of the adsorptive field. Takagi (1980) argues that the distribution of temperature and 'solid-like stresses' interacts to create a diffuse zone of 'partial' freezing within the liquid film. The Clausius-Clapeyron equation can only be applied in an approximate sense since the stresses must be 'averaged out' using special techniques and related to the 'average freezing temperature'.

Miller (1980a), however, presents a convincing argument that this view of 'solid-like' water is simply an illusion of perspective. When viewed from outside the adsorptive field, water may appear solid-like because it is able to support the weight of the overlying material. However, at close range, the water behaves exactly as ordinary water would under a force field which diminishes in intensity with distance from the particle surface and interacts more strongly with the liquid phase than the solid. These criteria are met by the double layer. Since the adsorbed water is locally in equilibrium with capillary water, a knowledge of the distribution of adsorptive forces is not required in order for the Clausius-Clapeyron equation to be applied. The equation remains valid regardless of whether the liquid phase is unfrozen capillary water (where P_w and Π are relatively low) or adsorbed film water (P_w and Π are much larger).

The same questions are also raised regarding anisotropic stress in ice. It seems unrealistic to assume that ice lenses experience a simple hydrostatic stress akin to gauge pressure. Ice is capable of sustaining shear stresses as well as anisotropic normal stresses, at least for short periods, although local stress

concentrations tend to be dissipated with time, owing to creep. In the case of microscopic, anisotropic stresses, O'Neill (1982) suggests that the stresses may average out somehow, so that P_i is uniform on the macroscopic level. Alternatively, P_i in the Clausius-Clapeyron eqn. may represent the pressure for an ice body which is 'thermo-mechanically equivalent' to the real situation, but isotropic.

Regardless of the microscopic situation, at the macroscopic level, anisotropy presents problems of its own. In the case of an ice lens which experiences a uniaxial stress due to the weight of the overburden, the question arises, how the state of stress within the ice relates to P_i in the Clausius-Clapeyron equation. The question might also be asked whether the pressure of the ice and water, at equilibrium, is dependent upon the orientation of the ice surface relative to the solid-liquid interface.

Ruil and Aguirre-Puente (1981) present a credible analysis which verifies the Clausius-Clapeyron eqn. regardless of whether the stress in the ice is hydrostatic or uniaxial (normal to the ice-water interface).[3] In the case of the latter P_i, in the Clausius-Clapeyron equation, refers to the uniaxial stress (stress in the direction of crystal growth). This also seems reasonable from a mechanical point of view, since ice crystals usually tend to grow in a direction normal to the interface and parallel to the direction of heat flow. In the case where the ice experiences a more complex state of stress, P_i refers to the sum of the hydrostatic and deviatoric stress components. If allowance is made for the creep of ice under shear, P_i becomes the

[3] The condition for hydrostatic stress, $\sigma_{11} = \sigma_{22} = \sigma_{33}$, $\sigma_{ik} = 0$, $i \neq k$.

product of both a stress tensor and a deformation tensor.[4]

2.4 Ice and Water Pressures in Different Freezing Scenarios

Of particular interest in the study of frost heaving pressures are 3 special cases of the Clausius-Clapeyron equation:

(1) If the water pressure remains constant at atmospheric pressure ($\delta P_w = 0$), for chemical equilibrium to occur between the ice and water, the ice pressure must increase with lower temperatures by $\frac{\delta P_i}{\delta T} = 1.127$ MPa $°C^{-1}$ (Fig. 2.2).

(2) Alternatively, if the ice pressure remains constant ($\delta P_i = 0$), the water pressure must decrease by $\frac{\delta P_w}{\delta T} = 1.220$ MPa $°C^{-1}$ for chemical equilibrium to occur.

(3) If the pressure of both phases remains equal ($P_i = P_w = P$), then

---

[4] The chemical potential of ice, μ_i, may be written as (Buil and Aguirre-Puente, 1981):

$$\mu_i = \mu_{io} + \frac{1}{2} \sigma_{jk} \varepsilon_{jk} v_i \qquad 2.2$$

where μ_{io} = chemical potential of ice at hydrostatic pressure,

v_i = molar volume of ice.

The stress tensor is written as:

$$\sigma_{jk} = \sigma^I_{jk} + \sigma'_{jk} \qquad 2.3$$

where the isotropic component $\sigma^I_{jk} = \frac{1}{3} \sigma_{\ell\ell} \delta_{jk}$ and the deviatoric component $\sigma'_{jk} = \sigma_{jk} - \frac{1}{3} \sigma_{\ell\ell} \delta_{jk}$ and δ_{jk} = kronecker's delta. A similar set of matrices describes the deformation tensor ε_{jk} corresponding to σ_{jk}.

FIGURE 2.2

EFFECT OF CHANGES IN ICE AND UNFROZEN WATER PRESSURE ON EQUILIBRIUM FREEZING TEMPERATURE ACCORDING TO CLAUSIUS-CLAPEYRON EQUATION (SPECIAL CASES 1 AND 2)

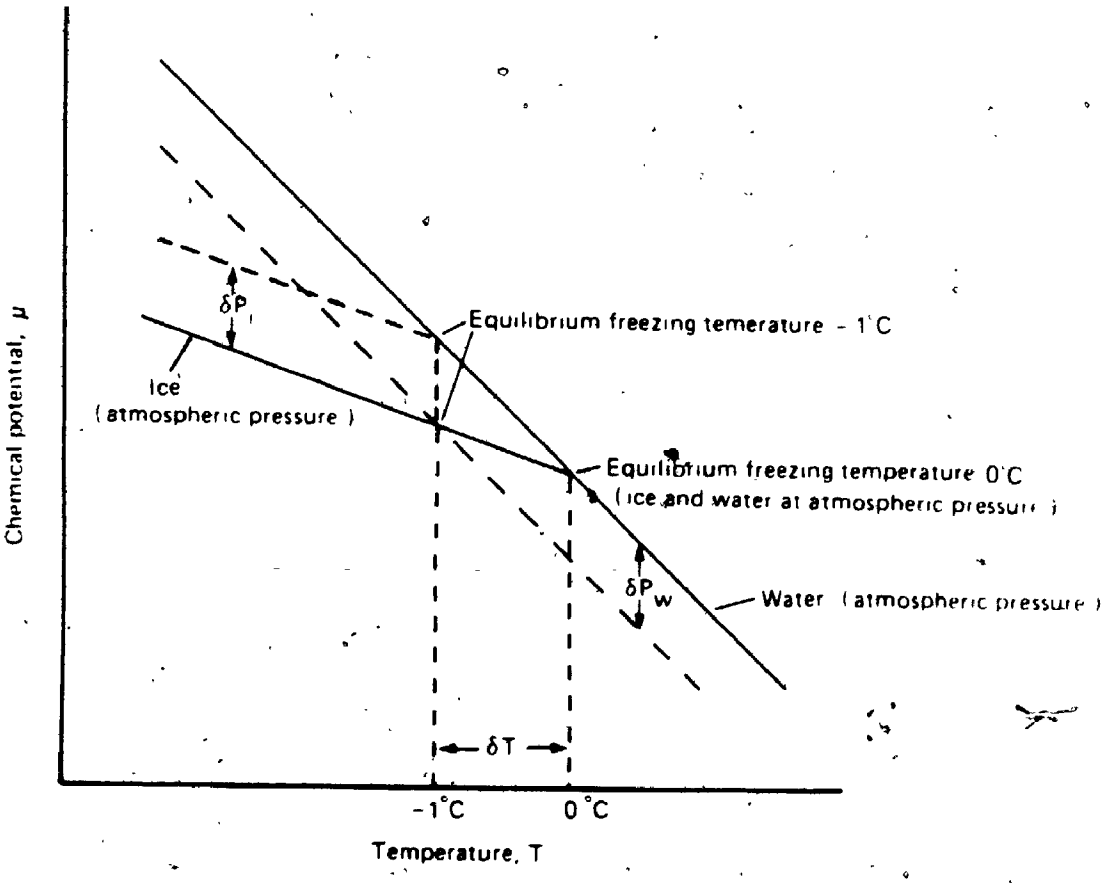

δP_i = increase in ice pressure = 1.127 MPa °C^{-1}

δP_w = decrease in unfrozen water pressure = 1.229 MPa °C^{-1}

δT = change in freezing temperature of system $\simeq$ - 1°C

chemical equilibrium occurs when the pressure increases by $\frac{\delta P}{\delta T} = 13.543$ MPa $^{\circ}C^{-1}$.

In freezing soils the Clausius-Clapeyron equation is normally satisfied by a simultaneous increase in the ice pressure and a fall in the pressure of the unfrozen water. The exact magnitude of each, depends upon the constraints imposed upon the system. The question does not appear to have been addressed directly in the literature although it is of major significance in describing the frost heaving pressures. The situation is controlled, ultimately, by whether there is a mechanical constraint or reactive stress for the ice pressure to rise against. In the absence of some form of resistance, the ice pressure cannot rise and the Clausius-Clapeyron equation is satisfied by a fall in the pressure of the unfrozen water instead. Heaving energy, or the work of frost heaving, is accomplished by unrestrained volume increases in the form of ice lenses. If there is resistance to volume change, the Clausius-Clapeyron equation is satisfied by a rise in ice pressure, at least until the ice pressure exceeds the restraining stress. In this case, the work of heaving is manifested entirely as an increase in pressure against the surroundings without the accompanying growth of ice lenses. The theoretical maximum ice pressure is fixed only by the temperature. Resistance to heave can take many forms, including external resistance provided by a load or a confining stress and/or internal resistance which originates within the soil itself and is dependent upon its mechanical properties. Both the compressibility of the soil as well as its strength and creep properties determine its ability to resist localized internal volume changes generated by growing ice lenses.

The third case, in which the pressure of both the water and ice remains equal, applies only in situations where water movement in or out of the system is restricted, thereby creating a 'closed system'. In this case, the pressures developed are enormous, far exceeding the strength of even rock. Natural materials, however, probably never behave as ideal closed systems although they are sometimes referred to as such. Instead, they are better regarded as 'grey box' or 'partly closed' since some water expulsion, however small, usually takes place. The question is one of degree.

The closest approximation of closed system freezing is the case of frost shattering of highly impermeable rock which is rapidly frozen. The pressures established depend upon the ratio of the permeability coefficient to the freezing rate, as well as its tensile strength (Lautridou and Ozouf, 1982). The permeability coefficient and the freezing rate determine the degree to which the hydrostatic pressure developed during freezing is dissipated by the flow of water away from the advancing ice. Shattering occurs when the pressure exceeds the strength of the material at some point of weakness.

In soils, closed system freezing is generally only associated with the formation of certain Arctic terrain features. The situation is more complicated than it is in rock since frozen soils are readily deformable (unlike rock which undergoes brittle failure) and are also moderately permeable (at least in comparison to rock). Certain types of permafrost features are often described as 'closed systems', including hydrolaccoliths and various types of ice-cored mounds associated with freezing of the active layer, as well as pingoes (cryostatic or 'closed-system' variety), produced by freeze-back of a talik beneath a

drained lake (Mackay, 1979). Realistically, however, these features are better described as 'partly closed' since considerable volume change obviously occurs and precludes the possibility of very large ice pressures developing. This is accommodated primarily by deformation and creep of the overlying frozen soil and possibly by some water flow through the frozen zone as well. P_i rises until it exceeds the bending strength of the overlying frozen material. P_w remains less than P_i as in special case 1 of the Clausius-Clapeyron eqn. but still develops a positive pressure (greater than atmospheric) because the water cannot flow out of the system fast enough to relieve the pressure.

2.5 Investigations of Frost Heaving Pressures in Soils

Although there has been a plethora of experimental studies of frost heaving, few of these have involved the measurement of the pressures established. The techniques used are simple (Fig. 1.1) and involve measuring the stress exerted by the surface of the soil on a surrounding fluid or a moveable piston. The 'heaving pressure' is defined as the pressure required to keep the volume of the soil constant. Although very small volume changes do occur owing to the elastic nature (volume modulus) of the cell, the heaving pressure is assumed to be the pressure of the fluid or the pressure (stress) on the piston.

Direct comparison of the results from different authors is difficult because test procedures are not standardized. Results are generally inconsistent and are often contradictory. For example, Hoekstra et al. (1965) and Penner (1967) concluded independently from experiments that each soil has a characteristic maximum heaving

pressure. They suggest that this is because the pore geometry controls the heaving pressure rather than the temperature. However, Sutherland and Gaskin (1973) and Loch and Miller (1975) found heaving pressures up to six times greater than the characteristic values predicted according to the pore geometry hypothesis. Similar observations were also made by Radd and Oertle (1973) and Takashi et al. (1980). They also found an inverse linear dependence of the heaving pressure on the cooling plate temperature at the cold end, in fine grained soils (warm end temperature, 0°C). The computed slope of the relationship was 1.118 MPa $°C^{-1}$ which compares almost exactly with the ice pressures specified by special case 1 of the Clausius-Clapeyron equation (section 2.4). A fairly thick ice lens formed at the cold end of the soil next to the cooling plate. Hysteresis was not apparent. That is, the pressure was independent of whether the soil was cooling or warming. Below a certain temperature (-4°C with a silt and -20°C with a clay) departures from a linear relationship were observed and the pressure instead increased at a diminishing rate.

McCabe and Kettle (1982) also observed a linear relationship between heaving pressure and cold plate temperature in a highly frost susceptible mixture of sand and ground chalk. Pressures, however, were about an order of magnitude smaller than those observed by Takashi et al. (1980) probably because of much higher temperatures at the warm end. Departures from linearity occurred when the cold end was below about -4.5°C.

Loch and Miller (1975) found a dependence of the heaving pressure upon the temperature gradient, but not a linear one.

Unfortunately they varied the temperature at both ends of the soil which makes direct comparison with Takashi's results difficult. Heaving pressures increased sharply with the temperature gradient up to a maximum of 600 kPa at 1-2°C cm^{-1} (for a silt), and then abruptly decreased as the temperature gradient was increased. Maximum pressures also increased inversely in proportion to the particle size of the silt.[5] When a surcharge (overburden pressure) was applied, after the maximum heaving pressure had been reached, the pressure of the soil increased accordingly, but then slowly dropped back to the previously established maximum. Loch (1975) hypothesized that the maximum observed heaving pressures may not be 'maxima' in the true sense but 'practical maxima' in which the rate of heave becomes smaller than a measurable limit. The implication is that heaving may go on at a very slow rate over geological periods of time, in the permafrost (Miller, 1977). This possibility, however, is probably limited to clays and colloidal materials rather than granular soils (Radd and Oertle, 1966).

2.6 Current Physical Theory of Frost Heaving

The increasing need for a practical understanding of frost heaving has prompted an expansion of the research into the physics of the phenomenon. A number of models have been developed which help to clarify some of the general thermodynamic and physical conditions which arise during ice segregation. Although these are limited to highly

---

[5] The opposite effect was observed in heaving tests by McCabe and Kettle (1981). Heaving pressures diminished in direct proportion to the amount of fines (chalk dust) added to the soil.

simplified situations, they help to provide a useful mental conception of the phenomenon as a whole. The main shortcomings with the current models are: (1) none deals with the effect of the soil mechanical propeties (creep and consolidation) on ice segregaton, (2) none allows for secondary frost heaving (i.e. only the warmest ice lens is assumed to be growing), (3) the models describe the situation where the soil is unconfined (i.e. unrestrained heaving). The possibility of frost heaving involving an increase in internal pressure, without the accompanying growth of ice lenses, is overlooked.

Current models define the location of ice lenses relative to the frost line as well as the conditions occurring in the frozen fringe. The simplest of these attributes the growth of ice lenses to the hydraulic conditions in the frozen fringe, in particular the changing permeability. Models in this category have been proposed by a number of authors including Harlan (1973), Taylor and Luthin (1978) and Guymon et al. (1980) and are referred to as the 'hydrodynamic approach' to frost heaving. Conservation of mass and heat in the frozen fringe is described by interrelated continuity equations. The Clausius-Clapeyron equation provides the link between the temperature gradient and the hydraulic gradient. Mass transfer across the frozen fringe is limited to the liquid phase and is assumed to obey Darcy's law:

$$J = -ki \qquad 2.2$$

where i = hydraulic gradient $mH_2O\ m^{-1}$

k = hydraulic conductivity (permeability coefficient) of the soil (decreases with colder temperatures), $m\ s^{-1}$

J = flux (flow rate), $m\ s^{-1}$

In order for mass to be conserved, the sharp decline in the hydraulic conductivity of the soil with colder temperatures induces an increasing divergence of flux within the frozen fringe.[6] The ice lens forms where the flux divergence is maximum. This corresponds to the point where $\frac{dk}{dT}$ is maximum (maximum slope, Fig. 2.3).

Numerical simulations of frost heaving with this model are generally compatible with observations of the spacing and thickness of ice lenses in experiments with columns of homogeneous soil. Following a step-wise decrease in the temperature at one end of the soil, the frost line advances so rapidly, initially, that the rate of water migration is too slow for distinct ice lenses to form, although some ice enrichment probably occurs. O'Neill (1982) suggests that a large number of closely spaced ice lenses form initially, but these are too thin to be visible. As the advance of the frost line slows, water is able to accumulate for longer periods of time and thin rhythmic lenses begin to appear. The thickness and spacing of these increases as freezing slows (Fig. 2.4). Allowing for the volume expansion of water during freezing (9.1%), the thickness of each lens is related to the flux of water through the frozen fringe, J, by:

$$\Delta z = 1.091 \int_0^t J \, dt \qquad 2.3$$

t = time.

The frozen fringe becomes progressively thicker with each lens, in response to the decline in the thermal gradient as the rate of freezing slows. Eventually, a thermal steady state is established and

---

[6] For mass to be conserved, when the divergence of flux is greater than zero, the water content of the soil must be increasing with time.

FIGURE 2.3

HYDRODYNAMIC MODEL OF FROST HEAVING
ASSUMING A LINEAR TEMPERATURE GRADIENT

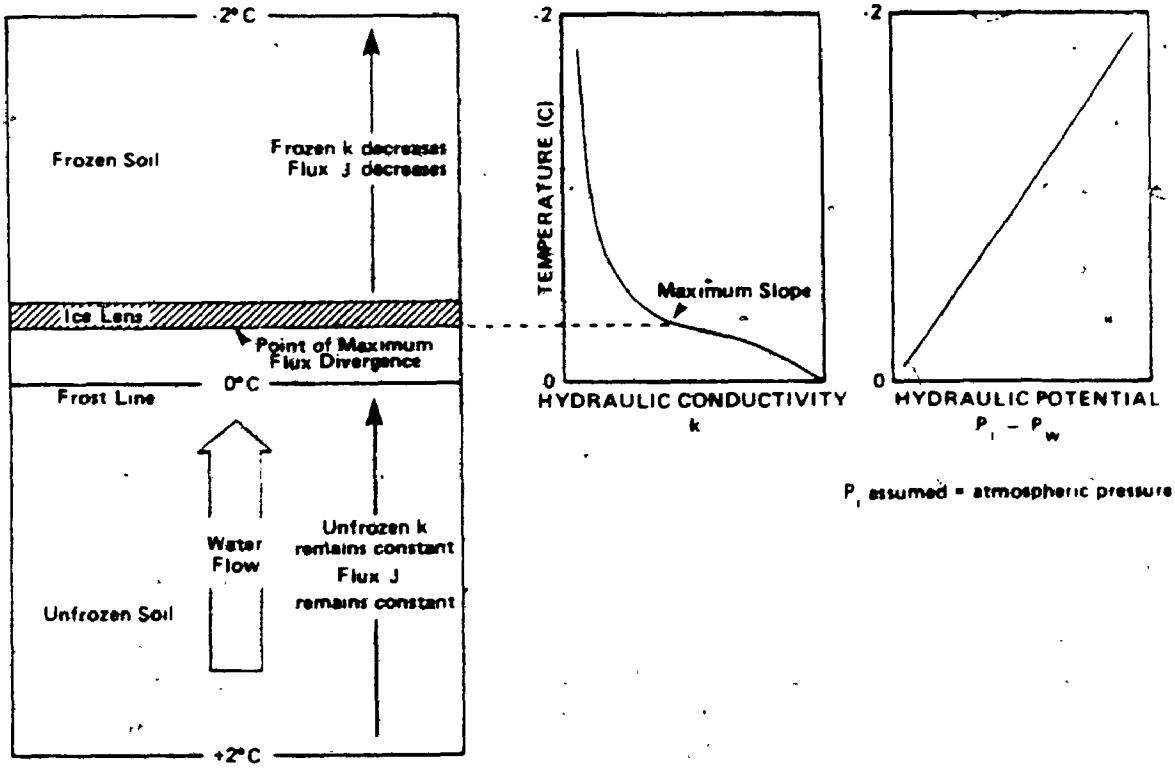

FIGURE 2.4

ICE LENS DISTRIBUTION IN A FREEZING SOIL COLUMN
FOLLOWING A STEP-WISE DECREASE IN TEMPERATURE AT ONE END

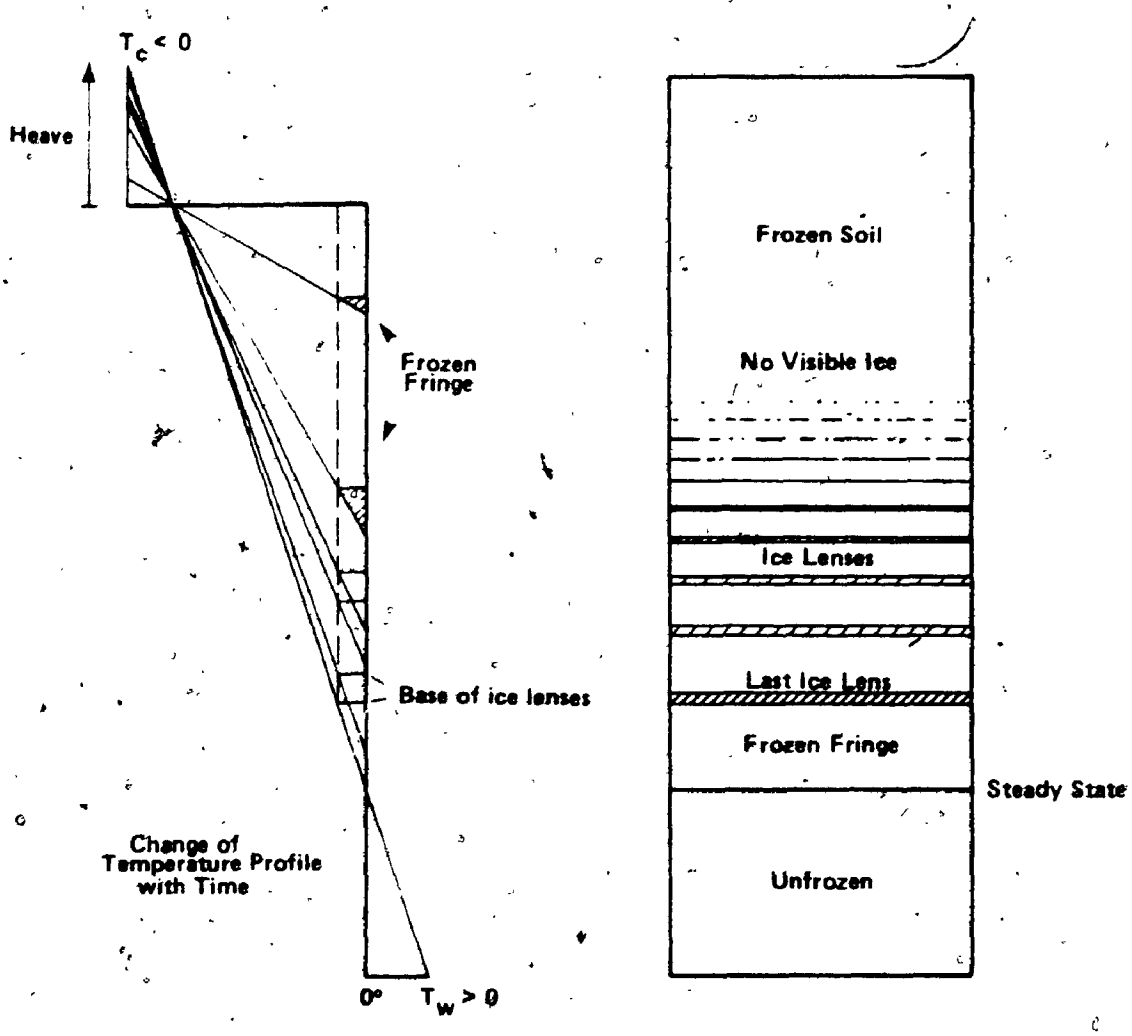

Konrad and Morgenstern (1980)

the frost line stops advancing. The liquid flux through the frozen fringe is obtained by substituting for the hydraulic gradient in Darcy's law from the Clausius-Clapeyron equation:

$$J = K\left[\frac{v_i}{v_w}\frac{(\Delta P_i)}{\ell} - \frac{L}{v_w T}\nabla T\right] \qquad 2.4$$

ℓ = thickness of the frozen fringe,

∇T = the temperature gradient,

ΔP_i = difference in ice pressure between the base of the warmest lens and the frost line.

The overall hydraulic conductivity of the frozen fringe, K, is the sum of a series of infinitesimal layers in which the conductivity is changing:

$$K = \frac{\ell}{\int_0^{\ell} \frac{1}{k(z)}\,dz} \qquad 2.5$$

Growth of the last lens continues at a declining rate and eventually stops over a long period of time, due to the increasing weight of the overlying ice.

Ratkje (1980) views frost heaving from a somewhat different perspective, employing irreversible thermodynamic theory to derive general thermal drive - water flux relations. This avoids the assumption of thermodynamic equilibrium occurring in the frozen fringe, as is done with the hydrodynamic model. Ratkje (1980) suggests that Darcy's law alone cannot be used to describe water transport during frost heaving because it is not valid where there is a temperature gradient. Instead, water flux is expressed in terms of temperature

and pressure gradients, which vary in proportion to phenomenological mass transfer coefficients and coupled (heat and mass) transfer coefficients. The model has similarities to the hydrodynamic model because it explains ice segregation as a result of the declining hydraulic conductivity of the soil with colder temperatures. One difficulty with this concept of frost heaving is that it implies the growth of dirty (diffuse) bands of segregation ice in the frozen fringe rather than discrete lenses with clearly defined boundaries.

An entirely different approach to frost heaving was conceived by Miller (1978, 1980). His model has a somewhat more elaborate physical basis than the other models, which avoids some of the problems these have encountered, particularly that of dirty ice lenses. Miller (1980) views the frozen fringe as a 'thermally-induced regelation engine' in which ice lenses are incidental by-products of the exhaust system rather than part of the engine itself. Because of this, the ice lens actually contributes nothing to the work of heaving. The work is done entirely by the frozen fringe. Water flows through the frozen fringe in response to hydraulic gradients, by two modes of transport: (1) transport entirely within the liquid films and (2) regelation transport, in which ice molecules move toward colder temperatures, changing phase at microscopic ice-water interfaces. Growth of ice lenses is described in terms of changing stress conditions occurring in the frozen fringe. The model is based on Terzaghi's theory of intergranular (effective) stress σ_e:

$$\sigma_e = \sigma - \sigma_n \qquad 2.6$$

σ = total stress (weight of overburden)

σ_n = 'neutral stress' generated by the pore contents

In frozen soil the neutral stress is produced by the combined effects of the ice and unfrozen water and acts to diminish the intergranular stress with colder temperatures. Equations depicting pressure profiles in the ice and unfrozen water define the stress conditions. According to this model, the ice lens forms where the intergranular stress falls to zero ($\sigma_n = \sigma$). The situation is analogous to the condition known as 'boiling' or 'liquefaction' in geotechnical engineering. Neutral stresses reduce the intergranular stress to zero and the overlying soil is lifted (Fig. 2.5).

Miller (1978) views the upper limit of heaving pressure, P_i, as determined solely by the thermodynamic conditions (temperature, ΔT^{**} and pore water pressure, P_w^{**}) at the base of the lens (Clausius-Clapeyron eqn.):

$$P_i = \frac{1}{v_i} \left[v_w P_w^{**} + \frac{L \Delta T^{**}}{T} \right] \qquad 2.7$$

He also suggests the possibility that the permeability of the frozen fringe may limit the heaving pressures established by reducing P_w^{**}.

2.7 Permeable Nature of Frozen Soils

An important advance in the understanding of frozen soils was the discovery that they are permeable. This confirmed the possibility of secondary frost heaving and explained how ice lenses are able to form behind the frost line. Burt and Williams (1976) used a relatively simple permeameter, in which a layer of frozen soil was sandwiched between two reservoirs of water containing dissolved lactose, to prevent

FIGURE 2.5

STRESS AND PRESSURE PROFILES IN THE FROZEN FRINGE DURING ICE SEGREGATION AS PROPOSED BY MILLER (1980)

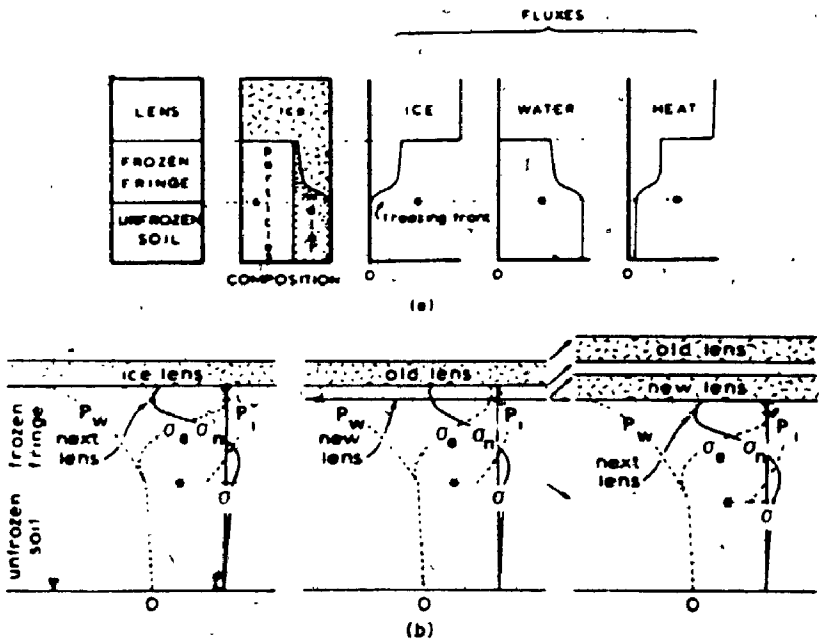

P_w = Unfrozen water pressure

P_i = Ice pressure

σ_e = Effective stress

σ_n = Neutral stress

σ = Total stress

(after Miller, 1980)

freezing. Semipermeable membrane filters prevented the lactose from entering and thawing the soil. The permeameter was immersed in a refrigerated bath. Application of a hydraulic pressure to one reservoir produced a slow discharge of water from the other. Their results demonstrated that frozen soils obey Darcy's law (eqn. 2.2).

Similar observations have also been made by Horiguchi and Miller (1983) with a permeameter in which supercooled water was used instead of lactose solution. Their results (Fig. 2.6) show a sharp decline in the hydraulic conductivity for different soils, by several orders of magnitude, within a few tenths of a degree below 0°C. This is attributed, in part, to the rapid decline in the thickness of the liquid film water in this temperature range.

An alternative approach was conceived by Aguirre-Puente and Gruson (1983). A layer of frozen soil was sandwiched between two layers of unfrozen soil which act as reservoirs for unfrozen water. The soil was cooled by circulation of cooling fluid in a hollow metal jacket. This was divided into three compartments each at different temperatures. Flow through the soil was induced by hydraulic pressures. The device is still in the developmental stage.

Perfect and Williams (1980) and Oliphant et al. (1983) measured the hydraulic conductivity of frozen soils, in which the flow was induced by a temperature gradient rather than a hydraulic gradient. At -2°C Oliphant et al. (1983) obtained a value of 4×10^{-13} m s^{-1} in a silt. This increased to about 5×10^{-12} m s^{-1} at -0.3°C, which is comparable to Horiguchi and Miller's (1983) results in silts at the same temperature. Similar values were also obtained by Loch and Kay (1978)

FIGURE 2.6

HYDRAULIC CONDUCTIVITY OF SEVERAL SILTS AND CLAYS AS A FUNCTION OF TEMPERATURE

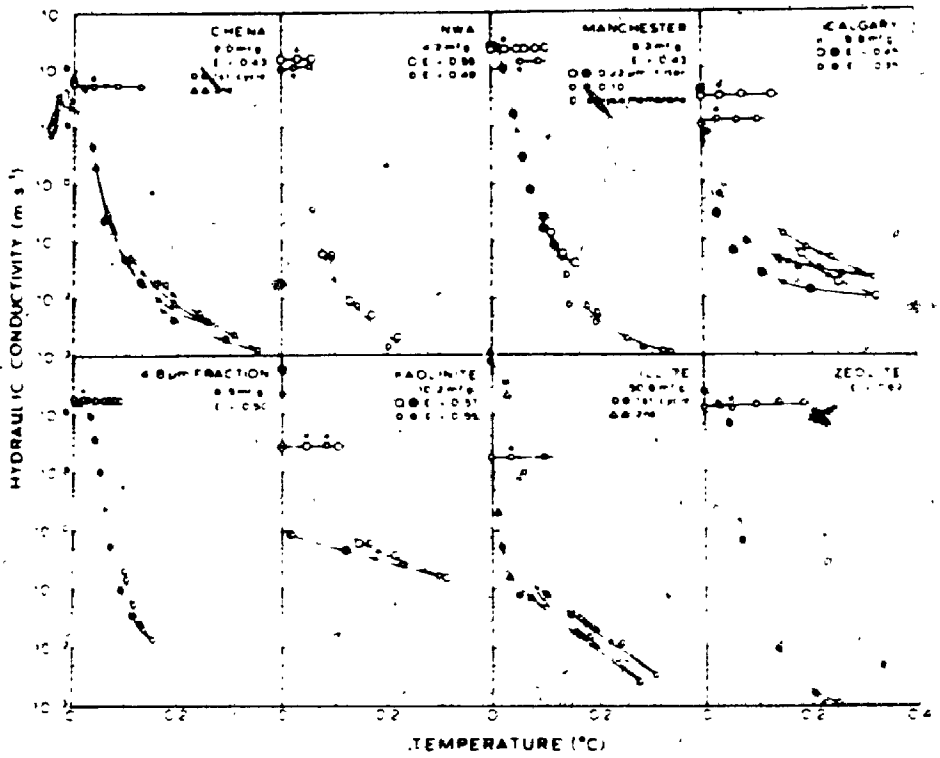

Freezing ○ Thawing ●

Nucleation indicated by a sharp break in slope of freezing curve

(after Horiguchi and Miller, 1983)

in an independent experiment. They determined the overall hydraulic conductivity of the frozen fringe in a frost heaving silt at about 10^{-12} m s^{-1}. (This was an inferred value rather than a direct measurement). The frozen fringe was about 2-4 mm thick.

2.8 Series-Parallel Transport

Miller et al. (1975) envisaged water movement in unconfined frozen soils as a 'series-parallel' transport process in which pore ice moves, as well as the liquid film water, in the direction of colder temperatures (Fig. 2.7). The parallel component refers to transport in the liquid phase only. The series component refers to regelation transport involving phase changes. Although the interfacial boundaries remain stationary within each pore, pore ice actually moves through the soil by continuous molecular replacement (freezing) along the upstream (warmer) boundaries and loss (thawing) along the downstream (colder) boundaries. Pore ice and ice lenses form a continuous rigid body, in which ice molecules move at a uniform translational velocity, provided that the rates of freezing and thawing along the interfacial boundaries remain equal (i.e. mass is conserved).[7] This is based on the assumption

---

7. A practical demonstration of the ability of an ice lens to undergo hydraulically-induced regelation was given by Burt and Williams (1976). A layer of pure ice was sandwiched between two layers of frozen soil in their permeameter. When pressure was applied to one reservoir there was a steady discharge from the other, indicating that even large ice lenses do not pose a barrier to water transport.

FIGURE 2.7

SERIES-PARALLEL TRANSPORT OF WATER IN A FROZEN SOIL

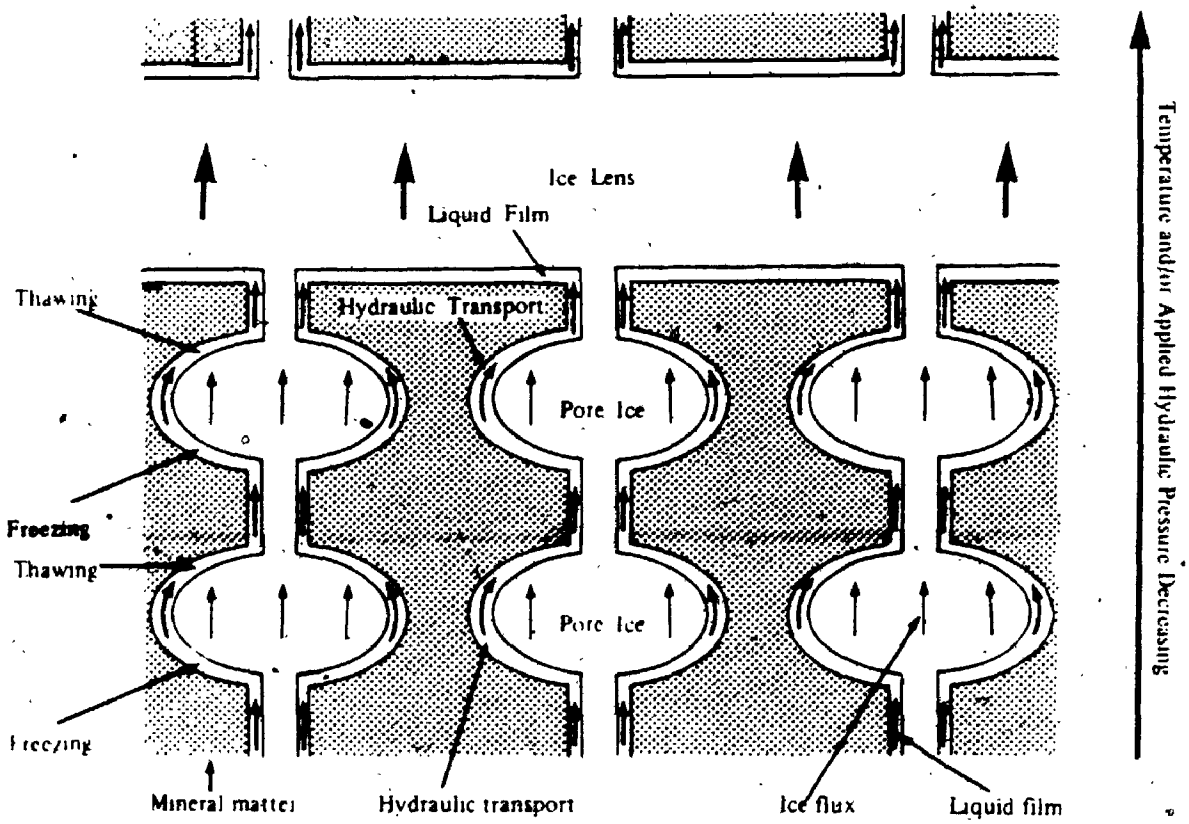

(modified after Loch, 1975)

that any pressure gradients in the ice are too low for significant creep deformation to occur.[8]

In a confined soil, where the ice pressures are able to build up, the flow of ice and water is more complex. Miller et al. (1975) envisaged a circulatory type of transport with the ice moving in the direction of warmer temperatures and the liquid film water in the opposite direction to produce zero net transport.[9] The pressure of the ice increases in the direction of colder temperatures and the pressure gradient is sustained thermodynamically by continuous freezing at the cold end of the soil and melting at the warm end. (This is discussed further in section 4.2).

Regelation transport is also coupled with a localized flow of sensible heat by conduction, as a result of latent heat released/absorbed during phase transitions at the boundaries of the ice. Microscopic temperature gradients within each pore depend upon the ice velocity, as well as the incident angle of the velocity vector. These secondary thermal effects are superimposed on the macroscopic temperature gradient, resulting in a very complex temperature field at

---

[8] Miller et al. (1975) acknowledge creep deformation as a distinct possibility, particularly at temperatures close to 0°C.

[9] The direction of movement of the ice when the unfrozen water pressure remains at atmospheric pressure (i.e. in a confined soil) is in the opposite direction to that when the flow is induced by a gradient in pressure of the unfrozen water (i.e. in an unconfined soil). In the former, the ice moves in the direction of warmer temperatures, whereas in the latter it moves toward colder temperatures. Miller (1980) views the flow of ice in unconfined soils as being due to a temperature induced gradient in the pressure of the unfrozen water.

the microscopic level. Miller et al. (1975) suggest that temperature gradients may even reverse direction at phase boundaries. However, this violates the second law of thermodynamics. The macroscopic flow of heat (primary thermal gradient) is independent of any secondary thermal effects because it acts as the driving force for induced phase changes. Instead, microscopic temperature fields would involve abrupt discontinuities in the temperature gradient along interfacial boundaries, rather than actual reversals.

Miller et al. (1975) raise doubts about whether simple expressions like Darcy's law can be used to describe liquid film (parallel) transport in frozen soils. They suggest that the driving force for film transport is somewhat less than the gradient in liquid pressure due to drag effects produced by the moving ice body. A term must be included, therefore, for momentum exchange with the ice. However, despite these theoretical objections, in permeabilty tests frozen soils still appear to obey Darcy's law, at least at temperatures close to 0°C. A possible reason for this is that the movement of pore ice itself obeys Darcy's law rather than a creep equation similar to Glen's (1975) law. The linear dependence of the rate of ice transport on the hydraulic gradient has been confirmed in experiments by Horiguchi and Miller (1980) with their 'ice-sandwich' permeameter.

Miller et al. (1975) derived analytic expressions for series-parallel transport in idealized soils with uniform cylindrical pores. Their results show that regelation transport forms a large component of the total water transport in frozen soils. Philip (1980) estimated "hydraulic conductivity coefficients" for an array of solid

spherical particles embedded in ice (porosity 50%). He obtained a value of 2.7×10^{-11} m s^{-1} per unit hydraulic gradient. This value is surprisingly large and is comparable to values for silts at temperatures of about -0.1°C (Fig. 2.6). Miller (1980) suggests that at progressively colder temperatures, regelation forms an increasing and even dominant component of the total water transport in soils. However, it is doubtful whether this assumption is true since experimental work discussed in the next section indicates that regelation flow declines exponentially with lower temperatures (about 1 order of magnitude for every 0.15°C temperature change). This suggests that the sharp decline in the permeability of frozen soils at temperatures within a few tenths of 0°C is due, not only to diminished rate of liquid transport, but also to the sharp decline in ice velocity with colder temperatures as well.

Horiguchi and Miller (1980) made a practical attempt to distinguish between the liquid (parallel) and regelation (series) components of flow with their frozen soil permeameter. They reasoned that regelation transport should be indicated by small changes in temperature at the inflow and outflow boundaries of the soil specimen. These are caused by the release/absorption of latent heat as a result of phase changes at the boundaries of the soil. If the ice were not moving the phase changes could not occur. Horiguchi and Miller (1980) actually observed very small changes in the temperature after hydraulic pressures were applied (several thousandths of a degree) but these quickly diminished and were lost in the background thermal noise. The chief difficulty with the experiment is the limited thermal resolution of the apparatus.

2.9 Irreversible Thermodynamics of Coupled Transport Phenomena in Frozen Soils

Experiments have shown that water movement through frozen soils can be induced by osmotic and electrical potential gradients in addition to thermal and hydraulic gradients. Hoekstra and Chamberlain (1964) found very substantial movements of water in the direction opposite to current flow under a relatively low voltage gradient (1 V cm^{-1}). In the region around the anode (+) the frozen soil was depleted of all visible ice, whereas large amounts were observed to accumulate in the vicinity of the cathode (-). In a separate experiment, Williams and Wood (1981) observed water movement through a frozen soil in an isothermal permeameter, which was osmotically induced by altering solute concentrations in the end reservoirs.[10] The flow was in the direction of the reservoir with the more concentrated solution (e.g. Fig. 2.8).

Various attempts have been made to analyse coupled transport of water, heat, ions and electrical current in frozen soils using irreversible thermodynamics (Ratkje, 1982, Miller et al., 1975, Groenvelt and Bolt, 1969).[11] Coupling effects are summarized by a system of linear equations relating the various fluxes, J_i, to the thermodynamic forces, X_j (i.e. $J_i = L_{ij} X_j$):

---

[10] The technique is described for the ice sandwich experiment, chapter 3.7.

[11] Römkens and Miller (1973) propose a theory in which dissolved ions in the liquid films play a key role in the migration of water toward colder temperatures in frozen soils.

FIGURE 2.8

FLOW OF WATER TO AND FROM A FROZEN SOIL PERMEAMETER INDUCED BY GRADIENTS OF OSMOTIC POTENTIAL BETWEEN THE RESERVOIRS AND THE SOIL, −0.30°C, ALLENDALE CLAY

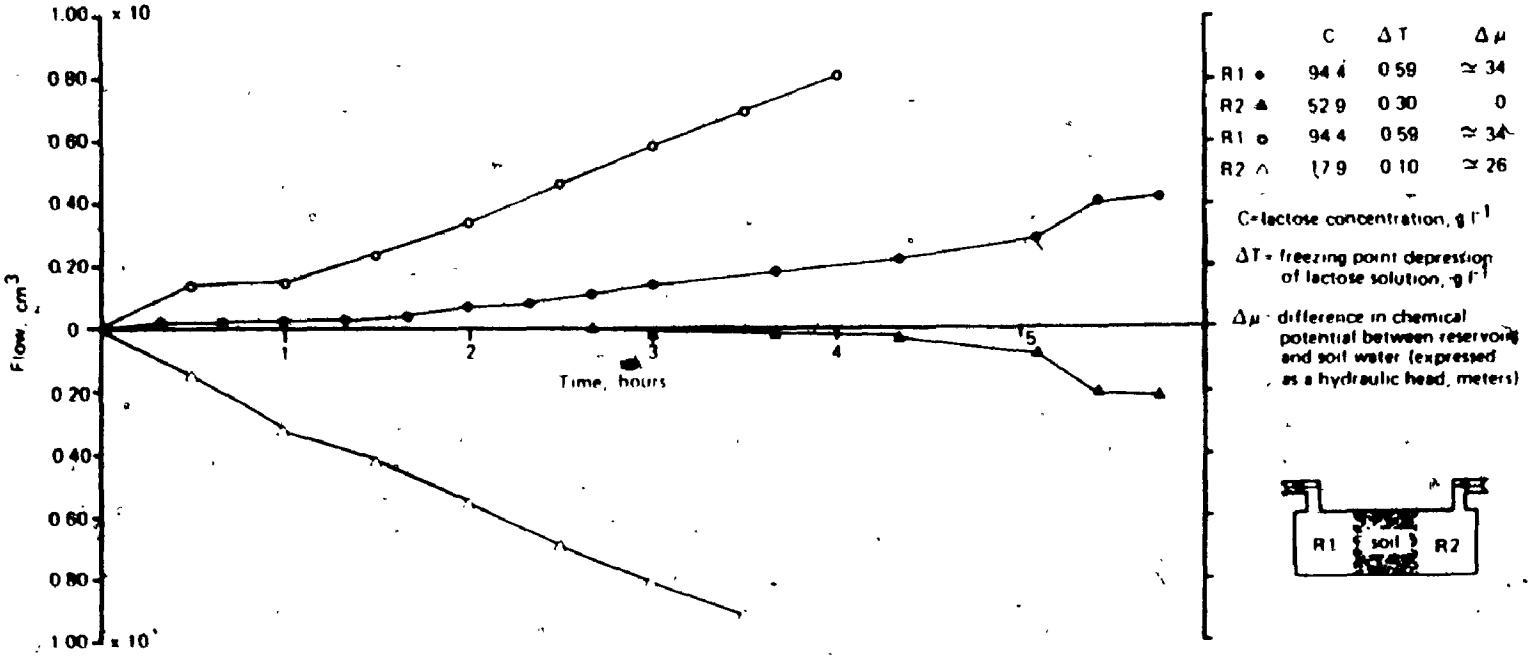

Negative values indicate flow from the reservoir into the soil

Positive values specify flow from the soil to the reservoir

$$J_1 = L_{11}X_1 + L_{12}X_2 + L_{13}X_3 + L_{14}X_4 \quad 2.6$$

$$J_2 = L_{21}X_1 + L_{22}X_2 + L_{23}X_3 + L_{24}X_4 \quad 2.7$$

$$J_3 = L_{31}X_1 + L_{32}X_2 + L_{33}X_3 + L_{34}X_4 \quad 2.8$$

$$J_4 = L_{41}X_1 + L_{42}X_2 + L_{43}X_3 + L_{44}X_4 \quad 2.9$$

where L_{ii} = transport coefficients

and subscripts 1, 2, 3, and 4 refer to the transport of heat, water, salts and electrical current, respectively.

The on-diagonal components (i = i) describe primary transport phenomena and are recognizable as Fourier, Darcy, Fick and Ohm's laws, driven by gradients of potential $X_1 = (-\frac{\Delta T}{\Delta x})\frac{1}{T}$, $X_2 = -\frac{\Delta P}{\Delta x}$, $X_3 = -\frac{\Delta \Pi}{\Delta x}$ and $X_4 = -\frac{\Delta V}{\Delta x}$; with direct transport coefficients, $\frac{L_{11}}{T} = \lambda$ thermal conductivity, $L_{22} = k$ hydraulic conductivity, $L_{33} = \frac{D_s M_s}{RT\rho_s}$, ($D_s$ = salt diffusivity for a single ion species), $L_{44} = \kappa$ electrical conductivity of the soil.

The equations above imply that establishment of a primary gradient in any medium (e.g. a thermal gradient) induces smaller secondary gradients (hydraulic, osmotic, electrical) with resultant flow of water, ions and current, coupled with the heat flow. Coupling coefficients (L_{ij}, $i \neq j$) are always smaller than the direct coefficient and may be positive or negative depending upon whether the flow is in the same direction, or counter to that of the primary gradient. According to Onsager's (1931) reciprocity principle, the cross-coefficients are identical, $L_{ij} = L_{ji}$ (e.g. $L_{12} = L_{21}$, $L_{13} = L_{31}$). The assumption of a linear relationship between the flux and the driving force is valid only if the system is relatively close to equilibrium. In the absence of this condition, fluxes must be approximated instead by non-linear phenomenological expressions (Srivastava and Abrol, 1966).

Unconfined frost heaving is a special case in which a primary thermal gradient induces a secondary hydraulic gradient (assuming ice pressures = atmospheric pressure). Because analytic expressions relating the direct and cross-coefficients are difficult to obtain, primary and secondary gradients are normally linked using the Clausius-Clapeyron equation. However, this is valid only if the soil does not differ significantly from an equilibrium condition. It may not be accurate in situations where an unsteady state prevails.[12]

---

[12] There is some uncertainty about this point because, in situations where the temperature of the soil is rapidly changing, it might be argued that the soil is in a state of dynamic equilibrium internally rather than disequilibrium.

III. EXPERIMENTAL INVESTIGATION OF REGELATION TRANSPORT IN AN ICE SANDWICH PERMEAMETER

3.1 Background

The classic regelation experiment involved the slow passage of a wire, with weights attached at either end, through a block of ice which remained undivided as a result of refreezing. The stress produced by the wire lowered the melting-point, which caused the ice to melt. Water flowed around the wire as a thin liquid film, toward a region of lower stress where the melting-point was higher, and there it refroze.

Miller, Loch and Bresler's (1975) hypothesis that pore ice moves through frozen soils by regelation stemmed from the 'ice-sandwich' experiment originally devised by Miller (1970). A thin disc of ice was sandwiched between two reservoirs containing distilled water. The apparatus was maintained at temperatures slightly below 0°C by a refrigerated bath. The water in the reservoirs was in a supercooled state. Membrane filters with very small pores (smaller than a stable ice crystal) separated the two phases, to prevent nucleation and freezing of the supercooled water by the ice. When pressure was applied to one reservoir, a steady outflow was observed from the other. Freezing occurred at the upstream (high pressure) side and thawing at the downstream side of the ice. This is different from the 'wire' experiment in which thawing occurred at the upstream (higher pressure) side. However, the ice sandwich is still explainable in terms of the effect of pressure on the equilibrium freezing temperature. Essential to the explanation is the difference in pressure between the ice and water, $(P_i - P_w)$, which is maintained at the ice-water interfaces by capillarity of the porous membrane. The Clausius-Clapeyron equation

(eqn. 2.1) relates changes in ice and water pressure to the equilibrium freezing temperature. The increase in water pressure, dP_w, at the upstream interface, raises the equilibrium freezing temperature there above ambient and water moves through the membrane to freeze on to the ice. The ice pressure then rises, and as the pressure increment is transmitted to the other end, where the water pressure has not changed, the equilibrium freezing temperature there is lowered, so the ice melts.

Horiguchi and Miller (1980) attempted to establish the temperature and pressure dependence of the flow rates in the ice sandwich. Their experiment, however, was confined to a narrow temperature range between 0°C and -0.13°C. They found a small temperature gradient across the ice which occurred as a result of phase changes at the upstream and downstream boundaries of the ice.

Several important questions remain to be answered about the ice-sandwich including: (1) the effect of colder temperatures (lower than -0.13°C) on the flow rates, (2) whether osmotic gradients can produce ice movements and (3) the effect of coupled heat flow on the rates of water transport through the ice sandwich. The author has attempted to answer these questions using modified versions of the ice sandwich experiment.

3.2 Apparatus and Procedure

The ice specimen (length 1.0 cm, diameter 5.4 cm) was confined in a perspex cylinder (wall thickness 1.0 cm), Fig. 3.1. This was located between two end reservoirs, also made of perspex, containing the supercooled water (volume approximately 58 cm^3). The reservoir walls were sprayed with PTFE (teflon) to inhibit ice nucleation by the perspex. The cell was immersed in a refrigerated bath which maintained

temperatures constant to within ±0.0025°C. The supercooled water was separated from the ice by cellulose acetate membranes, pore diameter = 0.005 μm (pores become ice filled at −10.0°C). A constant hydraulic pressure was applied to one reservoir and outflow from the other reservoir was recorded by the movement of a water meniscus in a glass capillary. To determine whether the impedance of the membrane significantly affected the flow rates, a coarser-pored nitrocellulose membrane was substituted (pore diameter = 0.05 μm, freezing temperature' −1.0°C), but the results were virtually identical.

Experiments were performed with bubble-free ice, prepared by slowly and undirectionally freezing a column of distilled water (0.3 PPM NaCl) within the ice chamber, while this was mounted on a thermo-electric cooling plate. The excess ice was then trimmed with a blade until flush with the ends of the specimen container. After the cell was assembled, the reservoirs were filled with distilled water. At each temperature decrement, at least 48 hours was allowed for establishment of thermal equilibrium. The experiment was generally limited to the temperature range between 0°C and −0.31°C because of the tendency for freezing to occur in the end reservoirs at lower temperatures.

3.3 Results

Figure 3.2 shows the rate of outflow for various temperatures and hydraulic pressures applied to the inflow reservoir. The flux is linearly related to the hydraulic gradient by a transport coefficient (Fig. 3.3). This confirms Horiguchi and Miller's (1980) finding that regelation flow of ice at temperatures close to the melting-point is described by a linear transport type of equation similar to Darcy's law:

FIGURE 3.1
CROSS-SECTION OF ICE SANDWICH PERMEAMETER

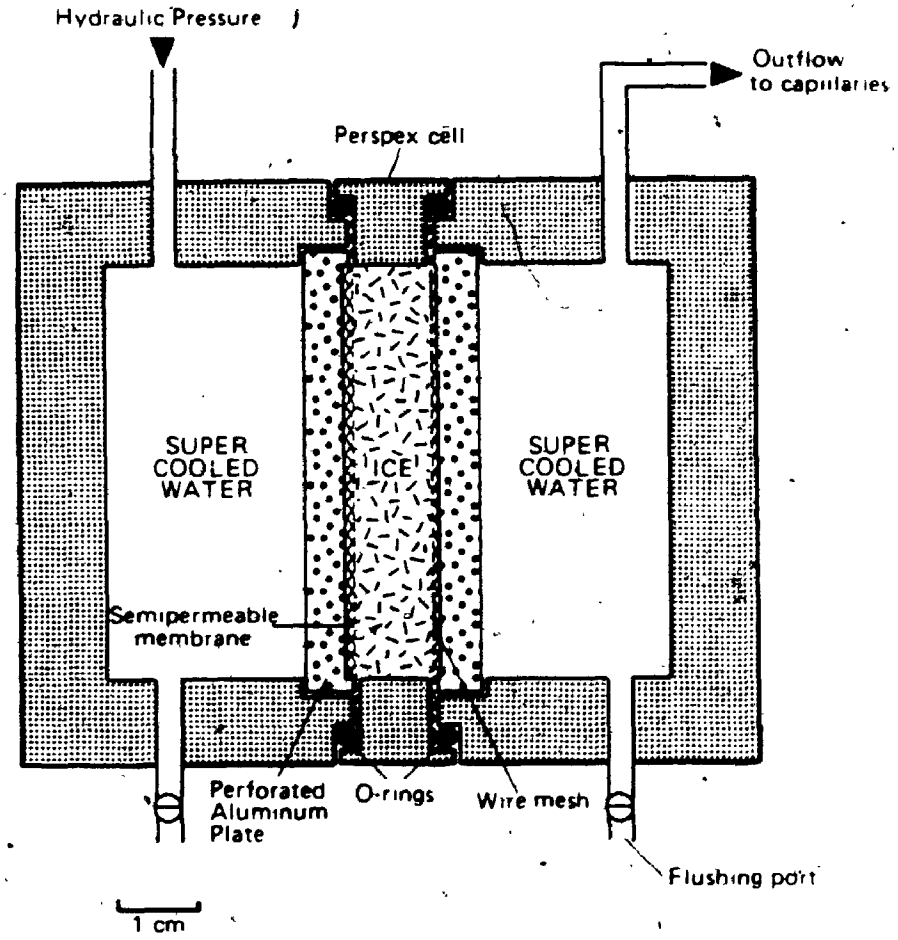

FIGURE 3.2
OUTFLOW VERSUS TIME FOR EXPERIMENT A4

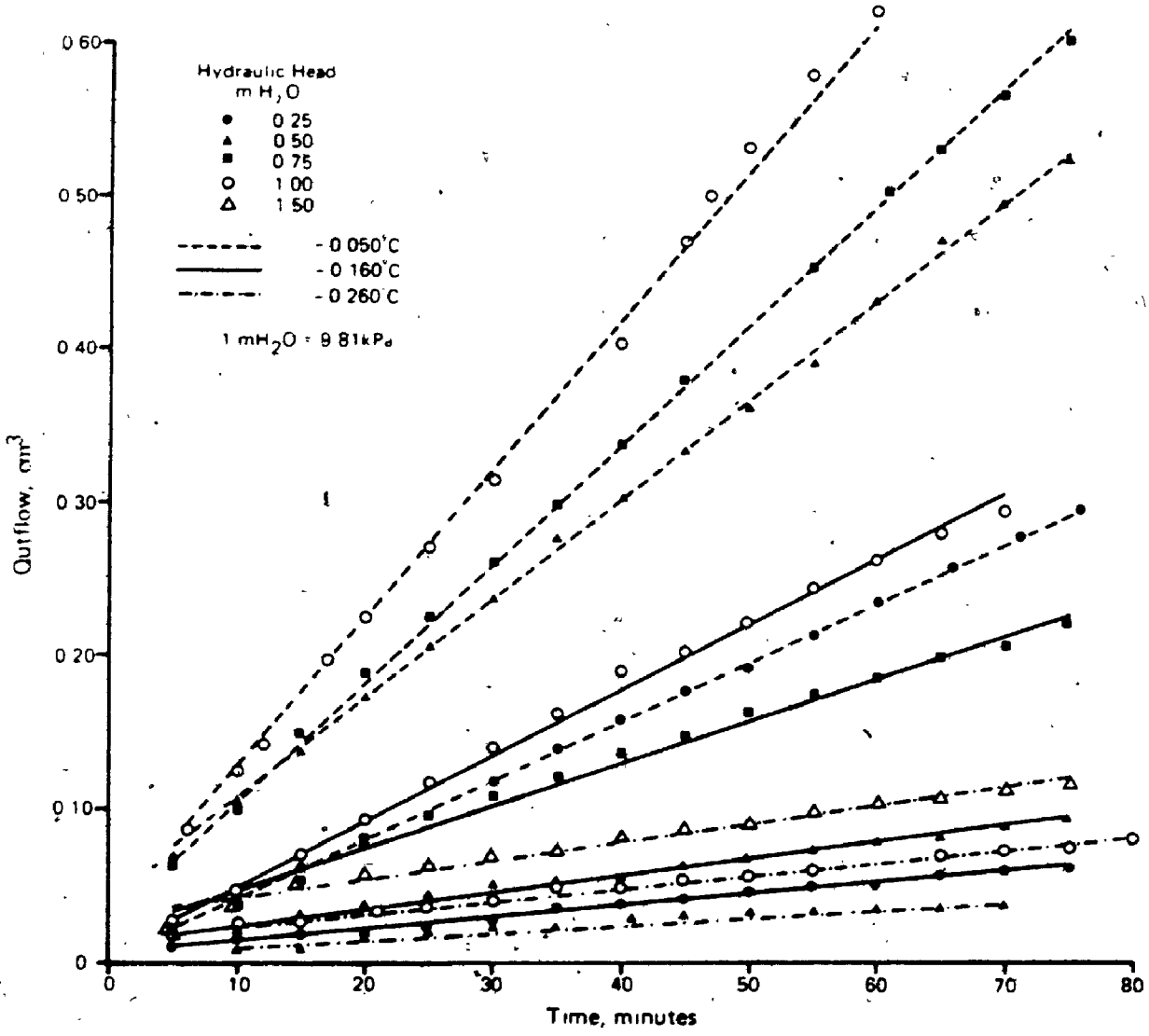

FIGURE 3.3

FLUX VERSUS HYDRAULIC GRADIENT FOR EXPERIMENT A4 AT VARIOUS TEMPERATURES

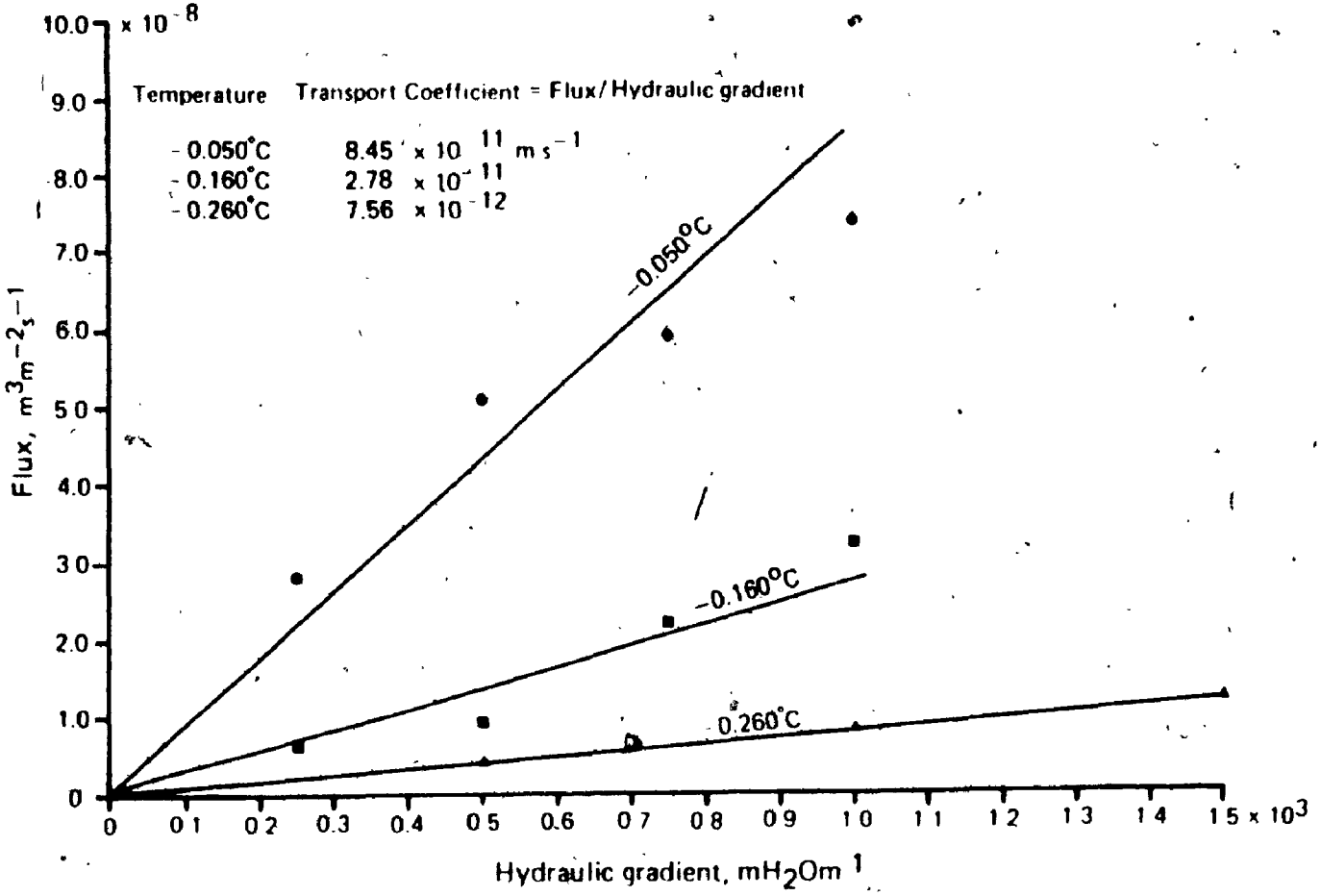

FIGURE 3.4

HYDRAULIC TRANSPORT COEFFICIENT VERSUS TEMPERATURE, EXPERIMENT A4 AND A8

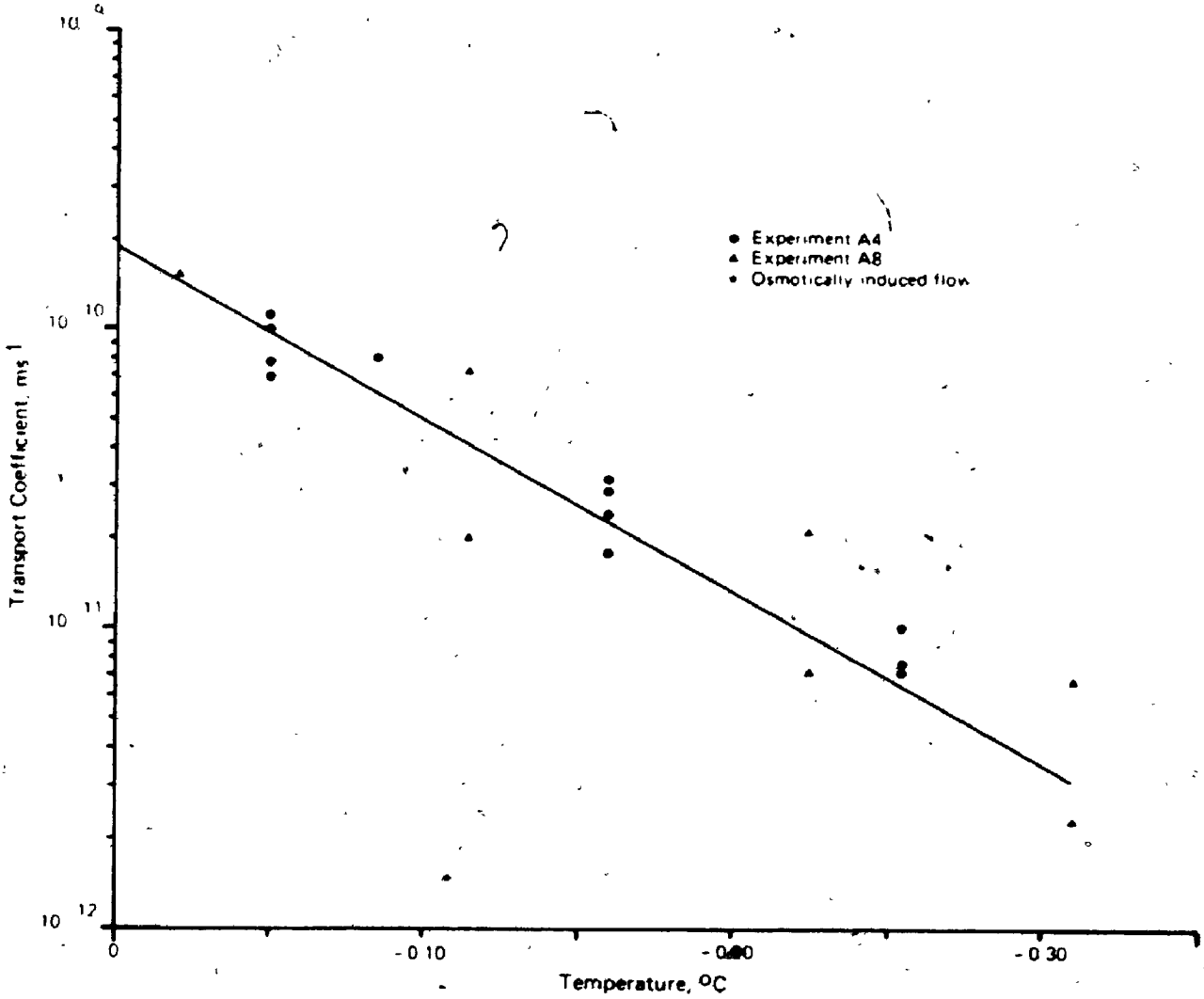

$$J = -L \frac{dH}{dx} \qquad 3.1$$

where J = flow velocity or flux, $m\ s^{-1}$

L = transport coefficient, $m\ s^{-1}$

$\frac{dH}{dx}$ = hydraulic gradient, $mH_2O\ m^{-1}$ ($1mH_2O = 9.81$ kPa)

The measured values of the transport coefficient (Fig. 3.4) show a much stronger temperature dependence than those obtained by Horiguchi and Miller (1980), changing by about 2 orders of magnitude in the temperature range investigated (0°C to −0.31°C). This is described by an exponential relationship (Fig. 3.4), in which the best fit line obeys the expression:

$$L = ce^{bT} \qquad 3.2$$

where T = temperature, °C

$b = 13.13$

and $c = 1.87 \times 10^{-10}\ m\ s^{-1}$.

3.4 Effects of Specimen Dimensions

The results in Figs. 3.2 and 3.3 were obtained from a series of tests (experiment A4) using a single ice specimen of cross-sectional area 22.86 cm^2 and 1 cm thickness. Subsequently, another specimen of the same dimensions was prepared and the experiment was repeated (experiment A8). The transport coefficients of the two experiments are compared in Fig. 3.4. It is apparent that the experiment is reproducible even though there is a greater scatter in A8 than A4.

A number of tests were carried out in which the sample thickness was 3.3 cm, rather than 1 cm (cross-sectional area also 22.86 cm^2). These did not produce comparable results. That is, the coefficients obtained were affected by the sample thickness. With an

ice specimen 3.3 cm thick, the transport coefficient was 3.7×10^{-12} m s^{-1} at -0.18°C, which is about an order of magnitude lower than in A4 and A8 with the thinner ice specimen at the same temperature (1.7×10^{-11} m s^{-1}, best fit line, Fig. 3.4). The transport coefficient also showed a much weaker temperature dependence, changing by about half the amount which occurred with the thinner ice specimen over the same temperature range. Thus, the regelation flow coefficient is unlike a Darcian permeability coefficient, in that the flow is affected by the thickness of the specimen. However, for a given thickness of ice the flow appears to obey Darcy's law with respect to the applied pressure. Changes also take place as a result of an apparent re-crystallization or other 'aging' of the ice. In some instances, although the bath temperature remained unchanged, the transport coefficient increased by half an order of magnitude when hydraulic gradients were re-established after a 48 hour period. In one or two instances the flow rates were actually higher at colder temperatures (e.g. Fig. 3.6). The findings suggest that regelation flow of pore ice in soil is influenced by the crystalline structure of the ice and the configuration of the pore spaces, as well as the temperature.

3.5 Threshold Pressures

There was also an effect seen in the initial behaviour of the ice sandwich when the hydraulic gradient was first applied. When the pressure was raised slowly on the water in the 'inflow' reservoir, the meniscus in the outflow capillary tube started moving only when a 'threshold' pressure was reached. This increased with colder temperatures, although the magnitude varied considerably with each ice specimen (eg. Fig. 3.5).

FIGURE 3.5

THRESHOLD PRESSURES REQUIRED TO INITIATE FLOW THROUGH THE ICE SANDWICH, EXPERIMENT A4 AND A8

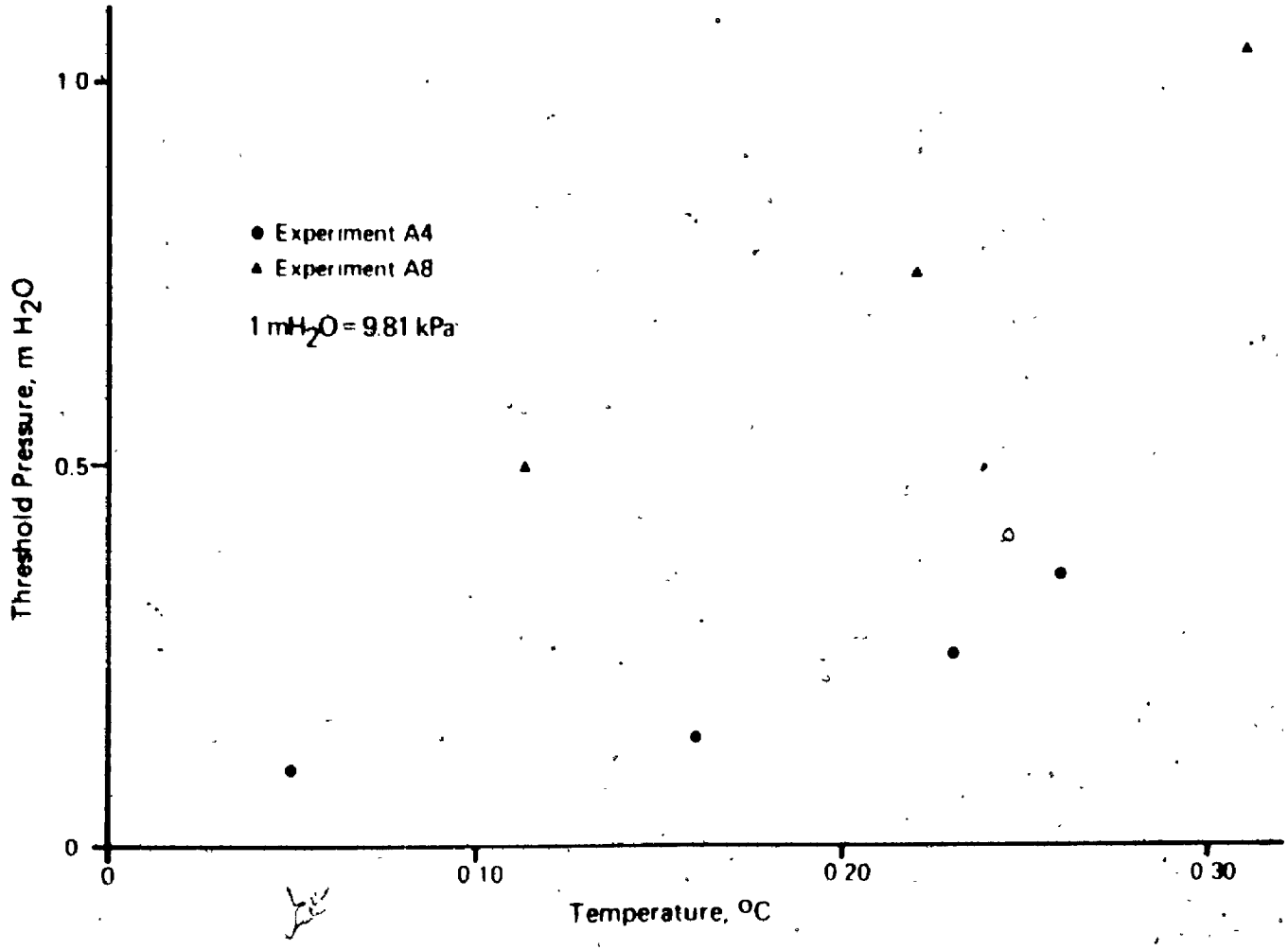

FIGURE 3.6
OUTFLOW VERSUS TIME FOR EXPERIMENT A2 AND A3

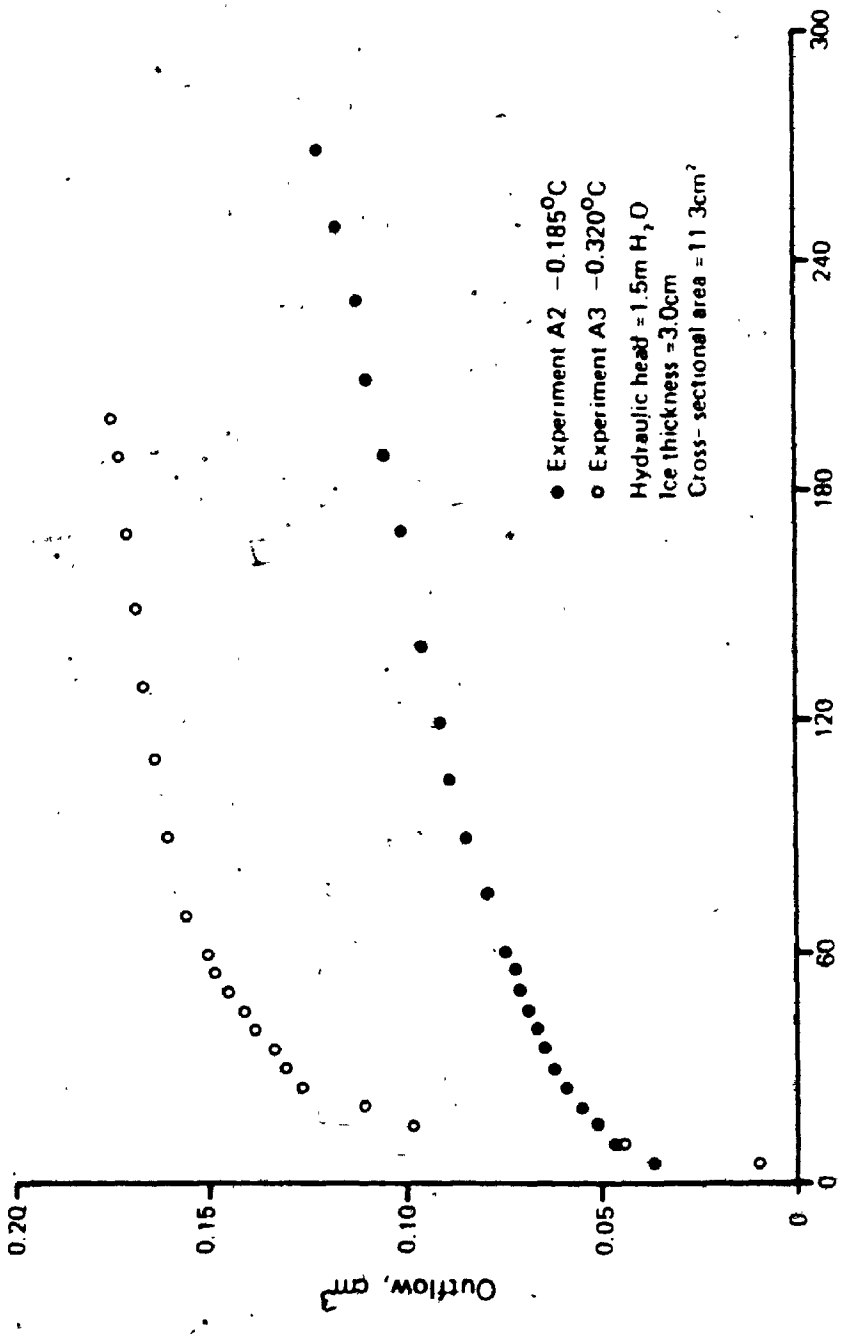

After the threshold pressure was exceeded and the desired test pressure established, the flow was rapid for an initial period. In experiments A4 and A8 (Figs. 3.2 and 3.3) this initial rapid flow declined to a steady value in less than 5 minutes, but with thicker ice specimens (3.0 cm, 3.3 cm), it took over an hour (Fig. 3.6). A similar phenomenon was observed in the experiments by Burt and Williams (1976), where it was described as a decline in the hydraulic conductivity of the soil during the course of the experiment (tests were also about an hour in duration).

The phenomenon may be caused by the coupled heat flow (i.e. the secondary thermal gradient), which tends to reduce the flow rate of the water (see section 3.8). Establishment of a stable (linear) thermal gradient within the ice may take somewhat longer with the thicker ice specimen and so the flow rate declines over a longer period. Alternatively, the phenomenon may be related to the establishment of a constant pressure gradient within the ice, which, presumably, takes longer in thicker ice specimens.

3.6 Osmotically-Induced Regelation

Experiments were also carried out with the ice sandwich, in which solutes were added to one or both reservoirs, to investigate whether flow could be induced by an osmotic gradient. Lactose monohydrate was used because its relatively large molecules were restricted from entering the ice chamber by the semi-permable membranes. In practice, the experiment was generally limited to relatively short periods because of the tendency for small quantities of lactose to diffuse through the membrane and gradually thaw the ice.

After the cell was assembled the reservoirs were flushed with distilled water and the system was allowed to equilibrate for about three days. Since the water pressure was constant and equal to atmospheric pressure, the Clausius-Clapeyron equation predicts that the ice pressure should increase by 1127 kPa $°C^{-1}$. In experiment A9 (Fig. 3.7), the temperature of the bath was −0.110°C, so the ice pressure should have been 124 kPa. Following this, reservoir R1 was flushed with lactose solution (concentration 52.9 g ℓ^{-1}, freezing-point-depression 0.30°C).[1] A steady rate of flow through the system from reservoir R2 into R1 was observed for about a day afterward, corresponding to a transport coefficient of 1.5×10^{-12} m s^{-1} (hydraulic head = difference in osmotic potential between the two reservoirs = 34 m H_2O). Subsequently, the rate decreased, presumably because lactose molecules slowly diffused through the membrane and began to thaw the ice. The explanation for the flow is as follows.

The addition of solutes lowers the chemical potential of the water μ_{R1} below that of the ice μ_i at its elevated pressure (Fig. 3.7). Consequently, the ice melts and flows through the membrane into reservoir R1. The resulting fall in ice pressure, when transmitted across the ice, disturbs the equilibrium between the ice and the pure water in R2. The equilibrium freezing temperature there is raised above ambient, so that water flows through the membrane to freeze onto the ice. There was a few minutes delay before flow from R2 was observed. The transport coefficient of 1.5×10^{-12} m s^{-1} is about an order of magnitude lower than the values in Fig. 3.4 at the same temperature.

---

[1] Freezing-point-depression of lactose solution, Appendix E.

FIGURE 3.7

FLOW THROUGH ICE SANDWICH INDUCED BY AN OSMOTIC GRADIENT, EXPERIMENT A9, -0.11°C

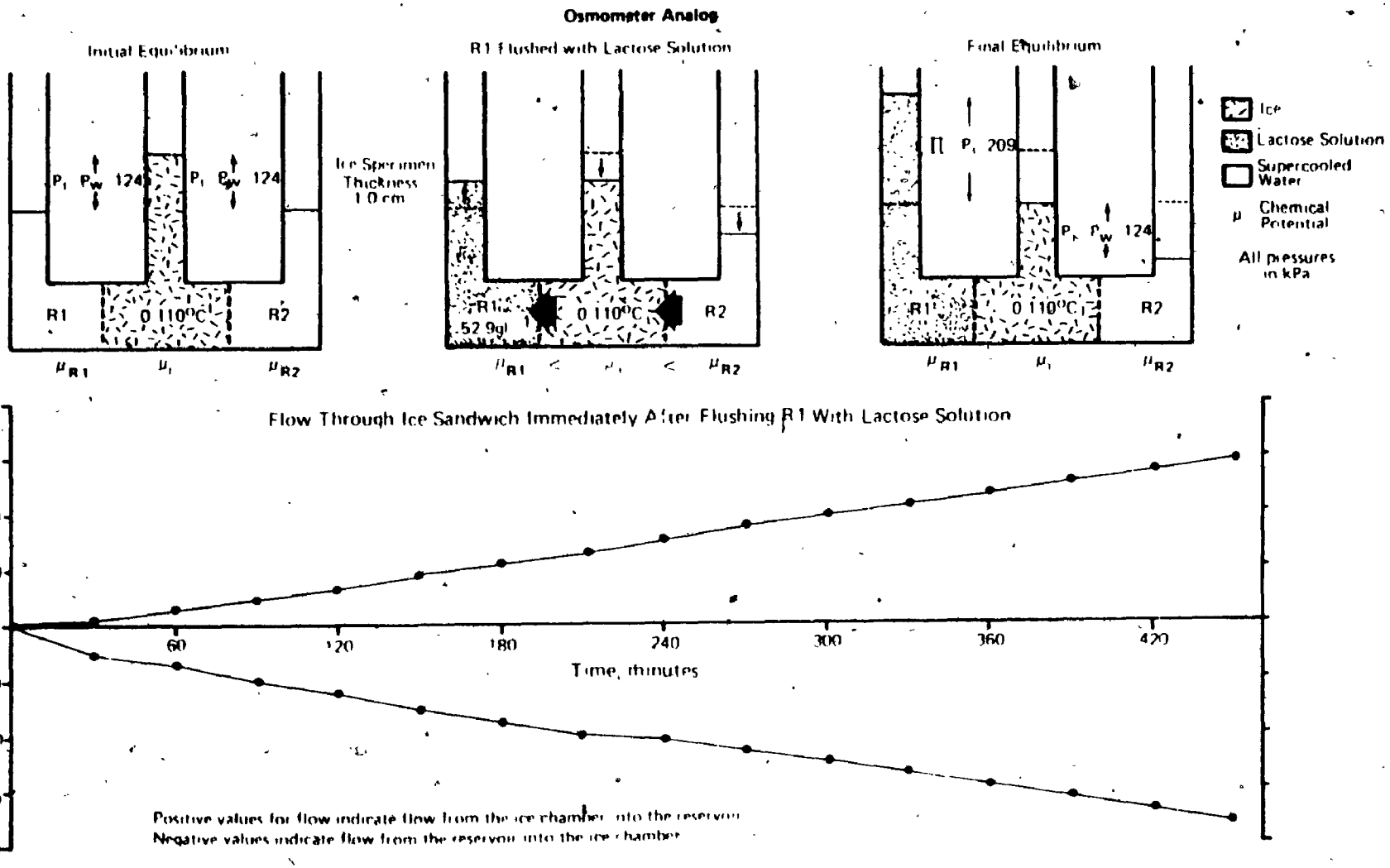

FIGURE 3.8

FLOW THROUGH ICE SANDWICH INDUCED BY AN OSMOTIC GRADIENT, EXPERIMENT A10, -0.30°C

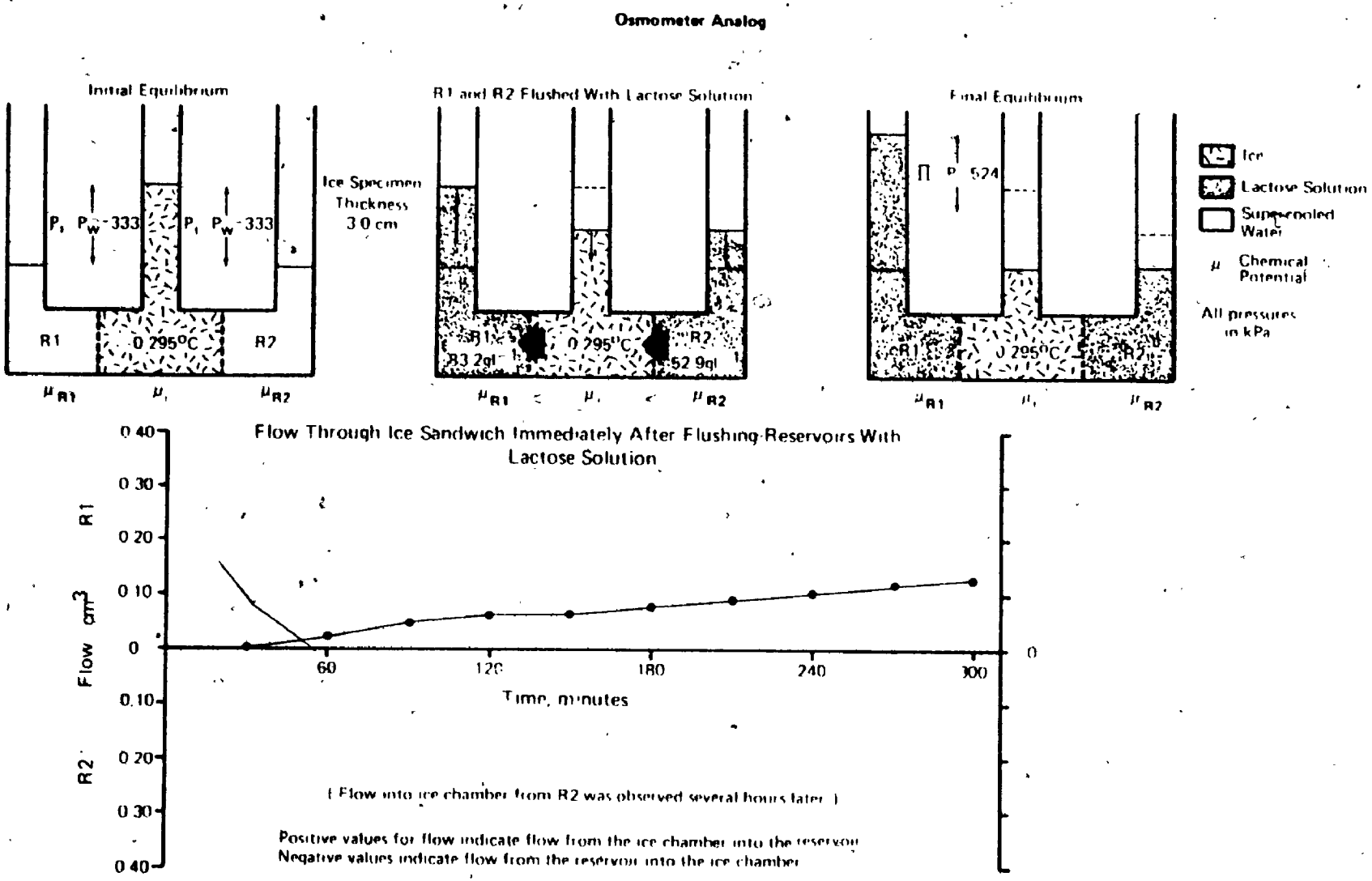

Figure 3.7 (osmometer analog) shows a hypothetical situation which would occur if pressure was allowed to build up in R1. Flow would eventually cease when chemical equilibrium was restored between the ice and the solution in R1 (final equilibrium condition). Ideally, this would occur when the osmotic pressure of the solution (333 kPa) exceeded the ice pressure (124 kPa) by 333 - 124 = 209 kPa (assuming the membranes are completely impermeable to lactose and the solution is dilute).[2] At the same time the ice pressure must have been 124 kPa greater than the pressure of the supercooled water in R2, which was atmospheric.

In experiment A10 (Fig. 3.8) the situation was more complicated than A9 because lactose solution was used in both reservoirs. The temperature was -0.30°C, so the flow rate (Fig. 3.8) was much slower. When the reservoirs contained pure water, the equilibrium ice pressure should have been 333 kPa (eqn. 2.1). The water was replaced with lactose solutions of 83.2 g ℓ^{-1} in R1 (freezing-point depression = -0.50°C) and 52.9 g ℓ^{-1} in R2 (freezing-point depression = -0.30°C). Initially, flow occurred into R1 (Fig. 3.8) which caused the

---

[2]The osmotic pressure, Π of a dilute solution is given by the Van't Hoff equation:

$$\Pi = \phi RT \sum_s C_s \qquad (3.3)$$

where ϕ = osmotic coefficient of the solute
R = universal gas constant, 0.848 m H_2O
T = temperature, Kelvins
C_s = molar concentration of solute = concentration, g ℓ^{-1} ÷ molecular weight (360.3 for hydrated lactose)

For an ideal solution, an osmotic coefficient = 1 is assumed. In the examples given above, the osmotic pressures are overestimated because the solutions are neither ideal nor dilute.

ice pressure to fall. The freezing-point depression of -0.30°C for the solution in R2 implies equilibrium with the ice at ambient (bath) temperature, assuming the ice is at atmospheric pressure. Since the ice pressure, initially, was much higher than this, flow into R2 might have been expected, at first. Subsequently, as flow into R1 continued because of the difference in the chemical potential between the ice and the solution there, the ice pressure presumably fell further below atmospheric, so that a flow from R2 into the ice was observed after several hours (not shown in Fig. 3.8) The slow response of reservoir R2, following the start of flow into R1, may be because the ice specimen was thicker (3.0 cm) and also colder in this experiment.

If the pressure was allowed to build up in R1, (osmometer analog Fig. 3.8), the flow would cease when the osmotic pressure of the solution in R1 exceeded the ice pressure (which eventually falls to atmospheric pressure) by 524 kPa.

3.7 Effect of Secondary Thermal Gradients on the Rates of Flow

Although in principle, the ice sandwich is isothermal, phase changes induce a coupled flow of sensible heat in the same direction as the mass flow. Latent heat released by freezing of the ice at the upstream ice-water interface, causes the temperature there to rise above ambient, while a similar effect causes the temperature to fall on the downstream side. To understand the implications, we assume P_i reaches a positive equilibrium pressure (greater than atmospheric) prior to applying pressure to the water, in accordance with the

Clausius-Clapeyron eqn. 2.1.[3] The established bath temperature = T and the pressure of the supercooled water, P_w = atmospheric pressure. The immediate effect of raising the water pressure at the upstream ice-water interface is to raise the equilibrium freezing-point dT (eqn. 2.1), so that freezing immediately occurs there. However, the liberated latent heat raises the temperature toward the new equilibrium temperature. The effect slows the rate of freezing as the equilibrium temperature is approached. A similar reasoning can be applied to the thawing occurring at the downstream face. The thermal effect, therefore, diminishes the mass flow rate. The magnitude of the secondary thermal gradient increases in direct proportion to the mass flow rate. It is also inversely related to the rate of heat exchange with the surrounding bath and, therefore, is dependent upon the thermal properties of the permeameter itself. Experiments by Horiguchi and Miller (1980) indicate that the induced temperature differences are very small, in the order of 0.01°C at flux rates of 1×10^{-7} m^3 m^{-2} s^{-1}. However, the effect may be significant.

Miller et al. (1975) give phenomenological equations for coupled mass J_m and heat J_q transfer in a one-dimensional system based on irreversible thermodynamic theory. For an ice sandwich these may be written as:

---

[3]The assumption as to P_i could be tested using pressure sensing apparatus in the ice chamber, similar to that described in chapter 5.2. A modified ice sandwich was fabricated for this purpose but experiments were not carried out owing to time limitations.

FIGURE 3.9

a

CROSS-SECTION OF ICE SANDWICH FOR MEASURING EFFECT OF SECONDARY THERMAL GRADIENTS ON MASS FLOW RATES

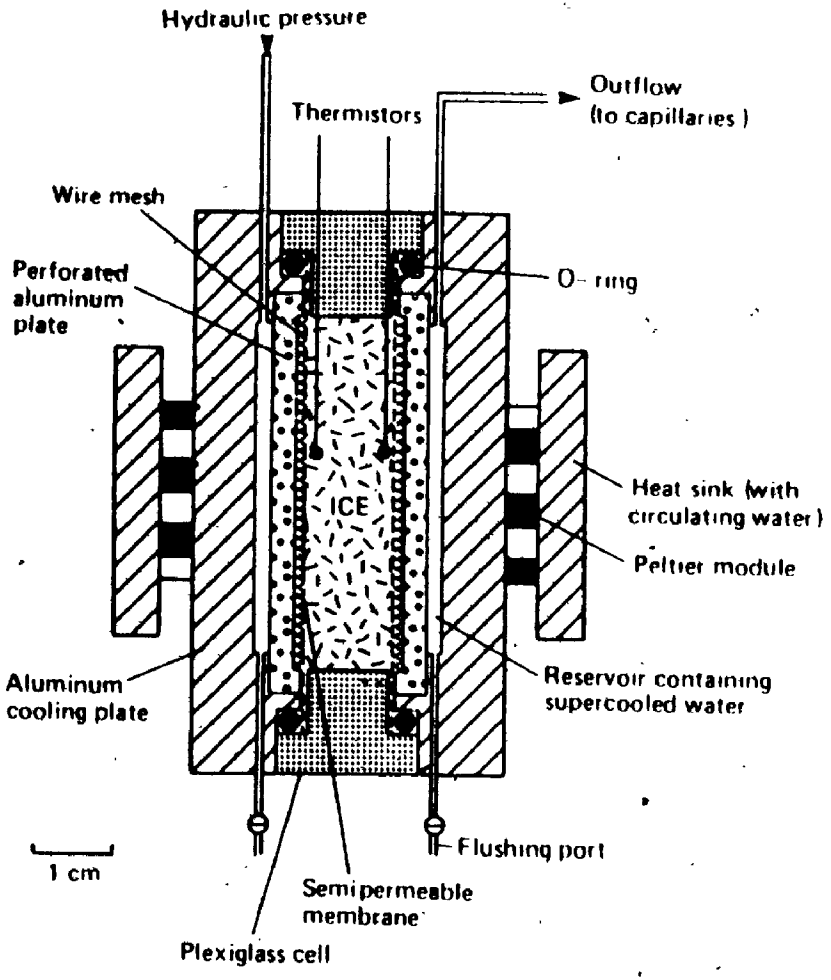

b

CIRCUIT DIAGRAM OF BRIDGE USED TO DETECT VERY SMALL RESISTANCE CHANGES TO THERMISTORS

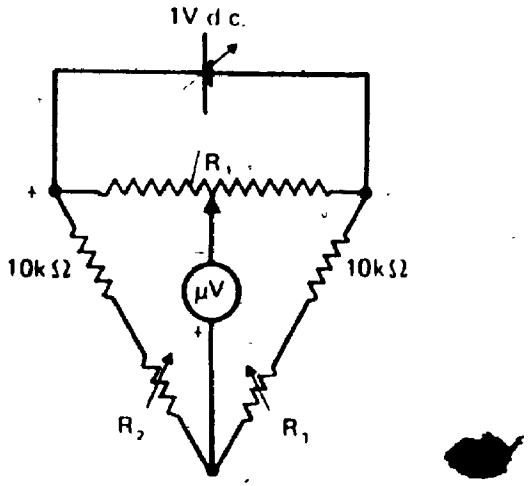

R_1 0.5k Ω (10 turn) pot

R_2, R_3 3k Ω thermistors

(μV) Microvoltmeter (output leads to digital multimeter)

$$J_m = -L_m \left(\frac{1}{\rho}\right) \frac{\Delta P}{\Delta z} - L_{mq} \left(\frac{1}{T}\right) \frac{\Delta T}{\Delta z} \qquad 3.4$$

$$J_q = -L_{qm} \left(\frac{1}{\rho_i}\right) \frac{\Delta P}{\Delta z} - L_q \left(\frac{1}{T}\right) \frac{\Delta T}{\Delta z} \qquad 3.5$$

where T = temperature, K

and ρ_i = density of ice.

$\frac{\Delta P}{\Delta z}$ and $\frac{\Delta T}{\Delta z}$ are the pressure and temperature gradients across the ice specimen as measured just inside the semipermeable membrane. L_m, L_q, L_{mq} and L_{qm} are the direct and cross coefficients for mass, m, and heat, q, transfer, respectively. According to Onsager's (1931) reciprocity principle, $L_{mq} = L_{qm}$, reducing the number of unknowns in the above equations from four to three.

With the ice sandwich experiment, the measured value for the mass transport coefficient, L, includes the effects of coupled heat flow (i.e. $L = L_m + L_{mq}$). Separating out the direct mass transport coefficient, L_m, from the coupling coefficient, L_{mq}, is difficult analytically. It is proposed that this could be accomplished by a rather simple experiment in which the induced temperature gradient across the ice specimen is nullified by very accurate temperature control at the ends of the ice. The transport coefficient should then increase to L_m since it excludes the coupled heat flow effect. The difference $L_m - L = L_{mq}$ represents the cross (coupling) coefficient (dimensions, m s kg^{-1}).

A special cell was fabricated for this purpose (Fig. 3.9a). Temperatures were controlled thermoelectrically by Peltier modules which cool two aluminium end plates containing small reservoirs. To eliminate radial heat exchange with the surroundings, the cell was wrapped in a jacket of foam rubber insulation and placed inside a low temperature incubator. Temperature differences were measured by YSI 3 kΩ thermistors positioned at the ends of the ice specimen. The very

small changes in resistance of the thermistors were measured by a modified Kelvin double bridge (Fig. 3.9b) which allows resolution to ±0.0005°C. Preliminary results suggest that the secondary thermal effect reduces the mass transport coefficient by a small amount. However, major modifications to the temperature control system are needed before further experiments are carried out. (These were not done owing to time and financial limitations). With the present system the resolution and stability of temperature control is about ±0.0025°C and so a fraction of the induced temperature gradient across the ice specimen is lost in the background thermal noise. An additional problem is the tendency for the supercooled water in the reservoirs to freeze after several hours.

3.8 Conclusions and Discussion

The ice sandwich experiment confirms the regelation flow phenomenon. While it does not provide much information directly on the possibility or magnitude of regelation flow of pore ice in frozen soils, it is a useful means of investigating the phenomenon as a whole. The flow rates were shown to be linearly dependent on the hydraulic head (Darcy's law) and exponentially related to the temperature. Tests also showed that regelation flow can be induced by osmotic gradients. However, the nature and configuration of the ice appear to affect the process. Phase changes at the boundaries of the ice specimen induce a secondary thermal gradient which reduces the rate of mass flow slightly, in accordance with the principles of irreversible thermodynamics. A similar phenomenon might also be expected to occur in a frozen soil permeameter. A modified permeameter with end-temperature control, similar to that shown in Fig. 3.9, would enable separation of the

secondary thermal effect from the mass transfer coefficient for the soil.

An interesting experiment would be to measure the regelation flow rates as a result of a thermal gradient rather than a hydraulic gradient. Tests of this nature could be carried out with the device shown in Fig. 3.9, by varying the end temperatures of the ice specimen. If the water in the reservoirs is supercooled more at one end than the other, this would result in an ice pressure gradient, the pressure being greater at the colder end (Clausius-Clapeyron eqn.). The movement of the ice would be in the direction of warmer temperatures. This situation might be expected in a frozen soil which is confined with a thermal gradient.

A point interesting to consider is whether the ice moves as a plug (uniform translational velocity) in the ice sandwich or whether it moves by creep and deformation, with the ice closer to the cell wall moving more slowly due to drag effects. Miller et al. (1975) acknowledge creep as a distinct possibility in the frozen fringe although it is ignored in their elaborate theories of frost heaving in favour of plug flow. The creep of ice is normally described by Glen's (1975) law which is based on observations of secondary (steady-state) strain. The particular mode of ice movement probably depends upon the extent of recrystallization. Recrystallization increases the flow rate because the new crystals are more favourably oriented for flow and are also relatively soft. Pressure-melting between the grains and grain boundary diffusion may also be significant factors. The mechanism of ice movement is important, not only with regard to the transport of ice in the soil, but also to the rheological behaviour of frozen soils as well.

IV. A THERMO-RHEOLOGICAL MODEL OF FROST HEAVE PRESSURES IN SOILS

4.1 Rheological Behaviour of Frozen Soils: Review

The creep behaviour of frozen soils is characterized by a family of creep curves in which the strain ε, resulting from a constant applied stress σ, is plotted as a function of time (e.g. Fig. 4.1). Creep is categorized into three distinct phases: (1) primary or decelerating creep, which is viscoelastic in nature, (2) secondary or steady-state creep and (3) tertiary or accelerating creep (viscoplastic). The transition from secondary to tertiary creep defines failure and is sometimes referred to as the 'strength' of the soil, although this term is also used in a general sense to refer to the mechanical resistance of the soil to an applied stress. If stresses are high enough, the soil will often go directly into tertiary creep without the transition through primary and secondary creep. The particular phase of creep which is dominant is very sensitive to the applied stress, as well as the temperature, especially in the region close to 0°C where the ice content of the soil is rapidly changing.

Creep behaviour is sometimes also described by a family of stress-strain curves plotted at constant strain rates. In this case the stress usually rises to a peak as the strain increases and then falls, often abruptly, as failure occurs. The stress at failure usually increases with higher strain rates (e.g. Fig. 4.2).

The dominant factor contributing to the strength of frozen soils is cohesion due to interactions between the ice and mineral matter, although interlocking of grains, friction and cohesion (between minerals) are also factors (Johnston, 1981). The strength of ice itself has an important effect and this is dependent upon the temperature,

pressure, crystal size, orientation and density, as well as the strain rate. At relatively cold temperatures, the dominant mode of ice deformation is the movement of dislocations, migration of crystal boundaries and recrystallization under stress. At warmer temperatures (close to 0°C) grain boundary sliding, diffusion along grain boundaries, as well as pressure-melting, diffusion and refreezing in zones of lower stress are dominant mechanisms.[1]

The viscosity of frozen soil is normally less than that of pure ice, implying faster deformation rates, chiefly as a result of unfrozen pore water (Williams, 1982). Although ice will deform under very low applied stresses, frozen soils require a critical threshold stress in order for secondary creep to occur because of interference effects between particles (i.e. static friction and cohesion). At very high ice contents the behaviour of the soil is similar to that of ice. At low ice contents, unfrozen film water has a dominant influence. Pressure-melting and refreezing play a key role in the creep behaviour of frozen soils (Czurda, 1983). This is a result of increased pressure on the ice, which lowers its freezing temperature (Clausius-Clapeyron eqn.), and also stress concentrations at points or edges of soil particles, with subsequent melting and migration to regions of lower stress, where the water refreezes.

---

[1] Pressure-melting is sometimes also referred to as 'regelation'. However, the process is distinctly different from that occurring in the ice sandwich. Freezing occurs on the high pressure side of the ice sandwich, whereas pressure-melting occurs because of a lowering of the freezing temperature of the ice by a direct application of pressure.

The strength of frozen soils is highly dependent upon the duration of application of the stress if it is constant, or the rate at which it is applied, in a constant strain rate test (Tsytovich, 1975). The more slowly stress is applied, the less the mechanical resistance of the soil to creep. Similarly, at constant stress, the stress at failure in the long term (several hours or days), $\sigma_{\ell t}$, is much lower than the instantaneous or short term value, by as much as 3-15 times, according to Tsytovich, 1975 (e.g. Fig. 4.3). The strength is also 2-6 times greater in compression than tension owing to the much greater number of contacts between mineral particles in compression (e.g. Table 4.1).

The decline in the strength of the soil with time is attributed to rupture of ice-mineral and structural bonds, pressure-melting and refreezing, as well as reorientation of ice crystals and mineral particles parallel to the direction of slip (Johnston, 1981).[2] Strain softening effects are eventually offset by the tendency for strain hardening to occur. This is a result of interference between ice crystals, accumulation of dislocations at nodes within the ice and establishment of new ice-mineral bonds. If the two effects counterbalance each other exactly, secondary (steady-state) creep results.

As the soil temperature decreases, both the instantaneous and the long-term tensile and compressive strengths increase, generally

---

[2]Although the ice is separated from the mineral surfaces by a layer of unfrozen water it can be regarded as being bonded to the mineral by interfacial energy. Any attempt to remove the mineral matter lowers the pressure of the unfrozen water, some of which then freezes and the liquid film becomes thinner and resists the motion.

FIGURE 4.1

STRESS-STRAIN CURVES AND CREEP CURVES (a,b,c)
FOR A FROZEN SILTY CLAY AT DIFFERENT TEMPERATURES

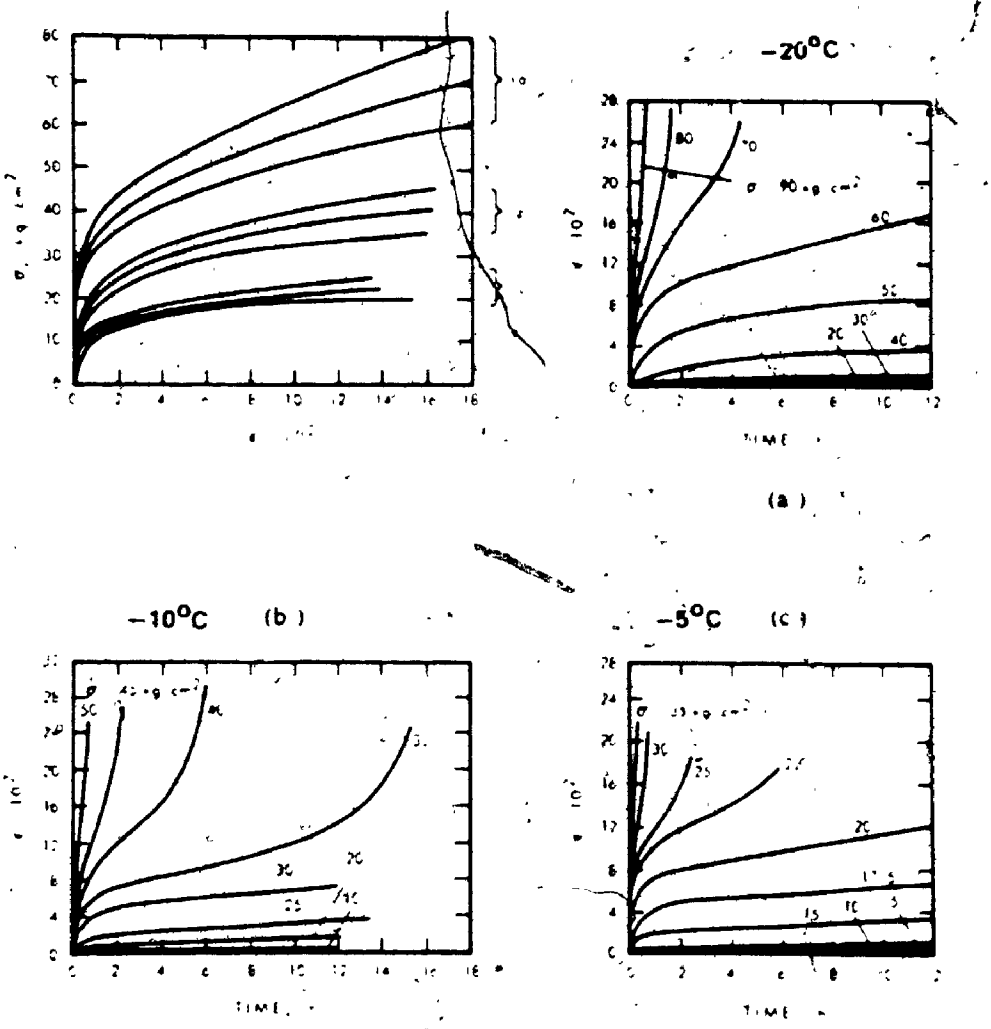

1 kg cm^{-2} = 98.07 kPa

(after Vyalov, 1962)

FIGURE 4.2

STRESS-STRAIN CURVES FOR SNEC SAND AT DIFFERENT STRAIN RATES, -2°C

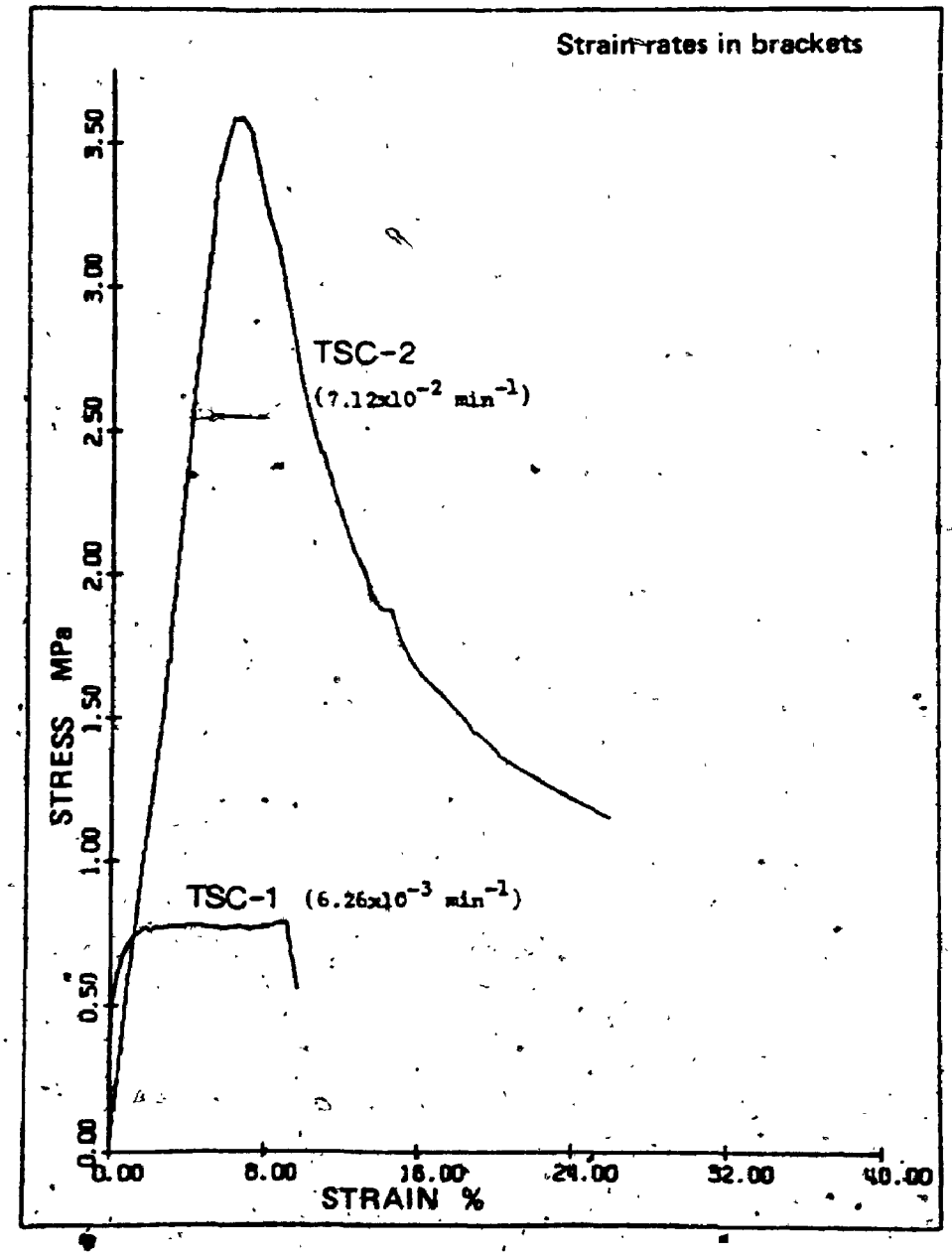

(after Ladanyi and Lauzon, 1985)

FIGURE 4.3

LONG-TERM AND INSTANTANEOUS COMPRESSIVE STRENGTHS OF TWO FROZEN SANDS AT VARIOUS TEMPERATURES

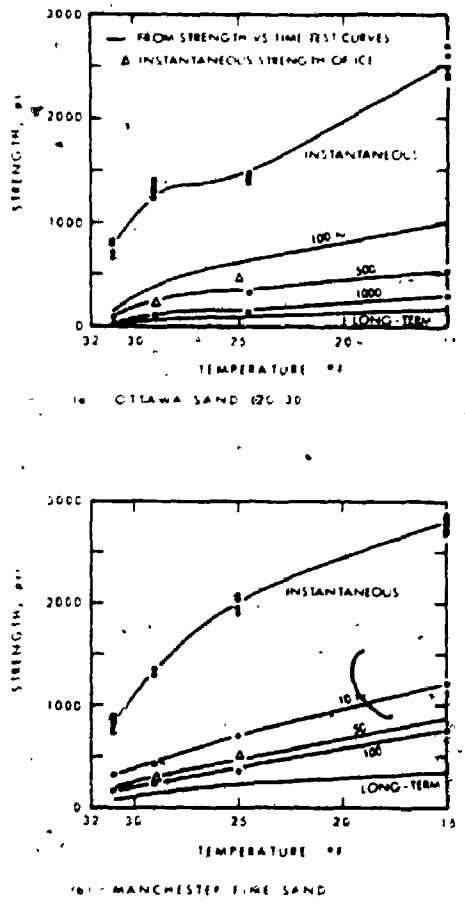

1 psi = 6.895 kPa $1^{o}F = 0.556^{o}C$ ($32^{o}F = 0^{o}C$)

(after Sayles, 1968)

Table 4.1

Instantaneous and Long-Term Strengths of Some Frozen Soils at Various Temperatures

	Water Content %	Temperature °C	Strength, kPa × 10^{-3} Instantaneous Compression	Instantaneous Tension	Long-Term Compression	Long-Term Tension
Polycrystalline ice[4]	100	-3.0	1.6-2.0	1.0-1.2	0	0
	"	-10.0	3.1-3.9	1.7-2.0	0	0
Segregation ice[2]	100	-0.2	5.0-7.0		0	
ductile failure	"	-0.5	7.0-8.0		0	0
	"	-1.0	8.0-11.0	3.0*	0	0
	"	-10.0	14.0	4.0*	0	0
	"	-20.0	17.0-23.0**	5.0*	0	0
Clay[1]	25-35	-1.0	1.47	0.49	-	0.16
	"	-5.0	3.43	1.27	-	0.15
Clay[3]	34.6	-0.5	-	-	0.88	-
	36.3	-1.6	-	-	1.27	-
	35.0	-3.4	-	-	2.26	-
	35.3	-8.2	-	-	4.41	-
Clay[2]	19.4	-1.2	-	0.96	-	-
	"	-2.5	-	1.65	-	-
	"	-4.0	-	2.12	-	-
Clayey silt[1]	35-40	-0.5	0.78-0.98	0.39-0.59	0.20	0.10-0.20
	30-35	-3.0	2.94-3.43	1.18-1.57	0.35	0.24
	20-25	-5.0	2.26	1.96	1.96	0.88-1.18
	"	-10.0	3.82	2.94	2.45	1.18-1.56
Fairbanks silt[4]	40-45	-0.5	-	-	0.3	-
	"	-1.0	-	-	0.5	-
	"	-2.0	-	-	0.9	-
	"	-3.0	-	-	1.2	-
	"	-5.0	-	-	1.9	-
	"	-10.0	-	-	3.4	-
Silty sand[1]	20-25	-0.3	0.98-1.18	0.49-0.79	0.20-0.29	0.10-0.15
	"	-5.0	2.94-3.92	1.96-2.45	0.59-0.98	0.34
	"	-10.0	5.88-6.86	3.92-4.90	3.43	1.08
	"	-20.0	11.77-13.73	4.90-5.88	5.88	2.06
Quartz sand[3]	14.7	-1.0	6.08	-	-	-
	14.0	-6.0	9.71	-	-	-
	14.9	-12.0	13.14	-	-	-
Quartz sand[2]	17.0	-2.2	-	-	0.62	-
	"	-5.0	-	-	0.77	-
	"	-10.0	-	-	1.57	-

* brittle failure
** load 90° to direction of crystal growth

Sources: 1 Voitkovskiy, 1968
2 Ohrai, et al., 1983
3 Tsytovich, 1975
4 Yuanlan and Carbee, 1983

FIGURE 4.4

EXAMPLE OF CHANGE IN SHORT-TERM COMPRESSIVE STRENGTH WITH ICE CONTENT (FINE SAND)

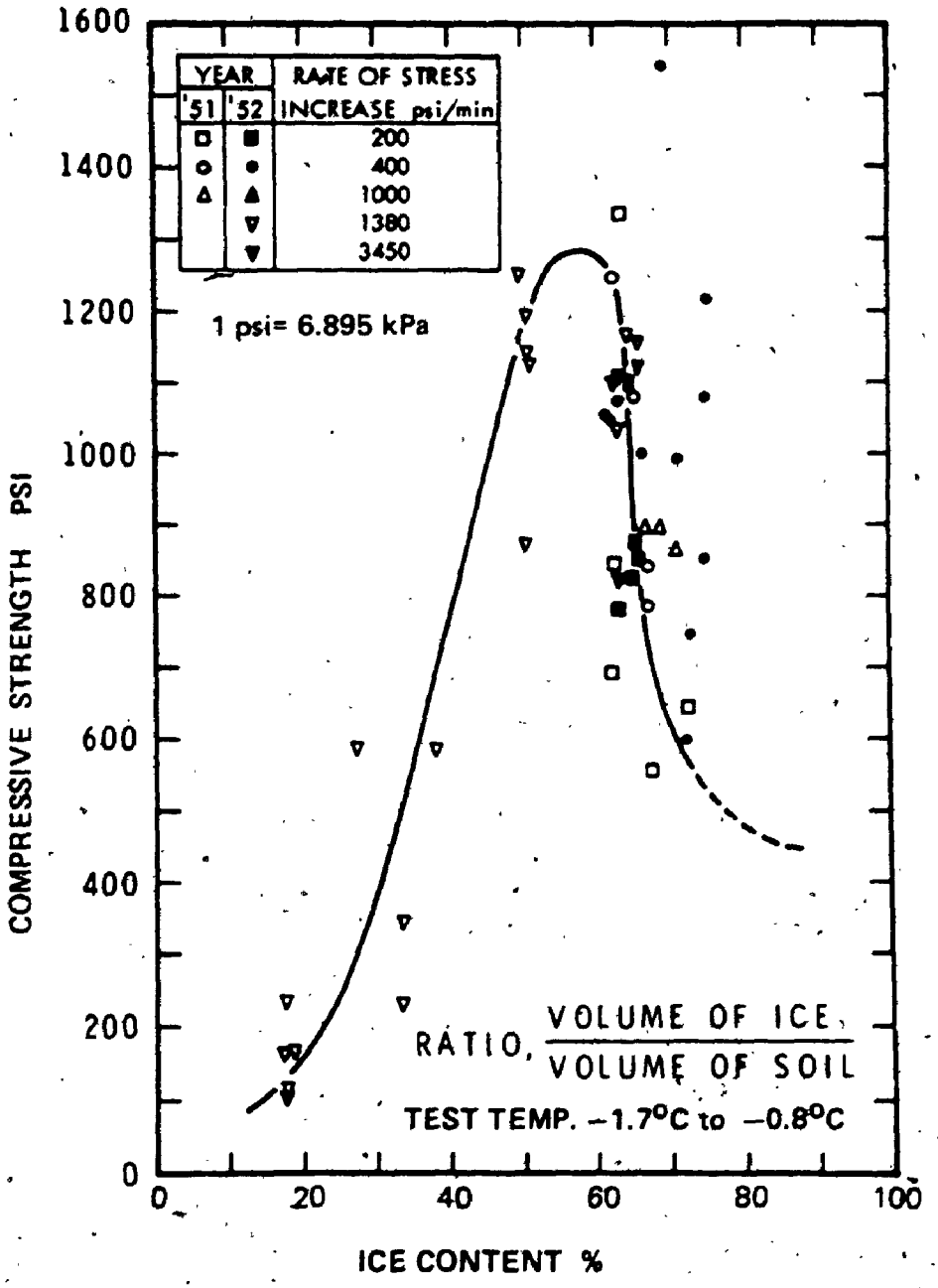

(after Kaplar, 1971)

FIGURE 4.5

LINEARIZED PLOT OF SECONDARY CREEP RATE VERSUS APPLIED STRESS

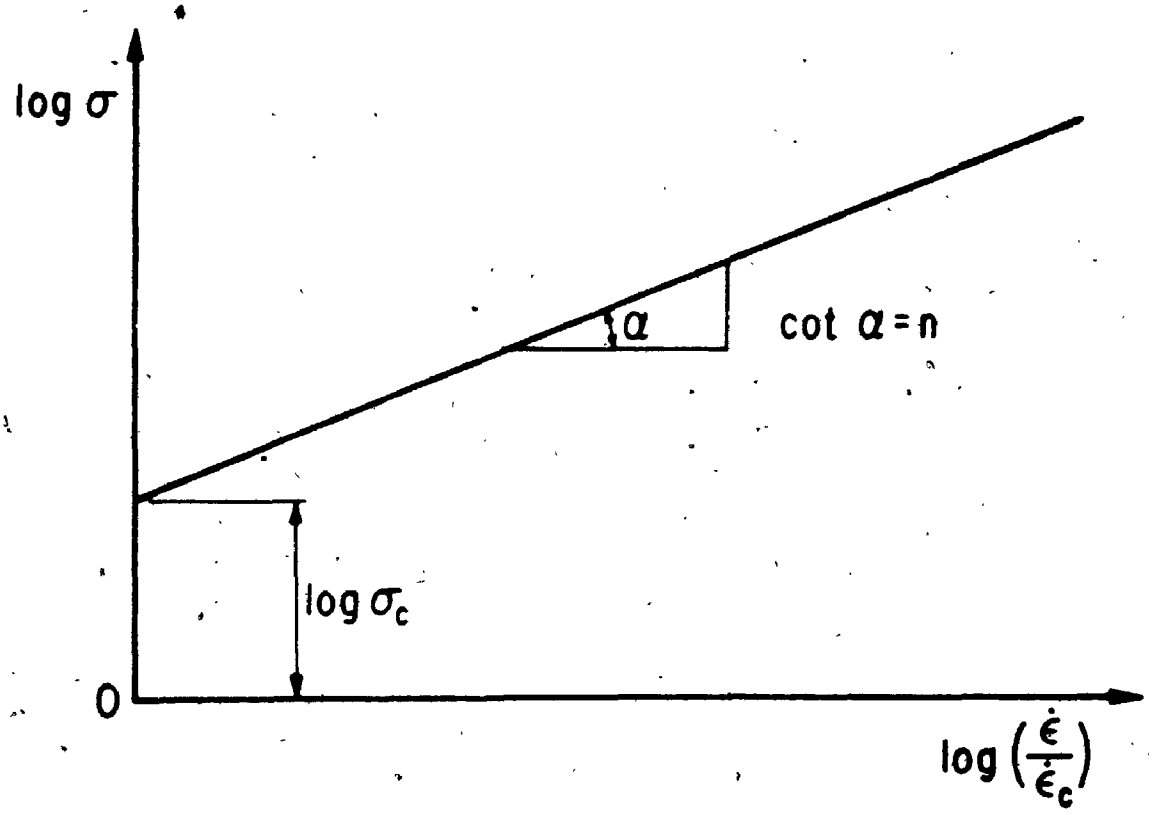

Ladanyi (1972)

obeying a power law. If the soil temperature remains constant and the ice content is increased, the change in strength follows a bell-shaped curve (e.g. Fig. 4.4). The strength increases rapidly with ice content due to increasing ice-mineral cohesion. The strength reaches a maximum at an optimum ice content and then begins to decline because of the decreasing angles of friction and dilatancy.[3] The curve eventually levels off at the strength of pure ice.

Ladanyi (1972) gives an expression which describes the primary and secondary phases of creep:

$$\varepsilon = \frac{\sigma}{E} + \varepsilon_k \left(\frac{\sigma}{\sigma_k}\right)^k + \dot{\varepsilon}_c \left(\frac{\sigma}{\sigma_c}\right)^n t \qquad 4.1$$

E = Young's modulus, σ_k is a temperature-dependent deformation modulus, σ_c and n are temperature-dependent creep parameters (σ_c more so than n). Parameter k is usually unaffected by the temperature. ε_k and $\dot{\varepsilon}_c$ are small arbitrary strain rates introduced in order to normalize the function. The first and second terms on the right side describe the 'pseudo-instantaneous' elastic and plastic components of strain respectively, while the third term describes the

---

[3] The angles of friction and dilatancy in a direct shear test are described by the Coulomb eqn:

$$\tau = c + \sigma \tan \phi$$

where τ = shear stress along a plane of failure

σ = normal stress

c = cohesion

$\tan \phi = \tan (\phi_f + \phi_d)$ = angle of the shear strength

(ϕ_f = angle of friction, ϕ_d = angle of dilatancy)

secondary (creep) strain which obeys a power law. For most practical problems with ice-rich soils under moderate loads, secondary creep is dominant and so the secondary phase can be linearized (Fig. 4.5).

Ladanyi (1972) also gives an expression for the long-term compressive strength (at constant temperature):

$$\sigma_{\ell t} = \sigma_c \left(\frac{\dot{\varepsilon}_f}{\dot{\varepsilon}_c}\right)^{1/n} \qquad 4.2$$

$\dot{\varepsilon}_f$ = average creep rate to failure.

$\sigma_{\ell t}$ can be determined directly from the linearized creep curve (Fig. 4.5) owing to the similarity in analytic form between this equation and eqn. (4.1).

4.2 Distribution of Frost Heave Pressures in Confined Soils

Consider the case of an ice sandwich, in which the driving force for flow is a temperature gradient rather than a hydraulic gradient, with the warmer end at temperature T_1 and the colder end at T_2 (both below 0°C). (The possibility of measuring this phenomenon was discussed in section 3.8). If the supercooled water in the reservoirs is at atmospheric pressure, the ice pressure will increase, according to the Clausius-Clapeyron eqn., to maintain local equilibrium with the water at each end. At the colder end the ice pressure required for local equilibrium, P_{i2}, is greater than at the warmer end, P_{i1} (i.e. $P_{i2} > P_{i1}$).

Lowering the temperature at the colder end causes the water to flow through the membrane and freeze onto the ice. This raises the ice pressure there toward P_{i2} in an attempt to restore local equilibrium.

As the ice creeps and the increase in pressure is transmitted to the warmer end, the ice pressure rises above P_{il}. This lowers the equilibrium freezing temperature there below ambient so some of the ice melts and flows into the reservoir. The ice pressure gradient is sustained thermodynamically by localized melting and freezing at the ends of the system and is independent of the wall friction. If a closed system is created by connecting the reservoirs at either end, the ice pressure gradient would still be maintained by recirculation of the water in the opposite direction to the flow of the ice. (This possibility was discussed by Miller et al., 1975).

Departures of the system from local equilibrium and, therefore, the ice pressure gradient, would depend upon the rheological properties of the ice. If the ice behaved like a rigid solid, perfect equilibrium would be maintained at each interface and there would be no flow through the system. In the opposite extreme, if the ice behaved like a fluid (which cannot sustain a shear stress), there would be no ice pressure gradient at all (i.e. the ice pressures would be uniform) and gross thermodynamic disequilibrium would occur at each end of the system. In reality, ice has the properties of both a rigid solid and a viscous fluid being able to sustain a shear stress in the short term but undergoing a slow deformation or creep with time. In the short term ice exhibits the properties of a solid while in the long term it behaves more like a fluid. The rheological or flow characteristics of the ice can be described as varying between 'semi-rigid' and 'quasi-viscous'. The former describes the situation where the ice is able to sustain a large shear stress while the latter refers to the situation where it deforms so rapidly that it cannot sustain shear.

The flow rate of the ice depends upon the crystal size, orientation, number of dislocations, grain boundary diffusion, temperature and time.

In principle, the ice sandwich simulates the thermodynamic and rheological conditions which occur in a single pore of a confined frozen soil in which there is a thermal gradient. On a macroscopic scale, the behaviour of a frozen soil can be regarded as similar to that in the ice sandwich except that there are millions of ice-water interfaces, instead of two, which are all attempting to maintain local equilibrium. In the ice sandwich the ice moves, although its boundaries remain stationary, whereas in the soil the ice-water interfaces and the soil particles may be moving as well as the ice.

The resistance of the soil to stress relaxation can be described as the 'strength' of the material. This is not a strict definition of the word 'strength' as used in engineering terminology, but rather refers to the rigidity of the material, or its mechanical reaction to its own stress. The effect of the rheological behaviour of the soil-ice matrix on the ice pressures established in a freezing soil is a complicated problem to deal with analytically because of the thermal gradient. In a confined soil with a linear thermal gradient, the equilibrium ice pressures should increase linearly with colder temperatures according to the Clausius-Clapeyron eqn. As in the case with the ice sandwich, the ability of the soil to sustain an increase in ice pressure and thereby approach local equilibrium, depends upon its strength. This also increases with colder temperatures.

Figure 4.6 shows two extreme modes of behaviour. In the diagram on the left, the soil behaves in a solid-like manner. The

Figure 4.6

Idealized Model Showing Distribution Of Frost Heave Pressure
In A Confined Soil With Different Rheological Properties

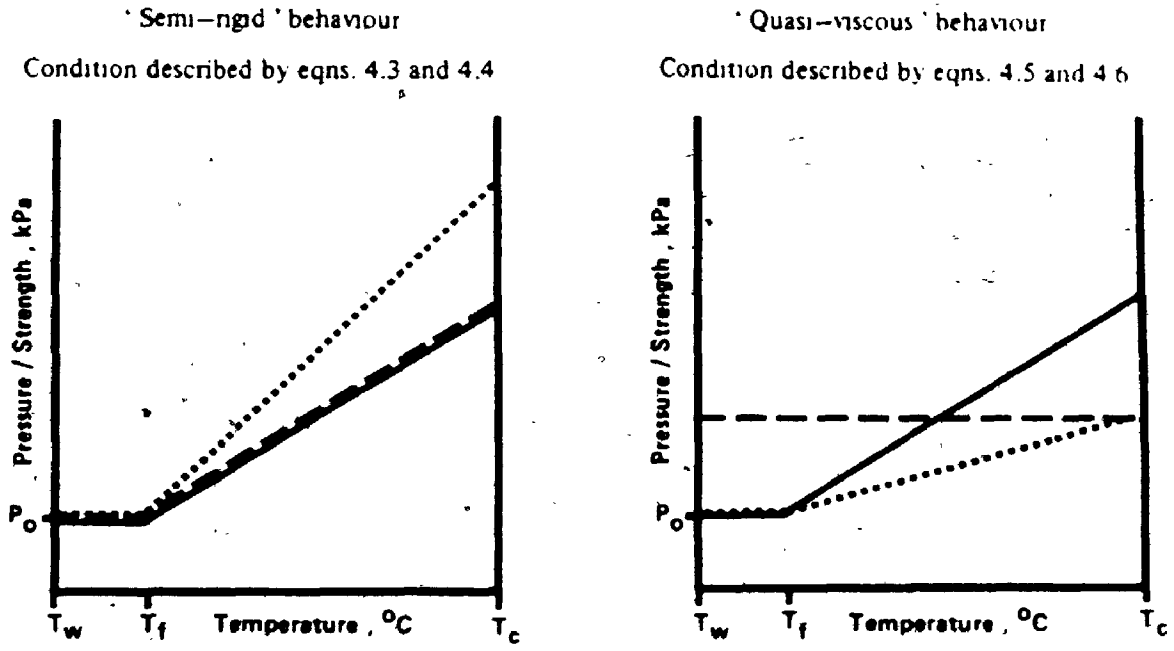

increase in the strength of the material with colder temperatures, $\frac{\delta\sigma}{\delta T}$, exceeds the increase in the equilibrium ice pressure, $\frac{\delta P_i}{\delta T}$, so that local equilibrium is maintained everywhere and the change in the observed ice pressures $\frac{\delta P}{\delta T} = \frac{\delta P_i}{\delta T}$. Stated mathematically:

$$\text{If} \quad \frac{\delta\sigma}{\delta T} > \frac{\delta P_i}{\delta T} \quad \text{then} \quad \frac{\delta P}{\delta T} = \frac{L}{v_i T} \qquad 4.3$$

The pressure at any location z is given by:

$$P = \frac{L\ \Delta T(z)}{v_i\ T} + v_w\ P_w \qquad 4.4$$

where $\Delta T(z)$ = equilibrium freezing temperature as a function of distance, °C

($\Delta T = T^* - T$, temperature of frost line, T^* and soil temperature, T)

and P_w = pressure of the unfrozen pore water (assumed equal to atmospheric pressure)

In the diagram on the right (Fig. 4.6), the material behaves more like a liquid (i.e. it cannot sustain large shear stresses). In this case, the increase in the strength of the material is insufficient to sustain the increase in the equilibrium ice pressure so the observed ice pressures are uniform (isotropic).

$$\text{That is} \quad \frac{\delta\sigma}{\delta T} << \frac{\delta P_i}{\delta T} \quad \text{therefore} \quad \frac{\delta P}{\delta T} \to 0 \qquad 4.5$$

In this case, the observed ice pressure would approach the equilibrium ice pressure given by the Clausius-Clapeyron equation at the <u>mean</u> temperature of the frozen section:

$$P = \frac{L}{v_i T}\left[\frac{\int_{z_1}^{z_2} \Delta T(z)\, dz}{z_2 - z_1}\right] + v_w P_w \qquad 4.6$$

where z_1 = location of the frost line

and z_2 = cold extremity of the frozen section.

Since the equilibrium and the observed ice pressures increasingly diverge toward the extremities of the frozen section the degree of thermodynamic disequilibrium increases with distance away from the centre of the frozen section. The following scenario is envisaged.

In the warmer half of the frozen section, the pressure of the ice is greater than the equilibrium ice pressure (see Fig. 4.6). This lowers the equilibrium melting-point, causing the ice there to slowly melt as the system attempts to restore thermodynamic equilibrium. Similarly, in the colder half of the soil where the pressure of the ice is too low the equilibrium melting-point is increased and freezing occurs. Although the system reaches a quasi-steady-state, thermodynamic equilibrium is not restored because of the continuous movement of the ice on a molecular scale toward warmer temperatures. The strength of the soil is insufficient to sustain a larger pressure gradient. Over a long period of time this might result in gradual redistribution of the ice within the soil toward colder temperatures, with water migrating from zones of pressure-melting to zones of refreezing. If the ice is redistributed, this might alter the rheological behaviour of the material so that eventually conditions may arise where the soil is able to sustain a larger pressure gradient. Over a very long period of time thermodynamic equilibrium may be restored.

The transition between the two extremes (equations 4.3 and 4.5) is gradual rather than abrupt. Departures from the equilibrium ice pressure distribution increase as the rate of stress relaxation of the soil increases. Stress relaxation is achieved at the molecular level by the movement of the ice toward warmer temperatures. Although the ice is actually moving, its boundaries remain stationary because of continuous crystallization in the colder regions of the soil and melting in the warmer regions. The ice pressure gradient is independent of any external water supply and is sustained by internal recirculation of unfrozen pore water in the opposite direction to the flow of ice (i.e. similar to the closed-system ice sandwich). The rheological behavior of the soil is more complex if there is any slow movement of the soil particles and the ice-water interfaces, in addition to the ice movement. In general terms, the rheological behaviour of the soil can be described as varying between semi-rigid (solid-like) behaviour and quasi-viscous (liquid-like) behaviour, the soil in the latter case being unable to sustain large differences in ice pressure.

Analysis of the pressure distribution during transient thermal conditions is made complicated because the rheological properties of the material are changing with time. Additional complications also arise because of changing rates at which stresses are established during the advance of the frost line, which has an effect on the rate of stress relaxation. If the stresses are established more slowly, the resistance offered by the soil is less and so the frost heave pressures would tend toward a more uniform distribution. This might be expected if the soil is frozen very slowly.

Failure to take into consideration the rheological behaviour of the frozen soil probably accounts for many inconsistencies and contradictions in the results observed by different investigators. The characteristic maximum heaving pressure for different soils reported by Hoekstra and Chamberlain (1965) and Penner (1965) can be explained in terms of the different rheological properties of these materials. Departures of the heaving pressure from the Clausius-Clapeyron equation observed by Takashi et al. (1980), may also be related to changes in the rheological behaviour of the soil with colder temperatures. The thermal gradient may also affect the rate of stress relaxation. This might explain Loch and Miller's (1975) observation of a maximum heaving pressure at an optimum temperature gradient.

Although it seems rather obvious that the rheological properties of the soil must play a significant role in the heaving pressures established, this factor appears to have been overlooked in the existing theories of frost heaving. There are, however, a few references to related concepts in the literature. Gilpin (1980) refers to a separation pressure required to force the soil fabric apart as heave occurs, but does not connect this with the rheological properties of the soil itself. More specifically, Ershov (1977) refers to a physical-mechanical ratio between the tensile strength of the soil and the expansive forces generated during freezing, which must be exceeded in order for an ice lens to grow. Once the sheaf strength of the soil is overcome, rupture occurs and water migrates into the fracture forming an ice lens. Although reference is made to a buckling pressure, Ershov (1977) neglected to relate the subsequent growth of the lens to the rheological behaviour of the material. (Ershov's concept of soil

2

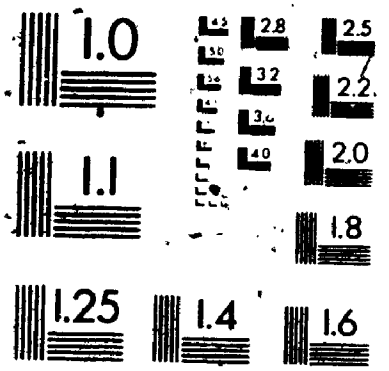

MicroD

freezing is distinctly different to the hypothesis presented in this thesis). Miller et al. (1975) suggest the possibility that creep deformation of the soil may be an important factor in frost heaving, but ignore the matter in their elaborate theories. Loch (1975), however, suggests that the continuous increase in heaving pressure over very long periods of time, predicted by Miller (1972), is probably limited by stress relaxation within the soil.

V. EXPERIMENTAL APPARATUS AND PROCEDURE

5.1 Frost Pressure Cell

The frost pressure cell and experimental layout (Figs. 5.1 and 5.2) evolved to its present form from tests conducted over several years. Successive modifications are described in the reports by Williams and Wood, 1981, 1982, 1984 and 1985 and by Torrance and Wood, 1983. Design specifications of the frost pressure cell and a list of the equipment used in the experiment are given in Appendices A and B.

The soil specimen (diameter 5.4 cm, length 3.5 cm) was located inside a perspex cylinder (wall thickness 1.90 cm).[1] Temperatures were controlled by aluminum cooling plates at either end of the soil, attached by 12 nylon screws. A large steel clamp prevented small volume changes which might otherwise occur due to elastic strain of the screws.

Although the cell itself was non-expansive, small volume changes may have occurred as a result of deflection of the wire mesh and perforated aluminum plates at each end of the soil under pressure.[2] The

---

[1] Total volume of the soil specimen allowing for the volume (1.38 cm^3) displaced by thermistor housings and pressure transducer bladders was 78.42 cm^3.

[2] To measure the volume displacement due to this effect an impermeable foil barrier was fitted over the perforated plate at one end of the cell and the adjacent reservoir was filled with water. When pressure was applied to the cell at the other end, volume displacement was measured by the outflow of water from the reservoir, the displacement being due to bending of the perforated aluminum plate. Although steel is a more rigid material, aluminum was preferred because of its very high thermal conductivity, 230 W m^{-1} K^{-1} (ten times that of steel) which allowed greater thermal control.

FIGURE 5.1
CROSS-SECTION OF FROST PRESSURE CELL

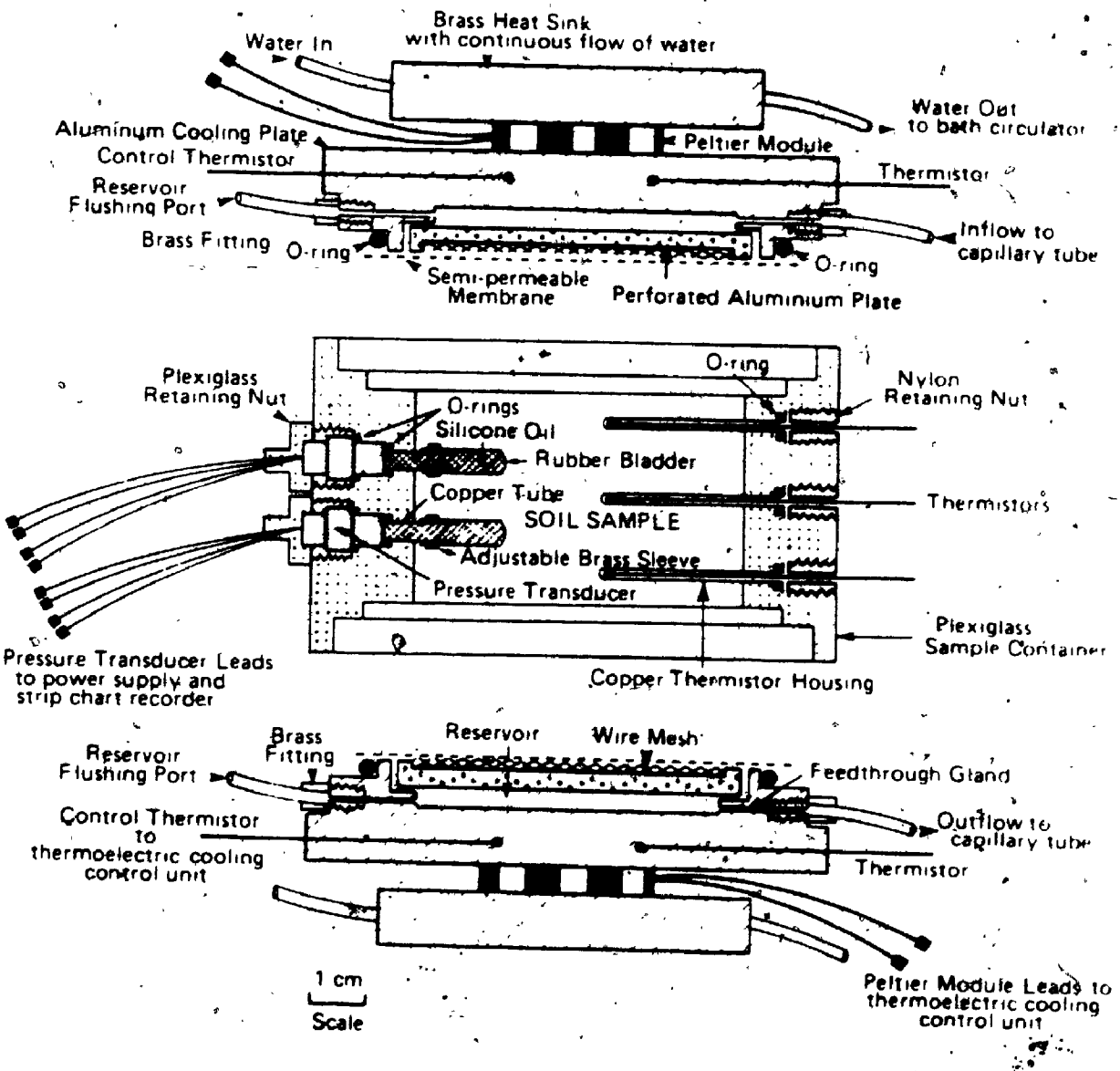

The steel clamp and nylon screws used to hold the apparatus together are not shown. Brass fittings and plexiglass retaining nuts are not drawn to scale.

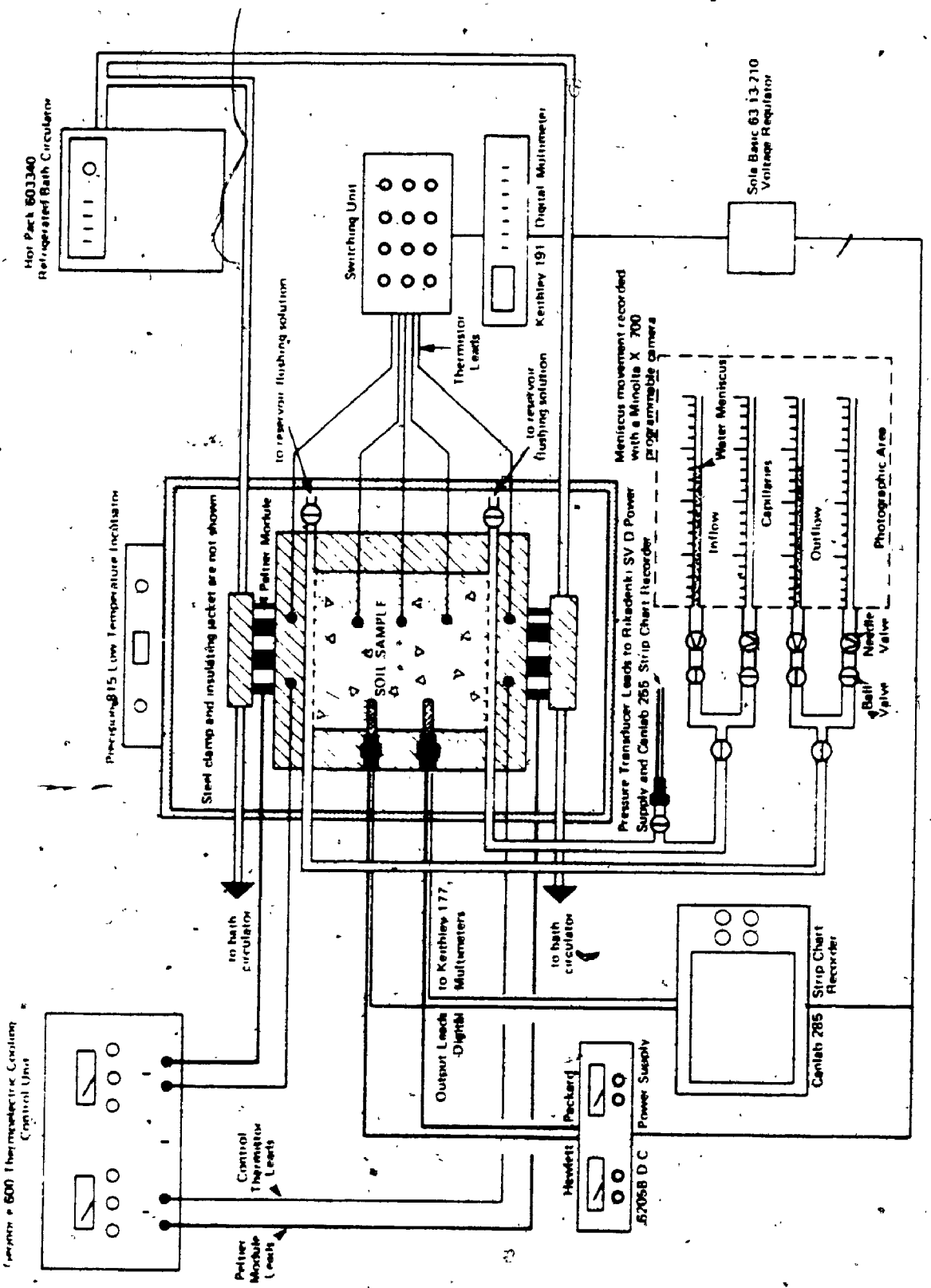

FIGURE 5.2
EXPERIMENTAL LAYOUT

PLATE 5.1

Exploded View of Frost Pressure Cell

PLATE 5.2

Vertical View of Specimen Container Showing Pressure Transducer Assemblies

FIGURE 5.3

VOLUME DISPLACEMENT DUE TO DEFLECTION OF PERFORATED ALUMINUM PLATES UNDER PRESSURE

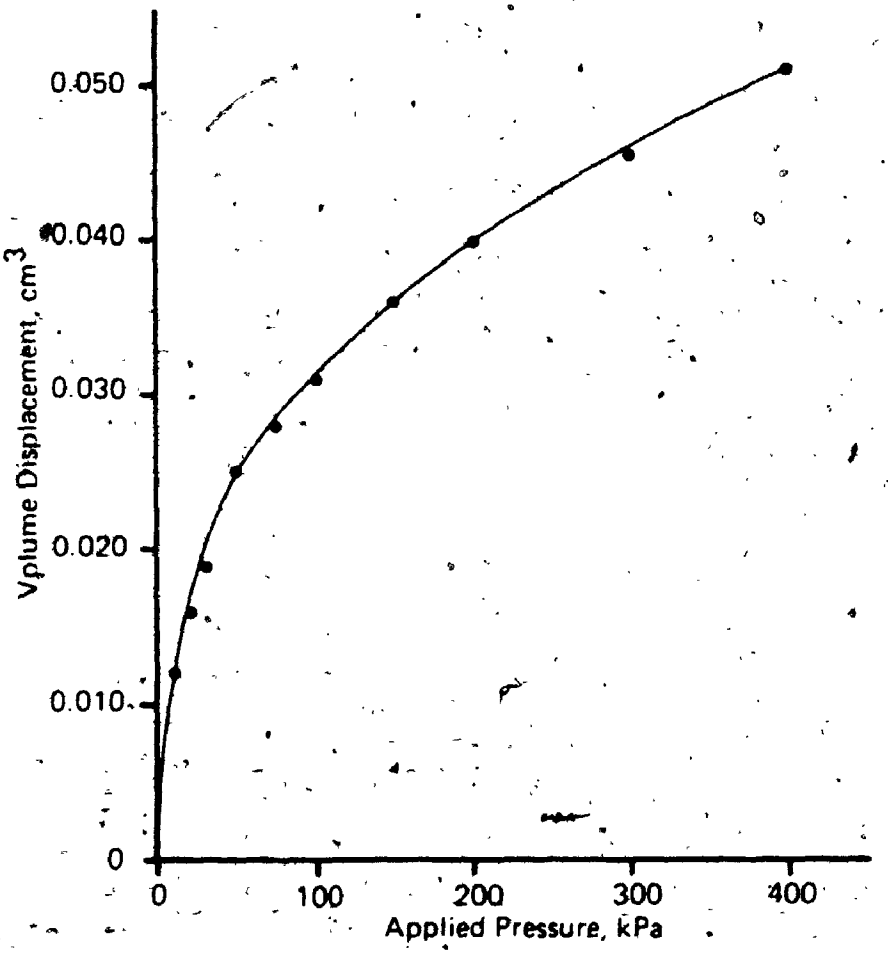

volume displacement due to this effect (Fig. 5.3), at the highest pressures experienced by the soil (300 kPa), was about 0.045 cm^3. This should not affect the pressures established within the soil significantly because ice lenses tend to enlarge until the pressures reach an equilibrium. However, slightly more ice would form than if the cell was perfectly rigid.

5.2 Pressure Transducers

Pressures within the soil specimen were measured by two small pressure transducer assemblies spaced 1.20 cm apart and 1.15 cm from the 'warm' and 'cold' extremities of the soil (calibration reports, Appendix C). The transducers (Kulite VQS-250, rated pressure 350 kPa) were mounted so that their entire length was accommodated within the walls of the cell to minimize external thermal disturbances.[3] The transducers were connected to small copper tubes over which were fitted oblong rubber bladders about 2 cm long and 0.35 cm outer diameter. The bladders were filled with Dow Corning 200 dimethyl silicone oil (freezing temperature -50°C, compressibility 0.01%/100 kPa, viscosity 350 centistokes at 25°C). Seals were made by small O-rings and an adjustable brass sleeve. The surface area of each bladder sensitive to pressure changes was about 1.8 cm^2. The bladders were replaced every 2 months due to the tendency for the rubber to decay slowly and lose its elastic properties (fabrication procedure, Appendix D).

---

[3] The transducers were activated by 1 V.d.c. This was lower than the recommended voltage (5 V.d.c.), to eliminate any heating effect on the transducer diaphragms caused by excitation of the wheatstone bridge. An 80% loss of sensitivity occurred because of the lower voltage but the results were unaffected. The transducer resolution was 0.01 kPa.

Although the silicone oil was very slightly compressible this did not have a significant effect on the pressures observed.[4] The behaviour and calibration of the transducers was checked periodically by filling the cell with water and applying pressure. Agreement between the transducers and a very accurate calibrated gauge was within 0.5 kPa. No significant change was observed during months of freezing experiments. The transducers have an internal compensation bridge to account for thermal effects and so the temperature dependence of the transducer calibration was negligible.

5.3 Temperature Control and Measurement

The soil was cooled by Peltier modules (cooling capacity 57 kJ hr^{-1}) and a thermoelectric cooling control unit which maintained the temperatures of the cooling plates constant to within ±0.0025°C. Soil temperatures were measured with YSI 3 kΩ thermistors (accuracy ±0.0025°C) spaced 1.25 cm apart and 0.50 cm from the ends of the soil specimen. These were housed within copper tubes, with O-ring seals, to prevent pressure loss in the cell. The tips of the thermistors were coated with heat conducting grease. To eliminate radial heat exchange with the surroundings, the cell was wrapped in a jacket of foam rubber insulation 15 cm thick and located inside a low temperature incubator

---

[4] The compressibility of the oil is due to small quantities of dissolved air (gas solubility, 0.259 $cm^3\ g^{-1}$ at 0°C and atmospheric pressure). Extrapolating from compressibility tables published by Dow Corning, the compressibility factor in the pressure range which occurred in this experiment (0-300 kPa) is approximately 0.01%/100 kPa, which is very low. Although there are other fluids which are less compressible, these may erode the silastic coating on the diaphragms and damage the transducer. Silicone oil was preferred because of its chemical compatibility.

set at 0°C ±0.1°C. Small fans were positioned above and below the cell to ensure good air circulation.

5.4 Water Supply

The soil imbibed or expelled water according to the potentials developed within the pores, from small reservoirs of distilled water at each end (volume about 5.5 cm^3). When the reservoir temperature was below 0°C, an exact concentration of lactose solution was used instead of pure water. This prevented freezing in the reservoir and it also lowered the chemical potential of the water in the reservoir, eliminating local osmotic gradients which would otherwise have occurred between the reservoir and the soil. The technique is described in Burt and Williams (1976) and Perfect and Williams (1980). The concentration required to equalize potentials was obtained directly from freezing-point depression tables for lactose solution (Appendix E). At -0.5°C, the temperature at the cold end, the required concentration is 87.3 g ℓ^{-1}.

The soil was separated from the reservoirs at each end by cellulose acetate membranes which readily transmit water but act as a barrier to lactose molecules.[5] The wire mesh and perforated aluminum plate, which supported the membranes, ensured the proper feed of water between the reservoir and the membrane surface. In practice, minute quantities of lactose were able to diffuse through the membrane, thawing the soil at the cold end at a very slow rate (0.2-0.3 cm in 3 weeks). The possibility of using larger solute molecules such as polyethylene

---

[5] Sartorius SM 117 cellulose acetate membrane: pore diameter <0.005 μm, thickness 80 μm, freezing temperature* −6°C, hydraulic conductivity* 1.5-3.5 × 10^{-12} $m\ s^{-1}$. (*determined directly from lab tests)

glycol was considered, but this had problems of its own and so it was dropped in favour of the lactose (discussed in Williams and Wood, 1982).

5.5 Data Record

Temperature measurements were made every half hour during the first 4-6 hours of each experiment and then at 24 hour intervals. Thermistors were calibrated at the N.R.C. Physics Division, temperature standards facility (Calibration reports, Appendix F).

Water flows were recorded by the movement of a water meniscus in glass capillaries (internal diameter 0.184 cm) which were connected to the end reservoirs. An automated camera (Minolta X-700) photographed the movement at intervals. The capillaries were filled with a red dye (propylene glycol) and were mounted on a finely divided scale with a white background to enhance contrast on the film. A network of copper tubing and valves (Fig. 5.2) mounted on a steel plate allowed the capillaries to be removed or changed without interruption to the flow record. The camera was mounted on a steel framework 1 meter above the capillaries. Photographic resolution allowed the meniscus position to be determined within ±0.05 cm. Negatives were developed in the laboratory darkroom (procedure, Appendix G) and were read with a microfilm projector.

Internal pressures were recorded by a Canlab 285 chart recorder. The recorder was adjusted to accommodate the sensitivity of each transducer as well as the anticipated range of pressure occurring within the soil (procedure, Appendix H). Changes in atmospheric pressure were incorporated into the results because the transducers were sealed with a constant internal reference pressure. Although the daily

change rarely exceeded 2 kPa, atmospheric pressure can vary by as much as 5 kPa.

5.6 Soil Specimens

Experiments were carried out with three different soils: Allendale clay, Caen silt and Snec sand. The Allendale clay is a highly frost susceptible material containing 45% clay (non-colloidal) and the remainder largely silt.[6] Some organic matter is also present. In its natural state, it is well flocculated with spheroidal aggregates 0.1 cm diameter. It has a relatively low bulk density and a high saturated water content and permeability (Table 5.1).

The majority of the experiments were carried out with Caen silt which has a very high frost heave susceptibility. This is an inorganic non-colloidal material with a granular (non-cohesive) structure. The bulk density is somewhat greater than the Allendale and the saturated water content and permeability (unfrozen) are less owing to its lower porosity.

One experiment was carried out on Snec sand which is a 'non-frost susceptible' material. This is a poorly graded sand with less than 0.5% in the clay-size fraction. Both the Snec and the Caen soils were obtained from the Canada-France ground pipeline freezing project at the Centre de Géomorphologie (C.N.R.S.) in Caen, France. The Allendale clay was obtained locally from an abandoned river channel in the east end of Ottawa.

---

[6] Frost heave susceptibility for the three soils based on U.S. Army Corps of Engineers classification (Chamberlain, 1981).

Table 5.1 Properties of Soils Used in the Experiments

Grain Size Distribution

	% Sand (>0.74 mm)	% Silt (0.74-0.002 mm)	% Clay (<0.002 mm)	Unified Soil Classification
Allendale	16	39	45	Clay, CL
Caen	4	74	22	Silt, ML
Snec	94	6	0	Sand, SP

Mineralogy

Allendale clay: Illite and chlorite present in large amounts. Smaller amounts of quartz, plagioclase and orthclase feldspar and traces of amphiboles (clay sized fraction).

Caen silt: Chiefly quartz with 7.2% calcite and small amounts of chorite.

Snec sand: Dominantly quartz with 3.1% calcite.

Physical Properties

	Allendale clay	Caen silt	Snec sand
ρ_B	1.2	1.5	1.85
ρ_s	2.68	2.67	2.67
W	≈43	≈26	≈10
ϑ	≈39(ρ_B=1.27g cm^{-3})	≈39(ρ_B=1.5g cm^{-3})	≈20(ρ_B=1.85g cm^{-3})
W_l	43.7	28.5	-
W_p	22.8	21.0	-
I_p	20.9	7.5	-
K_{uf}	8×10^{-5}(ρ_B=1.2g cm^{-3})	1×10^{-8}(ρ_B=1.30g cm^{-3})	-

Table 5.1 (cont'd)

	Allendale clay	Caen silt	Snec sand
λ_{uf}	1.1	2.0*	3.4*
C_{uf}	2.9×10^{6}	2.7×10^{6}	2.3×10^{6}*
$K_f(-0.3°C)$	5×10^{-11}	$.1\times10^{-11}$	-
$\lambda_f(-0.3°C)$	0.7	2.3	4.7
$C_f(-0.3°C)$	4.0×10^{6}	2.8×10^{6}	8.6×10^{6}*

*estimated values

ρ_B = bulk density (naturally occurring), g cm^{-3}

ρ_s = particle density, g cm^{-3}

W = saturated water content (gravimetric), % dry wt.

θ = saturated water content (volumetric), % total vol.

W_ℓ = liquid limit, % dry wt.

W_p = plastic limit, % dry wt.

I_p = plasticity index, % dry wt.

K_{uf} = hydraulic conductivity, unfrozen (saturated), m s^{-1}

λ_{uf} = thermal conductivity, unfrozen (saturated), W m^{-1} K^{-1}

C_{uf} = volumetric heat capacity, unfrozen (saturated), J m^{-3} K^{-1}

$K_f(-0.3°C)$ = hydraulic conductivity, frozen (saturated), m s^{-1}

$\lambda_f(-0.3°C)$ = thermal conductivity, frozen (saturated), W m^{-1} K^{-1}

$C_f(-0.3°C)$ = volumetric heat capacity, frozen saturated, J m^{-3} K^{-1}

FIGURE 5.4
GRANULOMETRY

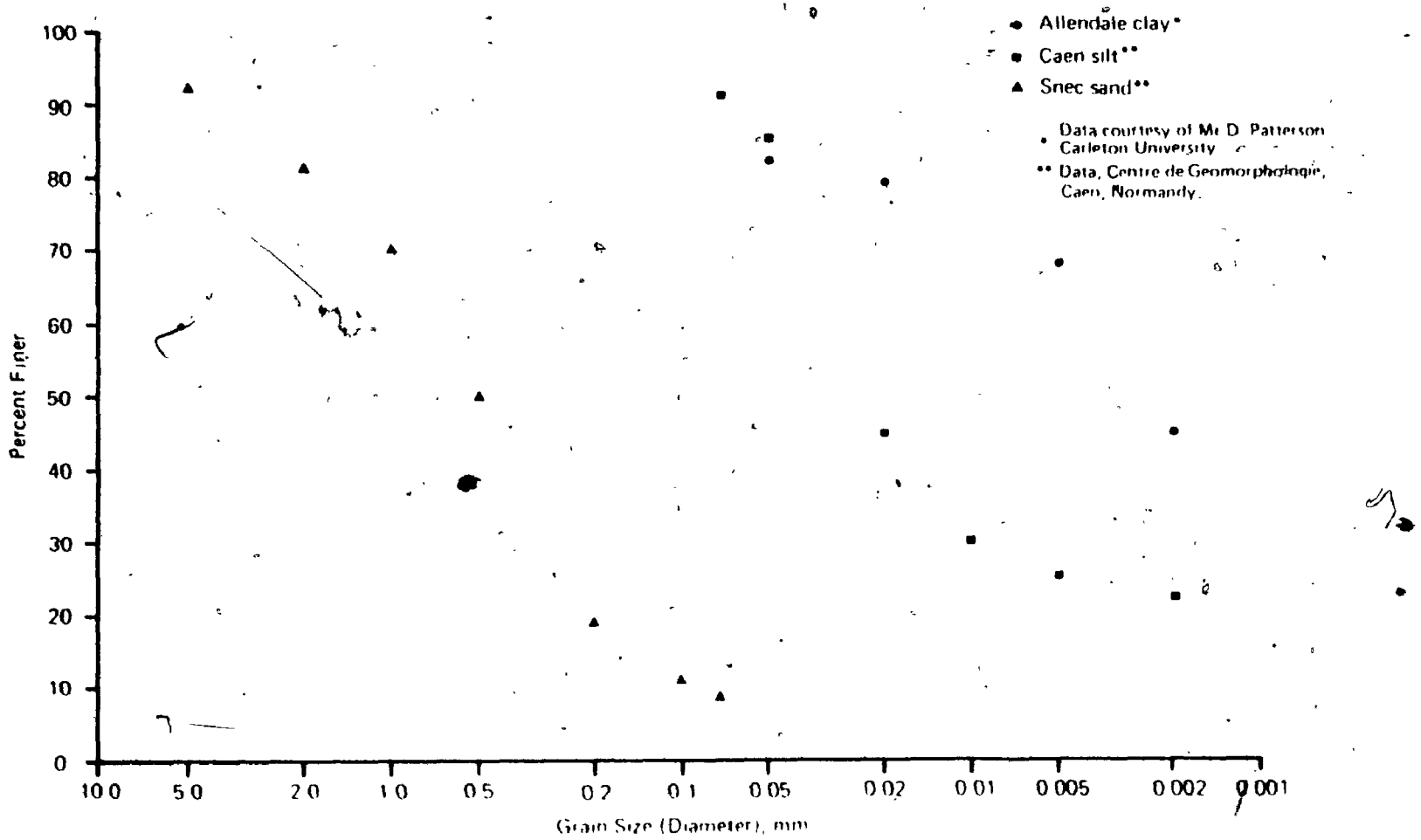

FIGURE 5.5
SOIL FREEZING CHARACTERISTIC CURVES

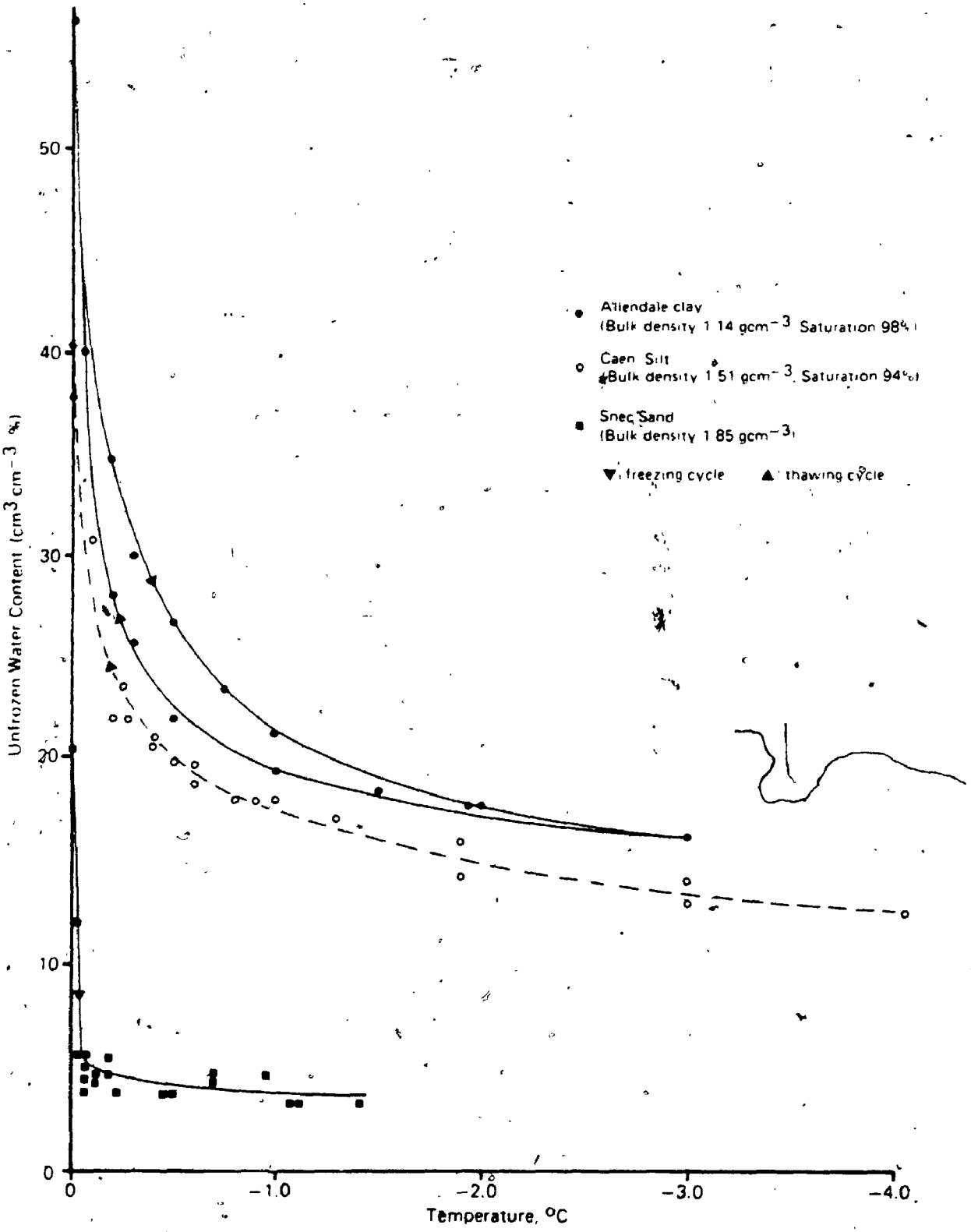

The mineralogy and physical properties of the soils are summarized in Table 5.1. Granulometric analysis and soil freezing characteristic curves are shown in Figs. 5.4 and 5.5.[7]

5.7 Soil Preparation

Careful attention was given to the preparation of soil specimens since this had a significant effect on the results obtained. In the majority of tests, the soil was prepared as a normally consolidated (uncompacted) saturated sediment. Soil specimens were saturated with distilled water and placed inside a vacuum chamber for about 30 minutes, breaking the vacuum several times to remove entrapped air from the soil pores. The soil was decanted into the partially assembled cell and allowed to consolidate under its own weight for 24-48 hours. (In some cases the soil was gently tamped with a rod). Gentle suction removed the supernatant liquid from the soil surface and further small quantities of soil were added until the sample container was deemed 'exactly full'. After this, the other cooling plate with semipermeable membrane was attached and the 'warm' reservoir was filled with distilled water.[8]

---

[7] Soil freezing characteristic curves for the Allendale and Caen soils determined by time domain reflectometry and, for the Snec sand, from suction-moisture content curves. Data courtesy of D. Patterson and S. Dallimore.

[8] Prior to assembly of the cell, the cellulose acetate membranes, which were stored in a solution of 25% ethanol and water, were washed in distilled water for 24 hours to remove all traces of ethanol from the pores. During assembly, care was taken to ensure that the membranes did not dry out as this would irreversibly damage the pore structure.

Tests were also carried out with soil specimens prepared as slurries (porosity and compressibility higher than normal) and with incompressible (compacted) soils (porosity reduced). Procedures for preparing the specimens are described in Appendix J.

5.8 Saturation of Soil Specimens

Although saturation was assumed, it appears that in all of the tests some air (generally less than 10% pore volume) remained trapped within the soil pores, probably as microscopic isolated bubbles. For example, in experiment 42A, Caen silt, the porosity of the specimen was 48.5% and the degree of saturation was 89.5% (Table 6.1).[9] The remaining 10.5% (by volume), presumably was occupied by air, although no bubbles were visible. A fraction of this air may have been due to the presence of aerophyllic substances within the soil.

Although additional precautions were taken to fully saturate the soil, including using de-aired water and vacuum dessication for longer periods, repeated attempts did not increase the degree of saturation by more than one or two percent. The presence of air, however, should not affect the pressures within the soil significantly, provided the air is present as isolated bubbles and pockets and not as a continuous phase (Williams, 1967).[10]

---

[9] The degree of saturation was probably slightly higher than the values given in Table 6.1 if allowance is made for certain errors in the determination of the water content. After the cell was dismantled the soil was allowed to thaw before it could be removed from the cell for weighing. Some evaporation probably occurred during this period although this was minimized by covering the cell with a plastic bag.

[10] As a continuous phase air lowers the water pressure which in turn reduces the ice pressures.

5.9 Nucleation and Freezing

After assembly, the frost heave cell was wrapped in its jacket of insulation, clamped and placed inside the incubator which was adjusted to 0°C. After thermoelectric cooling control was established, the soil was brought to +0.10°C and allowed to equilibrate with the 'warm' reservoir for about 24 hours. The soil was nucleated by momentarily lowering the temperature at the 'cold' end to about -1°C and giving the cell a sharp blow. Freezing was indicated by an immediate explusion of water from the warm reservoir, accompanied by an abrupt rise in soil temperature at the cold end as latent heat was suddenly released. Immediately after nucleation, the cold-end temperature was quickly raised and stabilized at -0.50°C.

Frost heaving tests were limited to temperatures warmer than -0.70°C. At colder temperatures, the heaving pressures (>790 kPa) might rupture the plexiglass cell or possibly damage the pressure transducers.[11]

The cold reservoir was not flushed with lactose solution until about 24 hours after freezing began. This is because the temperature at the cold end of the soil specimen was continuously decreasing during the early stages of the experiment. This would necessitate continuously changing the lactose concentration in the cold reservoir in order to maintain chemical equilibrium between the reservoir and the soil. In addition, if minute quantities of the sugar were allowed to pass through the semipermeable membrane before the soil was frozen, the sugar would

---

[11] Although the transducers were able to withstand pressures up to 690 kPa without damage, their accuracy was limited to pressures less than 350 kPa.

quickly diffuse through the soil, reducing the amount of pore ice that would otherwise form. By allowing the soil to freeze first, lactose diffusion was limited to a very narrow zone at the cold end of the soil and its effect was minimized.

3.10 Final Observations

At the end of each experiment, usually about 2-3 weeks, the frost pressure cell was quickly dismantled and the location of the frost line was determined. This was done by inserting a thin metal shaft (2 mm^2) into the soil which slides through the unfrozen layer until resistance is met at the boundary with the frozen section. The location of the frost line was assumed to be the average of several measurements (generally 6 or more).

After determining the position of the frost line, the specimen was dissected and examined with a hand lens and the location and thickness of visible ice lenses was noted. Finally, the soil was weighed and dried and its water content and bulk density were determined.

VI. RESULTS AND INTERPRETATION

6.1 Flows and Internal Pressures: General Observations

Sixteen frost heaving tests were carried out, of which two were with the Allendale clay, one with the Snec sand and the remainder with the Caen silt. These varied from about 8 days up to 30 days duration, depending upon the stability of the conditions inside the soil. In most of the experiments, the end temperatures (i.e. the temperatures of the cooling plates) were the same ('warm' end +0.10°C, 'cold' end -0.50°C). The thermal gradient varied slightly in each test (average gradient 0.145°C cm^{-1}).[1] Although there were minor variations in the results, the experiments showed a fairly consistent pattern provided the soil density was the same. Results from the experiments are summarized in Tables 6.1 and 6.2.

Immediately after nucleation, the soil began to expel water from the warm end (about 1.0-1.5 cm^3) at a diminishing rate which corresponded almost exactly with the rate of advance of the frost line (e.g. Fig. 6.1). A linear temperature gradient was established within about 24 hours. However, the frost line continued to advance very slowly for a further 24 hours. The outflow at the warm end stopped after 15-30 hours and the soil began to draw in water at a very slow but nearly constant rate for the remainder of the experiment (average inflow rate 0.02 cm^3 day^{-1}). In some cases the flow tended to be slightly faster initially, but then leveled off to a constant rate after a few

---

[1] Small changes in the thermal gradient were caused by variations in the thermal properties with different soil specimens and also slight variations in the heat flow at the cold end. The latter was affected by the thermal contact between the wire mesh and the perforated aluminum plate.

Table 6.1

Pressure and Flow Data for Experiments With Normally Consolidated Soil Specimens

(Warm end +0.10°C, Cold end −0.50°C)

Soil	Caen	Caen	Caen	Caen
Exp.	32A	42A	34	35**
Freeze	Second	Second	First	First and Second
$\Delta T/\Delta X$	0.152	0.146	0.138	0.138
ρ_B	1.35	1.37	1.35	1.32
n	51.7	48.6	49.3	50.5
W	38*	31.7	33.0	34.6
θ	–	43.4	44.6	45.7
θ_s	–	89.6	90.5	90.4
ℓ_f	2.42	2.56	2.03	2.03
T_f	-0.090	-0.065	-0.090*	-0.090
Q_i	1.59	1.52	1.20	1.12 (1.12)
Q_f	1.22	1.18	1.01	0.85 (0.80)
q	-0.26	-0.18	–	–
P_c	200	188	153	146 (153)
P_w	30	18	-4	1 (14)
P_r	–	–	142	103 (129)
Δt	406	378	168	381 (426)
P_{mc}	207	210	153	146 (156)
P_{mw}	130	75	67	37 (37)

*No data available. Value is assumed.

**Data from second freeze in brackets.

Table 6.1 (cont'd)

(Warm end +0.10°C, Cold end -0.50°C)

Soil	Allendale	Caen	Caen
Exp.	30	39B*	44A**
Freeze	First	Third	Second
$\Delta T/\Delta X$	0.158	0.148 (0.134)	0.140
ρ_B	1.31	1.32	1.49
n	51.1	50.4	44.1
W	38.7	35.1	28.4
θ	50.6	46.3	42.3
θ_s	99.0	91.9	96.8
ℓ_f	2.70	2.81	-
T_f	-0.050	-0.065	-0.065
Q_i	0.84	1.49 (0.66)	1.25
Q_f	0.52	1.32 (0.38)	0.92
q	0.10	- -	-
P_c	217	144 (70)	276
P_w	7	108 (0)	204
Δt	284	194 (507)	234
P_{mc}	234	146 (183)	277
P_{mw}	112	108 (159)	204

*Temperature gradient reversed midway through experiment. Flows and pressures after change, in brackets.

**Hydrostatic pressure of pore water raised to 100 kPa prior to freezing. (Same soil specimen as exp. 44 and 44B).

Table 6.1 (cont'd)

$\Delta T/\Delta X$ = thermal gradient, °C cm^{-1}

ρ_B = bulk density, g cm^{-3}

n = soil porosity, %

W = gravimetric water content, % (dry wt.)

ϑ = volumetric water content, % (total vol.)

ℓ_f = thickness of frozen section, cm

T_f = frost line temperature, °C (interpolated from thermal profile)

Q_i = initial outflow at warm end of soil, cm^3

Q_f = cumulative flow at warm end of soil (time Δt)*, cm^3

q = cumulative flow at cold end of soil (time Δt)*, cm^3

P_c = long-term pressure at colder transducer (time Δt), kPa

P_w = long-term pressure at warmer transducer (time Δt), kPa

P_r = cold-end reservoir pressure (time Δt), kPa (applies only to experiments 34 and 35 in which cell was modified to measure external heave pressure)

Δt = time since freezing began, corresponding to long-term pressure and flow observations, hours (in most cases, at the end of the experiment)

P_{mc} = maximum pressure observed at colder transducer, kPa

P_{mw} = maximum pressure observed at warmer transducer, kPa.

* Positive and negative sign conventions indicate outflow or inflow, respectively.

Table 6.2

Pressure and Flow Data for Experiments With Varying Soil Densities and Thermal Gradients

(Warm end +0.10°C, Cold end -0.50°C)

	Incompressible Soils		Slurries	
Soil	Caen	Snec	Caen	Allendale
Exp.	31	36	43A	29
Freeze	First	First	First	First
$\Delta T/\Delta X$	0.148	0.130	0.146	0.152
ρ_B	1.73	1.88	1.17	1.09
n	35.1	29.3	56.1	59.3
W	18.7	I4.2	51.2	48.3
θ	32.3	26.7	59.9	52.6
θ_s	92.0	91.1	-	88.7
ℓ_f	2.50	3.19	2.73	2.20
T_f	-0.065	-0.020	-0.060	-0.080
Q_i	0	0.99	1.84	0.83
Q_f	-1.13	0.47	1.62	0.37
q	0.13	-0.14	-0.34	-0.27
P_c	138	147	36	138
P_w	104	47	75	48
Δt	167	456	342	190
P_{mc}	181	182	62	143
P_{mw}	123	68	75	64
Comments	No visible ice lenses	No visible ice lenses	Increased ice lens density	Increased ice lens density

Table 6.2 (cont'd)

Changes to Thermal Gradient (Warm end +0.10°C)

Soil	Caen	Caen	Caen	Caen	Caen	Caen
Exp.	44B	40	33	44	44	44
Freeze	Third	First	First	First	"	"
T_c	-0.70	-0.70	-0.20	-0.30	-0.50	-0.70
$\Delta T/\Delta X$	0.188	0.188	0.074	0.082	0.120	0.166
ρ_B	1.49	1.22	1.34	1.49	"	"
n	44.1	54.3	49.7	44.1	"	"
W	28.4	43.1	34.7	28.4	"	"
θ	42.3	52.6	46.5	42.3	"	"
θ_s	96.0	96.8	93.6	96.0	"	"
ℓ_f	3.08	2.70	1.12	-	"	"
T_f	-0.065	-0.090	-0.065	-0.065	"	"
Q_i	1.75	2.79	0.62	0.72	1.00	1.04
Q_f	1.58	1.54	0.42	0.70	0.96	0.97
q	-	0.90	0.06	-	-	-
P_c	285	1.97	52	24	113	205
P_w	201	30	55	33	118	183
Δt	312	312	216	119	213	315
P_{mc}	310	240	52	31	113	205
P_{mw}	205	148	55	33	118	183
Comments	Few visible ice lenses	Large ice lens 0.5 cm thick at cold end	Ice lenses clustered near cold end	Few visible ice lenses		

Table 6.2 (cont'd)

T_c = cold-end temperature, °C

$\Delta T/\Delta X$ = thermal gradient, °C cm^{-1}

ρ_B = bulk density, g cm^{-3}

n = porosity, %

W = gravimetric water content, % (dry wt.)

θ = volumetric water content, % (total vol.)

ℓ_f = thickness of frozen section, cm

T_f = frost line temperature, °C (interpolated from thermal profile)

Q_i = initial outflow at warm end of soil, cm^3

Q_f = cumulative flow at warm end of soil (time Δt)*, cm^3

q = cumulative flow at cold end of soil (time Δt)*, cm^3

P_c = long-term pressure at colder transducer (time Δt), kPa

P_w = long-term pressure at warmer transducer (time Δt), kPa

Δt = time since freezing began, corresponding to long-term pressure and flow observations, hours (in most cases at the end of the experiment)

P_{mc} = maximum pressure observed at colder transducer, kPa

P_{mw} = maximum pressure observed at warmer transducer, kPa

* Positive and negative sign conventions indicate outflow or inflow, respectively.

days. At the cold end the flows were about an order of magnitude lower than at the warm end and also less predictable. In about half the experiments outflow occurred at the cold end. In the other half, the flow was in the opposite direction.

Pressures did not begin to rise until the frost line was midway between the two transducers, 3 or 4 hours after freezing began. The pressure at both transducers then increased rapidly by as much as 35 kPa hr^{-1} in the Caen silt (55 kPa hr^{-1} in the Snec sand). At the colder transducer the pressure increased for about 3 days, but then levelled off. In some cases the pressure declined slightly (30-40 kPa) after reaching a peak, or continued to increase very slowly for the duration of the experiment.

At the warmer transducer a very different pattern was observed. The pressure rose at a slower rate than the colder transducer, reaching a peak generally within 3-5 days and then began to decline at a very slow rate, eventually levelling off a few kPa above atmospheric pressure (e.g. Fig. 6.1). Peak values were not attained simultaneously. The colder transducer usually lagged by several days behind the warmer one.

The highest pressure observed at the colder transducer was 210 kPa in the Caen silt and 234 kPa in the Allendale clay. The mean temperature of the colder transducer was about -0.28°C (temperature gradient 0.15°C cm^{-1}). At the warmer transducer the peak pressure varied from 40-130 kPa (mean temperature about -0.10°C). The maximum observed pressure difference between the two transducers was 192 kPa in the Caen silt and 210 kPa in the Allendale clay. This corresponds to internal pressure gradients of 160 kPa cm^{-1} and 175 kPa cm^{-1}, respectively.

Significant deviations from the above described pattern occurred in soils prepared as slurries (densities lower than normal) and in incompressible (compacted) soils (densities higher than normal). Differences in internal pressure between the two transducers were reduced considerably (Table 6.2). The same effect, but even more pronounced, occurred in an experiment where the soil was frozen very slowly in stages (exp. 44).

6.2 Ice Contents and Ice Saturation

The initial outflow of water from the warm end was caused by the 9.1% volume increase due to the formation of ice within the soil. The volume of ice formed, V_i, can be calculated from the expression:

$$V_i = V_e \times \frac{100}{9.1} \qquad 6.1$$

V_e = volume of water expelled, cm^3.

For example, in exp. 32A Caen silt, the initial outflow from the warm end was 1.59 cm^3, therefore V_i = 17.47 cm^3 (Table 6.3). The volumetric ice content of the soil was 22.3%. The ice saturation was 43.1%, the remaining 56.9% being unfrozen water and a small amount of entrapped air.

The ice saturation of the Allendale clay (exp. 30) was only about half that of the Caen silt. This is a result of the dominant influence of the clay minerals. With the Snec sand the ice saturation was higher than either the silt or the clay owing to the larger pore sizes.[2]

---

[2]Although the ice saturation was higher in the Snec sand than the Caen silt, the ice content of the sand was lower because its total pore volume was lower.

Table 6.3

Freezing Data

	Normally Consolidated Specimens						
Soil	Caen	Caen	Caen	Caen	Allendale	Caen	Caen
Exp.	32A	42A	34	35*	30**	39B***	44A
$\Delta T/\Delta X$	0.152	0.146	0.138	0.138	0.158	0.148	0.140
V_f	55.42	58.63	46.49	46.49	61.83	64.36	-
R_f	70.7	74.8	59.3	59.3	78.9	82.1	-
V_e	1.59	1.52	1.20	1.14	0.84	1.49	1.25
V_p	40.54	38.11	38.66	38.60	40.07	39.52	34.58
V_i	17.47	16.70	13.19	12.53	9.23	16.37	13.74
θ_i	22.3	21.3	16.8	16.0	11.8 (14.9)	20.9	17.5
θ_{is}	43.1	43.8	34.1	32.5	23.0 (29.2)	41.4	39.7

*Data for first freeze and second freezes.

**Values in brackets are ice content and ice saturation of the frozen section alone (see * next page)

***Data applies to freeze prior to thermal gradient reversal.

Table 6.3 (cont'd)

	Incompressible Soils		Slurries		Changes to Thermal Gradient					
Soil	Caen	Snec	Caen	Allendale	Caen	Caen	Caen	Caen**	Caen	Caen
Exp.	31	36	43A	29*	44B	40	33	44	44	44
$\Delta T/\Delta X$	0.148	0.130	0.146	0.152	0.188	0.188	0.074	0.082	0.120	0.166
V_f	57.26	73.06	62.52	50.39	70.54	61.83	25.65	-	-	-
R_f	73.0	93.2	79.7	64.3	90.0	78.8	32.7	-	-	-
V_e	-	0.99	1.83	0.83	1.75	2.79	0.61	0.72	1.02	1.10
V_p	-	22.98	43.98	46.50	34.58	42.58	38.97	34.58	34.58	34.58
V_i	-	10.88	20.22	9.12	19.23	30.66	6.70	7.69	11.21	12.09
θ_i	-	13.9	25.8	11.6(18.1)	24.5	39.1	8.5	9.8	14.3	15.4
θ_{is}	-	47.4	50.4	19.6(30.5)	55.6	72.0	17.2	22.1	32.4	34.8

*Values in brackets are ice content and ice saturation of frozen section alone (i.e. $\theta_i^f = V_i/V_f$ and $\theta_{is}^f = V_i/V_p^f$ where $V_p^f = V_T \times$ porosity, see nomenclature page III).

**Same soil specimen as exp. 44A and exp. 44B.

Table 6.3 (cont'd)

$\Delta T/\Delta X$ = thermal gradient, $^{\circ}C\ cm^{-1}$

V_f = volume of frozen section (cross-sectional area, 22.90 cm^2 × thickness of frozen section), cm^3

R_f = $V_f/V_T \times 100$, fraction of total soil volume V_T(78.42 cm^3) that was frozen, %

V_e = initial outflow at warm end of soil, cm^3

V_p = pore volume (porosity × total volume of soil, 78.42 cm^3), cm^3

V_i = volume of ice formed, cm^3 (eqn. 6.1)

θ_i = $V_i/V_T \times 100$, volumetric ice content, % (total vol.)

θ_{is} = $V_i/V_p \times 100$, ice saturation % (pore vol.)

In the experiment with the Caen silt prepared as a slurry, the ice saturation was about 10-20% higher than in the normally consolidated silt specimens at the same end temperatures. More ice formed because of the increased porosity. Since the soil was also more compressible, there should be more segregation ice. This supposition is supported by observations of increased ice lens densities. The same is true of the Allendale clay specimen (exp. 29) prepared as a slurry. However, in this case, the ice saturation and the ice content appear lower than in the normally consolidated specimen (exp. 30). This is because the location of the frost line was about 0.030°C colder in the slurry and so the fraction of soil that was frozen was significantly smaller. If allowance is made for this, by expressing V_i as a fraction of the volume of the frozen section, V_f, rather than the total volume (values in brackets), the ice content appears proportionally larger in the slurry than in the normally consolidated specimen by a factor of 21%. Similarly, if Vi is expressed as a fraction of the pore volume of the frozen section, the ice saturation also appears slightly higher in the slurry.

With the incompressible (compacted) soils, the amount of ice formed should be less than in normally consolidated specimens because of the substantially reduced porosity. This is evident with the Snec sand; the amount of ice formed was about half that found in the normally consolidated silt specimens, although the ice saturation was actually higher because of the larger pores. With the highly compacted Caen silt (exp. 31), the ice content could not be determined directly because water flowed in at the warm end rather than out. This is physically incompatible with the fact that water expands upon freezing and should

flow out. The result is anomalous and may be due to experimental error, perhaps a leak in the apparatus itself. Whatever the reason, it is assumed that the ice content of the soil was substantially reduced because of the lower pore volume.

6.3 Observations of Segregation Ice

In the experiments with normally consolidated specimens the pattern of ice lenses within the soil was similar. When the cell was dismantled, the warmer transducer appeared to be located either exactly at the frost line (that is, the rubber bladder was half in and half out of the frozen soil), or in the frozen unlensed zone slightly behind it. The colder transducer was surrounded by a fairly dense reticulate pattern of discontinuous segregation ice (e.g. lower half of soil specimen, Plate 6.1). An unlensed layer about 0.2-0.3 cm thick was apparent at the cold end of the soil. Above this, ice lenses progressively increased in thickness with warmer temperatures, from barely visible up to 0.2 cm thick about 0.5 cm behind the frost line. Closer to the frost line, ice lenses diminished in thickness rather abruptly down to a hair's breadth. There were no visible ice lenses in the frozen zone about 0.2-0.3 cm behind the frost line.

In the colder regions of the soil horizontal lenses were interconnected by a splayed pattern of vertical ice-filled fissures, about 2 cm long, with the apex near the cold end. These increased in thickness toward the warm end of the soil (maximum thickness 0.2 cm). Fissures of this type are usually attributed to tensile stresses established in the unfrozen zone close to the frost line, which are normal to the direction of heat flow.

PLATE 6.1

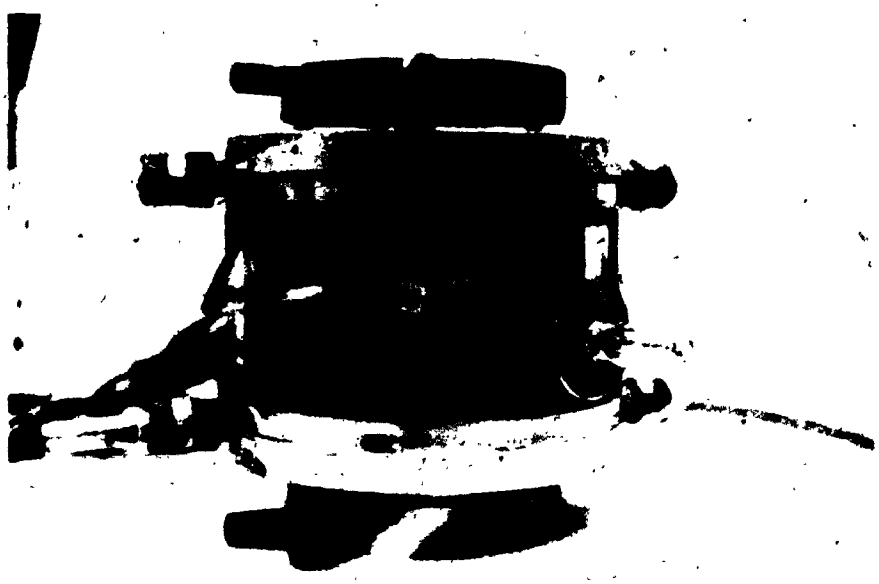

Ice Lenses In A Frozen Soil Specimen
(Lenses appear as dark areas)

In the specimens prepared with significantly reduced densities or increased densities, the pattern of ice lenses was very different. In the highly compacted (incompressible) soils there was no visible segregation ice. Similarly, in soils prepared as normally consolidated (uncompacted) specimens, but in which the density was somewhat higher than normal (e.g. exp. 44, 44A, 44B all the same soil specimen, Table 6.2), only a few very fine lenses were observed about 1.3 cm from the cold end. Some small vertical fissures were also apparent near the cold end but these were much smaller than those normally observed. In contrast, with slurries, the ice lens density was perceptibly greater than in normally consolidated specimens and vertical fissures were also more numerous. The lenses were about the same size as those normally observed. They were also concentrated in greater numbers closer to the frost line.

In one experiment, freezing apparently took place in the cold reservoir. A large ice lens (0.5 cm thick) formed between the semi-permeable membrane and the perforated aluminum plate at the cold end of the soil (exp. 40).

6.4 Graphical Presentation of Results

Results from a typical experiment are shown in Figs. 6.1 and 6.2 (next section). The internal pressures (dashed lines) are in kPa relative to atmospheric pressure, P_o. Water flows (solid line) are in cm^3, starting from the time freezing began. The slope of the flow curves indicates the flow direction (i.e. a positive slope for outflow and a negative slope for inflow). The positive and negative sign convention on the left hand vertical axis refers to the cumulative outflow (from the soil into the reservoir), or inflow (from the

reservoir into the soil), respectively, since freezing began. For example, in experiment 32A Fig. 6.1 at 144 hours, although there was a cumulative outflow of 1.50 cm^3 of water from the warm end since freezing began (indicated by positive flow values), this occurred during the first few hours of the test and the soil was still drawing in water at the warm end (indicated by a negative slope). At the cold end, there was a cumulative inflow of 0.12 cm^3 since freezing began and the inflow is still continuing. The internal pressures were 205 kPa at the colder transducer and 72 kPa at the warmer transducer.

The thermal profile at successive intervals during the approach to a steady-state is shown in Fig. 6.2. The location of the frost line is indicated by an arrow (in this case -0.090°C). For convenience, temperature profiles are plotted by connecting the points between thermistor temperatures. For this reason, the temperature appears slightly warmer than it actually is at the colder extremity (boundary E2) of the soil specimen and slightly colder at the warmer extremity (E1). For example, in Fig. 6.2, the temperature at the cold extremity reads as -0.42°C and at the warm extremity as +0.02°C (cold-end temperature -0.50°C, warm-end temperature +0.10°C).[3] Correcting for this, by extending the linear thermal profile at the three soil thermistors to the extremities of the soil specimen (E1 and E2), the true temperatures at the extremities are -0.46°C and +0.07°C.

---

[3]The terms 'cold end' and 'warm end' refer to the temperatures of the cooling plates rather than the temperatures at the extremities of the soil.

6.5 Analysis of Pressure Differences in Normally Consolidated Soil Specimens

If the pressure of the unfrozen water is assumed to be atmospheric, then, according to the Clausius-Clapeyron eqn., the equilibrium pressure of the ice lenses as a function of the soil temperature is:[4]

$$P_i = (T^* - T) \frac{\delta P_i}{\delta T} \qquad 6.2$$

T = soil temperature, °C

T* = frost line temperature, °C

$\frac{\delta P_i}{\delta T}$ = 1127 kPa $°C^{-1}$, (special case 1 of Clausius-Clapeyron eqn. section 2.4).

In the experiments with normally consolidated soils, the difference in the pressure recorded by the transducers is very close to the temperature-dependent difference in the equilibrium ice pressure specified by eqn. 6.2. For example, in exp. 32A the mean temperature of the rubber bladder at the colder transducer is −0.285°C and at the warmer transducer −0.105°C. Since the freezing temperature of the soil is −0.090°C (frost line temperature), the equilibrium ice pressure according to eqn. 6.2 is (−0.090°C + 0.285°C) 1127 kPa $°C^{-1}$ = 220 kPa, assuming the unfrozen water remains at atmospheric pressure (Table 6.4). This is slightly larger than the observed long-term pressure. At the warmer transducer, the equilibrium ice presure (eqn. 6.2) is 17 kPa, which is slightly less than the observed pressure (30 kPa).

The differences in pressure are similar in the other experiments with normally consolidated Caen silt and Allendale clay at

---

[4] Frost line temperature T* = freezing temperature of the soil <0°C.

Table 6.4

Observed Pressures and Equilibrium Ice Pressures for Normally Consolidated Soils

Soil	Caen		Caen	
Exp.	32A		42A	
T_f	-0.090		-0.065	
T	-0.105	-0.285	-0.095	-0.270
P_i	17	220	34	231
P	30	200	18	200

Soil	Caen		Caen		Allendale	
Exp.	35		34		30	
T_f	-0.090		-0.090*		-0.050	
T	-0.090	-0.255	-0.090	-0.255	-0.090	-0.255
P_i	0	186	0	186	45	231
P	16	156	-4	164	7	217

Soil	Caen		Caen	
Exp.	33		39B**	
T_f	-0.065		-0.065	
T	-0.030	-0.060	-0.105 (-0.125)	-0.285 (-0.290)
P_i	0	0	45 (68)	250 (254)
P	52	55	108 (0)	144 (70)

T_f = frost line, average temperature, °C

T = mean temperature of transducer, °C

P_i = equilibrium ice pressure, Clausius-Clapeyron equation (6.2), kPa

P = observed long-term pressure, kPa

*Approximate temperature

**Thermal gradient reversed halfway through experiment. Temperatures and pressures after change, in brackets.

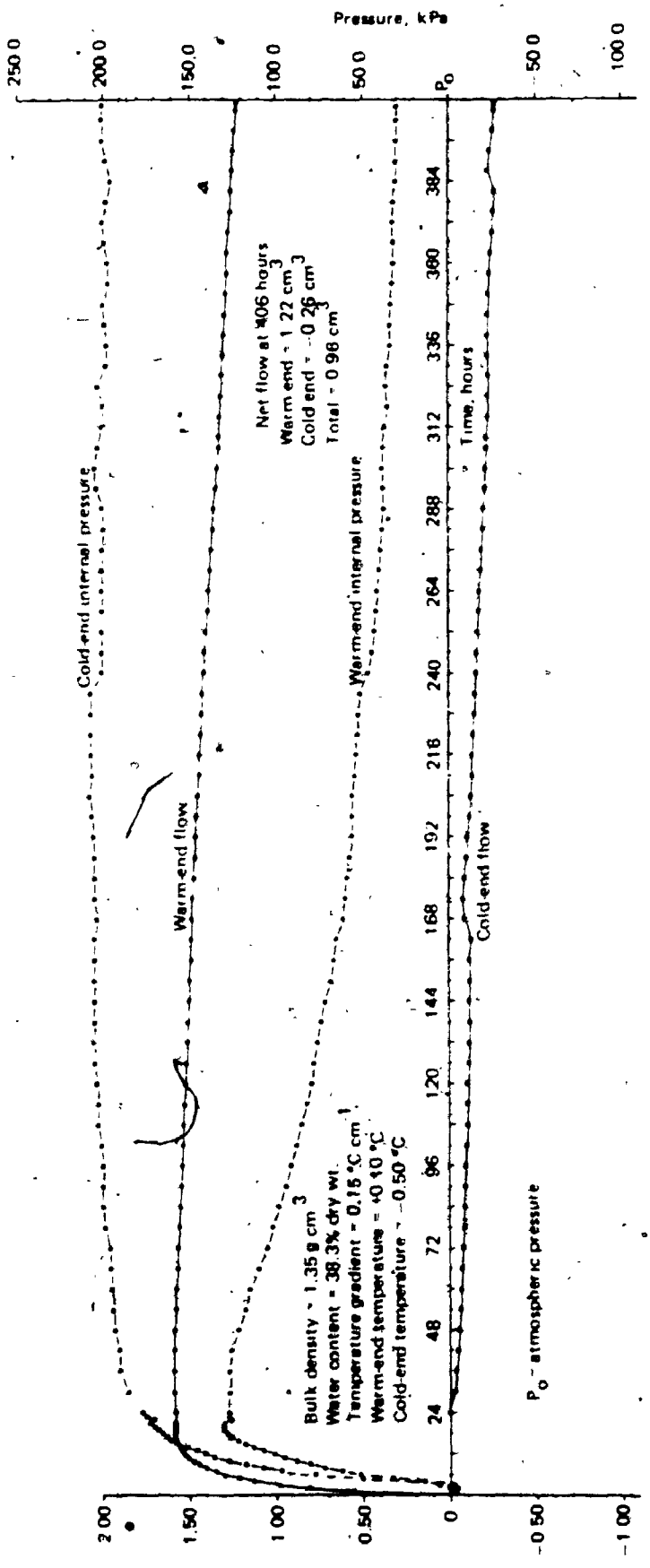

FIGURE 6.1

FLOWS AND INTERNAL PRESSURES, EXPERIMENT 32A, CAEN SILT

FIGURE 6.2

TEMPERATURE PROFILE DURING FREEZING, EXPERIMENT 32A, CAEN SILT

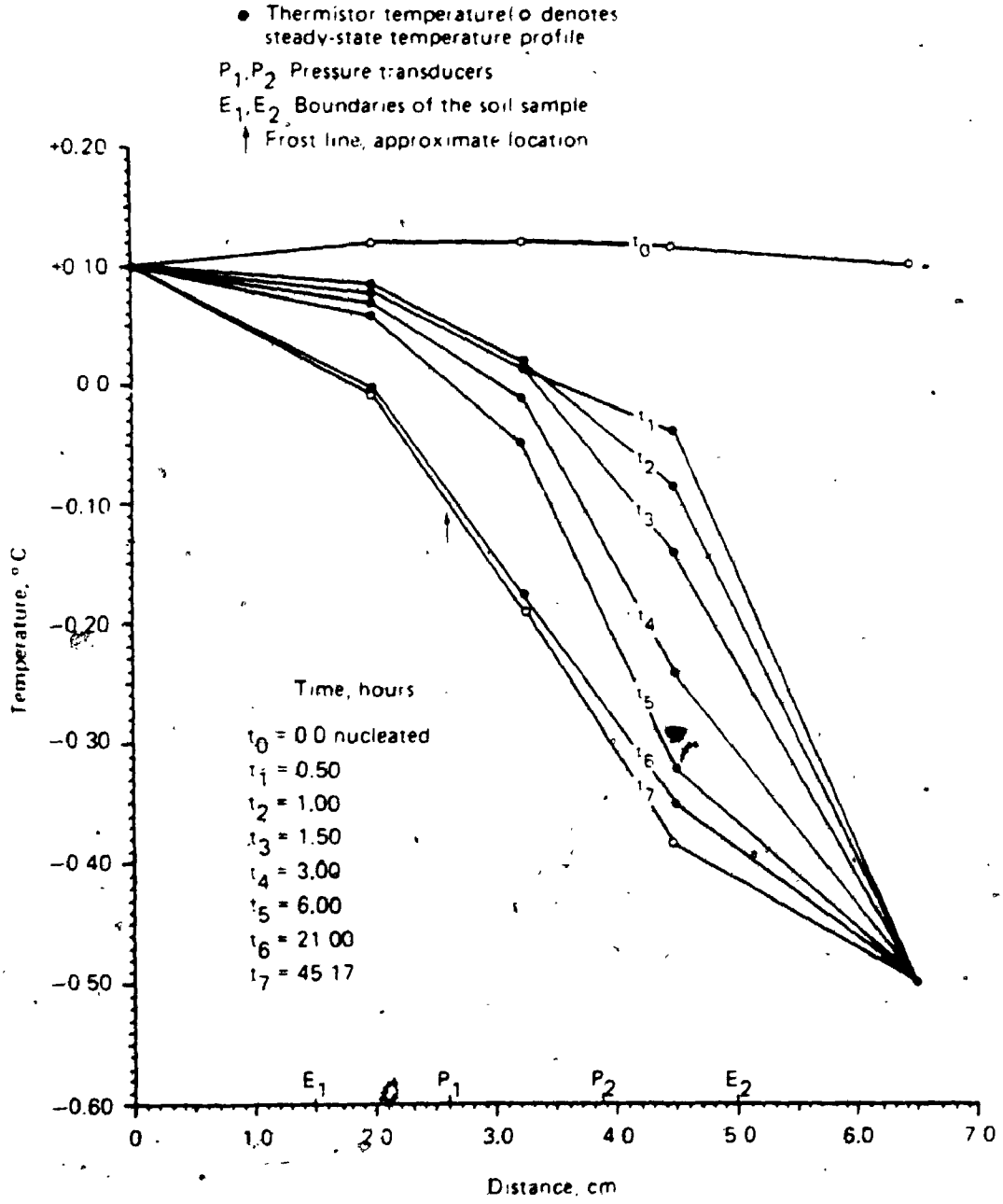

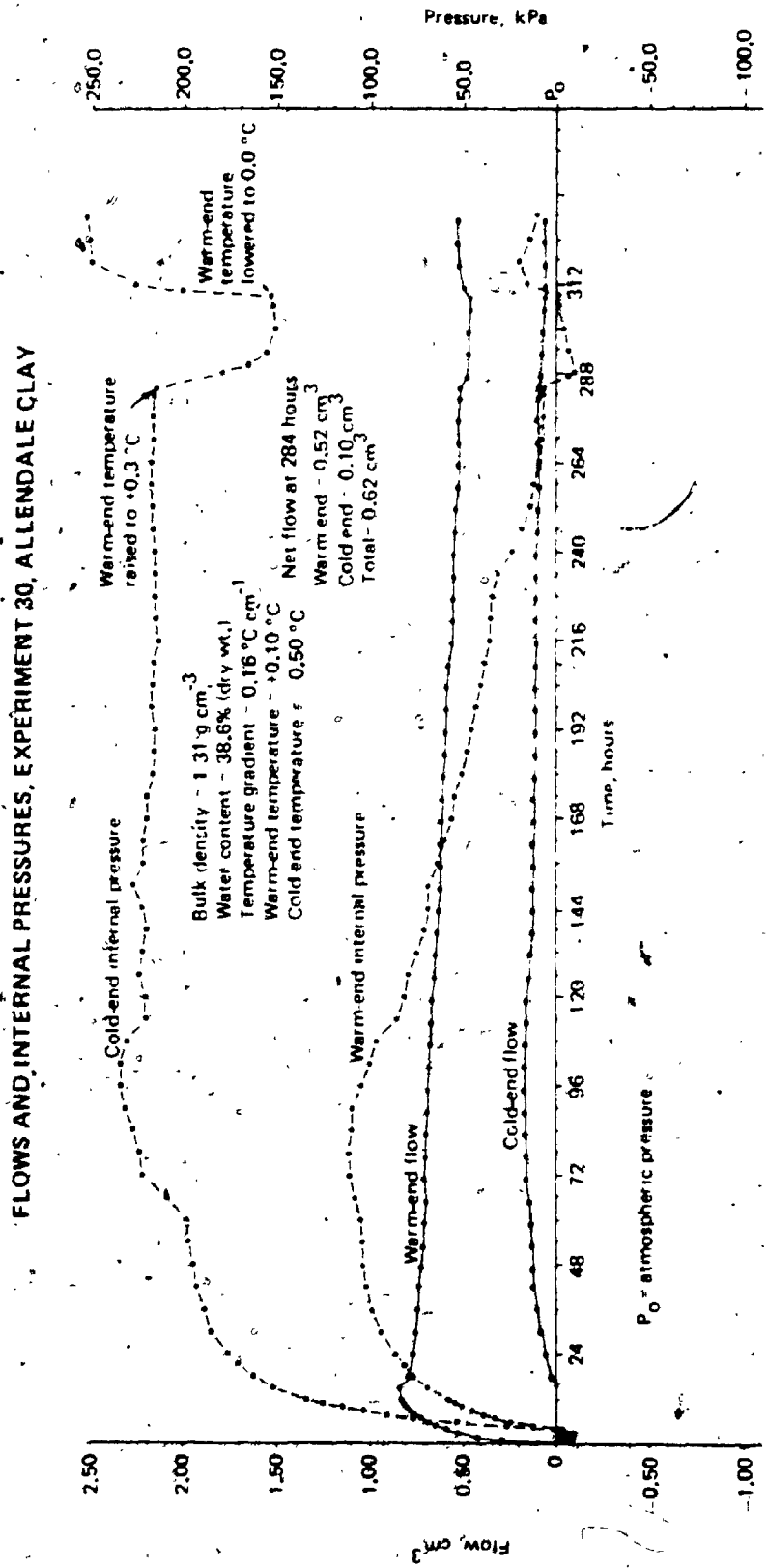

FIGURE 6.3
FLOWS AND INTERNAL PRESSURES, EXPERIMENT 30, ALLENDALE CLAY

FIGURE 6.4

TEMPERATURE PROFILE DURING FREEZING, EXPERIMENT 30, ALLENDALE CLAY

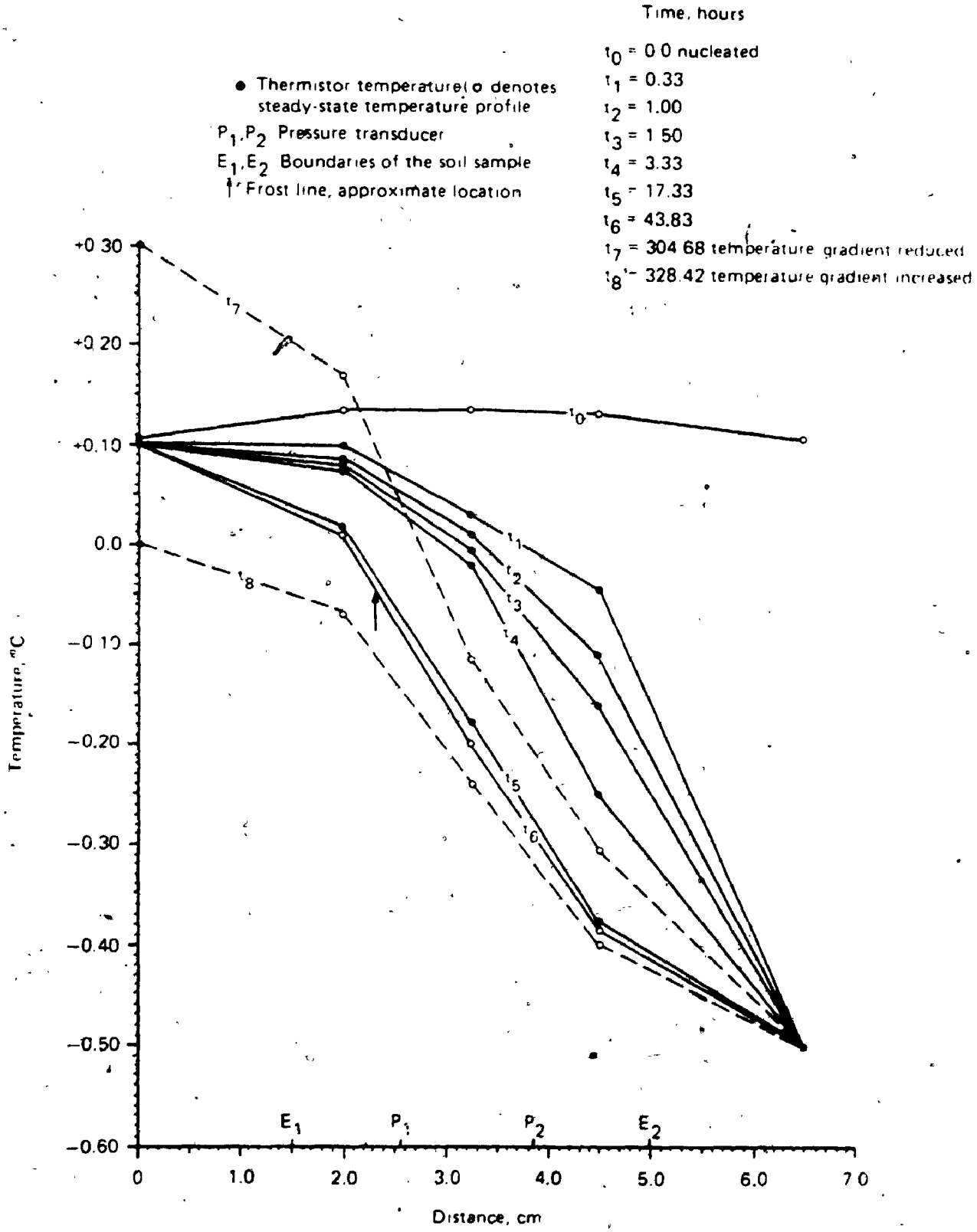

FIGURE 6.5

FLOWS AND INTERNAL PRESSURES, EXPERIMENT 33, CAEN SILT

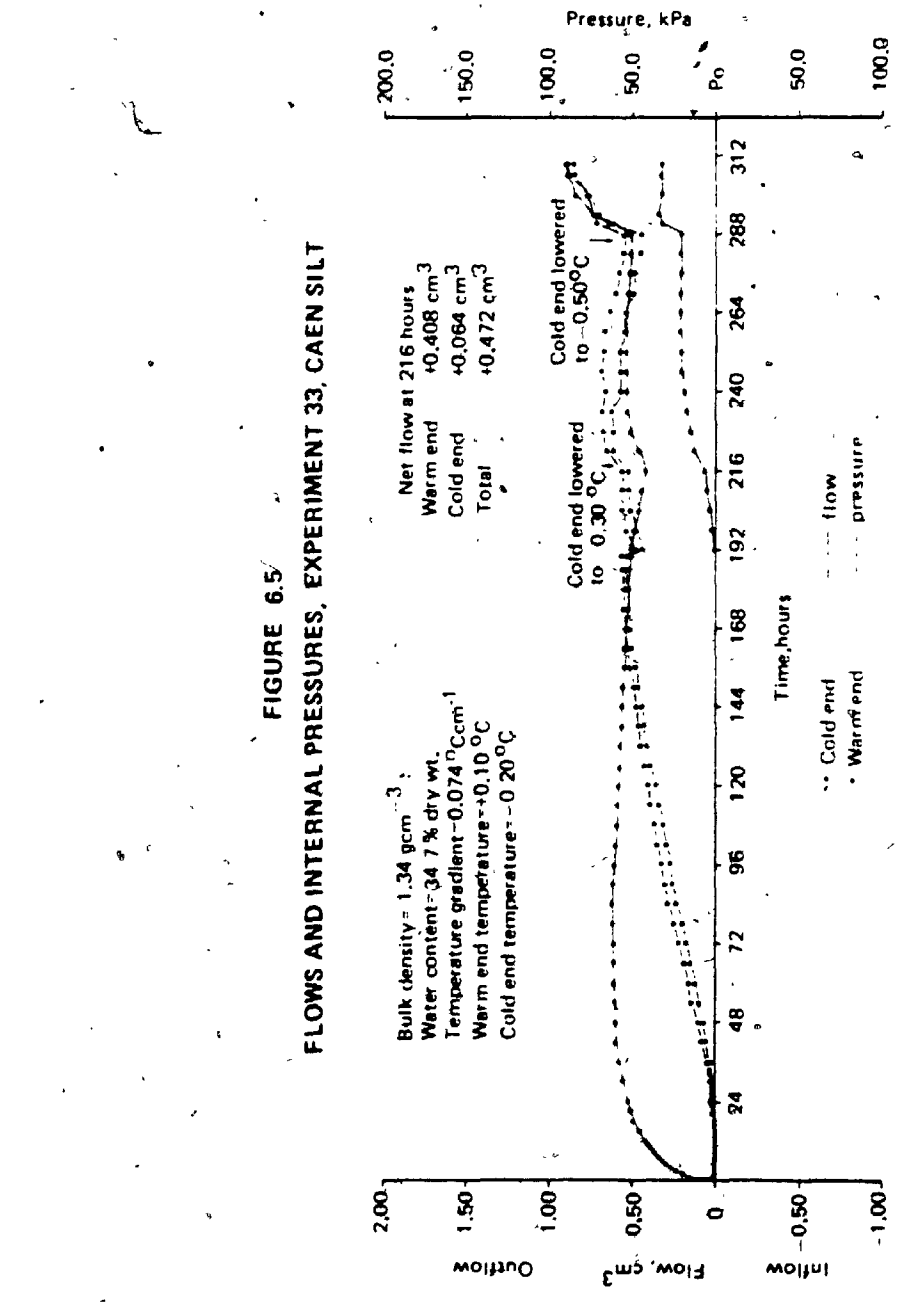

FIGURE 6.6

TEMPERATURE PROFILE DURING FREEZING, EXPERIMENT 33, CAEN SILT

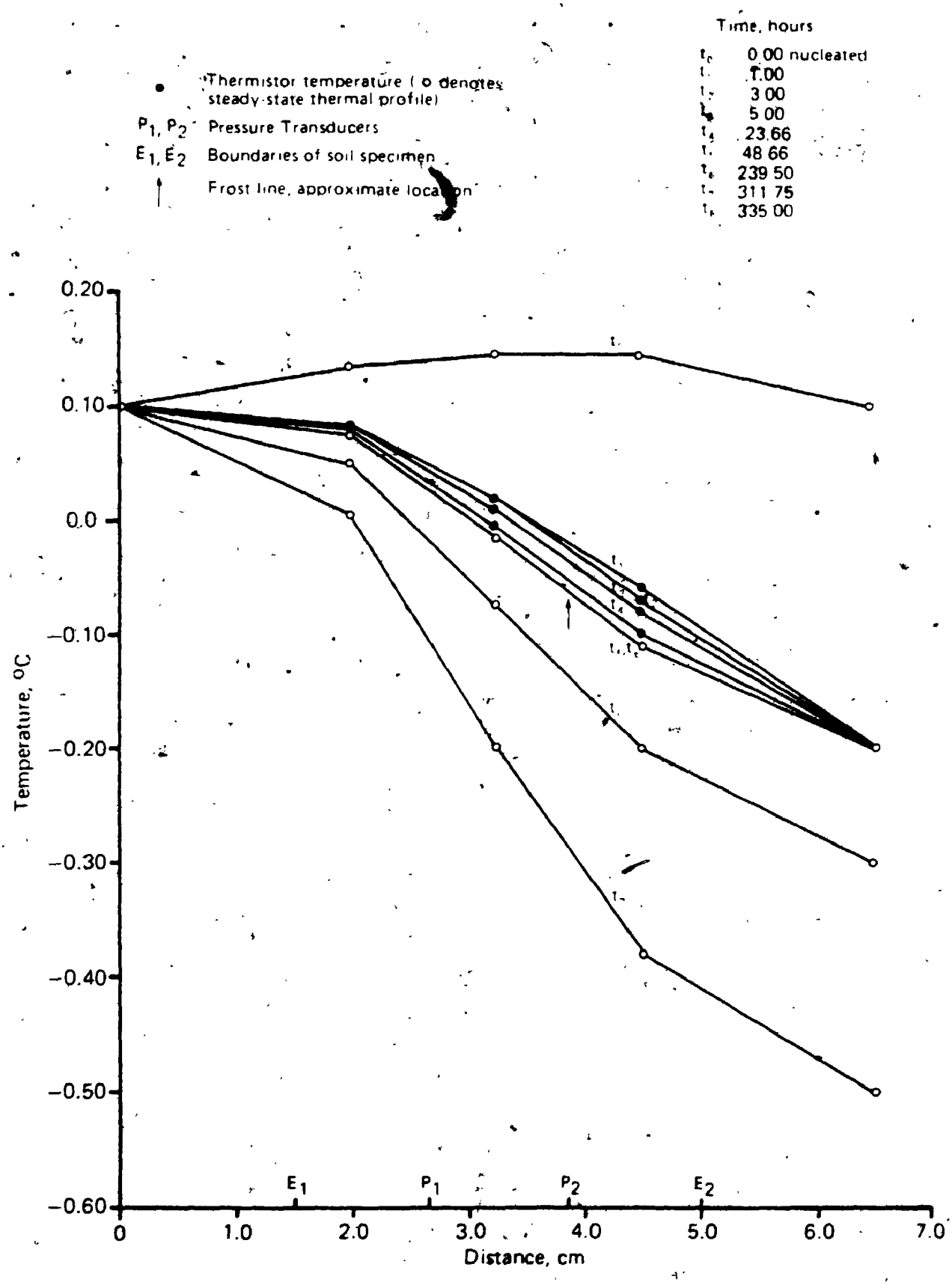

the same end temperatures (examples Table 6.4). At the colder transducer the observed pressure is slightly less than the equilibrium ice pressure (eqn. 6.2), by about 15-30 kPa. At the warmer transducer the observed pressure is usually slightly larger than the equilibrium pressure, by about 15-35 kPa, although in a few cases it is slightly less.

A certain element of potential error in the estimates of the equilibrium ice pressure is introduced as a result of the uneven topography of the frost line. Since the frost line temperature in Table 6.4 is the mean of several measurements, the temperature of the frost line at the point where the transducer is located may be slightly warmer or colder than the values indicated in the table (maximum error = ±0.02°C).[5] The maximum error in the estimate of the equilibrium ice pressure is, therefore, about (±0.02°C × 1127 kPa $°C^{-1}$) = ±22 kPa. This may account, in part, for the difference between the observed pressures and equilibrium ice pressures.

The very large difference in pressure between the two transducers (e.g. Figs. 6.1 and 6.3) can only be explained by the resistance to stress relaxation or 'strength' of the intervening material. The condition is similar to that described by eqns. 4.3 and 4.4. Stresses originating near the colder transducer are dissipated very rapidly over the relatively short distance (1.2 cm) between the two transducers. In the long-term, the increase in the strength of the material with colder temperatures must be greater than the increase in

---

[5] The location of the frost line varied by about 0.1-0.3 cm. This corresponds to a thermal variance of about 0.04°C. The potential error in the estimated temperature is therefore ±0.02°C.

the equilibrium ice pressures, otherwise the soil would tend toward an isotropic pressure distribution. Near uniform pressures actually occurred in frozen soil specimens prepared as slurries (ice contents higher than normal) and in compacted soils (ice contents lower than normal), presumably because these specimens had substantially reduced strengths.

In the normally consolidated specimens the pressures in the unfrozen zone should be isotropic because the soil has no significant strength. This is evident in exp. 33, Caen silt (Fig. 6.5) in which both transducers were located in the unfrozen zone above the frost line. The frost line stopped just short of the colder transducer because of the warmer cold-end temperature (-0.20°C). The observed pressures were almost identical at both transducers (Table 6.4). (The explanation for the positive pressures when the soil was unfrozen is discussed in section 6.6).

Figure 6.7 and 6.8 give an indication of the resistance to creep or stress relaxation for the Caen silt and also the Snec sand (data from Ladanyi and Lauzon, 1985). The creep strain is plotted at various constant applied stresses at -2°C, until failure occurs (i.e. transition from secondary to tertiary creep). With the Caen silt the transition is fairly abrupt and occurs between 800 and 900 kPa and at strains exceeding 9%. (Failure at 1000 kPa in the Snec sand, strains exceeding 3%). Since the stresses occurring in the frost pressure experiment are much lower than this, the resistance to stress relaxation offered by the soil is inversely related to the secondary creep rate. Creep data were fitted to eqn. 4.1. Parameters for secondary creep n, σ'_c and $\dot{\varepsilon}_c$, and for pseudo-instantaneous strain k, σ_k and ε_R are given in Table 6.5 (procedure, Appendix I).

FIGURE 6.7

CREEP CURVES FOR CAEN SILT AT VARIOUS APPLIED STRESSES, -2°C

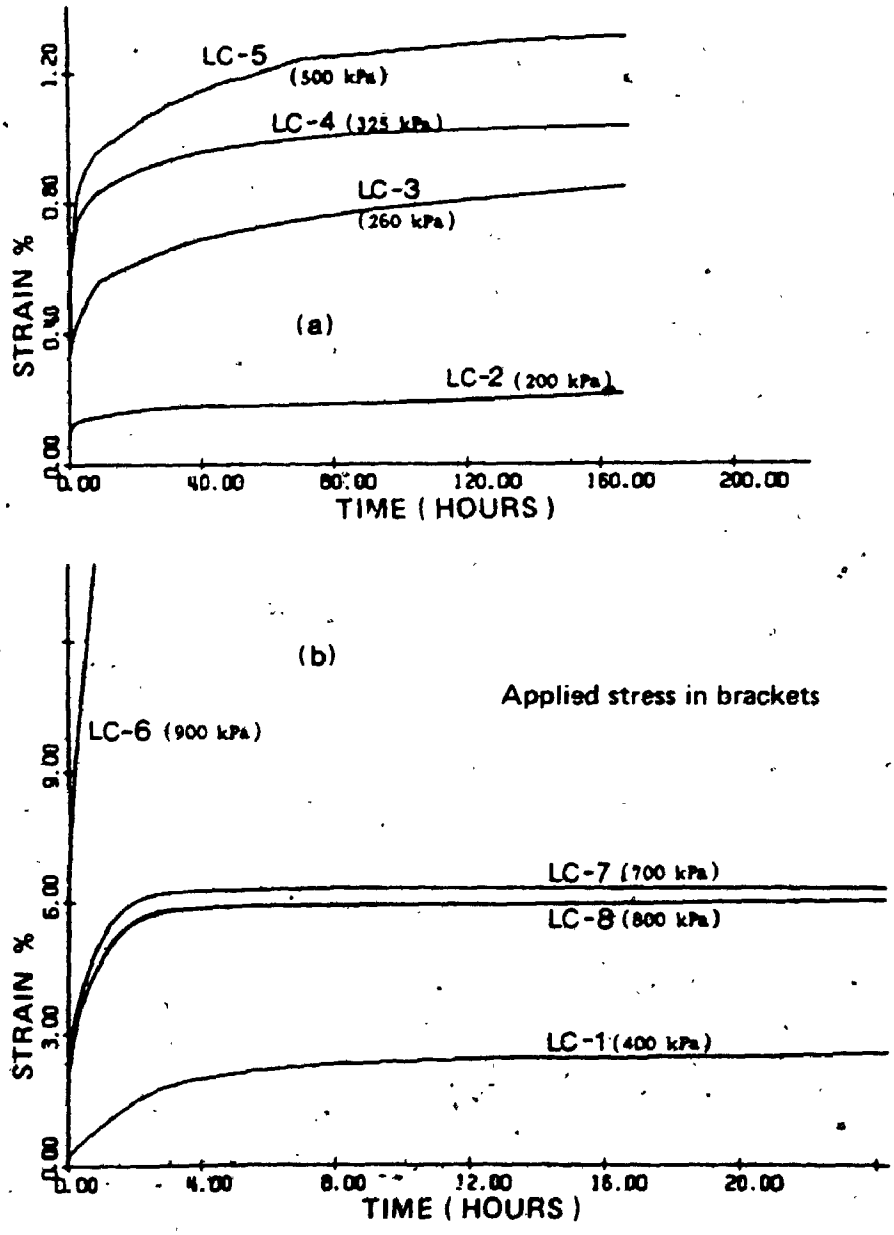

(Ladanyi and Lauzon, 1985)

FIGURE 6.8

CREEP CURVES FOR SNEC SAND AT VARIOUS APPLIED STRESSES, -2°C

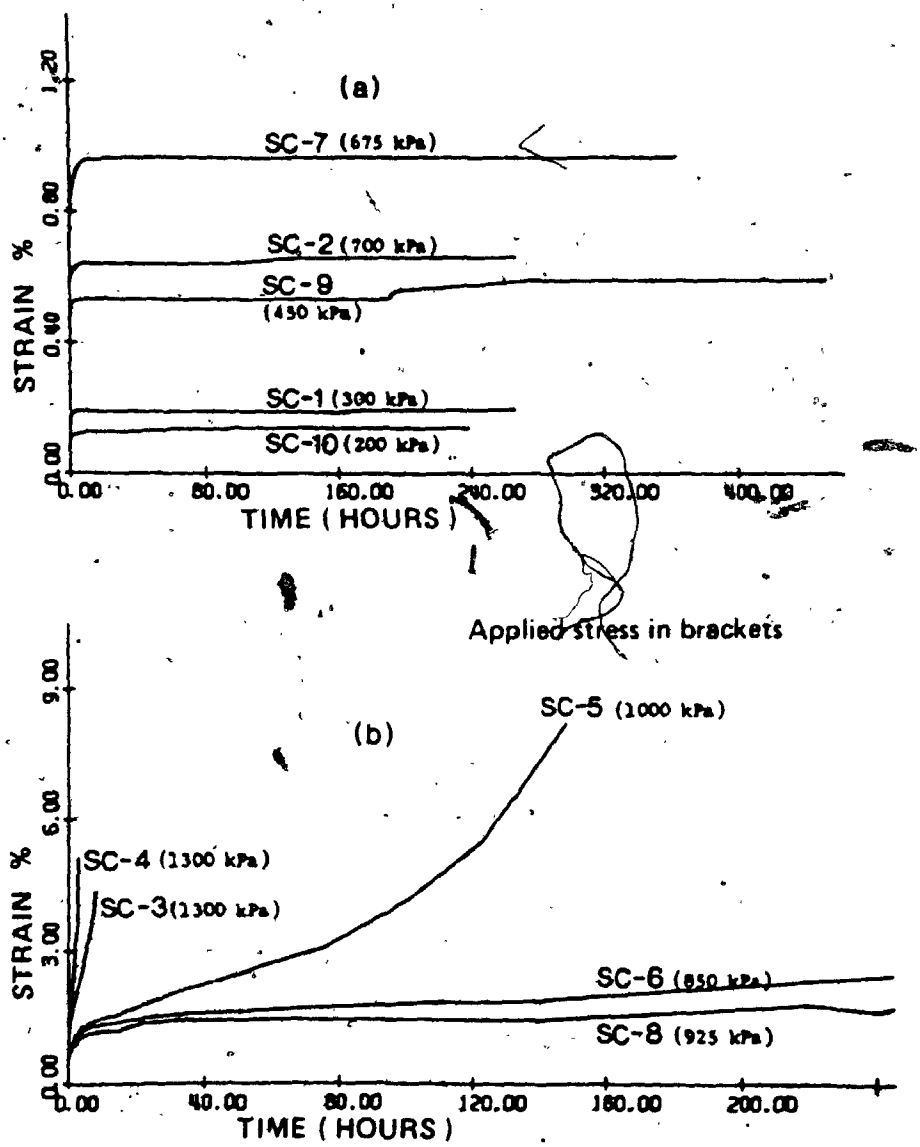

(Ladanyi and Lauzon, 1985)

Table 6.5

Creep Properties of Caen Silt and Snec Sand

Secondary Creep Parameters (eqn. 4.1)

	Caen Silt	Snec Sand	
n	10.6	5.6	14.0
σ_c	280	900 kPa	900 kPa
$\dot{\varepsilon}_c$	10^{-8} min^{-1}	10^{-6} min^{-1} ($\dot{\varepsilon}<10^{-6}$ min^{-1})	10^{-6} min^{-1} ($\dot{\varepsilon}>10^{-6}$ min^{-1})

Pseudo-Instantaneous Strain Parameters (eqn. 4.1)

	Caen Silt	Snec Sand
k	2.40	1.43
σ_k	140 kPa	170 kPa
ε_k	0.001	0.001

[Data: Ladanyi and Lauzon (1985)]

In Fig. 6.7 a load of 200 kPa on the Caen silt produced a very slow rate of secondary creep of about 0.008% day $^{-1}$.[6] This load is comparable to the long-term pressure occurring at the colder transducer. However, the rate of streess relaxation during an experiment is likely to be somewhat greater than this because the temperatures are warmer. At -0.47°C, the temperature at the cold end of the soil, 500-600 kPa seems a reasonable estimate for the strength of Caen silt, based on observations in similar materials.[7] Assuming the strength increases linearly with colder temperatures and that the unfrozen section has no significant strength, the gradient in strength of the frozen section is about 208-250 kPa cm^{-1}. This is slightly larger than the gradient in the equilibrium ice pressure, 169 kPa cm^{-1}, which is similar to the conditions described by eqn. 4.3. This explains why the gradient in the observed pressures, 150 kPa cm^{-1} (exp. 32A, Caen silt), is very close to the equilibrium ice pressure gradient.[8] Slight departures from the

---

[6] Secondary creep rate in the Snec sand = 0.002% day^{-1}.

[7] For a clayey silt similar in texture to the Caen or the Allendale soils (Table 4.1), the long-term compressive strength decreased by about 40% (350 kPa to 200 kPa) between -3°C and -0.5°C. Assuming the change is comparable in the Caen silt between -2°C and -0.47°C, the strength would decrease from 900 kPa to about 540 kPa.

[8] Since the thermal gradient is linear, changes in the strength σ, equilibrium ice pressure P_i, and observed pressure P, are expressed as a function of distance rather than temperature:
$\frac{\delta\sigma}{\delta z} = \frac{500 \text{ kPa}}{2.4 \text{ cm}} = 208 \text{ kPa cm}^{-1}$, $\frac{\delta P_i}{\delta z} = \frac{220 \text{ kPa} - 17 \text{ kPa}}{1.2 \text{ cm}} = 169 \text{ kPa cm}^{-1}$,
$\frac{\delta P}{\delta z} = \frac{170 \text{ kPa}}{1.2 \text{ cm}} = 150 \text{ kPa cm}^{-1}$. Thickness of frozen section exp. 32A = 2.4 cm. Distance between transducers = 1.2 cm.

equilibrium ice pressure gradient probably occur because of a very slow movement of the ice toward warmer temperatures. The respective differences between the gradient in the equilibrium ice pressure and the observed pressure gradient are similar in the other experiments with normally consolidated soils (e.g. 164 kPa cm^{-1} and 152 kPa cm^{-1}, exp. 42A, 155 kPa cm^{-1} and 117 kPa cm^{-1}, exp. 35, 155 kPa cm^{-1} and 144 kPa cm^{-1}, exp. 34, 164 kPa cm^{-1} and 152 kPa cm^{-1}, exp. 30).

6.6 Stress Relaxation and Consolidation During Transient Thermal Conditions

Figures 6.9 and 6.10 show the changes in the pressure at the transducers bladders as the temperature of the bladders decreased during transient thermal conditions (frost line advancing). The pressures did not begin to rise until about 3 or 4 hours after freezing began because the frost line was still fairly close to the cold end of the soil. Eventually, the pressures started to increase and this continued even after the system reached a quasi-steady-state (i.e. a stable temperature gradient). This is indicated in Figs. 6.9 and 6.10 by changes in pressure at constant temperature (numbers accompanying points are the time, in hours, since freezing began). It is interesting that the pressure at the colder transducer did not begin to rise until the frost line was well past the rubber bladder. In contrast, the pressure increased considerably at the warmer transducer before the frost line reached the bladder. The following explanation is suggested.

During the first 3 or 4 hours of freezing, the unfrozen soil is highly compressible and so it does not provide any reactive stress to the enlargement of ice lenses. The pressures, therefore, are unable to rise. Any tendency for the frozen section to push on the unfrozen soil

FIGURE 6.9

PRESSURE AS A FUNCTION OF BLADDER TEMPERATURE, EXPERIMENT 32A, CAEN SILT

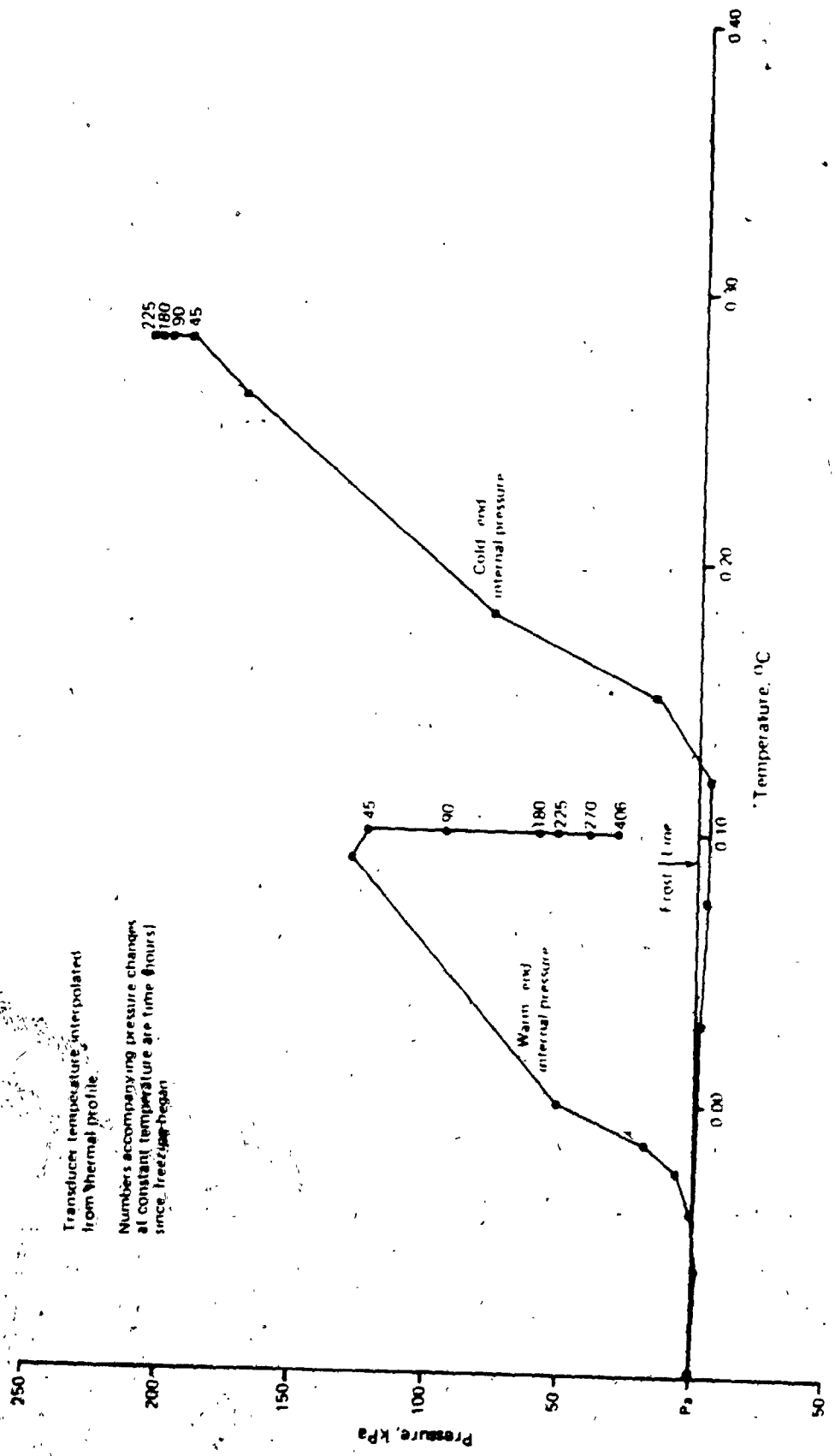

FIGURE 6.10

PRESSURE AS A FUNCTION OF BLADDER TEMPERATURE, EXPERIMENT 30, ALLENDALE CLAY

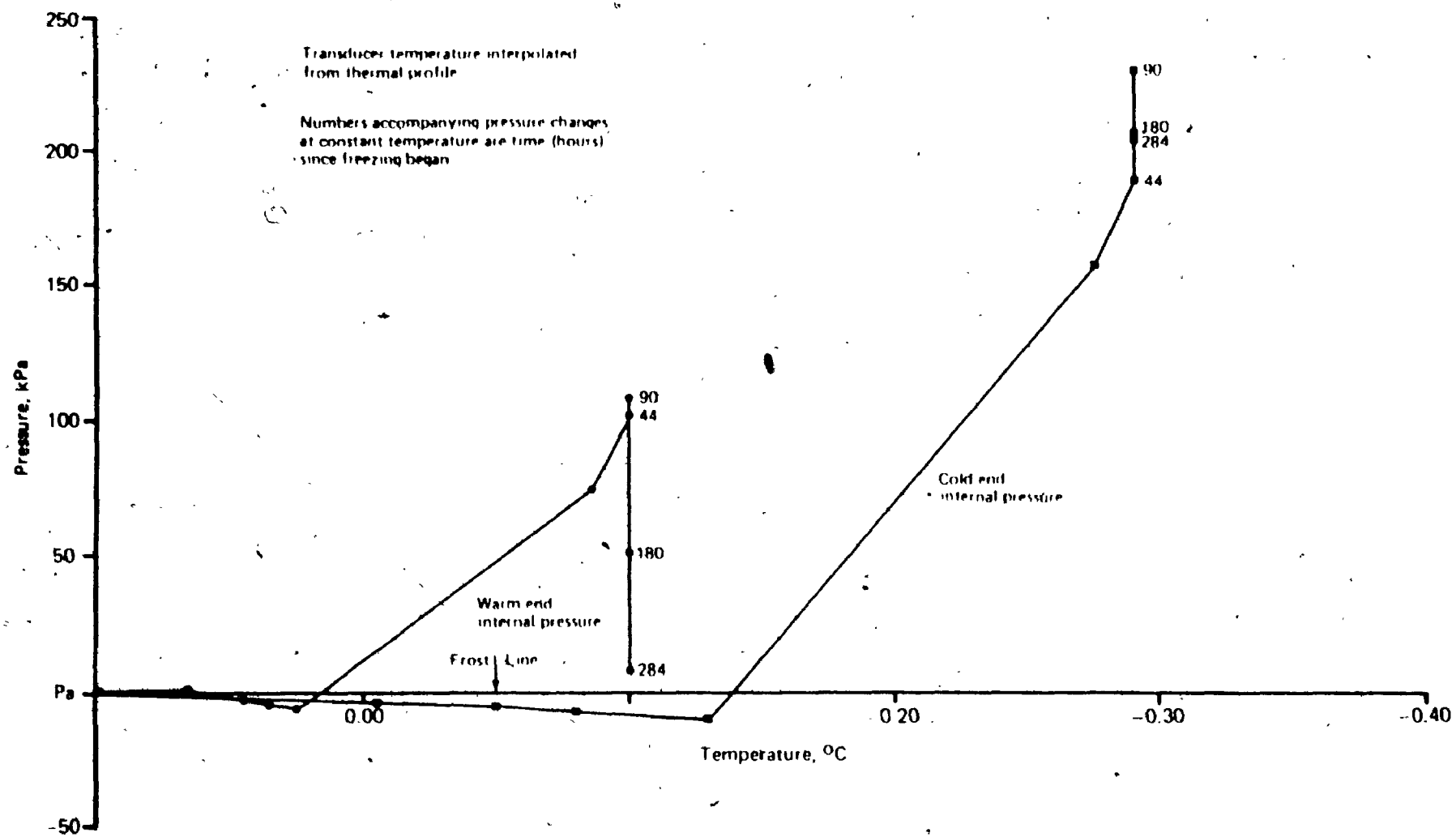

FIGURE 6.11
PRESSURE AS A FUNCTION OF BLADDER TEMPERATURE, EXPERIMENT 33, CAEN SILT

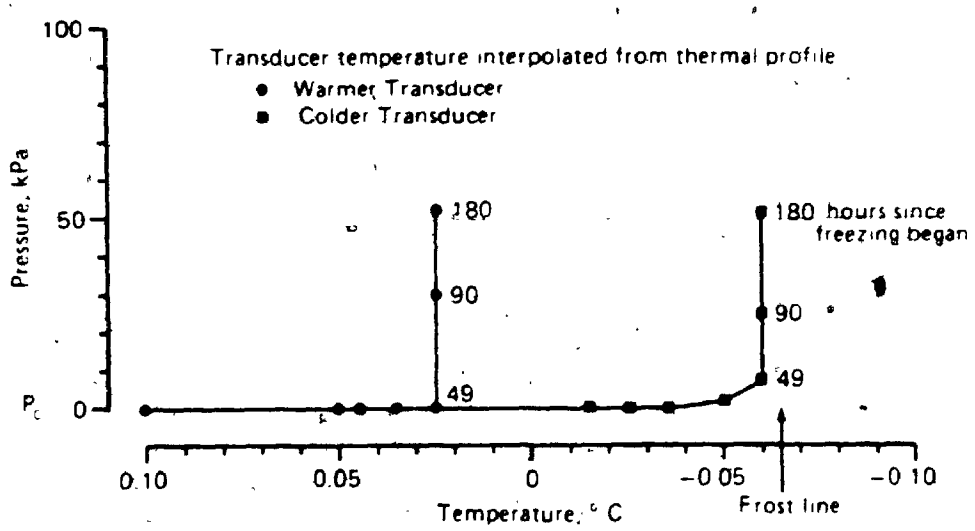

is transmitted immediately to the pore water in the unfrozen zone, which then flows out at the warm end. After the frost line advances past the colder transducer, the pressures are still unable to rise until the transducer is about 0.04°C to 0.08°C behind the frost line. This may be because the frozen zone close to the frost line has little strength during the transient thermal stage (i.e. it behaves in a quasi-viscous manner with the conditions similar to those described by eqns. 4.5 and 4.6). After the temperature stops decreasing, the strength increases so that conditions approach the semi-rigid type of behaviour described by eqns. 4.3 and 4.4.

As successive ice lenses form, consolidation of the unfrozen section reaches a limit and the stresses begin to be transmitted to the soil skeleton. Internal pressures rise rapidly at the warmer transducer although the frost line has not yet reached the rubber bladder. A similar situation evidently occurred in exp. 33 (Fig. 6.11), which explains why the internal pressures increased although both transducers remained within the unfrozen section (equilibrium ice pressures = 0 kPa, Table 6.4).

In order for a large positive pressure to occur at the warmer transducer while it remains in the unfrozen zone, it is evident that some form of quasi-viscous behaviour must occur in the warmer regions of the frozen section, otherwise the pressure would not rise at all. After the frost line reaches the warmer transducer, the pressure which occurs initially (i.e. peak pressure) is far in excess of the ice pressure required for thermodynamic equilibrium at the transducer temperature (Table 6.4). If it is assumed that the soil between the warmer transducer and the point of origin of the pressure offers no resistance

to deformation (at least initially), the temperature of origin of the peak pressure can be estimated by rewriting eqn. 6.2 as:

$$T = T^* - \frac{P_i}{\left(\frac{\delta P_i}{\delta T}\right)} \qquad 6.3$$

For example, in exp. 32A (Fig. 6.9) the maximum pressure at the warmer transducer is 130 kPa. Equation 6.3 indicates that the pressure originates at $-0.090°C - (130\ kPa/1127\ kPa\ °C^{-1}) = -0.205°C$. This is about 0.75 cm behind the frost line (distance interpolated from the steady-state thermal profile, Fig. 6.2). Similarly, in exp. 30 (Fig. 6.10), the maximum pressure at the warmer transducer (112 kPa) suggests a temperature of origin at -0.147°C, which is about 0.5 cm behind the frost line. In exp. 33 (Fig. 6.11), a pressure of 52 kPa at both transducers indicates a temperature of origin of the stress at -0.111°C, which is 0.60 cm behind the frost line.

Further evidence that the frozen soil just behind the frost line does not offer much resistance to deformation can be seen in Fig. 6.5. When the cold end temperature was later lowered from -0.2°C to -0.3°C, this caused the frost line to advance past the colder transducer and stop just short of the warmer transducer. The internal pressure of the two transducers did not diverge much although this might be expected if the frozen layer between the transducers offered significant resistance to deformation.

The analysis using eqn. 6.3 above is based on the assumption that the soil in the frozen zone at temperatures warmer than T, moves by a quasi-viscous (fluid-like) creep. T describes the temperature of transition between semi-rigid and quasi-viscous behaviour. At colder temperatures the soil's resistance to stress relaxation is sufficient to

prevent stresses from being transmitted to the warmer regions altogether. In reality, however, the transition is probably not as abrupt as this. At warmer temperatures there is probably some resistance offered by the frozen soil although this would be small. At colder temperatures the material is not perfectly rigid because of a very slow creep of the ice.

6.7 Pressure Changes and Flows During Quasi-Steady-State Conditions

A thermal steady-state was reached about 24-48 hours after freezing began. In most cases, the rubber bladder at the warmer transducer was located in the frozen soil just behind the frost line. (In some instances, the bladder was only half in the frozen soil). The pressure then began to fall continuing for about 9 or 10 days after this. There are 3 possible reasons:

(1) Initially, the frozen soil is unable to sustain completely the gradient in the thermodynamically generated (equilibrium) ice pressures (eqn. 6.2). As a result ice lenses in the warmer half of the frozen section (that is, above the colder transducer) experience pressures considerably higher than the equilibrium ice pressure. This results in gradual pressure-melting as the system attempts to restore thermodynamic equilibrium. (This possibility was discussed in chapter 4.2).

The 9.1% volume decrease due to pressure-melting of ice lenses would account for the steady influx of water at the warm end after the

frost line stopped advancing.[9] The influx is difficult to account for by any other mechanism. The pressures would increase if the influx of water were changing to ice.[10] The volume of ice melted can be calculated from the flow of water into the warm end (eqn. 6.1). For example, in exp. 32A (Fig. 6.1), the total influx over a period of 10 days was 0.37 cm^3, which is equivalent to melting about 4.07 cm^3 of ice. This is 23.3% of the volume of ice originally formed within the soil. (Examples from other experiments, Table 6.6).

This explanation is compatible with the observation that ice lenses steadily increase in thickness toward warmer temperatures, but then diminish rather abruptly to a hair's breadth at about the mid-point of the soil specimen (i.e. a few millimeters behind the frost line). Normally, in frost heaving of unconfined soils, the thickest ice lenses are the last to form and are the closest to the frost line.

---

[9] It has been suggested that the high pressures occurring at the warmer transducer are caused by an increase in the pore water pressure of the unfrozen section during freezing, because water cannot flow out of the soil rapidly enough to dissipate the rising pressure. If this is the reason, water should continue to flow out of the soil at the warm end as the pressure at the warmer transducer falls. The observed flow, however, was in the opposite direction.

[10] It has also been suggested that the inflow at the warm end may be due to an osmotic gradient at the cold end caused by lactose concentrations in the reservoir which are too high. However, this would not explain the observations of significant inflows at the warm end where there was no lactose solution in the cold reservoir (exp. 44, 44A, 44B, 34 and 35). In these experiments there was no flow at the cold end because the semi-permeable membrane was replaced by an impermeable rubber or foil barrier.

Table 6.6

Internal Pressure-Melting Data for Several Experiments

Soil	Caen	Caen	Caen	Allendale	Caen[1]	Caen[2]	Caen[3]
Exp.	32A	42A	35	30	43A	33	44B
V_u	0.37	0.33	0.31	0.32	0.21	0.21	0.16
V_m	4.07	3.63	3.41	3.52	2.31	2.31	1.76
V_i	17.5	16.7	12.5	9.23	20.22	6.70	19.2
ΔV	23.3	22.2	27.2	38.1	11.4	34.5	9.1

[1] Slurry

[2] Cold-end temperature, -0.20°C

[3] Cold-end temperature, -0.70°C

V_u = total influx of water at warm end after frost line stopped advancing, cm^3

$V_m = V_u \times \frac{100}{9.1}$ = volume of ice melted, cm^3 (eqn. 6.1)

V_i = initial volume of ice formed in soil, cm^3 (from Table 6.3)

$\Delta V = \frac{V_m}{V_i} \times 100$ = decrease in ice volume, %

The decline in pressure at the warmer transducer was about 100 kPa. The pressure gradually levelled off as it approached the equilibrium ice pressure. This possibility was not considered in the model described earlier (chapter 4.2). The soil was viewed as continuously attempting to reach a state of thermodynamic equilibrium, but unable to attain this state because of continued stress relaxation. Evidently, the water from melted ice lenses is not redistributed toward the cold end as suggested in chapter 4.2. If the melted water was refreezing near the cold end, there would be no inflow at the warm end. The continuous inflow at the warm end after the pressure levelled off probably occurred because of sequential pressure-melting of ice lenses at slightly colder temperatures further away from the warmer transducer.

(2) An additional reason for the decline in pressure may be an increasing resistance to stress relaxation with time, possibly as result of strain hardening. The pressures then begin to diverge according to the increase in strength. Strain hardening is caused by increasing interference between crystals during creep, which progressively acts to resist further deformation. However, this explanation alone does not account for the inflow at the warm end.

(3) A third possibility is that some combination of the above two effects occurs simultaneously. Pressures decline at the warmer transducer because of pressure-melting of warmer ice lenses, as well as the increasing resistance to stress relaxation with time.

6.8 Water Pressures and Hydraulic Gradients During Freezing

If the ice pressure is unable to rise, the Clausius-Clapeyron eqn. indicates that unfrozen water pressures become increasingly negative with lower temperatures. Frost heaving is explained as a result of water migrating along a pressure gradient in the direction of colder temperatures. In this experiment, however, the opposite conditions occur. At the start of the experiment water flows out of the soil at the warm end, implying positive pore water pressures and pressure gradients in the direction of warmer temperatures. The situation is not the same because the soil is confined. In a confined soil, the juxtaposition of ice and water is achieved by a rise in ice pressure while the unfrozen water pressure remains unchanged at atmospheric pressure. Volume expansion of water during freezing prohibits negative pore water pressures from developing. Any tendency for the water pressure to rise above atmospheric results in immediate outflow. The rate of outflow is controlled by the rate of advance of the frost line (this is shown in Fig. 6.12, next section).

As the frost line advances, the liquid pressures are probably slightly positive (greater than atmospheric) because of the impedance to flow of the soil itself and also the semipermeable membrane. After freezing stops, the soil begins to draw in water because of internal pressure-melting. In this case, the unfrozen water pressure must be slightly negative (i.e. less than atmospheric). However, departures of more than a few kPa from atmospheric pressure cannot occur, otherwise the ice pressures would be considerably lower. Hydraulic gradients, therefore, must be very small compared to the ice pressure gradient. Assuming Darcy's law (eqn. 2.2) remains valid for frozen soils, it

should be possible to calculate the hydraulic gradient established within the soil associated with the inflow at the warm end. For example, in exp. 32A (Fig. 6.1), the influx $J = 1.23 \times 10^{-8}$ cm s^{-1} (inflow = 0.37 cm^3 in 365 hours) and the overall hydraulic conductivity of the soil $K = 8.5 \times 10^{-10}$ cm s^{-1} (Fig. 7.6).[11] The hydraulic gradient $i = J/K = 14.5$ cmH_2O cm^{-1} = 1.42 kPa cm^{-1}, which is a very low value indeed.

6.9 Significance of Frost Line Temperature to the Pressures Established

Figure 6.12 shows the relative locations of the frost line for the different soils used in the experiments. This was much closer to the warm end in the Snec sand than the other two soils (temperature -0.020°C). This is because of lower natural solute concentrations in the sand and also larger pores sizes. It is interesting that the frost line was closer to the warm end in the Allendale day (temperature -0.050°C) than in the Caen silt (-0.090°C). The reverse might be expected to occur because of the smaller pore sizes in clays.[12] The lower freezing temperature for the silt is probably a result of the

---

[11] Measurement of the overall hydraulic conductivity of the soil with a temperature gradient is described in chapter 7.

[12] The temperature limits the size of a stable ice crystal. The relationship is described by the Thompson eqn. In theory, at least, ice cannot form in pores unless the pore size is larger than that of a stable ice crystal. This does not occur until a critical temperature is reached.

FIGURE 6.12
ADVANCE OF FROST LINE AND OUTFLOW FROM WARM END DURING FREEZING

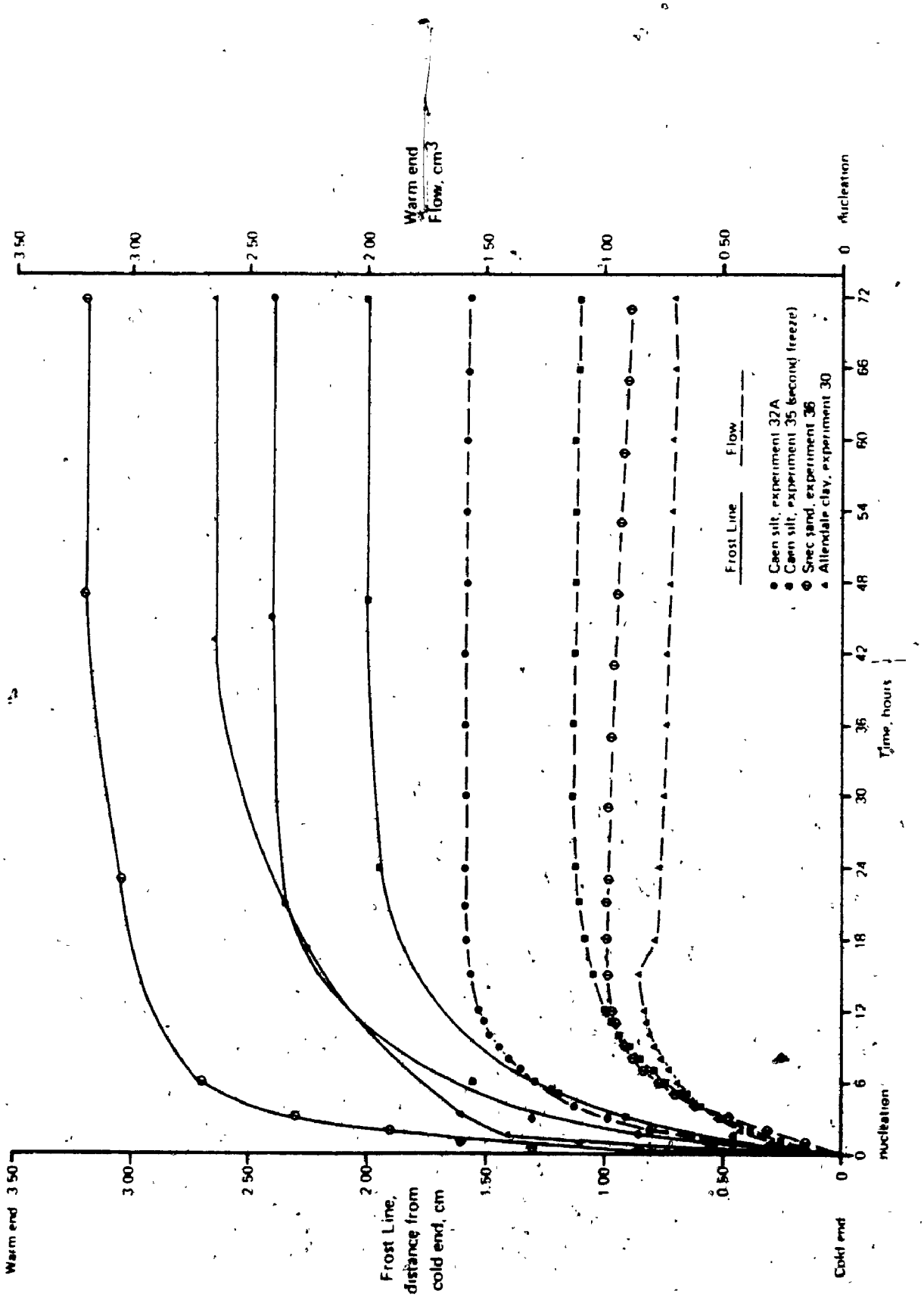

overriding influence of dissolved $CaCO_3$ in significant amounts in the silt (see mineralogy, Table 5.1).[13]

It is interesting that the frost line temperature varied by as much as 0.030°C in different experiments with the same type of soil. Since the frost line forms at the natural freezing-point depression of the soil, in principle, the location of the frost line should be independent of the thermal conditions. Variations in the freezing-point depression are probably a result of different amounts of dissolved solutes in the pore water of each individual soil specimen and possibly also because of slightly different pore size distributions. Small variations in the thermal gradient were also observed in different experiments although the cooling plate temperatures were the same. This is due to small changes in the thermal properties of each soil specimen, as well as the efficacy of the thermal contact between the soil specimen and the cooling plate at the cold end.

The variance in the temperature of the frost line as well as the temperature gradient in each experiment has a considerable effect on the internal pressures. For example, in exp. 35 (Table 6.4), the internal pressure at the colder transducer appears to be about 50 kPa lower than in the other experiments with normally consolidated Caen silt at the same end temperatures. This is partly a result of the increased thermal impedance of the cooling plate which slightly reduced the thermal gradient. (The cold reservoir was filled with mercury, see section 6.13). Allowing for the slightly colder frost line and also

---

[13] Although the Allendale clay is probably marine in origin, subsequent leaching over a very long period of time may have reduced the solute concentration so that the freezing-point depression was not very large.

slightly warmer soil temperatures overall, the equilibrium ice pressure at the cold transducer is 186 kPa.[14] This is slightly greater than the observed pressure, which is consistent with the findings in the other experiments.

6.10 Reversal of Thermal Gradient

It is important to establish that the pressure differences are not an artefact of the experimental apparatus itself. A convincing demonstration that this is not the case was done by reversing the direction of the thermal gradient after the pressure difference was established (Fig. 6.13). The internal pressures rapidly equalized and then slowly began to diverge in accordance with the new direction of the thermal gradient. The pressure at the warmer* transducer, following the reversal, was only about half the value established previously and also increased at a much slower rate. This can be attributed to a fairly thick central section (about 1.2 cm) which remained frozen during the reversal. This impeded the flow of water, from melting ice lenses near the warmer* transducer (originally the colder transducer), to new ice lenses forming near the colder* transducer (originally the warmer transducer). At the warmer* transducer, which remained in the frozen section slightly behind the frost line, the pressure declined steadily to atmospheric pressure.

The re-establishment of pressure at the colder* transducer following the reversal is evidence of secondary frost heaving. Before the reversal, the colder* transducer was located in the frozen zone just

---

[14] There may be a small error in the frost line temperature (-0.090°C) in exp. 35 because some thawing occurred before the location of the frost line was measured.

*After the temperature gradient reversal.

FIGURE 6.13

FLOWS AND INTERNAL PRESSURES, EXPERIMENT 39B, CAEN SILT, TEMPERATURE GRADIENT REVERSED

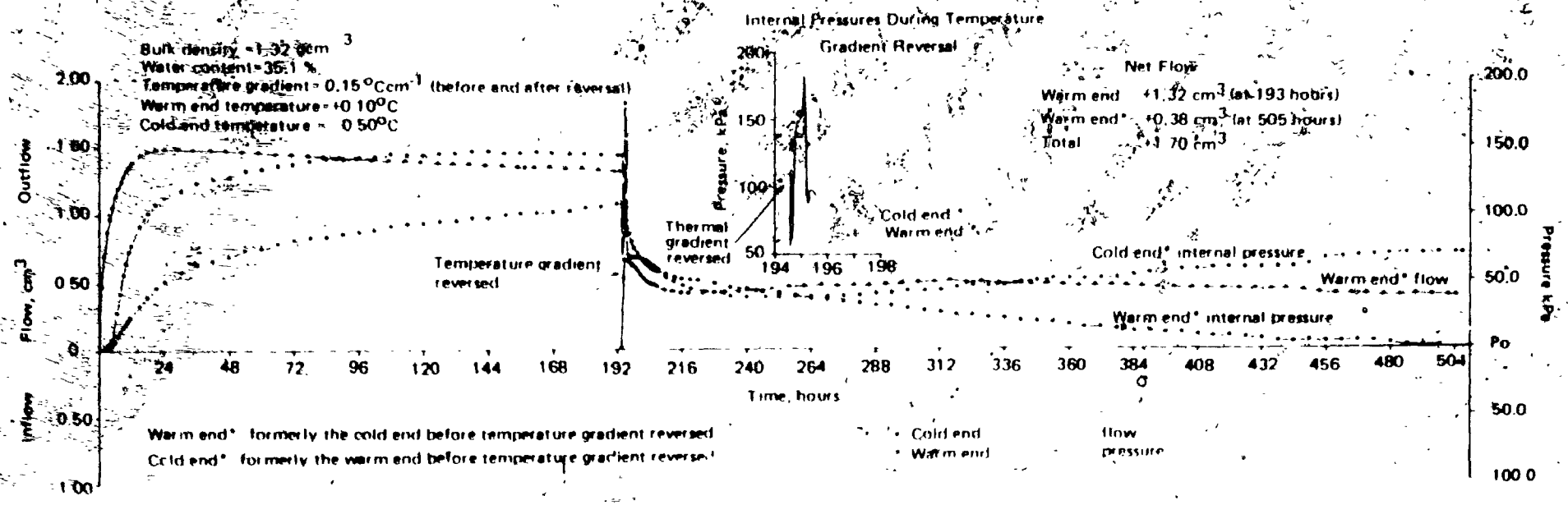

FIGURE 6.14

TEMPERATURE PROFILE DURING FREEZING, EXPERIMENT 39B, CAEN SILT

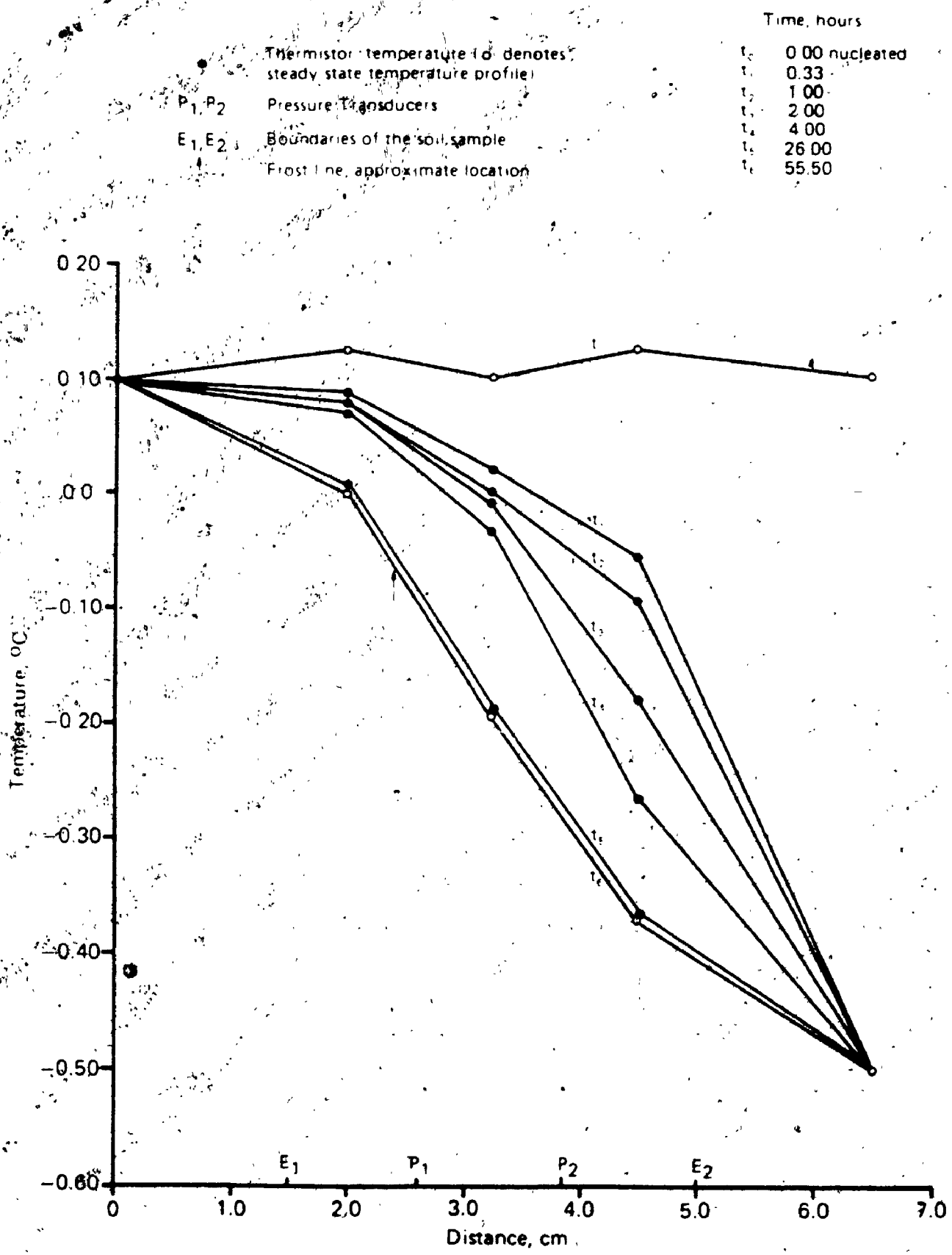

FIGURE 6.15

REVERSAL OF THERMAL GRADIENT, EXPERIMENT 39B, CAEN SILT

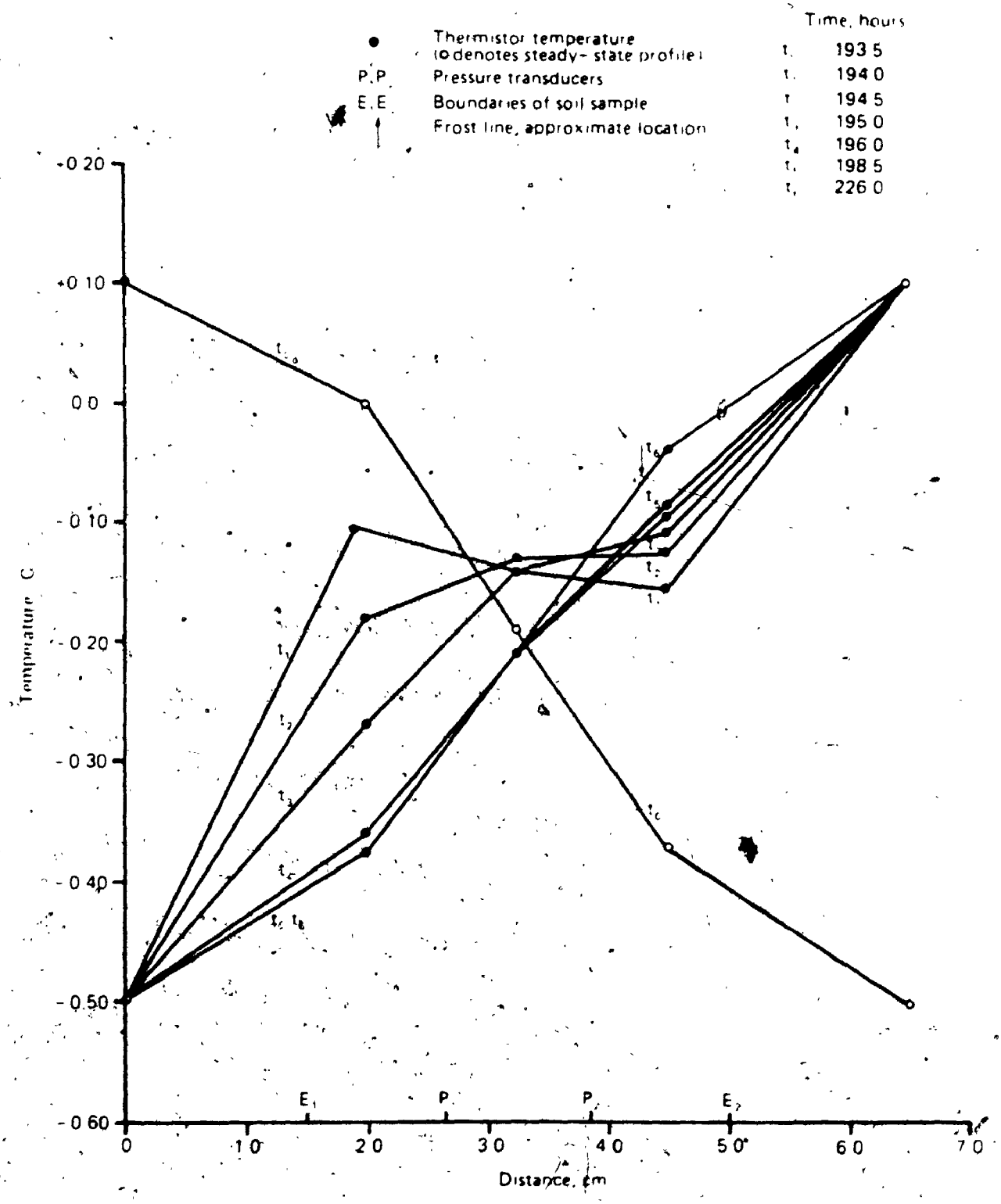

behind the frost line although there were no ice lenses in the immediate vicinity of the bladder. When the cell was dismantled, the colder* transducer was surrounded by ice lenses. In order for these ice lenses to form water must have moved toward colder temperatures, through the central frozen section, including any existing ice lenses. (The colder* reservoir was emptied of water just before the temperature gradient reversal so the soil had access to a water supply at the warm* end only). The ice lenses which formed near the colder* transducer appeared thin and poorly developed compared to those normally observed. This can be attributed to the impedance to flow of the central frozen section.

An interesting phenomenon is the abrupt fall and then rise in the pressure in the first 30 minutes after the thermal gradient was reversed (see inset, Fig. 6.13). The sudden fall in pressure probably occurs as a result of rapid thawing at the cold* end, as well as a slight rise in the soil temperature overall, for a short period after the reversal.[15] Immediately after this, however, the central frozen section, which remains colder than the extremities of the soil, acts as a heat sink for a brief period. Unfrozen water then flows along suction gradients temporarily established toward the central frozen section and freezes there, causing the ice pressures to rise briefly. As the water

---

[15] The equilibrium ice pressure, at the mean temperature of the frozen section, 30 minutes after the reversal, is about 68 kPa. This is approximately the mean observed pressure of the two transducers.

freezes, releasing latent heat, the soil warms and the pressure then falls off.[16]

To avoid complications, lactose solution, was not used in the cold reservoir during the experiment. The soil had access to water only at the warm end (i.e. the cold reservoir was left empty). The chief problem with lactose is that it diffuses slowly through the membrane in small quantities, thawing a thin layer of soil at the cold end. If the thermal gradient is then reversed, the sugar molecules quickly diffuse through the soil when it warms up, reducing the internal pressures.

It is interesting that the flow of water at the warm end reversed direction three times after the thermal gradient was reversed. The soil expelled water rapidly (0.68 cm^3) for an hour and then began to draw in water for the next 24 hours. The flow then reversed and a small amount (0.08 cm^3) flowed out for the next 4 days and then reversed again and started to flow into the soil, at a steady rate, for the remainder of the experiment. Outflow of water implies that the rate at which ice is forming exceeds the rate at which it is thawing, whereas inflow indicates the opposite conditions. Since there was a net outflow from the soil after the temperature change (0.38 cm^3 at 505 h), the ice content of the soil must have increased. Ice enrichment presumably took place in the central frozen section after the temperature change because the ice lenses near the cold* end were thin and poorly developed.

---

[16] Freezing in the central frozen section only occurs for a short period, at most, until the temperature reaches the natural freezing temperature of the soil. A similar phenomenon is apparent in exp. 35 (Fig. 6.24). After the cooling unit was switched off the pressure abruptly increased by about 30 kPa at both transducers. This is a result of water flow toward the interior of the soil, where it freezes. This occurs while the interior remains colder than the extremities.

6.11 Effect of Changes in Soil Density

Pressure differences established within the soil were highly sensitive to changes in soil density and porosity. Results with soil specimens in which the density was increased ('incompressible soils') or reduced ('slurries'), show similarities with each other and also some rather striking differences compared to normally consolidated specimens. This can be explained in terms of the effect of changes in the bulk density on the ice content of the soil. This, in turn, affects its resistance to stress relaxation.

Experiments with incompressible soils included Snec sand (Fig. 6.16), packed to a density of 1.88 g cm^{-3}, which is 92% of the absolute maximum density, and Caen silt (Fig. 6.17), prepared by Proctor compaction to a density of 1.73 g cm^{-3}, which is 96% of the absolute maximum (compaction procedure, Appendix J).[17] The density of the silt was 28% higher than the normally-consolidated specimens.

The slurries were prepared as saturated and de-aired soil specimens which were then agitated to form a suspension and decanted into the frost pressure cell. With the silt specimen (Fig. 6.18), freezing was initiated immediately after the cell was fully assembled, before the soil had a chance to settle out to form a sediment. The density of the silt was 1.17 g cm^{-3}, which is 18% lower than in the normally consolidated specimens. The Allendale clay (Fig. 6.19) was allowed to settle out, prior to freezing, so that a layer of supernatant water about 0.4 cm thick collected on top of the sediment. Experiments were carried out at the same end temperatures as the experiments with the normally-consolidated specimens (i.e. +0.10°C and −0.50°C).

---

[17] Thermal profiles Appendix K.

Table 6.7

Observed Pressures and Equilibrium Ice Pressures
for Incompressible (Compacted) Soils and for Slurries

Incompressible Soils

Soil	Caen		Snec	
Exp.	31		36	
T_f	-0.065		-0.020	
T	-0.080	-0.265	-0.120	-0.275
P_i	23	225	113	287
P	104	138	47	147

Slurries

Soil	Caen		Allendale	
Exp.	43A		29	
T_f	-0.060		-0.080	
T	-0.120	-0.300	-0.110	-0.290
P_i	68	271	34	237
P	75	36	48	138

T_f = frost line, average temperature, °C
T = mean temperature of transducer, °C
P_i = equilibrium ice pressure eqn. (6.2), kPa
P = observed long-term pressure, kPa

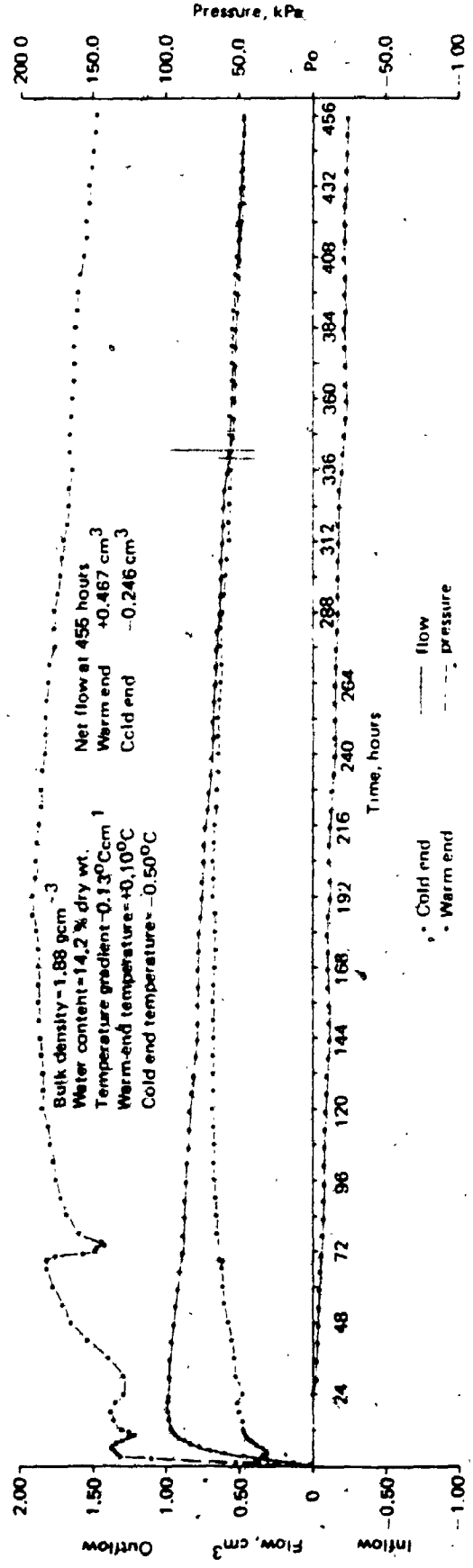

FIGURE 6.16

FLOWS AND INTERNAL PRESSURES, SNEC SAND, EXPERIMENT 36

FIGURE 6.17

FLOWS AND INTERNAL PRESSURES, COMPACTED CAEN SILT, EXPERIMENT 31

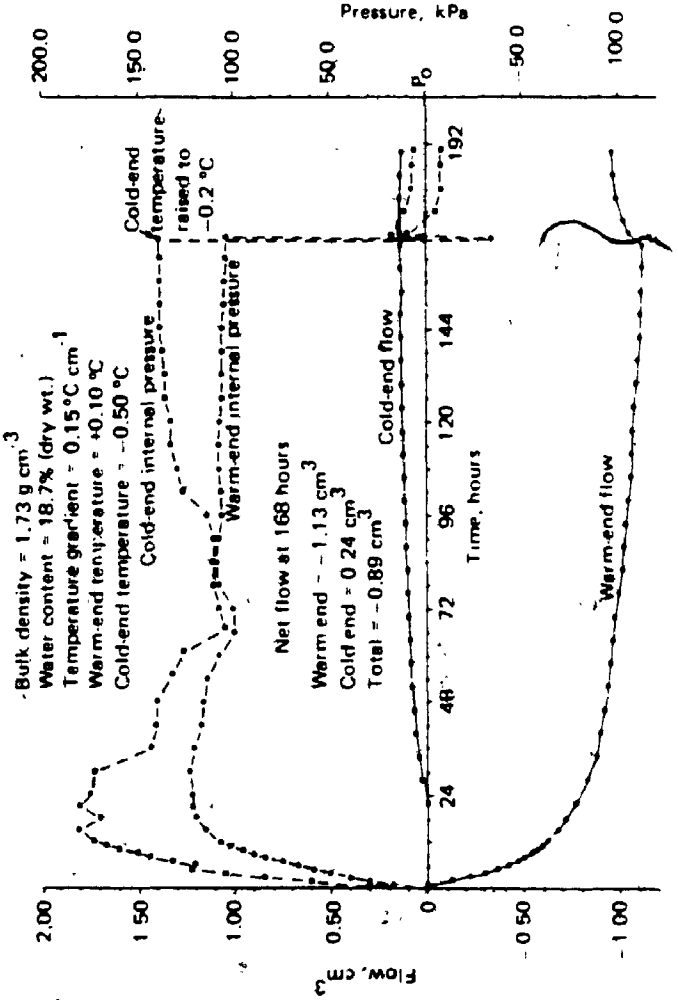

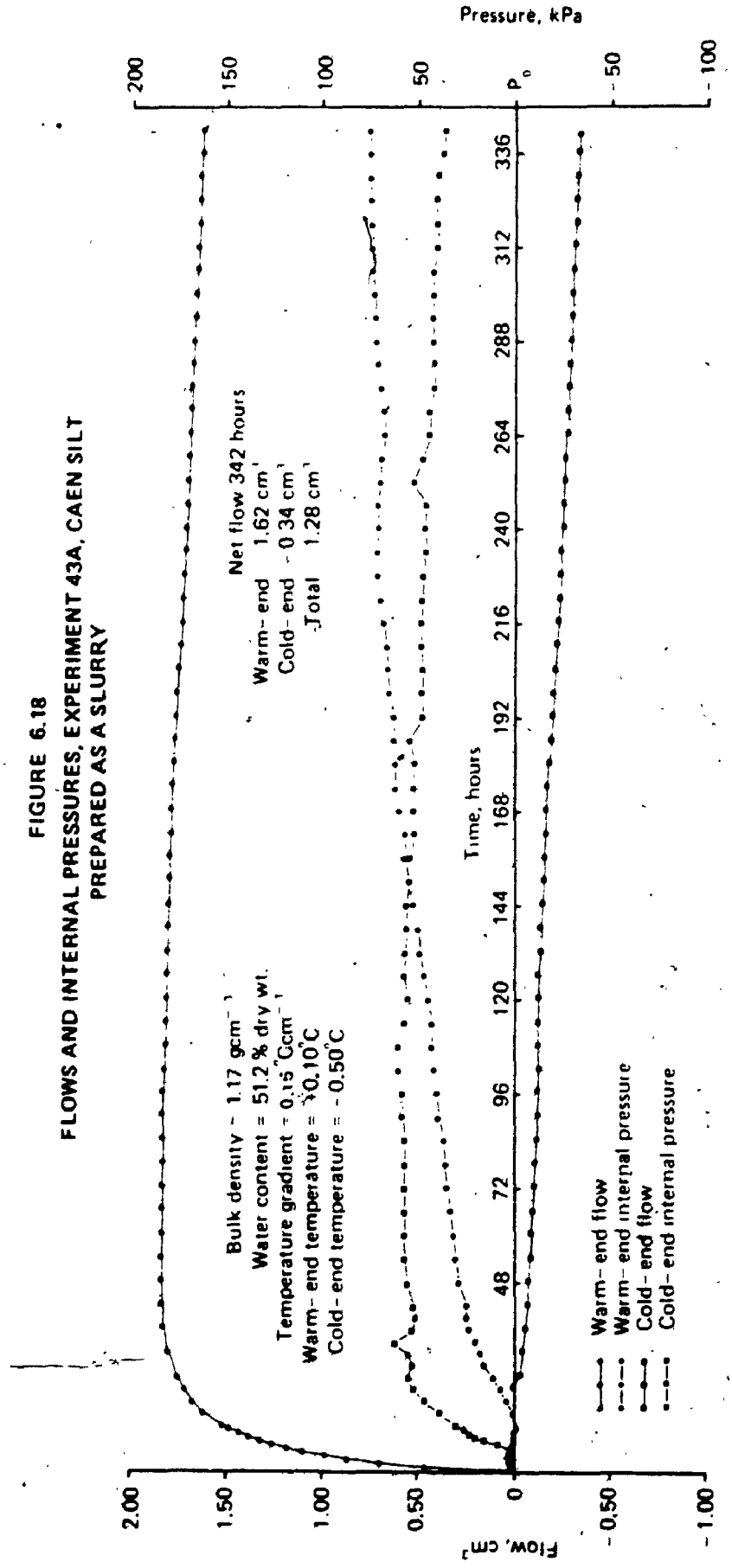

FIGURE 6.18
FLOWS AND INTERNAL PRESSURES, EXPERIMENT 43A, CAEN SILT PREPARED AS A SLURRY

FIGURE 6.19

FLOWS AND INTERNAL PRESSURES, EXPERIMENT 29, ALLENDALE CLAY PREPARED AS A SLURRY

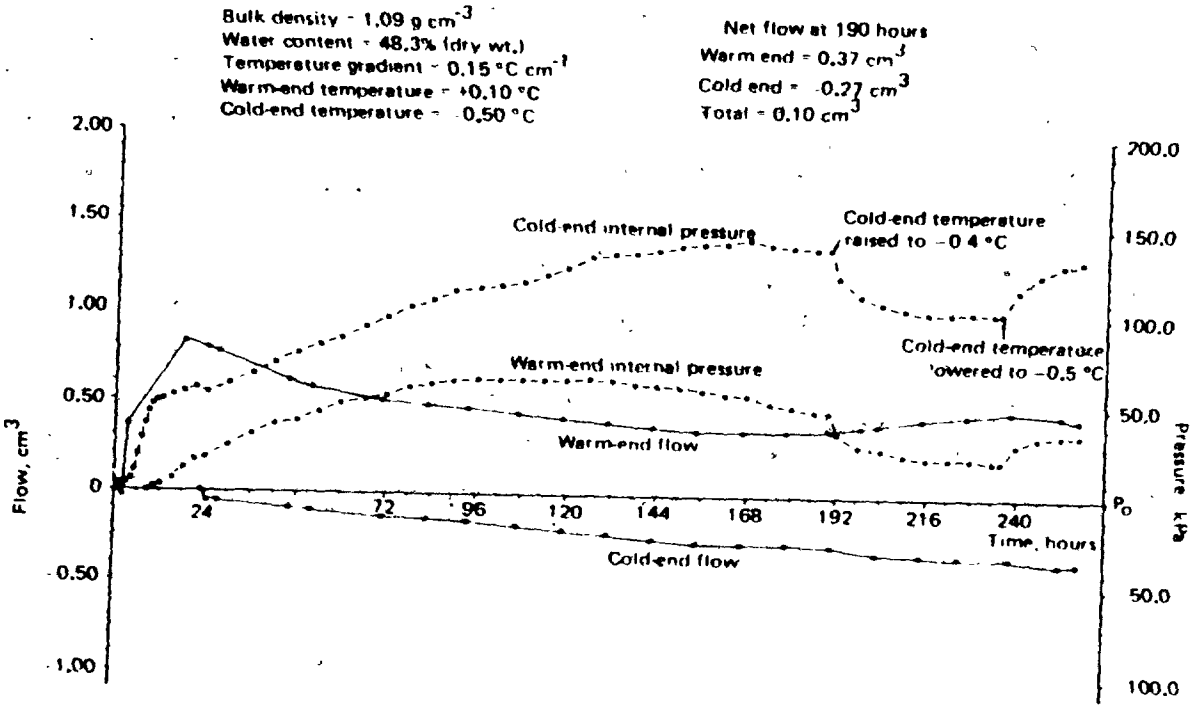

The most obvious difference in the results compared to those obtained with the normally consolidated specimens, is that the pressure differences between the two transducers were much smaller. This effect was more pronounced in the Caen silt (Figs. 6.17 and 6.18) than in the other two soils. The tendency toward more uniform pressures is chiefly a result of reduced pressures at the colder transducer (Table 6.7). Observed pressures were 87-235 kPa less than the equilibrium ice pressure at the colder transducer. Pressures at the warmer transducer were 81 kPa higher than the equilibrium ice pressure in the compacted Caen silt, although the opposite effect occurred in the Snec sand.

A distinct characteristic with the compacted (incompressible) soils is the abrupt fall in pressure which occurred at the colder transducer, followed by a partial recovery, suggestive of some form of rapid stress relaxation or sudden redistribution of stress near the colder transducer. There was no visible segregation ice in either soil, although this does not preclude the possibility that some segregation ice existed as diffuse non-visible bands of dirty ice.

An interesting phenomenon in the experiment with the Caen silt specimen prepared as a slurry, is that the pressures were considerably higher at the warmer transducer than at the colder transducer, during the latter half of the experiment. There is no obvious reason why this occurred. Since the temperature is lower at the colder transducer the ice pressure should be higher according to the Clausius-Clapeyron equation. The phenomenon may be only temporary, possibly a result of localized stress relaxation in the ice around the colder bladder.

It is interesting that, in this experiment, ice lenses were clustered in great numbers around the warmer transducer. In the normally consolidated specimens, the warmer transducer was located in the frozen unlensed zone just behind the frost line.

6.12 Significance of the Soil Strength to the Pressure Distribution

A suggested explanation, for the tendency toward more uniform pressures in compacted (incompressible) soils and slurries, is that the resistance to stress relaxation or the 'strength' of these specimens is substantially reduced. This is a result of changes in the amount of ice formed in the pores associated with increases/decreases in the soil porosity. In this case, the conditions approach those described by eqns. 4.5 and 4.6. The increase in strength of the soil with colder temperatures is insufficient to sustain the gradient in the equilibrium ice pressures and so the ice pressures tend toward a uniform distribution internally.

Various studies on silt-ice and sand-ice mixtures have shown that as increasing amounts of mineral matter are added to a block of ice at constant temperature, the strength of the ice, at some point, begins to increase rapidly, because of the increasing angles of friction and of dilatancy. The strength reaches a maximum at an optimum ice and then begins to decrease as the ice content decreases further because of loss of ice-mineral cohesion. Eventually, the strength levels off at a value

similar to that in unfrozen soil (Johnston, 1981, Goughnour and Andersland, 1968, Sayles and Carbee, 1981).[18]

An example of the curve for the short-term compressive strength for an isothermal sand was given earlier in Fig. 4.4. The long-term strength is generally an order of magnitude or more lower than this in sands and lower still in silts (Goughnoor and Andersland, 1968, Hooke et al. 1982). The shape of the curve (broad/narrow) and the location of the apex vary with the type of soil and probably also, with the individual soil specimen. In the normally consolidated Caen silt the apex of the strength-ice content curve at -0.5°C (the temperature at the cold end) probably occurs at a strength of about 500-600 kPa. Generally, the arms of the curve are steep in granular soils, which suggests that the soil strength is very sensitive to small changes in the ice content. For example, in Fig. 4.4, a change in the ice content of 10% from the optimum value (60%) results in a decrease in the strength of the mixture by more than 50% on the right arm of the curve and 25% on the left arm. In the situation where there is a thermal gradient, as occurs in the frost pressure experiment, the strength should increase with colder temperatures. In this case, the rheological

---

[18] With colloidal clays, Tsytovich (1975) suggests that the strength of the frozen soil is actually less than that of pure ice owing to high unfrozen water contents. The strength increases with ice content and eventually levels off at the value for pure ice, rather than following the bell-shaped curve for silts and sands. However, in the case of the Allendale clay, since this soil has a high silt content (i.e. it is almost a silty clay) and the soil freezing characteristic curve does not differ greatly from that of Caen silt, it probably behaves more like a granular soil with regard to the strength-ice content relationship.

behaviour is more appropriately described by the change in the overall strength, or the strength gradient in the specimen, with ice content.

Since the maximum difference in pressure occurred in the normally consolidated specimens, this suggests that the ice content of these specimens (about 22%) was close to the optimum value at which the strength of the soil was maximum. This is much lower than the value shown in Fig. 4.4 because of the effect of the thermal gradient (i.e. the ice distribution changes with temperature). In section 6.5 it was established that the strength gradient of these specimens was greater than the equilibrium ice pressure gradient although the difference was not very large. A relatively small reduction in the strength, therefore, could result in the conditions for uniform pressures being fulfilled. This may explain the apparent sensitivity of the soil to small changes in bulk density.

With the slurries, the amount of ice formed was higher than in the normally consolidated specimens because of the increased pore volume (reduced density). Presumably, this significantly altered the rheological properties of the material so that the strength was sufficiently reduced compared to normally consolidated specimens and the material was unable to sustain large differences in ice pressure internally. The Caen slurry probably resembled more a silty-ice mixture in texture rather than a soil, similar to that described by the right arm of the curve in Fig. 4.4. The reduction in strength of the Allendale may have been smaller because it was allowed to settle out first before freezing. This would explain why the observed differences in pressure were larger in the clay slurry than in the silt slurry.

With the compacted (incompressible) soils, the amount of ice formed may be significantly lower than in normally consolidated specimens because of the reduced pore volume. Assuming the ice content in these specimens is lower, the strength of the soil would be significantly reduced with respect to the normally consolidated specimens, similar to the left arm of the strength-ice content curve (Fig. 4.4).[19] As in the case with the slurries, the compacted soils are unable to sustain large differences in ice pressure because of the reduced strength. The change in the strength with ice content may be less steep on this side of the curve as it is in Fig. 4.4 (left side), which may explain why the differences in pressure tended to be slightly less in the compacted silt than in the slurried silt. The shape of the strength-ice content curve may also be somewhat different for the Caen silt than for the Snec sand. This might explain why the difference in pressure was less in the silt - its strength being reduced by a larger factor.

The results suggest that the transition between quasi-viscous (fluid-like) behaviour and semi-rigid (solid-like) behaviour is not abrupt. (This was discussed in chapter 4.2). Instead, the soil probably experiences a gradually increasing rate of stress relaxation as the ice content increases or decreases with respect to the optimum value, associated with the maximum strength. Observed pressures increasingly depart from the equilibrium ice pressures as the rigidity of the material decreases. Pressures that are very nearly uniform

---

[19] The reduction in the cohesive component of the strength due to the lower ice content would exceed any tendency for the frictional interference between the particles to increase the strength because of the lower pore volume configuration.

Table 6.8

Observed Pressures and Equilibrium Ice Pressures with Decrements in the Cold-End Temperature, Exp. 44, Caen Silt

Warm end = +0.10°C

T_f = -0.065°C

Cold End, °C	T	P_i	P	P_i*	P*
	-0.015	0	33		
-0.30	-0.115	56	24	28	30
	-0.090	28	118		
-0.50	-0.235	192	113	110	155
	-0.160	207	183		
-0.70	-0.360	332	205	220	195

T_f = frost line temperature, °C

T = transducer temperature, °C

P_i = equilibrium ice pressure (eqn. 6.2), kPa

P = observed long-term pressure, kPa

P_i* = mean equilibrium ice pressure, kPa

P* = mean observed long-term pressure, kPa

FIGURE 6.20

FLOWS AND INTERNAL PRESSURES DURING STEP-WISE DECREASES IN TEMPERATURE AT THE COLD END, EXPERIMENT 44, CAEN SILT

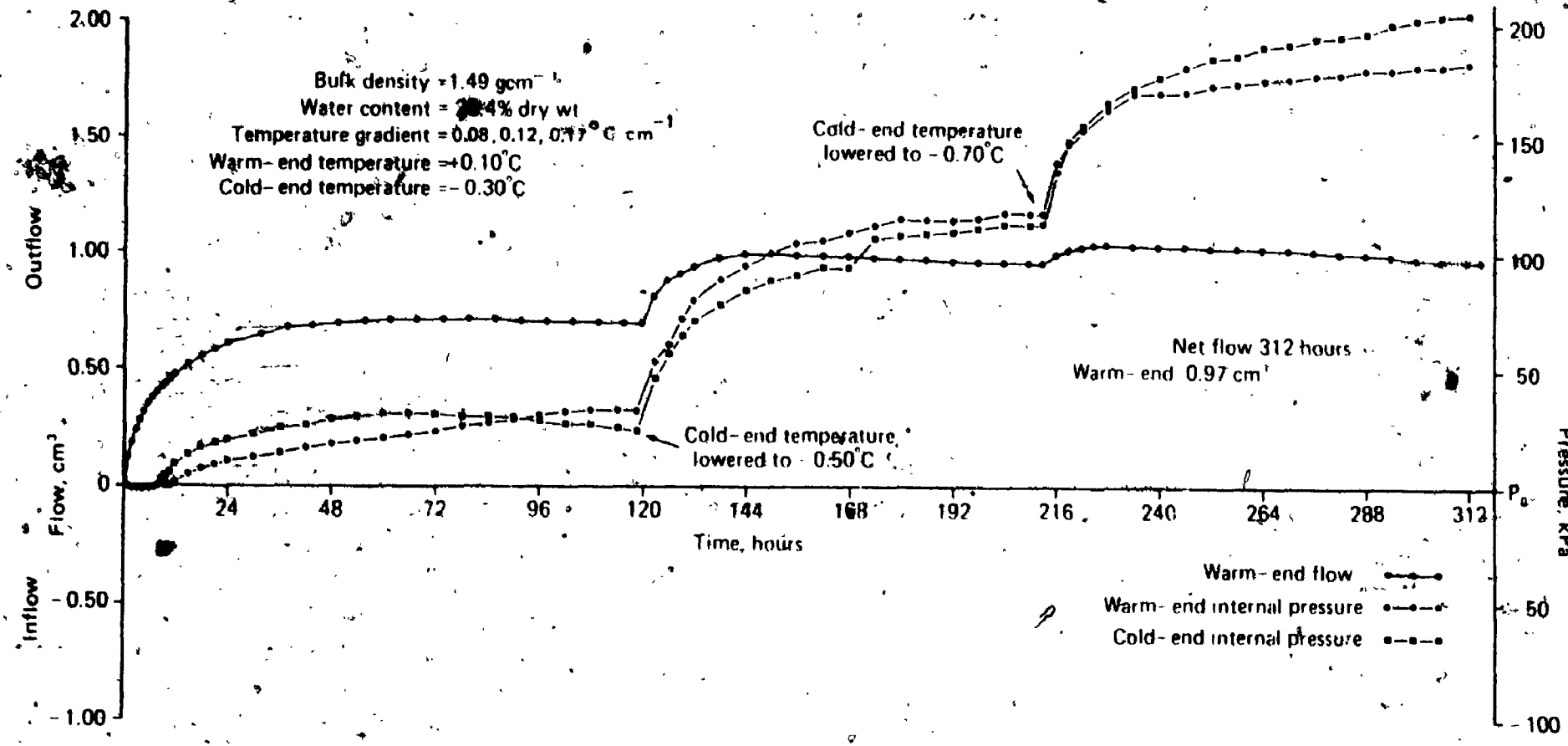

FIGURE 6.21

TEMPERATURE PROFILE DURING FREEZING, EXPERIMENT 44, CAEN SILT

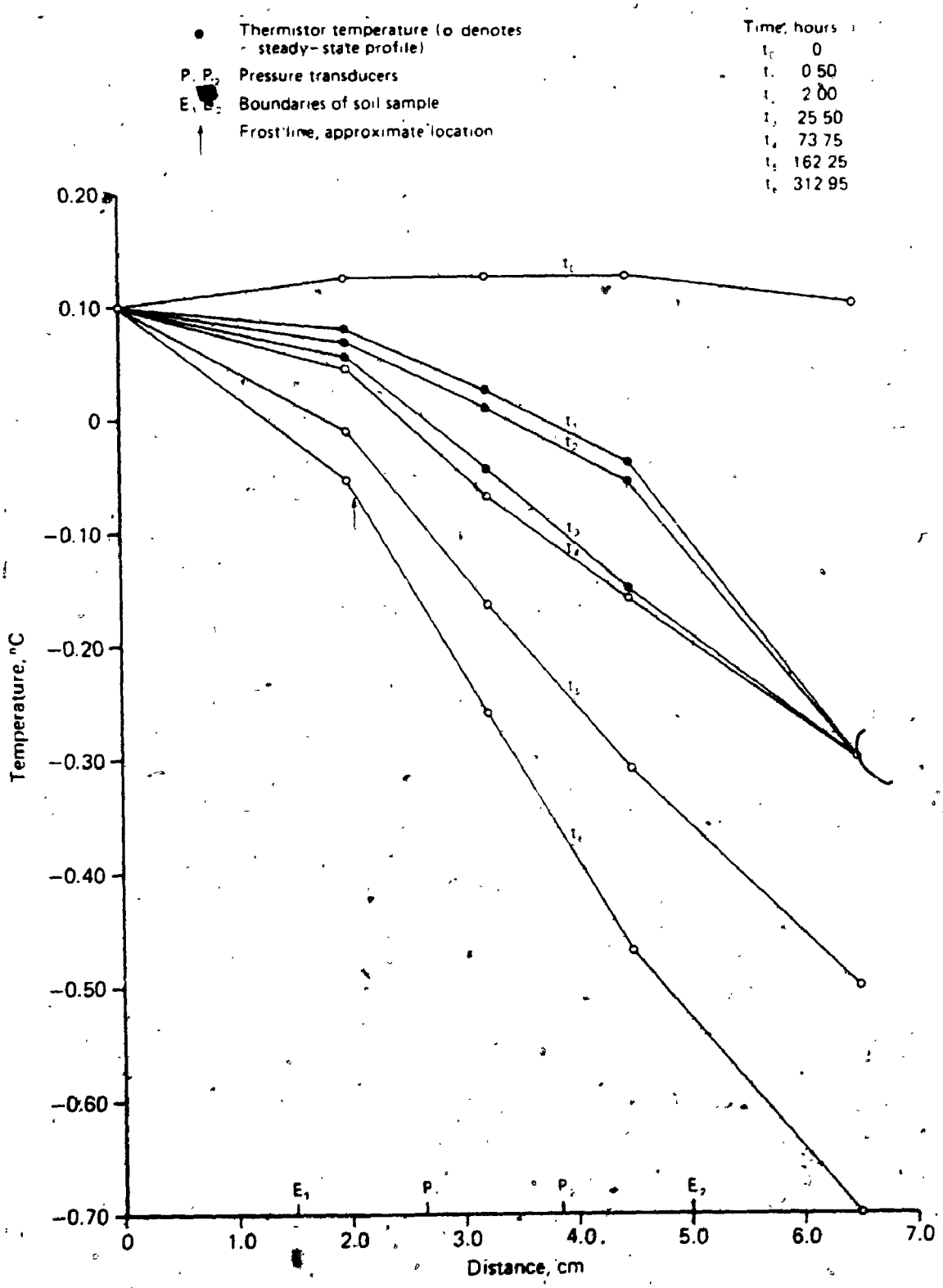

FIGURE 6.22

STRESS-STRAIN CURVE FOR CAEN SILT AT DIFFERENT STRAIN RATES, -2°C

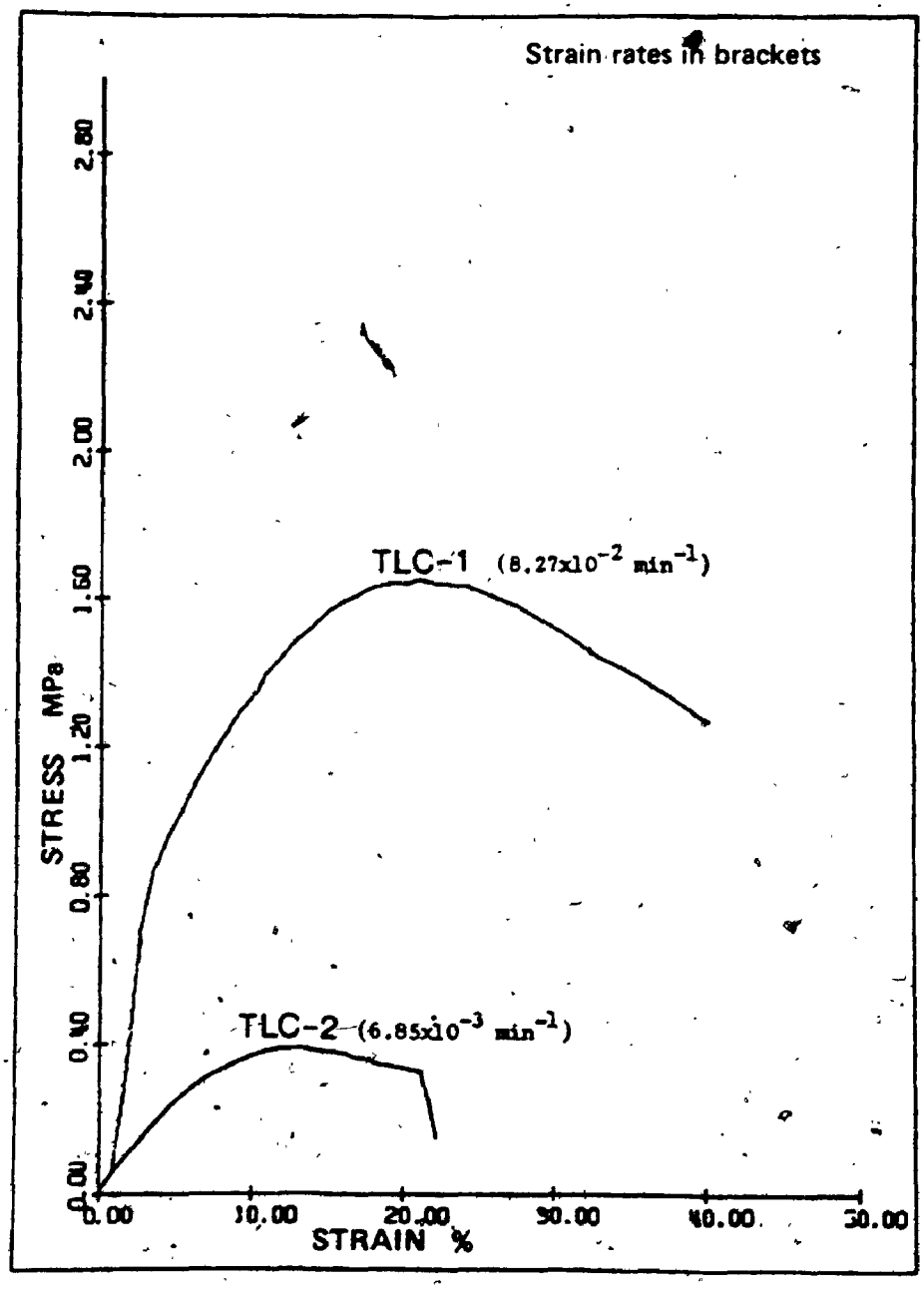

(Ladanyi and Lauzon, 1985)

probably only occur with the transition to true quasi-viscous type behaviour. In this case, the rate of stress relaxation is so rapid that the soil cannot sustain any significant ice pressure gradient. It is unlikely that this occurred in any of the soil specimens discussed above (Figs. 6.16-6.19) because the differences in pressure, although small, are still significant. Instead, the ice in the soil probably behaves more in a semi-rigid manner than a quasi-viscous manner although the rates of movement may have been higher in the silt specimens, which would explain why the differences in pressure were smaller than in the other two soils.

In one experiment with Caen silt (exp. 44, Fig. 6.21 and 6.22), true quasi-viscous behaviour probably occurred because the internal pressures were very nearly uniform. The results were very similar to the conditions described by the diagram on the right in Fig. 4.6. The soil was frozen very slowly by lowering the cold-end temperature in 0.2°C decrements every 4 or 5 days, starting at -0.3°C. The observed pressures did not differ by more than 20 kPa at any time during the experiment.

Although the soil was prepared as a normally consolidated specimen, the amount of ice formed within the soil was considerably less (up to 37%) than when the same soil specimen was frozen to -0.70°C in a single temperature decrement (e.g. exp. 44B, Table 6.3). The reasons for this are not clear, although it must be related in some way to the very slow rate of freezing. In this case, the reduction in the strength of the soil is probably considerable - enough for true quasi-viscous conditions to occur internally. It is interesting that the mean observed pressures which occurred within the soil were very close to the

equilibrium ice pressure at the mean temperature of the frozen section (Table 6.8). This condition was predicted by eqn. 4.5 in the model discussed earlier (chapter 4.2).

An additional reason for the uniform pressures may be reduced rates of stress relaxation associated with the temperature gradient being established in smaller decrements. The frost heave pressure is established more slowly, therefore, the rate of stres relaxation is lower. This may reduce the strength considerably in a manner similar to the effect of the strain rate on the stress-strain curve for Caen silt (Fig. 6.22).

6.13 Externally Effective Frost Heaving Pressures

One experiment was carried out in which the pressures exerted by the cold end of soil on the reservoir were measured by a few simple modifications to the frost pressure cell (Fig. 6.23). The perforated aluminum plate was removed from the cold reservoir and the semipermeable membrane was replaced with an impermeable rubber diaphragm. The reservoir was then filled with mercury and connected to a pressure transducer (Kulite XTM-190, rated pressure 690 kPa, Appendix C) by high pressure nylon tubing, with bleed valves. Care was taken to ensure that no air bubbles became trapped in the reservoir. Mercury was used instead of other non-freezing fluids because it conducts heat readily. However, the rate of freezing was slower than in the other experiments.[20]

---

[20] Although mercury has a high thermal conductivity (7.8 $W\ m^{-1}K^{-1}$) compared to water (0.5 $W\ m^{-1}K^{-1}$), the rate of heat extraction by the cooling plate was lower than normal. This was due to the absence of the perforated aluminum support which increased the heat flow through the reservoir (thermal conductivity of aluminum = 236 $W\ m^{-1}K^{-1}$).

It is suggested that the diaphragm is activated by a thin layer of ice which forms at the cold end of the soil in the same way it does around the rubber bladders (see discussion section 6.15). The pressure in the reservoir is, therefore, the ice pressure at the cold end. Results (Fig. 6.24) indicate that the pressure of the reservoir (i.e. the externally effective pressure) is lower than the pressure of the colder internal transducer.[21] This is puzzling since the soil temperature is coldest next to the reservoir, therefore, the highest pressures might be expected there. The equilibrium ice pressure (eqn. 6.2) at the cold extremity of the soil (-0.40°C) is 349 kPa (thermal profile, Appendix K).[22] However, the reservoir pressure never exceeded 150 kPa. There are two possible explanations: (1) A small amount of undetected air became entrapped in the reservoir which introduced a compressibility error into the results. This is the most probable explanation. The nylon tubing connecting the cold reservoir to the pressure transducer is aerophyllic which favours the entrapment of air. (2) An alternative explanation is that the ice pressure next to the bladder surface is much lower than the equilibrium pressure because the soil at the cold end was frozen very quickly. At the start of the experiment the soil was supercooled by momentarily lowering the cold end to -1°C. After nucleation the frost line may have progressed so rapidly during the first few minutes of freezing that significant ice pressures were unable to develop. Studies have shown that soils which freeze very rapidly do

---

[21] The negative pressures established after the cold-end temperature was raised to +0.1°C are discussed in section 7.4.

[22] P_i according to eqn. 6.2 = (-0.090°C + 0.400°C) 1127 kPa $°C^{-1}$ = 349 kPa.

FIGURE 6.23

MODIFIED CELL FOR MEASURING EXTERNALLY-EFFECTIVE FROST HEAVE PRESSURES AT THE COLD END

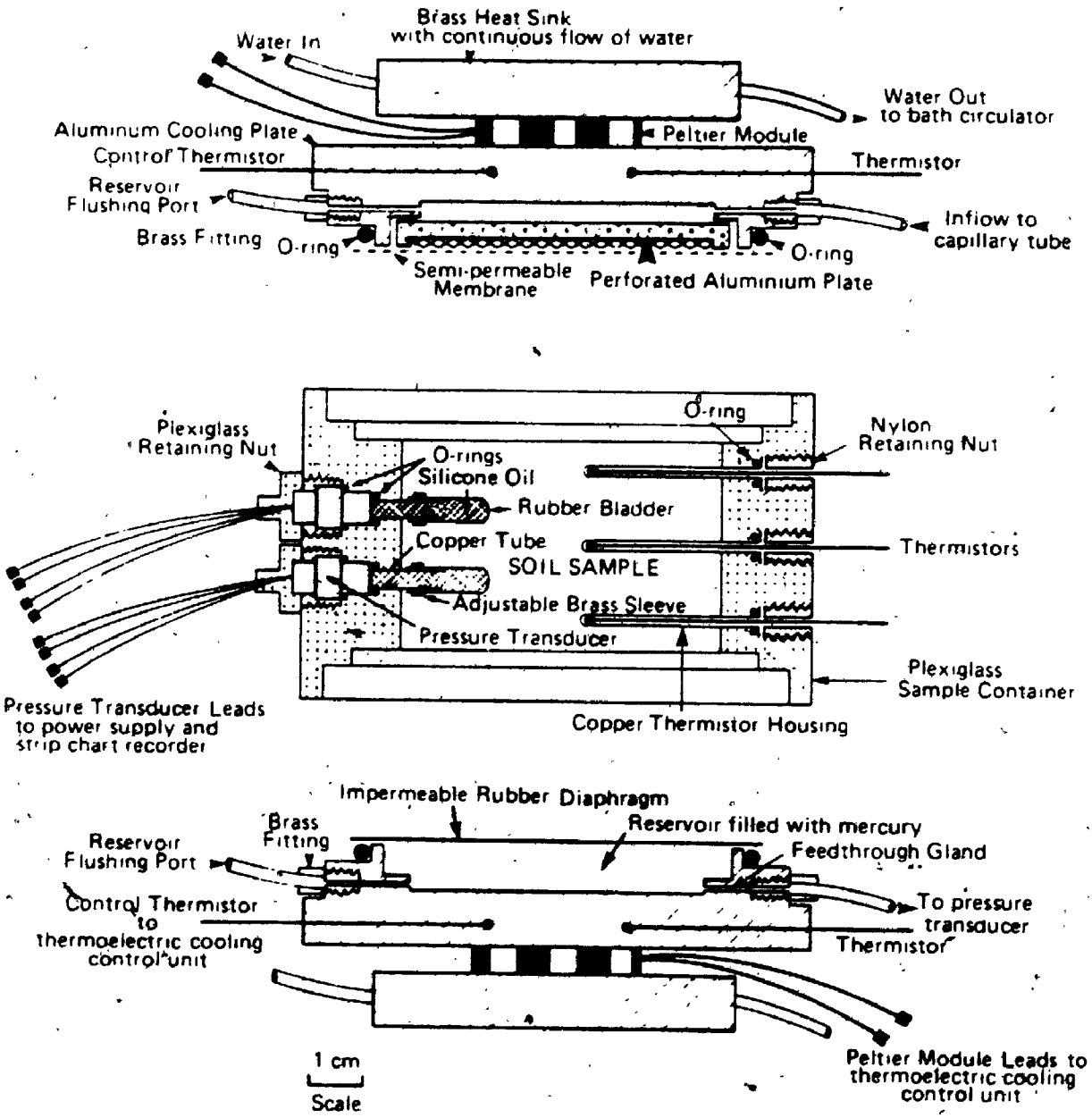

The steel clamp and nylon screws used to hold the apparatus together are not shown. Brass fittings and plexiglass retaining nuts are not drawn to scale.

FIGURE 6.24

FLOWS, INTERNAL PRESSURES AND COLD-END RESERVOIR PRESSURE, EXPERIMENT 35, CAEN SILT

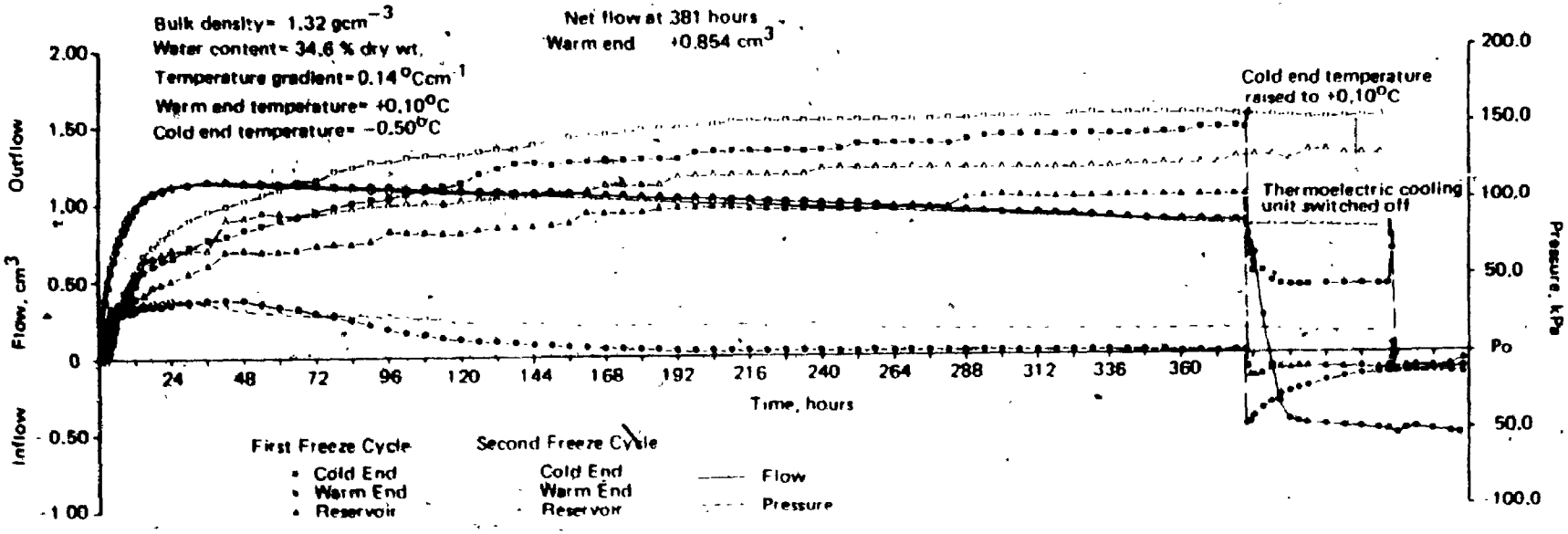

not develop ice lenses or large heaving pressures (Penner, 1960). In a situation where the rate of freezing is rapid, equilibrium thermodynamics may not be applicable, because it is based on the assumption that any change to the system is slow enough that the process is reversible (i.e. thermodynamic equilibrium occurs between the ice and unfrozen water). In this case, ice pressures may not be controlled by the temperature, at least not in the manner given by the Clausius-Clapeyron eqn. After the frost line slows, reversible conditions begin to prevail and the ice pressure slowly begins to increase at the cold end toward the equilibrium value (e.g. Fig. 6.24).

6.14 Frost Heave Pressures in Unconfined Soils

The confined nature of the soil implies that the resistance offered by the cell itself contributes to the heaving pressures established in the frozen soil. The confining effect of the cell, however, would not account for the differences in pressure between the transducers. If the soil has a significant restraining effect on ice segregation, it should be possible for heaving pressures to develop in unconfined soils. In this case, the pressures would probably be lower because the soil is able to develop negative (subatmospheric) pressures in the unfrozen water. An interesting possibility would be to repeat the experiment with an unconfined soil specimen.

There are a number of references in the literature which suggest that significant ice pressures and differences in pressure can develop in unconfined soils close to the soil surface. Tsytovich (1975) described temperature related differences in pressure up to 70 kPa in seasonally frozen ground. Mackay (1980) recorded fluctuating positive pressures up to 110 kPa in the active layer using small pressure cells

buried at depths down to 1 meter. This is much greater than the overburden pressure. At the Canada-France pipeline ground-freezing project, pressure differences up to 100 kPa were detected in the annulus of frozen soil around the pipe, by Glotzl cells buried at depths down to 1 m.

6.15 Location of the Ice with Respect to the Bladders

A matter interesting to consider is the location of the ice lenses relative to the rubber bladders. One possibility is that an ice lens forms as a very thin (non-visible) layer around each rubber bladder. Since the bladder is the weakest material in the system it favours the growth of segregation ice. The observed pressure in this instance, represents that of a single ice lens at the respective temperature. An alternative possibility is that both pore ice and segregation ice are in contact with the bladder surface. According to the Clausius-Clapeyron eqn., where the temperature of the soil is constant, the pressure of the ice is the same regardless of whether it is pore ice or segregation ice.[23]

The reason for the design with the oil held within the rubber bladder was to avoid damage to the transducer diaphragm by a point or an edge of a particle. Since the oil within the bladder cannot sustain

---

[23] If the pressure of the segregation ice begins to exceed the pressure of the pore ice (both at the same temperature), this increases the equilibrium freezing temperature of the ice-water interface in the pore and some of the liquid film water freezes. This raises the pore ice pressure back to the segregation ice pressure. Pore ice and segregation ice are maintained at the same pressure by the liquid films being thinner in the soil pores.

shear, the pressure of the oil is hydrostatic. The situation with the oil in a bladder, is different from a rigid stress sensor embedded in a visco-elastic material, where the stress measured by the sensor must be resolved into isotropic and deviatoric components. In the present case, any deviatoric stresses (i.e. shear or anisotropic normal stresses) occurring within the soil-ice matrix would result in distortion and/or displacement of the bladder rather than an increase in the pressure of the oil. The pressure indicated by the transducer, therefore, is the isotropic stress component.

An interesting question concerns the effect of the small difference in temperature across the rubber bladder and its effect on the ice pressures established. At a thermal gradient of about 0.15°C cm^{-1} (the average thermal gradient in the experiments), this was about 0.04°C. This corresponds to a difference in the equilibrium ice pressure (eqn. 6.2) of about 45 kPa between the warmer and the colder sides of the bladder. However, any significant increase in the pressure on the colder side of the bladder is immediately transmitted by the oil to the ice on the warmer side, which then rises above its equilibrium pressure. This lowers the equilibrium freezing temperature of the ice there, which then melts and the ice pressure increment is dissipated. Since the oil within the bladder cannot sustain shear, the ice pressures around the bladder must be uniform and equal to the equilibrium ice pressure at the mean temperature of the bladder. In effect, the bladder artificially induces the conditions described by eqns. 4.5 and 4.6 (right-hand side of Fig. 4.6) to the ice in direct contact with it's surface.

6.16 Stress Concentrations

An important question concerns the possible effects of stress concentrations developing in the frozen soil around the rubber bladders. This is also known as the 'arching effect'. A consideration in the design of any pressure or stress sensing device for soil is the elastic modulus of the device itself. If it differs significantly from that of the surrounding soil, it will alter the stress field in the soil (Brown, 1973, Cox and Johnson, 1983). A device which is more rigid than the surrounding soil supports more of the stress than would otherwise be borne by the soil itself. Stresses tend to be concentrated on the sensor. If it is less rigid than the soil, the stresses are concentrated in the soil around the sensor.[24] In this case, the stress indicated by the sensor may be too low. If the stress concentrations are high enough, this may cause localized yielding of the soil around the sensor (Cox and Johnson, 1983).

For this experiment, several different methods of measuring the internal pressure in the soils were considered, including a rigid cylindrical sensor with a photoelastic stress meter or a vibrating wire device inside, or a flat piezoelectric type of transducer. However, all of these devices are fairly large (usually several cm3) and also introduce potential difficulties of their own. The configuration with the oil held within a rubber bladder is the only practical device which can be kept very small - a requirement for this experiment.

---

[24] The stress concentration factor is also dependent upon the geometry of the sensor (in this case a cylinder).

The effect of an inclusion on the stress distribution in a host material is normally described by the relationship between the principal stresses in the two materials (Williams, 1973):

$$\sigma_1 = C\sigma_1' + c\sigma_2' \qquad 6.4$$

$$\sigma_2 = C\sigma_2' + c\sigma_1' \qquad 6.5$$

where σ_1 and σ_2 = principal stresses in the host body, which would have existed at the site of the inclusion if it were absent,

σ_1' and σ_2' = principal stresses in the inclusion.

The inclusion factors, C and c, are expressed as a function of the elastic modulii and Poisson's ratio of the inclusion (E' and ν') and the host material (E and ν), respectively. For an oil-filled rubber bladder, E' and ν' cannot be evaluated because they are meaningless parameters in a fluid. The device obviously exhibits some elastic properties, due to the rubber itself. However, equations 6.6 and 6.7 are more applicable to the situation where a pressure sensor has significant rigidity. In the case of the stress distribution around a hole the concentration factor is given by (Peterson, 1974):

$$C = \frac{\sigma_{max}}{\sigma} \qquad 6.6$$

where σ_{max} = maximum stress at the edge of the hole

σ = applied stress some distance from the hole.

In one experiment (end temperatures, +0.10°C, -0.50°C), an external stress of 100 kPa was applied at the cold end by increasing the

pressure in the cold reservoir. An impermeable foil barrier was placed across the cold end of the soil specimen. The response of the transducers, 1.15 cm and 2.35 cm away, was instantaneous, the pressure increasing by about 40 kPa at both transducers. The pressures continued to increase very slowly by another 20 kPa, for an hour or two after the stress was applied. When the external stress was later released, the internal pressure returned to its original value.

Although this result implies a rather large concentration factor, this is only relevant to the situation where the stresses are externally applied. In the freezing experiments, stress concentrations have no relevance to the measured pressures because the ice pressure develops at the bladder surface rather than externally. In other words the bladder pressure equals the ice pressure.

An additional factor which may introduce potential errors into the results is differential thermal expansion between the rubber bladder and the soil. However, in this experiment, it is unlikely that this had any significant effect because of the narrow range of temperature in which the experiment operates (+0.10°C to -0.50°C).

6.17 Wall Friction

Tests were carried out to measure the wall friction of the cell (procedure, Appendix L). When the soil was unconfined (i.e. the end plates were removed) and isothermal, the wall friction was about 10 kPa at a temperature of -0.5°C. However, the confined nature of the soil during the freezing experiments suggests that the wall of friction was probably larger than this. Since the ice pushes laterally on the walls of the cell, the wall friction probably increases in direct proportion to the increase in ice pressure with colder temperatures.

3 of/de 3

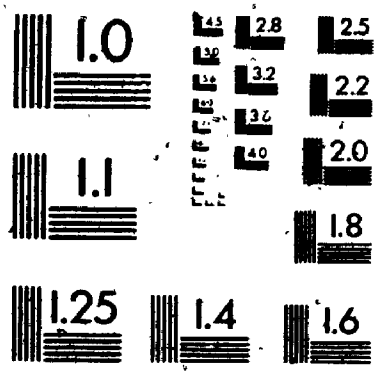

However, any drag effects due to wall friction should not affect the ice pressures measured by the bladders because the bladders are located in the middle of the soil away from potential sources of friction.

An additional consideration is the frictional interference caused by the copper tubing (i.e. thermistor housings) which protrudes into the soil. This cannot be measured directly without possible damage to the apparatus. However, its effect must be fairly small because the pressures remained the same when the experiment was repeated with the copper tubing removed.[25] The copper tubing does not present a barrier to the movement of the ice in the soil because the ice flows around any obstruction by the same mechanism in which it moves through the soil pores.

6.18 Compressibility of the System

An important question concerns the effect of the soil compressibility including the pore contents (ice and water), as well as the elastic properties of cell, on the pressures established. The isothermal volume compressibility is given by the expression (Gray and Issacs, 1975):

$$\kappa = \frac{1}{v}\left(\frac{\delta v}{\delta P}\right)_T \qquad 6.7$$

where δP and δv = the change in pressure and the corresponding volume changes at constant temperature,

v = the initial volume.

---

[25] This test was carried out with an earlier version of the apparatus (described in Williams and Wood, 1982). The pressure sensing apparatus was different to that shown in Fig. 5.1.

For water, κ is very low (4.7×10^{-5}/100 kPa, at 0°C, between 0 and 50 MPa, Dorsey, 1940). The additional volume required to raise the pressure of the water by 200 kPa (= the pressure at the colder transducer) is very small (0.0001%). For ice, the compressibility is about an order of magnitude larger (33.0×10^{-5}/100 kPa) and the extra volume required to change the pressure by 200 kPa is about 0.0007%.

The compressibility of the soil is distinguished from consolidation, the former being due to the elastic properties of the soil, whereas the latter is caused by the flow of pore water out of the soil under an applied stress. For a frozen sand at -0.6°C, Tsytovich (1975) gives a coefficient of compressibility of 1×10^{-4}/100 kPa (between 0 and 200 kPa). This is somewhat larger than the compressibility of pure water and ice because of compression of entrapped air.

Some small volume expansion probably also occurs due to the compressible nature of the cell itself. This is mainly due to deflection of the perforated aluminum plates in the end reservoirs (see Fig. 5.3). The compressibility associated with this effect is about 5×10^{-4}/100 kPa.[26]

Any slight expansion of the cell or compression of the contents within, implies that more ice must form than would otherwise occur if the system was absolutely incompressible. However, this should not affect frost heave pressures established because the soil behaves as an open system. That is, the soil tends to work toward establishing an

---

[26] Between 0 and 200 kPa the volume displacement is 0.08 cm^3 (Fig. 5.3). The compressibility (eqn. 7.2) $\kappa = \frac{1}{78.42\ cm^3}\left(\frac{0.08\ cm^3}{200\ kPa}\right) = 5.1\times10^{-6}$/kPa = 5.1×10^{-4}/100 kPa.

equilibrium ice pressure regardless of any slight elasticity in the system. Ice pressures are sustained provided the volume expansion of the cell remains less than the 9.1% expansion when the pore water changes to ice. In the present case, the former is about 2 orders of magnitude less than the latter.

6.19 Flows at the Cold End

The inconsistency in the direction of flow at the cold end is puzzling. Since the pressure of the unfrozen water is atmospheric, it would be reasonable to expect no flow at all at the cold end, provided the correct amount of lactose was used in the cold reservoir. The small volume changes due to thawing at the cold end may be the reason for the inflows that occurred there. However, this would not explain the cases where outflow occurred at the cold end. Inflow also occurred at the cold end in the experiment with the Snec sand (Fig. 6.16), although there was no evidence of thawing at the cold end. One suspects that the flows may be a result of freezing or thawing of segregation ice near the cold end in response to minute deformations within the soil.

It is interesting that the flows at the cold end had no significant effect on the internal pressure. In the experiments where there was an impermeable rubber or foil barrier at the cold end, the observed pressures and the flows at the warm end were not significantly altered. Similarily, thawing at the cold end, due to the diffusion of lactose molecules into the soil, did not affect the internal pressures (thickness of thawed layer 0.1-0.2 cm). This is because there were no ice lenses for about 0.2-0.3 cm from the cold end and so the soil there was incompressible.

VII. ADDITIONAL RESULTS AND ANALYSIS

7.1 Reproducibility

To demonstrate the reproducibility of the experiment, tests were repeated with normally consolidated Caen silt specimens prepared to the same bulk density as in exp. 32A (Fig. 6.1) and exp. 35 (Fig. 6.24) and the same end temperatures (+0.10°C and −0.50°C). The freezing history of exp. 32A was duplicated by freezing the soil for 24 hours and allowing it to thaw completely before it was refrozen.

Flows and internal pressures (Figs. 7.1 and 7.2, exp. 42A and 34) were very similar to those in exp. 32A and exp. 35, respectively.[1] Departures between the observed long-term pressures and the equilibrium ice pressures were also about the same (Table 6.4). However, there were some minor differences. The internal pressure at the warmer transducer in exp. 42A (Fig. 7.1) and exp. 35 (Fig. 6.24) increased to a maximum which was only about half as large as that observed in the other two experiments. This may be due to differences in the bulk density and ice content of the soil near the frost line in these specimens which affects their strength slightly. The pressures also declined much more abruptly at the warmer transducer in exp. 42A and 34, levelling off fairly early in the experiment. The frost line in exp. 32A was about 0.03°C warmer than in exp. 42A. However, any effect that this had was offset by slightly warmer soil temperatures overall, so the internal pressures remained about the same.[2]

---

[1] Thermal profiles, Appendix K.

[2] The location of the frost line was not measured in exp. 34. The frost line temperature given in Tables 6.1 and 6.4 is an estimate, based on the assumption that it is the same as that in exp. 35.

FIGURE 7.1

FLOWS AND INTERNAL PRESSURES, EXPERIMENT 42A, CAEN SILT

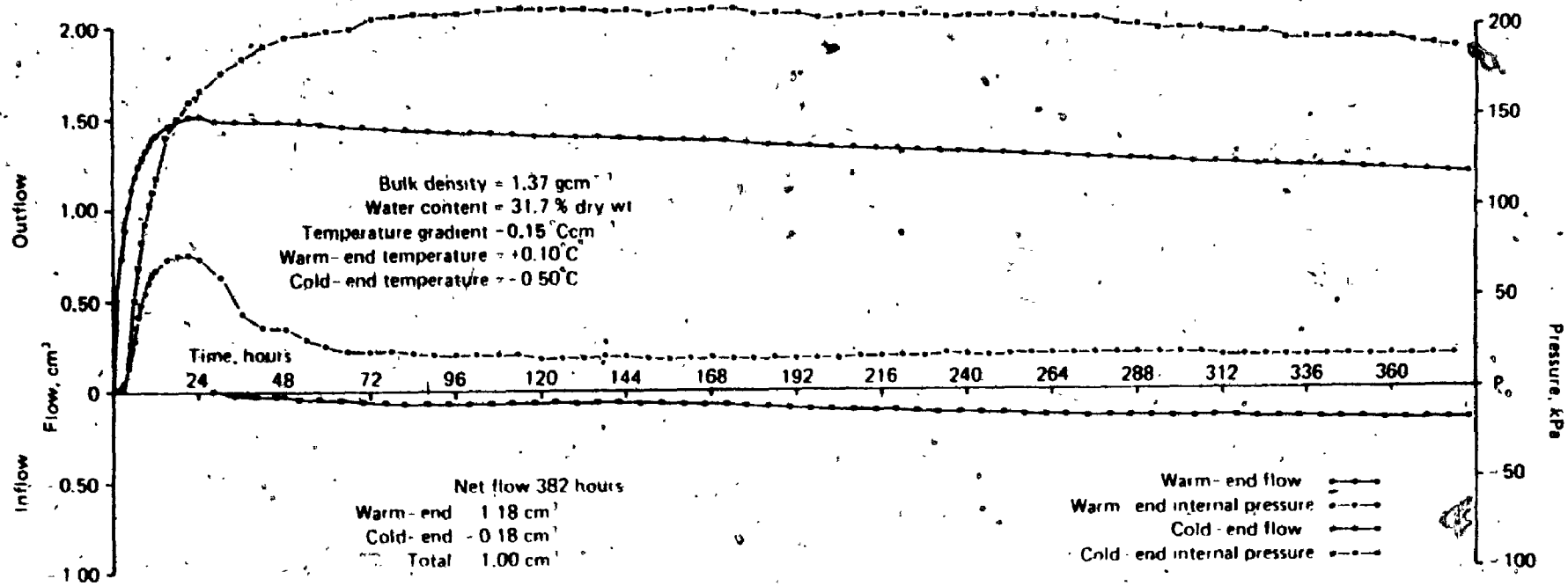

FIGURE 7.2

FLOWS AND INTERNAL PRESSURES, EXPERIMENT 34, CAEN SILT

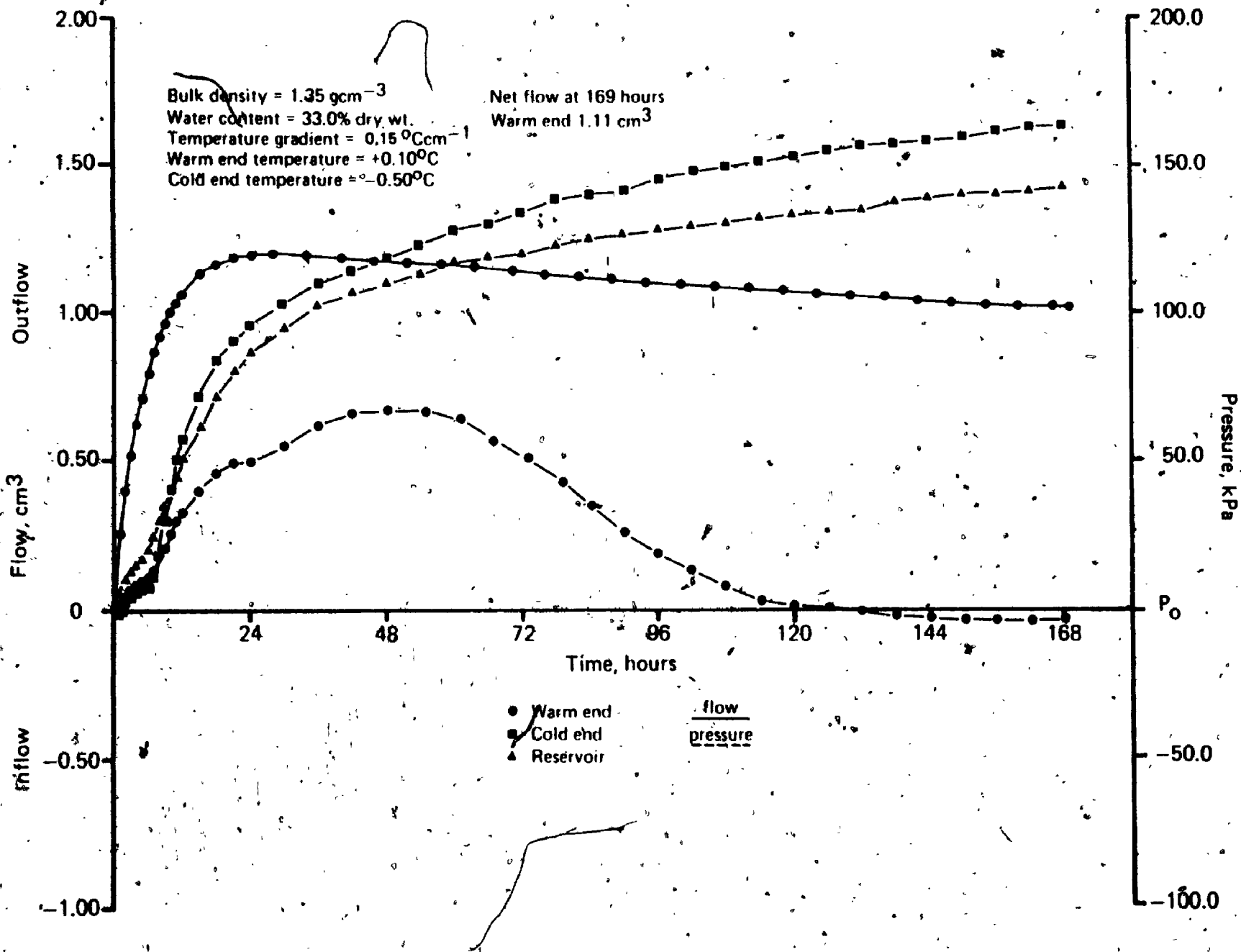

7.2 Effect of a Positive Pore Water Pressure on the Heaving Pressure

The Clausius-Clapeyron eqn. specifies the temperature-dependent difference between the ice and unfrozen water pressures. The magnitude of the ice pressure relative to atmospheric pressure depends upon additional constraints such as the expansive nature of the system and the pore water pressure. If allowance is made for varying unfrozen water pressures, eqn. 6.2 becomes:

$$P_i = P_w + \left[(T^*-T)\,\frac{\delta P_i}{\delta T}\right] \qquad 7.1$$

where P_w = unfrozen pore water pressure relative to atmospheric pressure, kPa.

Equation 7.1 indicates that the heaving pressures are much lower in unsaturated ('drained') soils because the pore water pressures are substantially negative (i.e. less than atmospheric). Similarly, when the water pressures are greater than atmospheric, the pressures should increase accordingly.

In unsaturated frozen soils, the presence of air influences the strength of the soil. A more uniform distribution of pressures might be expected because of reduced pore ice contents and increased creep rates. However, in a saturated soil which is frozen with a positive pore water pressure, the pressure should not affect the rheological behaviour of the soil - provided that the pressure is established before the soil is frozen. The distribution of frost heave pressures within the soil would remain unchanged, although larger pressures might be expected according to eqn. 7.1.

To test the latter possibility, an experiment was carried out with a large positive pressure in the pore water. The end temperatures were the same as in the other experiments (i.e. +0.10°C, -0.50°C). The soil was prepared as a normally consolidated, saturated sediment, although the density in this case (1.49 g cm^{-3}) was about 13% higher than normal. (There was no apparent reason for this). To prevent water from flowing out of the soil under pressure, the semipermeable membrane at the cold end was replaced with an impermeable foil barrier. After the warm reservoir was filled with water, the glass capillary at that end was connected to a regulated air pressure source. The water pressure was then raised to 100 kPa, about 24 hours prior to freezing.

Results (Fig. 7.3) appear to confirm the above hypothesis in a general way. Observed pressures were about 100 kPa higher than in the other experiments at the same end temperatures (at least at the colder transducer). This is a direct result of the elevated pore water pressure. Although there were some departures from the normal pattern, these were probably caused by the higher soil density rather than any direct effect of the elevated pore water pressure. The pressures showed a tendency toward a more uniform distribution. The difference in the observed pressures was less than half that of the equilibrium ice pressures (Table 7.1).[3] The pattern was similar to that in compacted Caen silt, in which the density was substantially increased. However, the difference in pressure was larger in exp. 44A, because the density did not increase by as large a factor. When the same soil specimen was

---

[3]Thermal profiles for exp. 44A, 44B and 40, Appendix K.

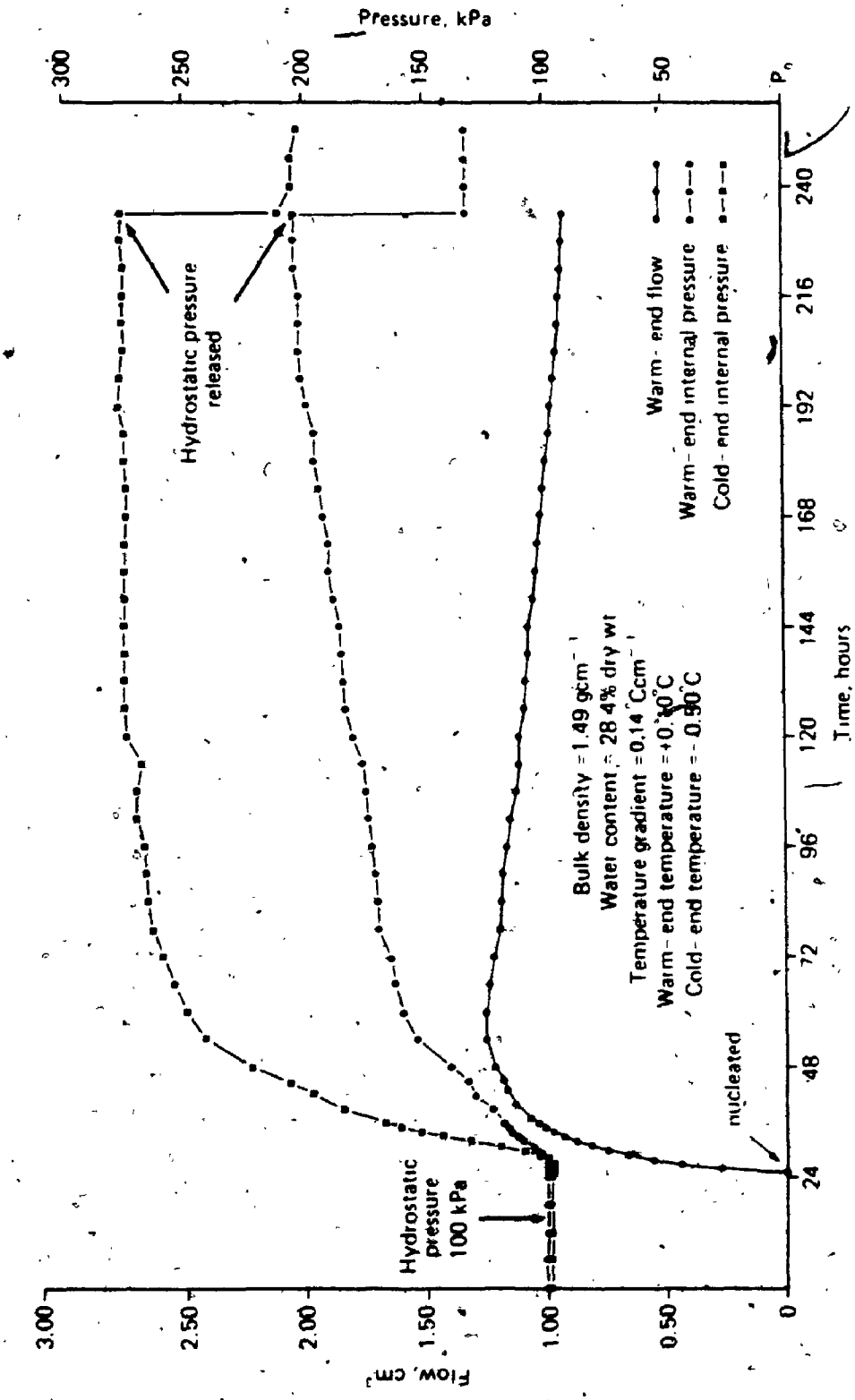

FIGURE 7.3
FLOWS AND INTERNAL PRESSURES WITH A POSITIVE HYDROSTATIC PRESSURE, EXPERIMENT 44A, CAEN SILT

Table 7.1

Observed Pressures and Equilibrium Ice Pressures with a Positive Pore Water Pressure and a Larger Thermal Gradient

Pore Water Pressure 100 kPa

Soil	44A	
Exp.	Caen	
T_f	-0.065	
T	-0.110	-0.280
P_i^*	151	342
P	204	276

Thermal Gradient 0.188°C cm^{-1}

Soil	Caen		Caen	
Exp.	44B		40	
T_f	-0.065		-0.085	
T	-0.195	-0.420	-0.155	-0.380
P_i	147	400	79	333
P	201	310	30	190

T_f = frost line, average temperature, °C

T = mean temperature of transducer, °C

P_i = equilibrium ice pressure (eqn. 6.2), kPa

P = observed long-term pressure, kPa

*Equilibrium ice pressure (eqn. 7.1), kPa

refrozen with the pore water at atmospheric pressure (exp. 44B, discussed next section), the difference in pressure was about the same.

It is interesting that the pressure continued to increase at the warmer transducer despite the steady inflow at the warm end. The inflow implies internal melting, therefore, the pressure might be expected to decrease with time. The apparent conflict can be explained by the rate at which these processes occur. In this case, the rate of stress relaxation exceeded the rate of internal melting.

7.3 Experiments with Increased Thermal Gradients

Experiments (Figs. 7.4 and 7.5) were carried out with lower cold-end temperatures (-0.70°C) to determine the effect of larger thermal gradients (0.188°C cm^{-1}). In exp. 44B, temperatures were lower by about 0.14°C at the colder transducer and 0.075°C at the warmer transducer. Although the long-term pressures were higher, the difference in the observed pressures in exp. 44B was only about 40% of the difference in the equilibrium ice pressures (Table 7.1). In exp. 40, the difference in the equilibrium ice pressures was about 100 kPa less than in exp. 44B (Table 7.1). This is a result of slightly warmer soil temperatures overall (about 0.04°C) and also the frost line temperature, which was about 0.02°C colder.[4] The difference in the observed pressures in exp. 40 about 60% of the difference in the

---

[4] Warmer temperatures may be a result of reduced thermal contact between the wire mesh and the perforated aluminum plate at the cold end. The wire mesh had a slight inverted dish shape. In soils with a reduced density, an air gap sometimes formed between the mesh and the perforated plate, which reduced the heat flow significantly.

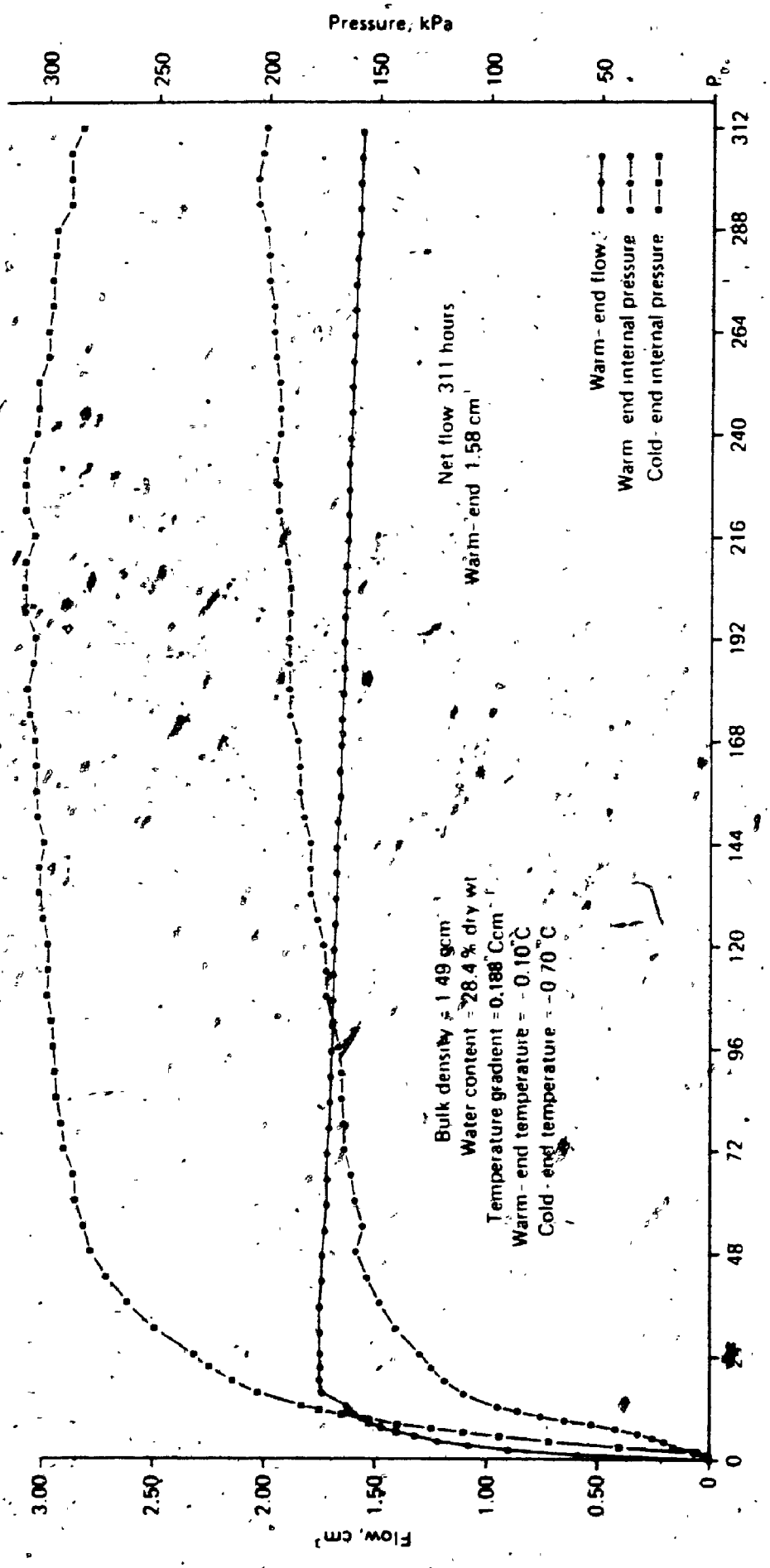

FIGURE 7.4
FLOWS AND INTERNAL PRESSURES; EXPERIMENT 44B, CAEN SILT

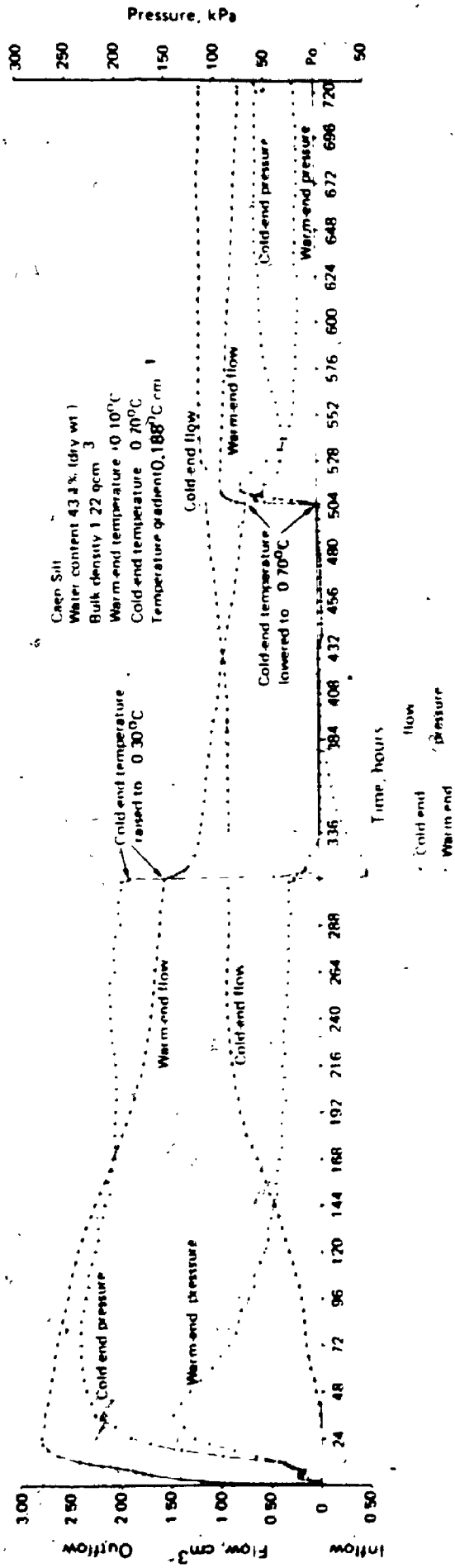

FIGURE 7.5

FLOWS AND INTERNAL PRESSURES, EXPERIMENT 40, CAEN SILT

equilibrium ice pressures. In this case, the pressure at the warmer transducer was less than the equilibrium ice pressure.

The tendency toward a more uniform distribution of pressure is probably a result of reduced strength in these specimens, associated with significant departures in the soil density from normal (1.35 g cm^{-3}). Although both specimens were prepared as normally consolidated, saturated sediments, the density was higher than normal in exp. 44B (1.49 g cm^{-3}) and lower than normal in exp. 40 (1.22 g cm^{-3}).[5] The pattern of pressure was similar to that in compacted (incompressible) soils and in slurries, although the pressure differences were much larger because the soil densities were closer to the norm. The ice contents and ice saturation were higher in both specimens (Table 6.3) because the soil temperatures were colder. However, there was a considerable difference in the ice content and ice saturation between exp. 44B and exp. 40, which reflects the difference in density between the two specimens. This is also supported by visual observations. Only a few very fine (barely visible) ice lenses were apparent in exp. 44B, about midway between the frost line and the cold end. In exp. 40, the amount of visible segregation ice appeared higher than normal, including a very large ice lens (0.5 cm thick) which formed at the cold end, underneath the semipermeable membrane..

An interesting feature of exp. 40 is the excessive flow rates which were much higher than normal. The inflow during the entire course

---

[5]The variations in density may have occurred because more time was allowed for the soil to settle out, during preparation, in exp. 44B than exp. 40.

of the experiment was 2.04 cm^3. This cannot be attributed entirely to internal pressure-melting of ice lenses (discussed in chapter 6.7), since it would imply thawing of 73% of the ice initially formed in the soil. This was not supported by the visual observations.

It is suggested that the increased flow rates, in this particular case, were artificially induced by an osmotic gradient at the cold end.[6] This was caused by lactose concentrations which were too high in the cold reservoir. The effect is similar to that in the ice sandwich (Fig. 3.7). The osmotic gradient induced a steady flow of water, from the soil, into the cold reservoir. This component of flow was added to whatever flow might have occurred if there was no osmotic gradient. The outflow slightly lowered the unfrozen water and ice pressures in the soil, which caused water to flow in at the warm end, at a faster rate, in an attempt to restore the equilibrium. In exp. 40, the influx at the warm end was more than 6 times faster than in exp. 44B (same thermal gradient), where the cold reservoir was left empty. The increased flow rates at the cold end may be responsible for the large ice lens which formed in the cold reservoir, underneath the

---

[6] The concentration of lactose used in the cold reservoir was 111.3 g ℓ^{-1} (including correction for the hydration of lactose). Available data on the freezing-point depression curve for lactose is limited to the temperature range between 0°C and -0.5°C. The concentration required for -0.7°C was estimated by projecting the curve an additional 0.2°C. However, significant deviations from a linear relationship began to occur below -0.35°C and increased with lower temperatures. It seems likely that, in this experiment, the required concentration was overestimated.

semipermeable membrane. The accelerated outflow may have caused significant dilution of the lactose solution next to the membrane surface, so that nucleation occurred and a layer of ice started to form.[7]

7.4 Effect of Changes in the End Temperatures

In a number of cases the end temperatures were changed during the experiment, to determine the effect on the internal pressure. It is interesting that the pressures increased relatively slowly when the temperature was lowered, but were released abruptly when the soil temperature was increased (e.g. exp. 31, Fig. 9.19, exp. 35, Fig. 6.24, exp. 40, Fig. 7.5). This is probably a result to the irreversible nature of consolidation. During freezing, pressures build up slowly because of gradual deformation and consolidation of the soil between ice lenses. This eventually stabilizes and the pressures level off. When the temperature is raised and the soil thaws, the pores do not expand to their original configuration and the pressure falls abruptly.

Table 7.2 compares changes in the internal pressure and flow direction, resulting from changes in the temperature at the cold end (exp. 30, Fig. 6.3) and at the warm end (exp. 29, Fig. 6.19). The observed changes in pressure were always less than the change in the equilibrium ice pressure (eqn. 6.2). This is probably because of a certain thermo-mechanical inertia in the system. In other words, insufficient time was allowed for equilibrium to be fully established.

---

[7] For dilution to occur, the rate of outflow must exceed the diffusion rate of lactose molecules. (Diffusion acts to restore a uniform solute concentration).

Table 7.2

Effect of Changes in End Temperature to the Internal Pressures

Soil	Allendale		Allendale	
Exp.	29		30	
T_{p1}	-0.50		0.10	
T_{p2}	-0.40	-0.50	0.30	0.00
	Colder Transducer		Colder Transducer	
ΔT	0.085	-0.085	0.085	-0.110
ΔP_i	-96	96	-96	124
ΔP_o	-35	29	-62	98
	Warmer Transducer		Warmer Transducer	
ΔT	0.050	-0.050	0.120	-0.175
ΔP_i	-34*	-34*	-22*	85*
ΔP_o	-27	15	-7	11
ΔQ	0.11	-0.04	-0.05	0.07

T_{p1} = initial temperature of cooling plate, °C

T_{p2} = temperature of cooling plate after the change, °C

ΔT = temperature change at transducer, °C (interpolated from thermal profiles)**

ΔP_i = change in equilibrium ice pressure to (eqn. 6.2), kPa**

(*temperature at transducer increased above frost line temperature. At temperatures warmer than this the ice thaws so the pressure should remain at atmospheric pressure.)

ΔP_o = observed change in pressure, kPa**

ΔQ = change in flow at warm end, cm^3 (positive sign)

**Positive values indicate an increase in ΔT, ΔP_i or ΔP_o. Negative values indicate a decrease.

It is puzzling that the flow of water in exp. 29 was in the opposite direction to that observed in exp. 30. When the soil is warmed, water should flow in at the warm end, as a result of thawing. When the temperature is lowered, the water should flow in the opposite direction.

In exp. 40 (Fig. 7.5), thawing of ice and associated volume decreases caused an accelerated influx of water at the warm end after the cold-end temperature was raised from -0.7°C to -0.3°C. A large negative pressure developed temporarily at the warmer transducer. This was located in the zone which thawed completely. A similar effect also occurred in exp. 31 (Fig. 6.17) and exp. 35 (Fig. 6.24) when the end temperature was raised. Negative pressures occurred because the rate at which the volume decreased, due to thawing, exceeded the rate of inflow. The inflow was impeded, temporarily, by the very low hydraulic conductivity of the frozen soil which remained around the transducers.

It is interesting that the pressure at the colder transducer declined to atmospheric after the cold-end temperature was increased (exp. 40). The transducer actually remained within the frozen section and so positive pressures might be expected there. When the cold-end temperature was later lowered to -0.70°C, the high pressures, which occurred previously, were not re-established. The amount of ice that formed during refreezing was less than the amount melted when the end temperature was raised. This may be caused by the diffusion of minute quantities of lactose through the soil when the temperature was raised.

7.5 Effect of Repeated Freezing

Repeated freezing generally increased the pressures by about 20%. This is evident in Fig. 6.24 (exp. 35). Pressures increased by about 30 kPa (including the reservoir pressure) although the flow remained identical in both cases. There was no further increase during subsequent freeze cycles.

A similar effect also occurred in heaving tests with unconfined Caen silt (S. Dallimore, 1985, personal communication). The volume displacement doubled during the second freeze. The increase can be attributed to vertical cracks and fissures formed during the initial freeze, which increased the hydraulic conductivity of the unfrozen soil (Chamberlain and Gow, 1979).[8] Further changes in displacement after the second freeze were diminishingly small, because the vertical fissures, once formed, do not enlarge much with subsequent freezing.

In a confined soil, the formation of vertical fissures probably has little to do with the increased pressures because pressures are established as a result of freezing of pore water in situ. The pressures, therefore, are independent of any increase in the hydraulic conductivity of the soil caused by vertical fissures. Instead, the

---

[8] An interesting question concerns the mechanism by which vertical fissures form in the soil. Normally these are attributed to a large negative (sub-atmospheric) pore water pressure that develops during freezing of unconfined soils. This increases the intergranular stress laterally, which causes the soil to crack, much like the formation of dessication cracks in drying soils (Chamberlan and Gow, 1979). However, in a confined soil, this cannot be the reason because the pore water pressures remain at atmospheric pressure.

higher pressures may be related to consolidation of the soil skeleton during the first freeze, which reduced its compressibility, although the total pore volume of the soil remained unchanged. This facilitates the growth of ice lenses during the second freeze so the pressures were established more rapidly.

7.6 Significance of Frost Susceptibility Classification to the Pressures Established

It is interesting to consider how large heaving pressures can develop in a material classified as 'non-frost susceptible', such as the Snec sand (Fig. 6.16, p. 147). The frost susceptibility classification generally refers to the expansive ability of a soil in the situation where it is unconfined. In an unconfined sand, ice lens growth is severely impeded by the very low hydraulic conductivity of the soil. This restricts the flow of water toward potential segregation sites behind the frost line - thus, the designation 'non-frost susceptible'.

However, the situation is different when a sand is confined. In this case, ice forms as a result of freezing of pore water in situ rather than the addition of water from an external supply. Ice pressures, therefore, are independent of the frozen hydraulic conductivity of the soil. Since the growth of segregation ice is not necessary for ice pressures to develop, the frost susceptibility classification is no longer applicable.

7.7 Hydraulic Conductivity of Caen Silt

Experiments were carried out to determine the hydraulic conductivity of the Caen silt. The soil was prepared as a normally consolidated, saturated sediment which was frozen inside the frost pressure

cell by first lowering the temperature to -0.30°C at one end and then, 24 hours later, at the other end. This avoided creating a closed system by simultaneously freezing both ends of the soil, which would burst the cell.[9] The soil was allowed to equilibrate for about 4 days. After this, both reservoirs were flushed with the appropriate concentration of lactose solution (Appendix E) and a hydraulic pressure of 20 mH_2O (196.2 kPa) was applied to one reservoir for about 30 minutes (flow readings taken at 10 minute intervals). The reservoirs were then purged with air, the soil temperature was raised and the process repeated. At temperatures warmer than -0.15°C, the cellulose acetate membrane (pore size <0.005 μm) was exchanged for a nitrocellulose membrane (<0.05 μm) because of the impedance to flow by the smaller pores.[10]

---

[9] In one test, both ends of the soil were frozen simultaneously. After several hours, the internal pressures were so high that the experiment had to be stopped to prevent damage to the cell.

[10] Ideally, the hydraulic conductivity of the membrane filter should be greater than that of the soil, otherwise, significant error will occur in the results. (Hydraulic conductivity of the nitrocellulose membrane = 2.5×10^{-9} m s^{-1}, freezing temp. -1°C). For practical purposes this rule was not strictly adhered to because coarser pored membranes would allow significant lactose diffusion into the soil, which would introduce an even larger component of error into the results. Hydraulic conductivity values for the soil, k_s, are corrected for the impedance of the membrane by:

$$k_s = \frac{\ell_s}{\frac{\ell}{K} - \frac{\ell_m}{k_m}}$$

ℓ_m = thickness of membrane
ℓ_s = thickness of frozen soil
K = hydraulic conductivity of system (soil plus membrane)
ℓ = thickness of system (soil plus membrane).

FIGURE 7.6

HYDRAULIC CONDUCTIVITY OF FROZEN CAEN SILT AS A FUNCTION OF TEMPERATURE

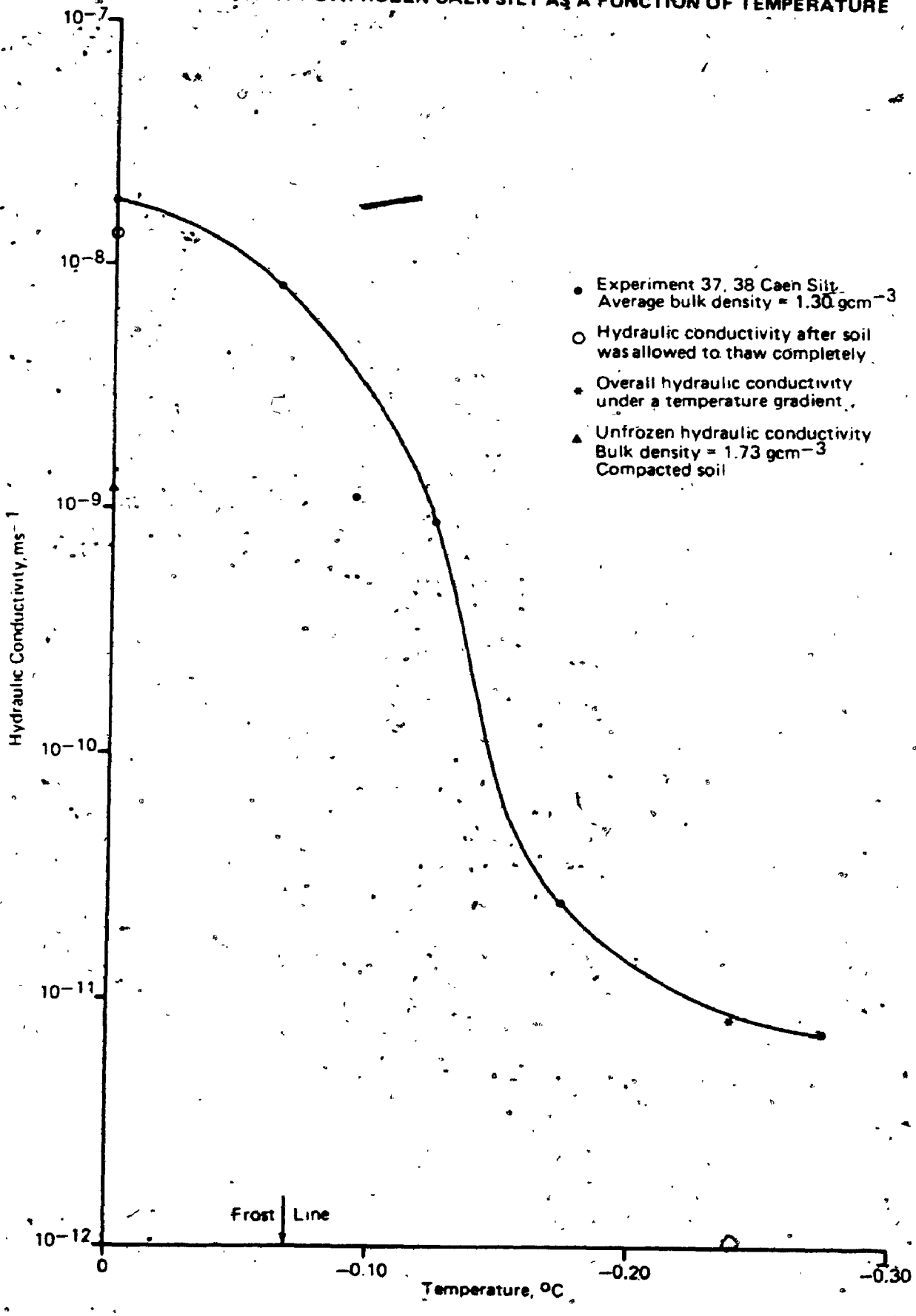

The hydraulic conductivity of Caen silt was calculated from Darcy's law (eqn. 2.2). The hydraulic conductivity versus temperature curve (Fig. 7.6) is comparable to the curves obtained by Horiguchi and Miller (1983) for similar materials (Fig. 2.6). An interesting observation is that the hydraulic conductivity continued to increase at temperatures warmer than the natural freezing temperature of the soil (about -0.07°C). This probably occurred because of continued thawing of ice-filled fissures within the soil. At 0°C, even after 4 days was allowed for the soil to thaw, ice fissures were still visible surrounded by a layer of liquid water.[11] These thawed more slowly than the rest of the soil because of the greater heat input required to thaw pure ice. When the cooling unit was switched off and the soil was allowed to thaw completely, the hydraulic conductivity dropped slightly (Fig. 7.6), as a result of subsequent setting of the soil and loss of macroporous channels associated with the ice fissures.

In one experiment the overall hydraulic conductivity of the soil (eqn. 2.5) was measured with a thermal gradient (0.15°C cm^{-1}) across the specimen (end temperatures, to 10°C, -0.50°C). The flux, J, resulting from the imposed hydraulic gradient, was obtained by subtracting the flow rate, before pressure was applied, from the flow

---

[11] A similar phenomenon also occurred in exp. 35 (Fig. 6.24). When the cold-end temperature was raised to +0.10°C, the internal pressure at the colder transducer dropped rapidly, but then levelled off at about 44 kPa. Ice lenses around the colder transducer appeared to be only partially melted, although the soil should have thawed completely. When the cooling unit was switched off 48 hours later, the soil thawed rapidly and the pressure dropped to atmospheric.

rate afterward (i.e. $J = J_f - J_i$). The overall hydraulic conductivity (8.5×10^{-12} m s^{-1}) is plotted at the mean temperature of the frozen section (about −0.24°C) in Fig. 7.6.

The observed changes in the internal pressure during the isothermal hydraulic conductivity tests leave some doubt as to the assumption of a linear hydraulic gradient implied by Darcy's law. In one instance, the observed hydraulic gradient (46.7 kPa cm^{-1}) was close to the hydraulic gradient given by Darcy's law (56 kPa cm^{-1}).[12] In most instances, however, the observed gradient was much smaller than the gradient given by Darcy's law. This was because the hydraulic pressures within the soil were too large.

---

[12] The observed hydraulic gradient is the pressure difference between the two transducers (56 kPa) ÷ distance (1.2 cm). The hydraulic gradient, according to Darcy's law is the difference in pressure between the end reservoirs (196 kPa) ÷ thickness of soil specimen (3.5 cm).

VIII. SUMMARY AND CONCLUSIONS

1. A thermo-rheological model of frost heaving has been proposed. The central hypothesis of the model is that the rheological properties of the soil exert a control on the frost heave pressures that develop. The ice pressures and their internal distribution are dependent not only upon the thermodynamic conditions (soil temperature and unfrozen water pressure), in accordance with the Clausius-Clapeyron equation, but also upon the rheological properties of the soil-ice matrix. The latter determine its ability to resist stress relaxation and, therefore, sustain an ice pressure gradient.

In the case of a confined soil with a temperature gradient, the system continuously attempts to reach a state of thermodynamic equilibrium (that is, an equilibrium ice pressure distribution) dictated by the temperature gradient and the unfrozen water pressure. This results in a slow movement of the ice toward warmer temperatures (lower pressures). The ice pressure gradient is sustained thermodynamically by freezing in the colder regions of the soil and melting in the warmer regions. The degree to which an equilibrium ice pressure distribution is achieved is determined by the resistance of the material to stress relaxation or its 'strength'. If the strength of the material is sufficient, then the gradient in the observed ice pressure would be close to or equal to the gradient in the equilibrium ice pressure given by the Clausius-Clapeyron eqn. If the strength of the soil is substantially reduced so that it is unable to sustain an ice pressure gradient, then the observed pressures would be uniform. In the case of the former, the soil behaves in a 'semi-rigid' (solid-like) fashion whereas in the latter, its behaviour is more fluid-like or

'quasi-viscous'. The transition between the two extremes is gradual rather than abrupt.

2. This hypothesis has been confirmed by an experiment in which the internal pressures were measured in freezing soils with a thermal gradient. Ice pressures were monitored by two very small transducers inserted 1.2 cm apart in a 3.5 cm soil column. Differences in the long term pressure up to 210 kPa were observed in a normally consolidated, saturated silt and also in a clay with a high silt content, associated with a temperature difference of about 0.20°C. When the thermal gradient was reversed, the pressures rapidly equalized and then slowly began to diverge again in accordance with the new direction of the thermal gradient.

3. The differences in the observed long-term pressures were very sensitive to small changes in soil density. The maximum difference occurred in specimens prepared as normally consolidated sediments. The gradient in the observed pressure was slightly less than the gradient in the equilibrium ice pressure. In this case, the behaviour of the soil can be regarded as 'semi-rigid'. This is attributed to a significant 'strength' or a resistance to stress relaxation of the material.

4. With compacted soils and slurries, the gradient in the observed pressure was much less than the gradient in the equilibrium ice pressure. This is due to a substantial reduction in the 'strength' of these materials so that they are unable to sustain a large increase in ice pressure with colder temperatures. In this case, the behaviour of the material can be regarded as 'quasi-viscous'.

5. It is suggested that the soil is able to sustain much larger ice pressure gradients when it is prepared as a normally consolidated

sediment because the ice content of the soil is close to an optimum value at which the strength of the material is maximum. In compacted soils and slurries, changes in the ice content of these materials with respect to the optimum (due to decreases/increases in the porosity), result in substantial reductions in the strength. As a result the observed pressures tended toward a uniform distribution.

6. In one experiment, the observed pressures at successive decrements in temperature were almost uniform. This was attributed to substantially reduced ice contents in this particular experiment and also slower rates of freezing which may also affect its strength. In this case the behaviour of the soil was almost fluid-like.

7. In the normally consolidated specimens, the pressure at the colder transducer increased rapidly at first, levelling off at a value close to the equilibrium ice pressure, two or three days after freezing began. At the warmer transducer, which was located in the frozen zone just behind the frost line, the pressure was initially much greater than the equilibrium ice pressure. This gradually decreased over a long period, toward the equilibrium ice pressure. The decline in pressure was accompanied by a very slow flow of water into the soil at the warm end. These phenomena were attributed to internal pressure-melting of ice lenses close to the frost line as the system attempted to restore thermodynamic equilibrium.

8. When the soil was frozen with a large positive pore water pressure, the ice pressures were proportionally larger in accordance with the Clausius-Clapeyron equation. However, the distribution of ice pressure with colder temperatures remained about the same as that normally observed, presumably, because the positive pore water pressure

did not affect the rheological properties of the soil. This may not be the case if the pore water pressures are substantially negative. The presence of air would reduce the strength so the pressures would tend toward a more uniform distribution.

9. Repeated freezing increased the pressures by about 20%. This was attributed to the reduced compressibility of the soil after the initial freeze.

10. Frost susceptibility criteria cannot be applied to the situation where the soil is confined because there is no volume displacement. This was confirmed by observations of large internal pressures in a sand which was classified as 'non-frost susceptible'. This is because the heaving pressures established were independent of the frozen hydraulic conductivity of the soil which, in the case of an unconfined sand, would otherwise limit the volume displacement.

BIBLIOGRAPHY

Aguirre-Puente, J. and Gruson, J., 1983. "Measurement of permeabilities of frozen soils". Fourth Int. Conf. Perm. Proc., Fairbanks, Alaska, Nat. Acad. Sci., Wash., p.5-9.

Anderson, D.M. and Morgenstern, N.R., 1973. "Physics, chemistry and mechanics of frozen ground": A review. Second Int. Conf. Perm. Proc., Yakutsk, U.S.S.R., Nat. Acad. Sci., Wash., p. 257-288.

Anderson, D.M. and Tiu, A.R., 1973. "The unfrozen interfacial phase in frozen soil water systems". Physical Aspects of Soil Water and Salt in Ecosystems, Springer Verlag, Berlin, p. 107-124.

Assur, A., 1980. "Some promising trends in ice mechanics", in Physics and Mechanics of Ice, Int. Symp. Copenhagen, Springer Verlag.

Bedford, R.E., Dauphinee, T.M. and Preston-Thomas, H. "Temperature Measurements". Nat. Res. Coun. Canada, Div. Phys., p. 80.

Biermans, M.B.G.M., Dijkema, K.M., and deVries, D.A., 1978. "Water movement in porous media towards an ice front". J. Hydrol. V.37, p. 137-148.

Bishop, A.W. and Blight, G.E., 1963. "Some aspects of effective stress in saturated and partly saturated soils". Géotechnique, V.13, p. 177-197.

Bolt, G.H. and Peech, M., 1953. "The application of the Gouy theory to soil-water systems". Soil Sci. Soc. Am. Proc., V.17, p. 210-213.

Bresler, E., 1972. "Interacting diffuse layers in mixed mono-divalent ionic systems". Soil Sci. Soc. Am. Proc., V.36, p. 891-896.

Brown, S.F., 1973. "The measurement of in-situ stresses and strain in soils". Symp. Field Instr. in Geotech., Eng., p. 38-51.

Ruil, M. and Aguirre-Puente, J., 1981. "Thermodynamic and experimental growth study of the crystal growth of ice". Am. Soc. Mech. Eng., Wash.

Burt, T.P. and Williams, P.J., 1976. "Hydraulic conductivity in frozen soils". Earth Surf. Processes, V.1, p. 349-360.

Chamberlain, E.J., 1981. "Frost susceptibility of soil: Review of index tests". U.S. Army Cold Reg. Res. Eng. Lab. Mon. 81-2, 121 p., Hanover, N.H.

Chamberlain, E.J. and Gow, A.J., 1979. "Effect of freezing and thawing on the permeability and structures of soils". Eng. Geol., V.13, p. 73-92

Colbeck, S.C., 1982. "Configuration of ice in frozen media". Soil Sci., V.133, p. 116-123.

Cox, G.F.N. and Johnson, J.B., 1983. "Stress measurements in ice". U.S. Army Cold Reg. Res. Eng. lab. Report 83-23, 38 p.

Czurda, K.A., 1983. "Freezing effects on soils: Comprehensive summary of the ISGF 82". Cold Reg. Sci. Tech., V.8, p. 93-107.

Defay, R. and Prigogine, I., 1951. "Tension Superficielle Adsorption". Liège Addition Desoer, 295 p. In: Traité de thermodynamique conformement aux methodes de Gibbs et de Donder., V.3.

Dorsey, N.E., 1968. "Properties of ordinary water substance", Hafner, N.Y., p. 239-247.

Ershov, E.D., 1977. "The mechanism of migration-segregation ice separation in freezing and thawing dispersed soils". (in english). Vestnik Moskovskogo Universiteta, Geologiya, V.32, n.2, p. 97-108.

Everett, D.H., 1961. "Thermodynamics of frost damage to porous solids". Trans. Far. Soc., V.57, p. 1541-1551.

Fish, A.M., 1984. "Thermodynamic model of creep at constant stress and strain rate". Cold Reg. Sci. Tech., V.9, p. 143-161.

French, H.M., 1976. "The periglacial environment", Longman, London, 309 p.

Gardner, A.R., Jones, R.H. and Harris, J.S., 1984. "A new creep equation for frozen soils and ice". Cold Reg. Sci. Techn., V.9, p. 271-275.

Geotechnical Science Laboratories, 1984. "Experimentation sur la gel d'un sol et d'une canalisation enterée et refroidie dans une installation d'essai de grandes dimensions". Direction de le Physique du Globe, Energie, Mines et Resources, Canada, 63 p.

Gilpin, R.R., 1982. "A frost heave interface condition for use in numerical modelling". Proc. Fourth Can. Perm. Conf., Calgary, Alta., p. 459-465.

Glen, J.W., 1975. "The mechanics of ice". U.S. Army Cold Reg. Res. Eng. Lab., Hanover, N.H., Mon. II-C2b, 47 p.

Gold, L.H., 1957. "A possible force mechanism associated with freezing of water in porous materials". Highway Res. Bd. Bull., V.168, p. 65-72.

Goughnour, R.R. and Andersland, O.B., 1968. "Mechanical properties of a sand-ice system". Proc. Am. Soc. Civil Eng., V.94 (SM4), p. 923-950.

Gray, H.J. and Issacs, A. (eds)., 1975. "A new dictionary of physics", Longman, London, 619 p.

Guymon, G., Hromadka, T.V., and Berg, R.L., 1980. "A one-dimensional frost heave model based upon simulation of simultaneous heat and water flux". Cold Reg. Sci. Tech., V.3, p. 253-262.

Groenevelt, P.H. and Bolt, G.H., 1969. "Non-equilibrium thermodynamics of soil-water system". Journ. Hydr., V.7, p. 358-388.

Groenvelt, P.H. and Kay, B.D., 1979. "Water and ice potentials in frozen soils". Water Resour. Res., V.13, p. 445-449.

Groenvelt, P.H. and Kay, B.D., 1980. "Pressure distribution and effective stress in frozen soils". Second Int. Symp. Ground Freezing, V.1, p. 597-610.

Harlan, R.L., 1973. "Analysis of coupled heat-freeze transport in partially frozen soil". Water Resourc. Res., V.9, p. 1314-1323.

Harlan, R.L., 1974. "Dynamics of water movement in permafrost: A review". In Perm. Hydrol., Proc. of Workshop Sem., Calgary, Can. Nat. Comm. Int. Hydr. Decade, p. 103-163.

Hesstvedt, E., 1964. "The interfacial energy ice/water". Norwegian Geotechnical Inst., Pub. n.64, p. 7-10.

Hoekstra, P. and Chamberlain, E., 1964. "Electro-osmosis in frozen soil". Nature, V.203, p. 1406-1407.

Hoekstra, P., Chamberlain, E. and Frate, T., 1965. "Frost-heaving pressures". U.S. Army Cold Reg. Res. Eng. Lab., Report 176, 12 p.

Hooke, R. Le B., Dahlin, B.B. and Kauper, M.T., 1972. "Creep of ice containing dispersed fine sand". J. Glaciology, V.11, n.63, p. 327-336.

Horiguchi, K. and Miller, R.D., 1980. "Experimental studies with frozen soil in an 'ice-sandwich' permeameter". Cold Reg. Sci. Tech., V.3, p. 177-183.

Horiguchi, K. and Miller, R.D., 1983. "Hydraulic conductivity functions of frozen materials". Fourth Int. Conf. Perm. Proc., Fairbanks, Alaska, p. 504-508.

Johnston, G.H. (ed.), 1981. "Permafrost engineering, design and construction". Associate Committee on Geotechnical Research, N.R.C., Wiley, N.Y., 540 p.

de Jong, E., 1967. "Application of thermodynamics to the study of soil moisture". Proc. Hydr. Symp., Univ. Sask., n.6, p. 25-47.

Kaplar, C.W. "Some strength properties of frozen soil and the effect of loading rate". U.S. Army Cold Reg. Res. Eng. Lab., Res. Rep. 159, 25 p.

Kay, B.D. and Groenevelt, P.H., 1983, "The redistribution of solutes in freezing soil: Exclusion of solutes". Fourth Int. Conf. Perm. Proc., Fairbanks, Alaska, p. 584-588.

Konrad, J.M. and Morgenstern, N.R., 1980. "A mechanistic theory of ice lens formation in fine-grained soils". Can. Geotech. J., V.17, p. 473-486.

Konrad, J.M. and Morgenstern, N.R., 1981. "The segregation potential of a freezing soil". Can. Geotech. J., V.18, p. 482-491.

Koopmans, R.W.R. and Miller, R.D., 1966. "Soil freezing and soil water characteristic curves". Soil Sci. Soc. Am. Proc., V.30, n.6, p. 680-685.

Ladanyi, B., 1972. "An engineering theory of creep of frozen soils". Can. Geotech. J., V.9, p. 63-90.

Ladanyi, B. and Lauzon, M., 1985. "Mechanical properties of Caen silt and Snec sand". Geotechnical Science Labs., Carleton Univ., Int. Rep.

Lautridou, J.P. and Ozouf, J.C., 1982. "Experimental frost shattering". Bulletin du Centre de Géomorphologie du CNRC, V.6, n.2, p. 215-232.

Lewis, G.N. and Randall, M., 1923. Thermodynamics and the free energy of chemical substances. McGraw-Hill, N.Y., p. 180-185.

Loch, J.P.G., 1975. "Secondary heaving: Experiments and analysis of frost heave pressures in soils". Ph.D. thesis, Cornell Univ., 102 p.

Loch, J.P.G., 1979. "Influence of heat extraction rate in the ice segregation rate in soils". Frost i Jord., V.20, p. 19-30.

Loch, J.P.G. and Kay, B.D., 1978. "Water redistribution in partially frozen saturated silt under several temperature gradients and overburden loads". Soil Sci. Soc. Am. J., V.42, p. 400-406.

Loch, J.P.G. and Miller, R.D., 1975. "Tests of the concept of secondary frost heaving". Soil Sci. Soc. Am. Proc., V.39, n.6, p. 1036-1041.

Mackay, J.R., 1979. "Pingos of the Tuktoyaktuk penninsula area, N.W.T.". Géogr. Phys. Quat., V.23, n.1, p. 3-61.

Mackay, J.R., 1980. "The origin of hummocks, western Arctic coast, Canada". Can. J. Earth Sci., V.17, p. 996-1006.

Mahar, L.J., Vinson, T.S. and Wilson, R., 1982. "Effects of salinity on freezing of granular soils". Third Int. Sym. on Ground Freezing, Hanover, N.H., 12 p.

McCabe, E.Y. and Kettle, R.J., 1982. "Heaving pressures and frost susceptibility". Proc. Third Int. Symp. Ground Freezing, Hanover, N.H., p. 285-294.

Miller, R.D., 1970. "Ice sandwich: Functional semipermeable membrane". Sci., V.169, p. 584-585.

Miller, R.D., 1972. "Freezing and heaving of saturated and unsaturated soils". Highway Res. Rec., V.393, p. 1-11.

Miller, R.D., 1977. "Lens initiation in secondary frost heaving". Proc. Int. Symp. on Frost Action in Soils, Lulea, Sweden, V.2, p. 68-74.

Miller, R.D., 1978. "Frost heaving in non-colloidal soils". Third Int. Conf. Perm. Proc., p. 708-713.

Miller, R.D., 1980. "Freezing phenomena in soils", in Applications of soil physics, D. Hillel ed., Academic Press, N.Y., p. 254-299.

Miller, R.D., 1980a. "The adsorbed film controversy". Cold Reg. Sci. Tech., V.3, p. 82-86.

Miller, R.D., Loch, J.P.G. and Bresler, E., 1975. "Transport of water and heat in a frozen permeameter". Soil Sci. Soc. Am. Proc., V.39, p. 1029-1036.

Ohrai, T., Takashi, T., Yamamoto, H. and Okampto, J., 1983. "Uniaxial compressive strength of ice segregated from soil". Third Int. Conf. Perm. Proc., p. 945-950.

Oliphant, J.L., Tiu, A.R. and Nakano, Y., 1983. "Water migration due to a temperature gradient in frozen soil". Fourth Int. Conf. Perm. Proc., p. 951-956.

O'Neill, K., 1983. "The physics of mathematical frost heave models: A review". Cold Reg. Sci. Tech., V.6, p. 275-291.

O'Neill, K. and Miller, R.D, 1982a. "Numerical solutions for a rigid-ice model of secondary frost heave". Second Int. Symp. on Ground Freezing, Trondheim, Norway, V.1, p. 656-669.

Onsager, L., 1931. "Reciprocal relations in irreversible processes II". Phys. Rev., V.38, p. 2265-2279.

Outcalt, S., 1971. "An algorithm for needle ice growth", Water Resources Res., V.7, n.2, p. 394-400.

Patterson, D. and Smith, M.W., 1981. "The measurement of unfrozen water content by time domain reflectometry; results from laboratory tests". Can. Geotech. J., V.18, n.1, p. 131-144.

Perfect, E. and Williams, P.J., 1980. "Thermally induced water migration in frozen soils". Cold Reg. Sci. and Tech., V.3, p. 101-109.

Penner, E., 1959. "The mechanism of frost heaving in soils". Highway Res. Bull., n.225, p. 1-13.

Penner, E., 1960. "The importance of freezing rate in frost action in soils". Am. Soc. Testing Materials, Proc. V.60, p. 1151-1165.

Penner, E., 1967. "Heaving pressures in soils during unidirectional freezing". Can. Geotech. J., V.4, p. 398-408.

Penner, E., 1972. "Soil moisture redistribution by ice lensing in freezing soils". 17th Annual meeting, Can. Soc. Soil Sci., Lethbridge, Alta., p. 44-62.

Penner, E. and Goodrich, L.E., 1980. "Location of segregated ice in frost susceptible soil". Second Int. Symp. on Ground Freezing, Trondheim, Norway, p. 626-639.

Penner, E. and Ueda, T., 1978. "A frost susceptiblity test and a basis for interpreting heaving rates". Third Int. Conf. Perm., V.1, p. 721-727.

Peterson, R.E., 1974. "Stress concentration factors". Wiley, N.Y., p. 1-13.

Philip, J.R., 1980. "Thermal fields during regelation". Cold Reg. Sci. Tech., V.3, p. 193-204.

Phukan-Morgenstern-Shannon, 1979. "Development of a frost heave classification system". Revised Interim Report, V.1, Fluor Northwest Inc., Fairbanks, Alaska, 81 p.

Prigogine, I. and Defay, R., 1954. "Chemical thermodynamics", Longmans Green, Toronto, 543 p.

Radd, F.J. and Oertle, D.H., 1973. "Experimental pressure studies of frost heave mechanisms and the growth-fusion behaviour of ice". Second Int. Perm. Conf., Yakutsk, U.S.S.R., p. 377-384.

Ratkje, S.K., 1982. "On the energetics of coupled transport processes: A theoretical and experimental irreversible thermodynamic investigation", Det. Konglelige Norske Videnskabers Selskab. Skrifter, n.6, p. 96-106.

Römkens, M.J.M. and Miller, R.D., 1973. "Migration of mineral particles in ice with a temperature gradient". J. Coll. Interf. Sci., V.42, p. 103-111.

Sayles, F.H., 1968. "Creep of frozen sands". U.S. Army Cold Reg. Res. Eng. Lab. Tech. Rep. 190, 54 p.

Sayles, F.H. and Carbee, D.L., 1981. "Strength of frozen silt as a function of ice content and dry unit weight". Eng. Geol., V.18, p. 55-66.

Skapski, A., Billings, R. and Rooney, A., 1957. "The capillary cone method for determination of surface tension of solids". J. Chem. Phys., V.26, p. 1360.

Smith, M.W., 1985. "Observations of soil freezing and frost heave at Inuvik, N.W.T., Canada". Can. J. Earth Sci., V.22, n.2, p. 283-290.

Srivastava, R.C. and Abrol, I.P., 1966. "Nonlinear thermodynamics of irreversible processes and flow of water through soils". Soil Sci., V.102, p. 416-417.

Sutherland, H.B. and Gaskin, P.N., 1973. "Pore water and heaving pressures developed in partially frozen soils". Int. Conf. Perm. Proc., Yakutsk, U.S.S.R., p. 409-419.

Sheeran, D.E. and Yong, R.N., 1975. "Water and salt redistribution in freezing soils". Proc. Conf. on Soil-Water Problems in Cold Regions, Calgary, Alta., p. 58-69.

Taber, S., 1930. "The mechanics of frost heaving". J. Geol., V.38, p. 309-317.

Taylor, G.S. and Luthin, J.N., 1978. "A model for coupled heat and moisture transfer during frost heaving". Can. Geotech. J., V.15, p. 548-555.

Takagi, S., 1980. "The adsorption force theory of frost heaving". Cold Reg. Sci. Tech., V.3, p. 57-81.

Takashi, T., Ohrai, T., Yamomoto, H., and Okamoto, J., 1980. "Upper limit of heaving pressure derived by pore water pressure measurements of partially frozen soil". Second Int. Symp. Ground Freezing, Trondheim, Norway, p. 713-724.

Takashi, T., Yamomoto, H., Ohrai, T. and Masuda, M., 1978. "Effect of penetration rate of freezing and confining stress on the frost heave ratio of soil". Third Int. Conf. Perm. Proc., Edmonton, Alta., p. 737-742.

Templeton, J.S., 1979. "Measurement of sea ice pressures". Proc. Fifth Int. Conf. Port and Ocean Engineering Under Arctic Conditions, Oslo, Norway, p. 73-87.

Ting, J.M., 1981. "Creep of frozen sands qualitative and quantitative models". Final report, part II, M.I.T., p. 241-259.

Torrance, J.K. and Wood, J.A., 1983. "Investigation of temperature-induced stresses and water movements in freezing soils". Final Report to Dept. of Energy, Mines and Resources, Ottawa, Canada, DSS File No. 24SU.23235-2-0581.

Tsytovich, N.A., 1975. "The mechanics of frozen ground". Scripta Book Co., Wash., D.C., 349 p. (G.K. Swinzow, ed.).

Voitkovskiy, K.R. (ed.), 1968. "Foundations of structures in frozen soils in Yakutia". Nauka, Moscow, 199 p. (in Russian).

Vyalov, S.S. (ed.), 1962. The strength and creep of frozen soils and calculations for ice-soil retaining structures. U.S. Army Cold Reg. Res. Eng. Lab., Transl. 76, (1965) 321 p.

Washburn, A.L., 1979. "Geocryology: A survey of periglacial processes and environments". Edward Arnold, London, 406 p.

Williams, F.T., 1973. "The behaviour of stress measuring devices in rocks of various properties". Symp. Field Instrumentation in Geotechnical Engineering, p. 463-474.

Williams, P.J., 1967. "Properties and behaviour of freezing soils". Norwegian Geotech. Inst., Publ. n.72, 119 p.

Williams, P.J., 1982. "The surface of the earth: an introduction to geotechnical science". Longman, N.Y., 212 p.

Williams, P.J. and Wood, J.A., 1981. "Investigation of pressure changes in frozen soils during thermally-induced moisture migration". Final Report to Dept. Energy, Mines and Resources, Ottawa, Canada. DSS File 05SU.23235-0-0496, 131 p.

Williams, P.J. and Wood, J.A., 1982. "Investigation of moisture movements and stresses in frozen soils". Final Report to Dept. Energy, Mines and Resources, Ottawa, Canada. DSS File 24SU.23235-2-0700, 134 p. (Supplementary issue in Sept. 1982. DSS File 09SU.23235-2-0777, 46 p.)

Williams, P.J. and Wood, J.A., 1984. "Internal stresses in soils during frost heaving". Final Report to Dept. Energy, Mines and Resources, Ottawa, Canada, DSS File 24SU.23235-3-1098, 53 p.

Williams, P.J. and Wood, J.A., 1985. "Investigation of internal stresses in freezing soils and their effects on long-term migration of moisture". Final Report to Dept. Energy, Mines and Resources, Ottawa, Canada, DSS File 24ST.23235-4-0559, 38 p.

Williams, P.J. and Wood, J.A., 1985a. "Internal stresses in frozen ground". Can. Geotech. J., V.22, n.3, p. 413-416.

Wood, J.A. and Williams, P.J., 1985. "Stress distribution in frost heaving soils". Fourth Int. Symp. Ground Freezing, Sapporo, Japan, p. 165-171.

Wood, J.A. and Williams, P.J., 1985a. "Further experimental investigation of regelation flow with an ice-sandwich permeameter". Symp. Freezing and Thawing of Soil Water Systems, Am. Soc. Civil Eng., Technical Council on Cold Regions Engineering, p. 85-94.

Yariv, S. and Cross, H., 1979. "Geochemistry of colloid systems". Springer Verlag, Berlin, 450 p.

Yuanlin, Z. and Carbee, D.L., 1983. "Creep behaviour of frozen silt under constant uniaxial stress". Fourth Int. Conf. Perm. Proc., p. 1507-1513.

APPENDIX A

DESIGN SPECIFICATIONS OF FROST PRESSURE CELL

1. Plexiglass sample container

	Inner diameter	5.39 cm
	Inner length	3.55 cm
	Wall thickness	3.41 cm

2. Aluminum cooling plates

	Overall thickness	1.78 cm
	Outer flange diameter	8.12 cm
	Outer flange thickness	0.83 cm
	Inner flange diameter	6.75 cm
	Inner flange thickness	0.62 cm
(i)	O-ring outer diameter	7.00 cm
	O-ring thickness	0.36 cm
	O-ring flange diameter	6.35 cm
	O-ring flange thickness	0.32 cm
(ii)	Reservoir diameter	5.40 cm
	Reservoir thickness	0.17 cm
	Feed through gland diameter	0.20 cm

3. Porous aluminum plates (membrane supports)

	Thickness	0.62 cm
	Diameter	6.03 cm

Holes 0.20 cm diameter drilled vertically 0.25 cm apart

(i)	Wire mesh diameter	5.50 cm
	Wire mesh thickness	0.03 cm

4. Brass heat sinks

Diameter	6.30 cm
Thickness	1.05 cm

5. Peltier modules (15 amp 120 V.d.c.)

Length	3.00 cm
Thickness	0.45 cm

6. Pressure Transducers (Kulite VQS-250 series)

	Length	1.72 cm
	Inner diameter	0.64 cm
	Outer (flange) diameter	0.78 cm
(i)	O-ring outer diameter	0.95 cm
	O-ring thickness	0.18 cm
(ii)	Copper tubes	
	Length	1.55 cm
	Outer diameter	0.31 cm
	Inner diameter	0.21 cm
	Flange diameter	0.62 cm
(iia)	O-ring outer diameter	0.95 cm
	O-ring thickness	0.18 cm
(iii)	Adjustable brass sleeve	
	Diameter (approx.)	0.53 cm
	Width	0.50 cm
(iv)	Plexiglass retaining nuts	
	Length	0.90 cm
	Outer thread diameter	0.89 cm

	Thickness of head	0.19 cm
(iva)	Plexiglass extention tubes	
	Length	1.90 cm
	Outer diameter	0.65 cm
	Inner diameter	0.33 cm

7. Thermistors (YSI 3000 Ω)

(i)	Copper housing tubes	
	Length	2.45 cm
	Outer diameter	0.31 cm
	Inner diameter	0.21 cm
	Flange diameter	0.60 cm
(ii)	O-ring outer diameter	0.95 cm
	O-ring thickness	0.18 cm

8. Spacing of Pressure Transducers and Thermistors

T_1 Cooling plate thermistor, 1.50 cm from E_1

E_1 Boundary of soil specimen

T_2 Soil thermistor, 0.50 cm from E_1

P_1 Pressure transducer, 1.15 cm from E_1

T_3 Soil thermistor, 1.75 cm from E_1

P_2 Pressure transducer, 2.35 cm from E_1

T_4 Soil thermistor, 3.00 cm from E_1

E_2 Boundary of soil specimen, 3.50 cm from E_1

T_5 Cooling plate thermistor, 5.00 cm from E_1

APPENDIX B

LIST OF EQUIPMENT USED IN THE EXPERIMENT

1. Precision low temperature incubator, model 815
2. Hotpack refrigerated bath circulator, model 603340
3. Geonor thermoelectric cooling control unit, model e-600
4. 2 Keithley digital multimeters, model 177
5. Keithley digital multimeter, model 191
6. Keithley digital multimeter, model 160
7. Hewlett Packard twin channel d.c. power supply, model 6205B
8. Rikadenki zero suppression voltage unit, model SV-D
9. Canlab twin channel strip-chart recorder, model 285
10. 4 Kulite pressure transducers, model VQS-250 (rated pressure 50 psi)
11. Canlab single channel strip-chart recorder, model 255
12. 1 Kulite pressure transducer, model XTM-1-190 (rated pressure 100 psi)
13. 7 YSI 3000 Ω precision thermistors, model 44030
14. Sola Basic (single phase, 60 Hz, 120 volt) voltage regulator, model 63-13-210
15. Minolta camera and multifunction back, model X-700 (film, panatomic-x ASA 32)
16. 2 Hammond 125 V power bars, cat. no. 1584 H8A
17. 2 Boxer 115 V fans, model WS2107 FL-1002
18. 2 Triple-channel switching units
19. 1 Multi-channel switching unit
20. 10 Whitey stainless-steel ball valves, model 42S4
21. 4 Nupro brass v-stem valves, model 4-J

APPENDIX C

CALIBRATION REPORTS FOR PRESSURE TRANSDUCERS

PRESSURE TRANSDUCER TEST REPORT

MODEL NO VQS-250-50 SG SERIAL NO. 4505-5-76

CUSTOMER DURHAM CUSTOMER P.O. No. R831401

STANDARD ELECTRICAL CONNECTIONS (Per ISA 37.)

Red - + Input Green - + Output
Black - - Input White - - Output

SPECIAL CONNECTIONS

TEST CONDITIONS.

Rated Pressure 50 psi SG ___ Gage X Sealed Gage
Maximum Pressure 100 psi SG
Maximum Reference Pressure ___ psi ___ Absolute ___ Differential
Tested at 5 VDC Excitation Maximum Excitation 7.5 VDC

SPECIFICATIONS:

Sensitivity .902 mV/psi
Zero Pressure Output. < ±3% F.S.
Thermal Effect on Zero: < ±1 % FS/100°F ___ Not Compensated
Thermal Effect on Sensitivity: < ±2 %/100°F ___ Not Compensated*
Compensated Temperature Range 14°F to 86°F (-10°C to 30°C)
Output Impedance 364 ohms Input Impedance 732 ohms
*See Bulletin ___ for external compensation method

REMARKS:

SILASTIC COATING ON DIAPHRAGM. O-RING SUPPLIED.

UNIT PARYLENE-COATED.

NEW TEST REPORT BEING ISSUED AFTER REPLACEMENT OF COMPENSATION MODULE.

QUALITY ASSURANCE:

Tested by H. S. Inspected by A47

Date ___ Date AUG 10 1983

PRESSURE TRANSDUCER TEST REPORT

MODEL NO. VQS-250-50 SG SERIAL NO 1025-7-126

CUSTOMER DURHAM CUSTOMER P.O. No 883140

STANDARD ELECTRICAL CONNECTIONS: (Per ISA 37.1) SPECIAL CONNECTIONS

Red - + Input Green - + Output
Black - - Input White - - Output

TEST CONDITIONS:

Rated Pressure 50 psi SG ____ Gage X Sealed Gage
Maximum Pressure 100 psi SG
Maximum Reference Pressure ____ psi ____ Absolute ____ Differential
Tested at 5 VDC Excitation Maximum Excitation 7.5 VDC

SPECIFICATIONS:

Sensitivity .902 mV/psi
Zero Pressure Output: < ±3% F.S.
Thermal Effect on Zero: < ±1 % FS/100°F ____ Not Compensated
Thermal Effect on Sensitivity: < ±2 %/100°F ____ Not Compensated*
Compensated Temperature Range 14°F to 86°F (-10°C to 30°C)
Output Impedance 359 ohms Input Impedance 646 ohms
*See Bulletin ____ for external compensation method

REMARKS:

SILASTIC COATING ON DIAPHRAGM. O-RING SUPPLIED.

UNIT PARYLENE-COATED.

REPLACEMENT FOR S. N. 4417-2-19

QUALITY ASSURANCE:

Tested by H. S. Inspected by A47

Date SEP 30 1983 Date OCT 4 1983

PRESSURE TRANSDUCER TEST REPORT

MODEL NO VBS-250-50 SG SERIAL NO 1025-7-73

CUSTOMER DUR-AM CUSTOMER PO RE31689

STANDARD ELECTRICAL CONNECTIONS (Per ISA 37.) SPECIAL CONNECTIONS

Red — +Input Green — +Output
Black — -Input White — -Output

TEST CONDITIONS

Rated Pressure 50 psi SG ____ Gage X Sealed Gage
Maximum Pressure 100 psi SG
Maximum Reference Pressure ____ psi ____ Absolute ____ Differential
Tested at 5 VDC Excitation Maximum Excitation 7.5 VDC

SPECIFICATIONS

Sensitivity .889 mV psi
Zero Pressure Output ± = 3% F.S.
Thermal Effect on Zero < ±1 %FS/100°F ____ Not Compensated
Thermal Effect on Sensitivity < ±2. %/100°F ____ Not Compensated*
Compensated Temperature Range 14°F to 86°F (-10°C to +30°C)
Output Impedance 362 ohms Input Impedance 649 ohms
*See Bulletin ____ for external compensation method

REMARKS

XX O Ring Supplied ___ Copper Washer Supplied
___ 4 Screen Added ___ 8 Screen Added

UNIT PARYLENE-COATED.
SILASTIC COATING ON DIAPHRAGM.
REPLACEMENT FOR S. N. 4505-5-79

QUALITY ASSURANCE

TESTED BY H. S. INSPECTED BY A47
DATE 12-13-83 DATE DEC 14 1983

PRESSURE TRANSDUCER TEST REPORT

MODEL NO VGS-250-50 SG SERIAL NO 1025-7-106

CUSTOMER DURHAM CUSTOMER P.O. R531689

STANDARD ELECTRICAL CONNECTIONS Per ISA 37.1 SPECIAL CONNECTIONS

Red — Input Green — Output
Black — Input White — Output

TEST CONDITIONS.

Rated Pressure 50 psi SG ____ Gage X Sealed Gage
Maximum Pressure 100 psi SG
Maximum Reference Pressure ____ psi ____ Absolute ____ Differential
Tested at 5 VDC Excitation Maximum Excitation 7.5 VDC

SPECIFICATIONS.

Sensitivity .897 mV/psi
Zero Pressure Output < ± 3% F.S.
Thermal Effect on Zero < ±1 %FS 100°F ____ Not Compensated
Thermal Effect on Sensitivity < ±2 %/100°F ____ Not Compensated*
Compensated Temperature Range 14°F to 86°F (-10°C to +30°C)
Output Impedance 352 ohms Input Impedance 668 ohms
*See Bulletin ____ for external compensation method

REMARKS X O-Ring Supplied ☐ Copper Washer Supplied
☐ M Screen Added ☐ B Screen Added

UNIT PARYLENE-COATED.
SILASTIC COATING ON DIAPHRAGM.
REPLACEMENT FOR S. N. 4505-5-81

QUALITY ASSURANCE.

TESTED BY H. S. INSPECTED BY A47

DATE 12-13-83 DATE DEC 4 1983

PRESSURE TRANSDUCER TEST REPORT

(ORDERED AS XTM-T-190-100 SG)

MODEL NO. XTM-190-100 SG NEW MODEL SERIAL NO 375-5-114 (R4-40)

CUSTOMER DURHAM CUSTOMER P O No 1890

STANDARD ELECTRICAL CONNECTIONS: (Per ISA 37.1) SPECIAL CONNECTIONS

Red	+ Input	Green	+ Output
Black	- Input	White	- Output

TEST CONDITIONS

Rated Pressure 100 psi SG ___ Gage X Sealed Gage

Maximum Pressure 200 psi SG

Maximum Reference Pressure ___ psi ___ ___ Absolute ___ Differential

Tested at 5 VDC Excitation Maximum Excitation 7.5 VDC

SPECIFICATIONS:

Sensitivity .403 mV/psi

Zero Pressure Output < ±3% F.S.

Thermal Effect on Zero < ±2 %FS/100°F ___ Not Compensated

Thermal Effect on Sensitivity < ±2 %/100°F ___ Not Compensated*

Compensated Temperature Range 14°F to 86°F (-10°C to +30°C)

Output Impedance 328 ohms Input Impedance 965 ohms

*See Bulletin ___ for external compensation method

REMARKS

O-RING SUPPLIED.

MAXIMUM TORQUE 15 INCH POUNDS.

QUALITY ASSURANCE:

Tested by M. S. Inspected by ___

Date 12-29-81 Date DEC 9 1981

APPENDIX D

FABRICATION AND INSTALLATION OF RUBBER BLADDERS

Materials:

1. Vultex 1-F-5501 latex: available from General Latex and Chemicals, Brampton, Ontario.
2. Moulds: copper tubing 15 cm long, 0.32 cm outer diameter.
3. Coagulant: calcium nitrate tetrahydrate.
4. Ethyl alcohol.
5. Talcum powder.

Procedure:

1. Clean moulds first with deoxidizer (Brasso) followed by glassware detergent and allow to dry.
2. Prepare a solution of 20% by weight calcium nitrate tetrahydrate in ethyl alcohol. Stir until crystals are completely dissolved.
3. Dip mould in coagulant and shake off excess droplets.
4. Dip mould slowly into latex at an angle and then withdraw.
5. Allow latex to air dry at room temperature for 12 hours.
6. Oven dry bladders at 60°C for 12 hours.
7. Cool bladders and dust with talcum powder. Slowly peel bladder off mould applying talc to inner surface.
8. Immerse bladders in water for 12 hours.
9. Store in a cool place away from light.
10. The formation of clots of latex on the mould during coagulation will result in a bladder with a lumpy surface. Thicker bladders are generally preferred because this improves the seal made by the brass sleeve, reducing the possibility of oil leakage between the bladders and the copper tubing. For thicker bladders, the concentration of the coagulant may be increased or the mould may be dipped two or three times into the latex rather than once.

Installation Notes:

After the bladder has been fitted over the tubing and the brass sleeve attached, silicone oil is injected into the orifice with a syringe until the copper tubes are filled. Care must be taken to ensure that no air bubbles become entrapped within the oil by alternately squeezing and releasing the bladders while filling them. A drop of oil is placed on the diaphragm of each transducer to displace air from the small depressions in which the diaphragms are located. As the transducers are inserted into the holes in the walls of the cell, the bladders are squeezed and slowly released to exclude air.

APPENDIX E

FREEZING TEMPERATURE OF LACTOSE SOLUTION AS A FUNCTION OF LACTOSE CONCENTRATION

Raw data obtained from the Handbook of Chemistry and Physics 58th ed., p. D232-233. Lactose concentration determined at intervals of 0.01°C by Lagrangian interpolation. Since the data given in the table below is for anhydrous lactose (mol. wt. 340.3) a small correction is necessary to allow for the hydration of lactose (mol. wt. 360.3). The correction factor is (360.3 - 340.3)/340.3 = 0.05. The required concentration of lactose monohydrate is:

$$C_h = C \times 0.05$$

C = anhydrous lactose concentration, g ℓ^{-1}

Freezing Temperature °C	Lactose Concentration g ℓ^{-1}
0	0
-0.01	1.78
-0.02	3.56
-0.03	5.35
-0.04	7.16
-0.05	8.94
-0.06	10.74
-0.07	12.54
-0.08	14.34
-0.09	16.14
-0.10	17.94
-0.11	19.74
-0.12	21.54
-0.13	23.33
-0.14	25.12

Freezing Temperature °C	Lactose Concentration g ℓ^{-1}
-0.15	26.90
-0.16	28.68
-0.17	30.46
-0.18	32.22
-0.19	33.99
-0.20	35.75
-0.21	37.50
-0.22	39.25
-0.23	40.94
-0.24	42.71
-0.25	44.44
-0.26	46.15
-0.27	47.86
-0.28	49.55
-0.29	51.24
-0.30	52.90
-0.31	54.57
-0.32	56.22
-0.33	57.86
-0.34	59.48
-0.35	61.09
-0.36	62.68
-0.37	64.26
-0.38	65.82
-0.39	67.37

Freezing Temperature °C	Lactose Concentration g ℓ^{-1}
-0.40	68.90
-0.41	70.41
-0.42	71.91
-0.43	73.38
-0.44	74.84
-0.45	76.27
-0.46	77.69
-0.47	79.09
-0.48	80.47
-0.49	81.83
-0.50	83.17
-0.51	84.49
-0.52	85.78
-0.53	87.07
-0.54	88.33
-0.55	89.58
-0.56	90.81
-0.57	92.02
-0.58	93.23
-0.59	94.42
-0.60	95.60

APPENDIX F

CALIBRATION REPORTS FOR THERMISTORS

DATE 27 January 1988

REPORT NO. APH 2426
RAPPORT NO.

Calibration of 7 thermistors

for/pour
Carleton University
Geography Dept., Loeb Bldg. Rm. 8347
Ottawa, Ontario
Attn: John Wood

AUTHOR Don Lawlor
AUTEUR

APPROVED
APPROUVÉ for Director/pour le directeur

The thermistors were calibrated in a stirred liquid bath between -0.6° and 0.1°C with the readings listed in the table below. The thermistor (serial number 0) was calibrated with a Keithley digital multimeter model 177 serial number 096877 and readings were taken on the 20 K ohm range. The remaining thermistors were calibrated with a Keithley digital multimeter model 191 serial number 17059 and the readings were taken on the 200 K ohm range.

Temp	No.0	No.1	No.12	No.14	No.16	No.15	No.13
-0.641	10.115	10.152	10.134	10.168	10.139	10.153	10.149
-0.607	10.097	10.134	10.117	10.151	10.123	10.135	10.132
-0.503	10.043	10.080	10.063	10.097	10.069	10.081	10.077
-0.421	10.001	10.038	10.021	10.054	10.026	10.039	10.035
-0.310	9.944	9.981	9.964	9.997	9.969	9.982	9.978
-0.198	9.867	9.923	9.906	9.940	9.911	9.924	9.921
-0.077	9.826	9.863	9.845	9.879	9.850	9.863	9.860
-0.021	9.799	9.835	9.818	9.851	9.822	9.836	9.832
+0.005	9.790	9.826	9.808	9.842	9.813	9.827	9.823
0.111	9.733	9.768	9.751	9.784	9.756	9.769	9.765

Thermistor temperatures interpolated from the expression (Bedford, Dauphinee and Preston-Thomas):

$$\frac{1}{T} = A + B \ln R + C (\ln R)^3 \quad -$$

R = thermistor resistance, ohms

T = temperature, °C

A,B,C = constants.

APPENDIX G

PROCEDURE FOR DEVELOPING PANATOMIC-X BLACK AND WHITE FILM

Materials:

1. Wire developing spool.
2. Light-proof container.
3. Kodak D76 developing solution, 8 oz.
4. Tap water, 8 oz.
5. Kodak rapid fix 16 oz.

Procedure:

1. Mix D76 and tap water in plastic container.
2. Keep all lights out.
3. Remove film from metal cannistor and wind on spiral developing spool threading it from the right.
4. Place film in light-proof container making sure lid is properly attached.
5. Add developer solution to container through slot in the light-proof lid. (Film is washed in developing solution for 9 minutes).
6. Gently agitate container for 30 seconds and then shake twice every 30 seconds for the remaining time period.
7. Pour out developer and add fixer to film for 2 minutes, gently agitating the container during this period.
8. Remove film from container and wash in cold tap water for 5 minutes.
9. Rinse briefly in soapy water, to prevent water marks.
10. Allow film to dry for 30 minutes before handling.

APPENDIX H

ADJUSTMENT PROCEDURE FOR CHART RECORDER

Apparatus:

1. Rikadenki Model SV-D zero suppression voltage unit (ZSVU) (used as a millivolt power supply for adjusting input to the recorder).
2. Keithley 177 digital multimeter.
3. Canlab 285 twin channel strip chart recorder.

Scale:

1. Horizontal axis, 1 small division = 5.0 kPa.
2. Vertical axis, chart speed set at 1 cm $hour^{-1}$.
3. Anticipated stress range is -50.0 to 250.0 kPa.

Strip chart recorder must be calibrated to accommodate the sensitivity of the particular transducer being used, as well as the anticipated stress range.

Example:

1. Sensitivity of transducer = 0.02634 in mV kPa^{-1} at 1 V d.c. (input).
2. 7 mV output from transducer indicates a stress of

$$\frac{7 \text{ mV}}{0.02634 \text{ mV kPa}^{-1}} = 265.76 \text{ kPa} \approx 266 \text{ kPa}.$$

3. Mark off pressure units on horizontal axis in 50 kPa increments and note location of 266 kPa.

Procedure:

1. Set ZSVU range at 1 V and polarity switch on positive.
2. Set power at 70% (X 10 mV = 7 mV).
3. Adjust recorder pen to zero position (atmospheric pressure) on chart.
4. Connect ZSVU to channel 1 at rear of recorder.
5. Set recorder scale to 1 V.
6. Adjust attenuation until recorder pen is set at 266 kPa on chart.

7. Test zero position of pen.
8. Disconnect ZSVU and apply zero correction procedure below.
9. Repeat steps 3-8 for channel 2 of recorder.

Usually the silicone oil next to the transducer is under a slight back pressure due to the elastic strain of the rubber membrane. Hence, the transducer normally registers a value of a few kPa in excess of atmospheric pressure. Because of this, a correction procedure must be applied to the zero position (atmospheric pressure) of the pen on the chart.

Zero Correction Procedure:

1. Connect pressure transducer to digital multimeter.
2. Set multimeter scale to 20 mV.
3. Record value (V) indicated by multimeter in mV.
4. Back pressure due to membrane $P_b = \frac{V}{\text{sensitivity}}$
5. If back pressure is positive, shift pen to a negative position P_b by adjusting zero control knob.
6. Connect multimeter to recorder.

APPENDIX I

PROCEDURE FOR DETERMINING RHEOLOGICAL PROPERTIES OF FROZEN CAEN SILT AND SNEC SAND

Creep tests were carried out by Ladanyi and Lauzon (1985) in a cold room at -2°C with a triaxial cell. Soil specimens were loaded by a pneumatic "Bellofram" piston and the deformation measured by a dial gauge. Axial strains ϵ were calculated from the linear displacement L by:

$$\epsilon = \int_{L_o}^{L} \frac{1}{L} dL = -\ln \left(1 - \frac{L}{L_o}\right)$$

L_o = initial length of soil (assuming volume of soil remains constant).

Creep data were then fitted to eqn. 4.1 enabling total strain to be expressed as a function of the applied stress and time. Creep parameters n and σ_c (Table 6.5) correspond to the slope and intercept of a log-log plot of the stress versus minimum strain rates observed in the creep tests. Similarly, pseudo-instantaneous strain parameters k and σ_k are obtained from a log-log plot of the stress versus the instantaneous strain.

Controlled strain rate tests were also carried out with a 50 ton testing machine. The compressive strength was measured with a force transducer. Volume changes were incorporated into the calculation of the strength. Further details of the testing procedure are described in Ladanyi and Lauzon (1985).

APPENDIX J

COMPACTION PROCEDURE FOR CAEN SILT AND SNEC SAND

The Caen silt was prepared by proctor compaction. Compaction curves predict that the maximum density (1.80 g cm^{-3}) is obtained by packing the soil at 15% water content (dry wt). Since the volume of the frost heave cell is 78.42 cm^3, the required amount of dry soil is 78.42 cm^3 × 1.80 g cm^{-3} = 141.2 g. This amount was wetted with 21.1 g of water to give a water content of 15%. The soil was then packed into the partially assembled cell with a tamping device, care being taken to ensure that the packing was as uniform as possible. A small quantity of soil was left over indicating that the density was slightly less than maximum.

Next a porous stone was placed over the open (upper) end of the soil, the cell was clamped and the reservoir at the other end was filled with water. Air was purged from the soil pores by applying 400 kPa hydraulic pressure to the reservoir forcing the water to flow up through the soil displacing the air. Saturation was indicated by the presence of water oozing through the porous stone at the upper end.

With the Snec sand, coarse sand and gravel (>2 mm) were removed from the specimen first to prevent possible damage to the semipermeable membrane and the pressure sensitive bladders by a point or an edge of a particle. The procedure used to pack the soil was slightly different.* The soil was prepared by packing small quantities of sand into the cell which was already filled with water. The object of this was to achieve a very high degree of saturation at the expense of a

---

*Proctor compaction curves for the Snec sand predict that the maximum density (2.04 g cm^{-3}) occurs when the soil is compacted at 7.5% water content.

slightly lower degree of compaction. It is interesting, however, that the saturation (91.1%) remained about the same as that of the compacted Caen silt (92%). The procedure, therefore, does not appear to have any effect on the degree of saturation.

APPENDIX K

THERMAL PROFILES FOR SEVERAL EXPERIMENTS

FIGURE K.1

TEMPERATURE PROFILE DURING FREEZING, EXPERIMENT 29, ALLENDALE CLAY

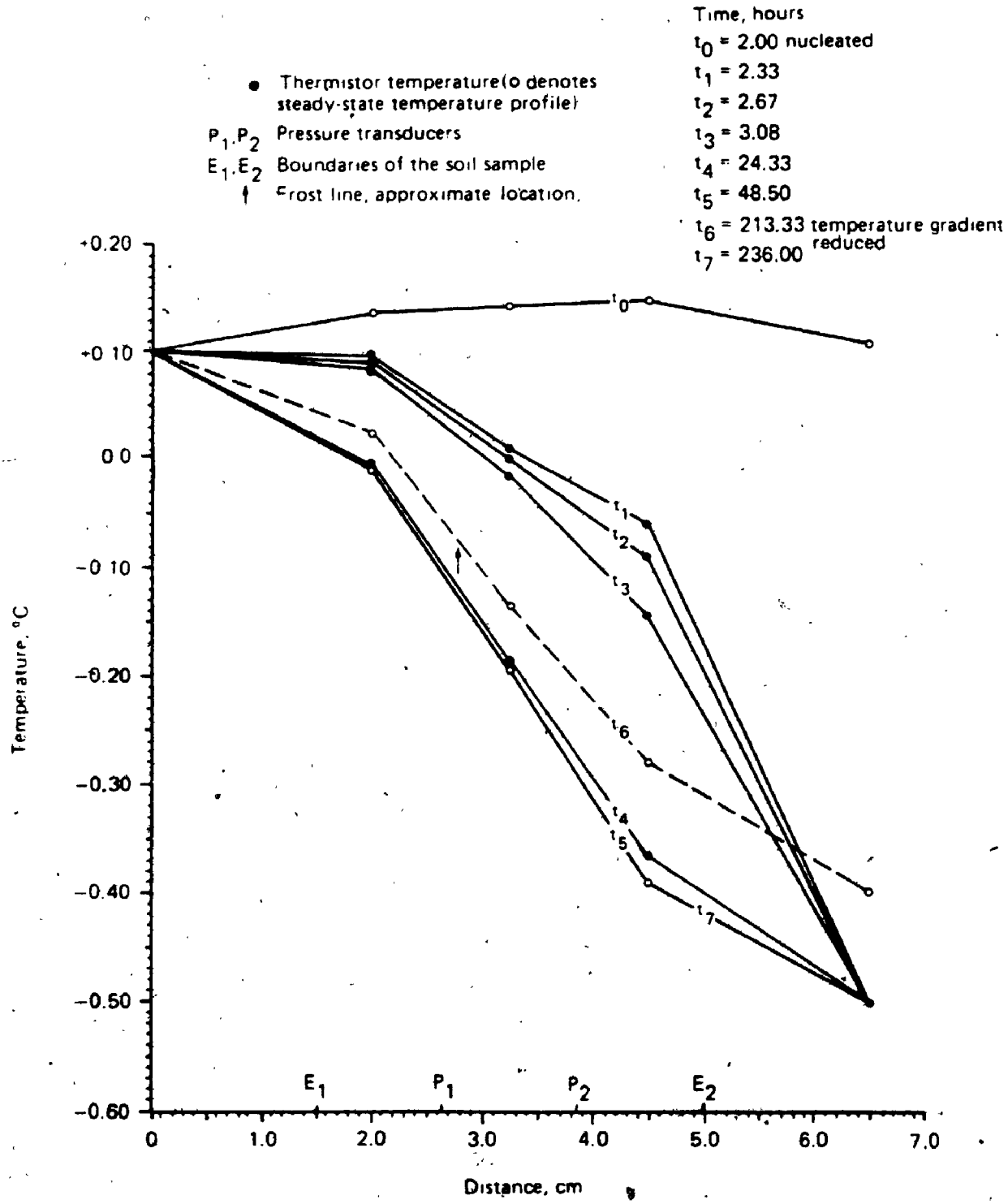

FIGURE K.2

TEMPERATURE PROFILE DURING FREEZING, EXPERIMENT 31, CAEN SILT

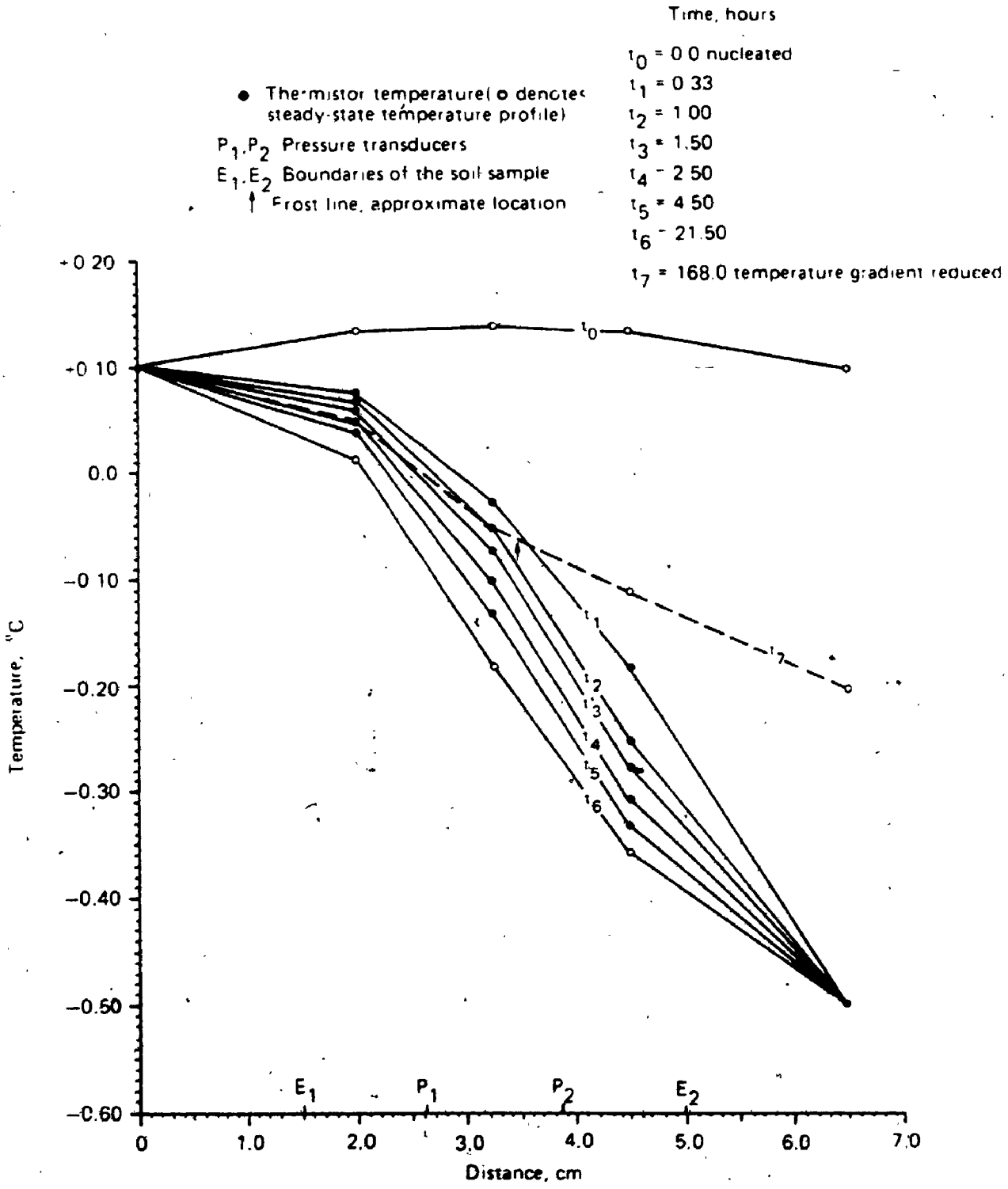

FIGURE K.3
TEMPERATURE PROFILE DURING FREEZING, EXPERIMENT 35, CAEN SILT

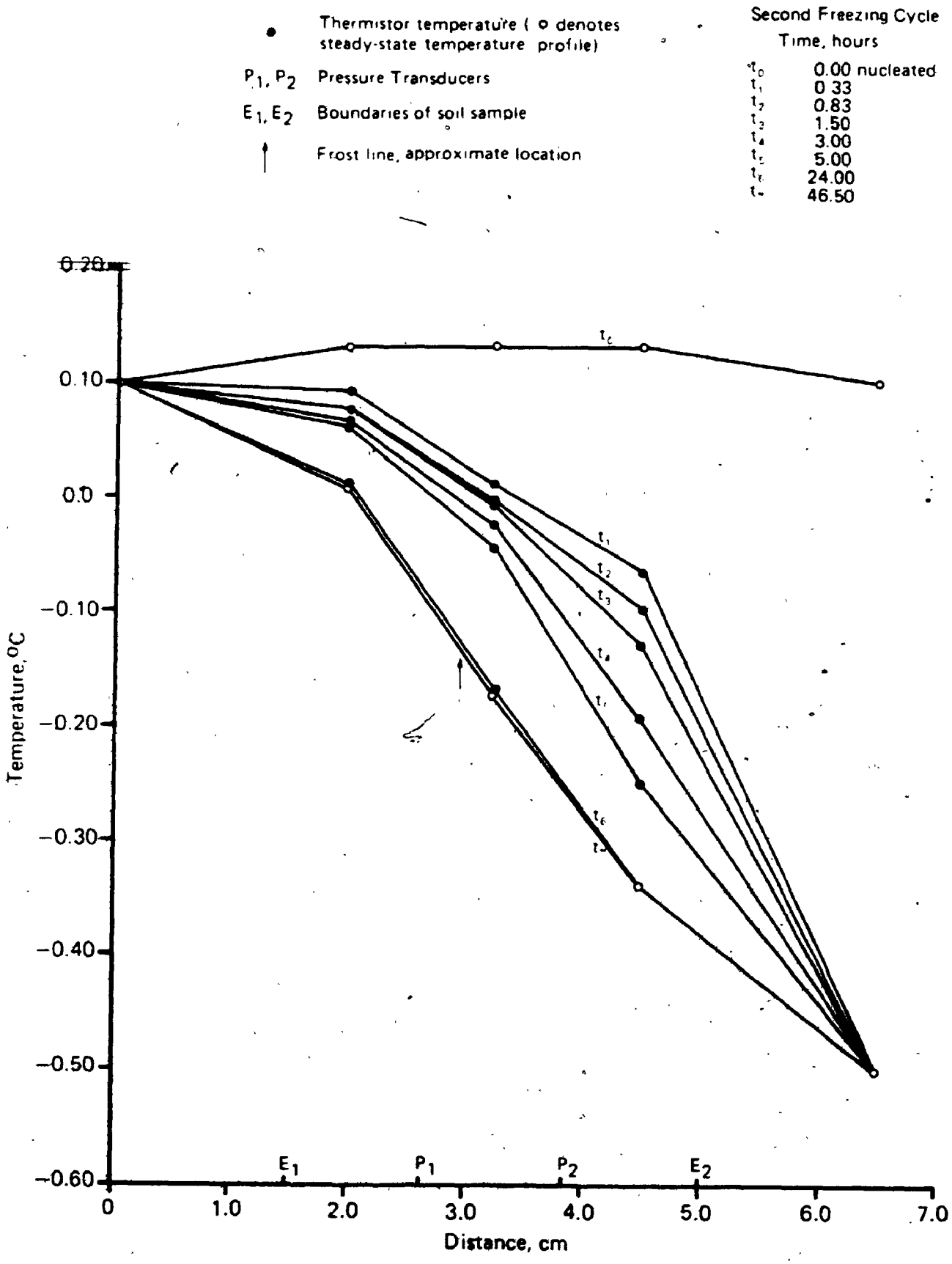

FIGURE K.4

TEMPERATURE PROFILE DURING FREEZING, EXPERIMENT 36, SNEC SAND

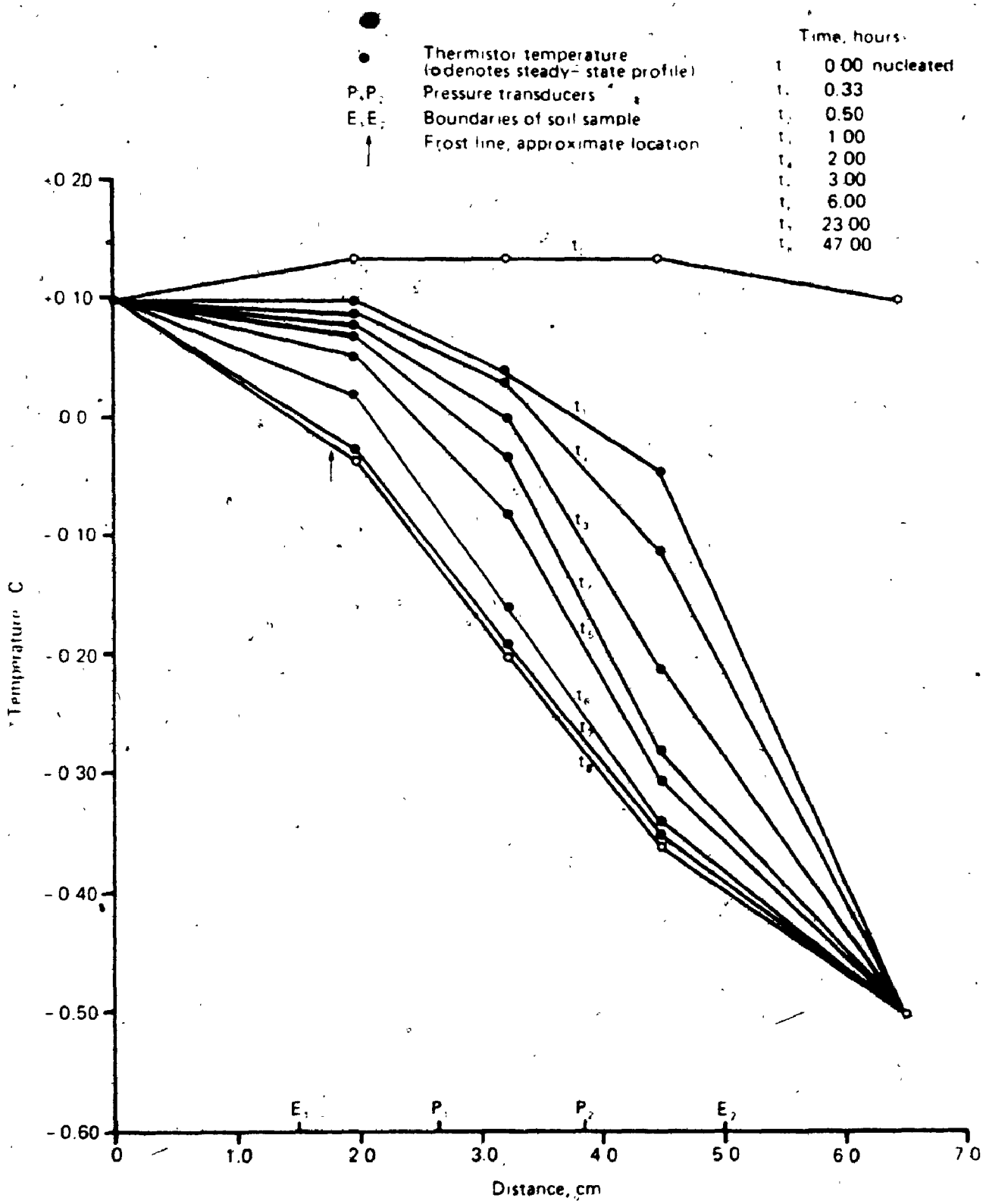

FIGURE K.5

TEMPERATURE PROFILE DURING FREEZING, EXPERIMENT 40, CAEN SILT

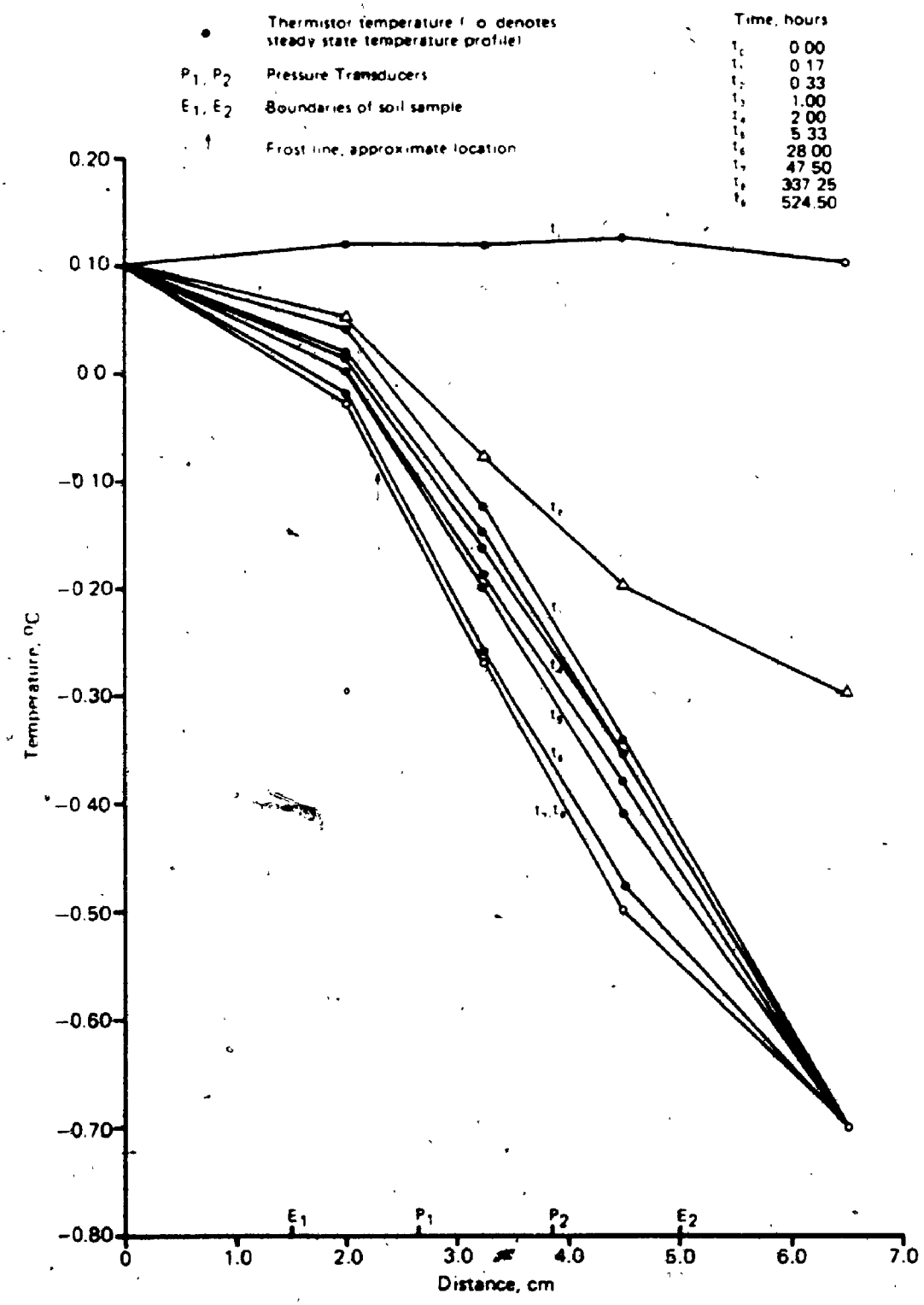

FIGURE K.6
TEMPERATURE PROFILE DURING FREEZING, EXPERIMENT 42A, CAEN SILT

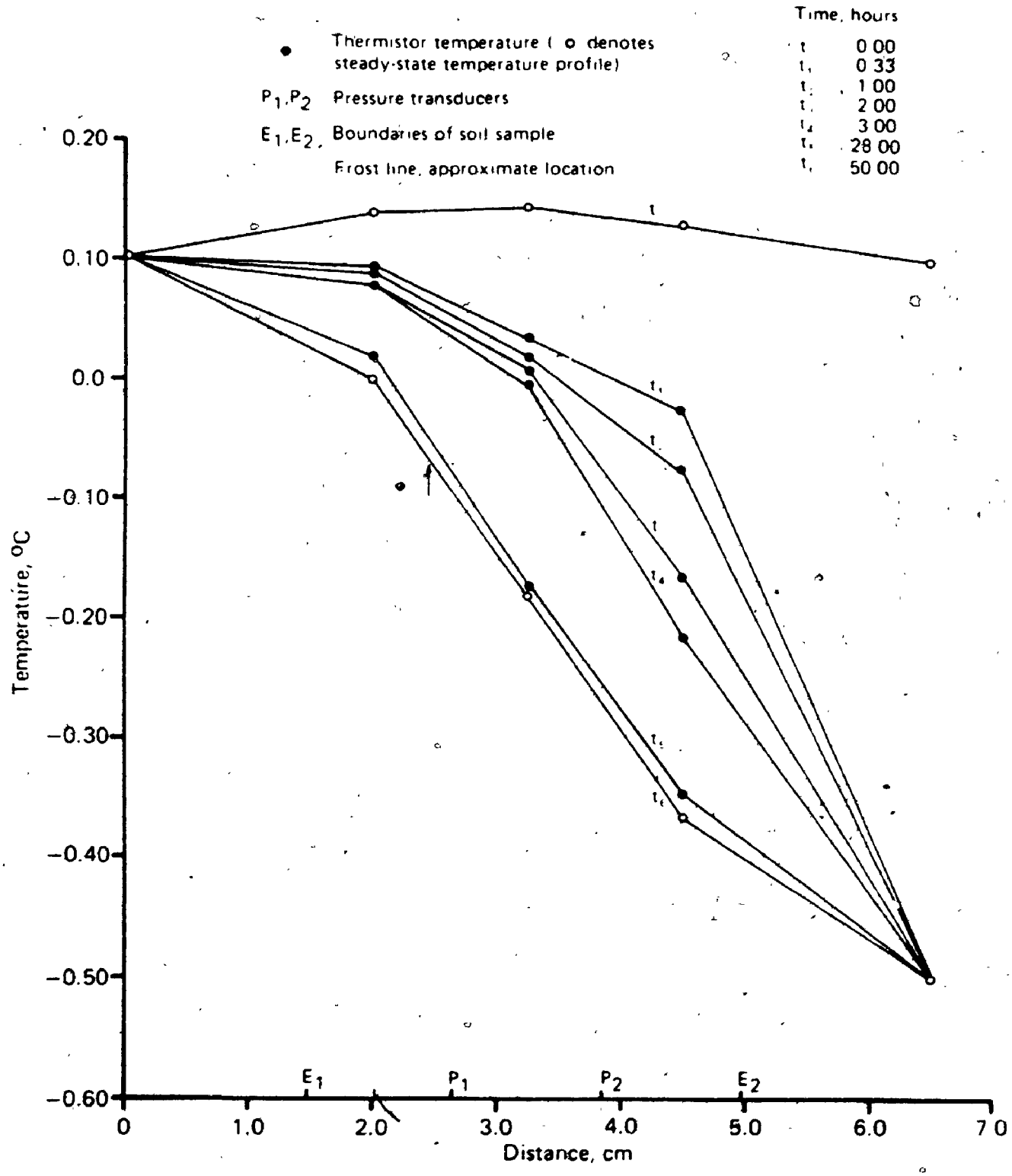

FIGURE K.7

TEMPERATURE PROFILE DURING FREEZING, EXPERIMENT 43A, CAEN SILT

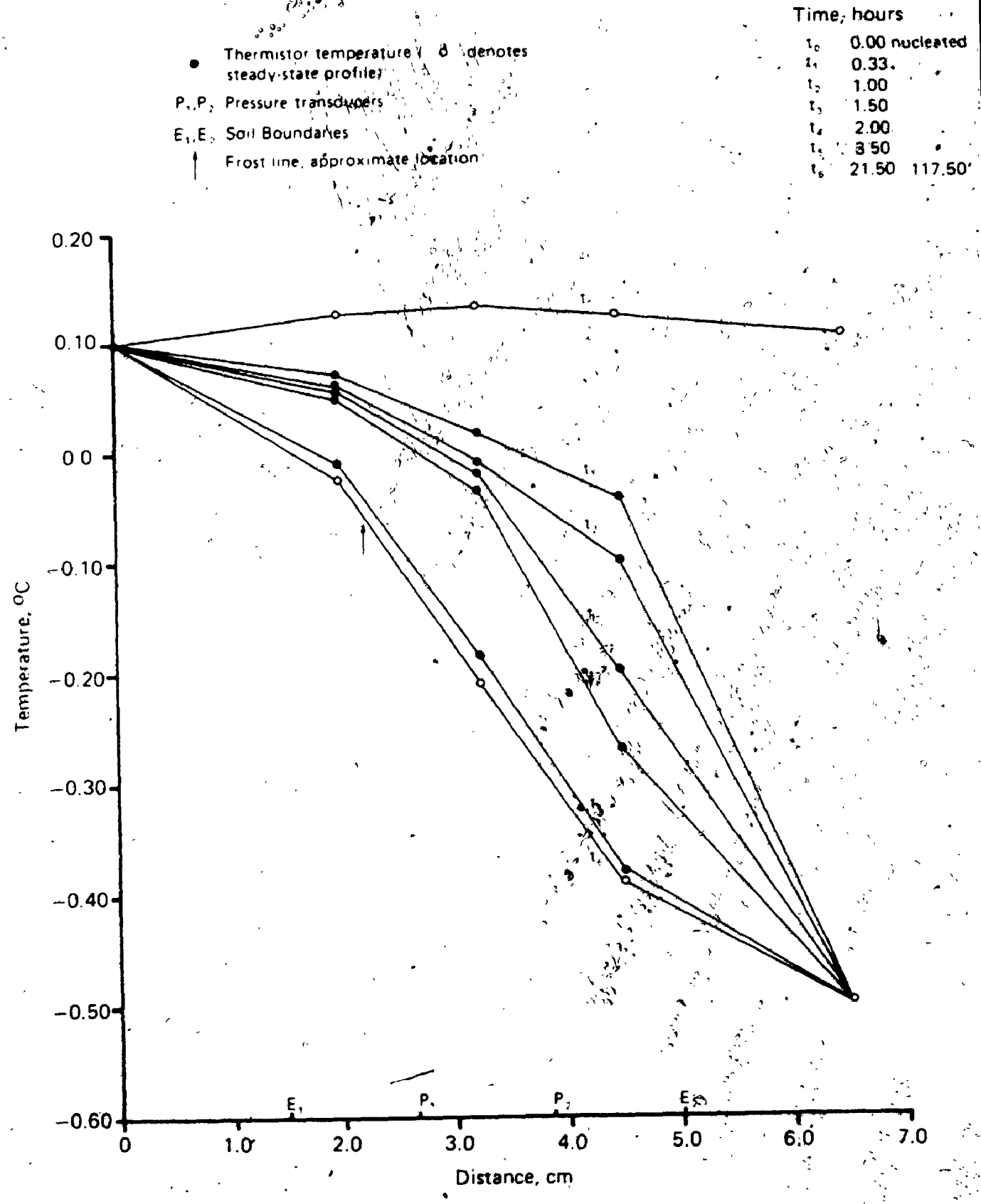

FIGURE K.8

TEMPERATURE PROFILE DURING FREEZING, EXPERIMENT 44A, CAEN SILT

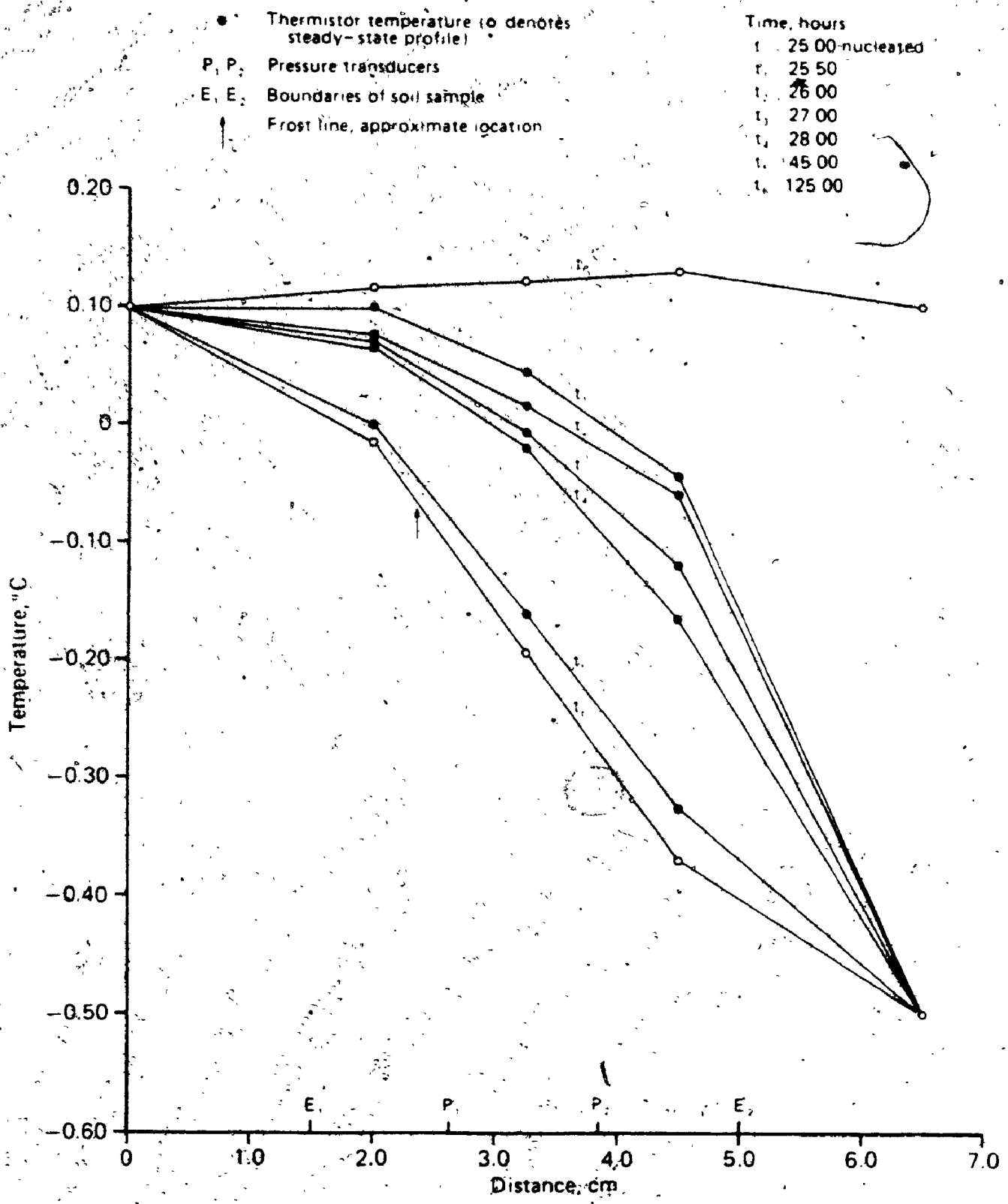

FIGURE K.9

TEMPERATURE PROFILE DURING FREEZING, EXPERIMENT 44B, CAEN SILT

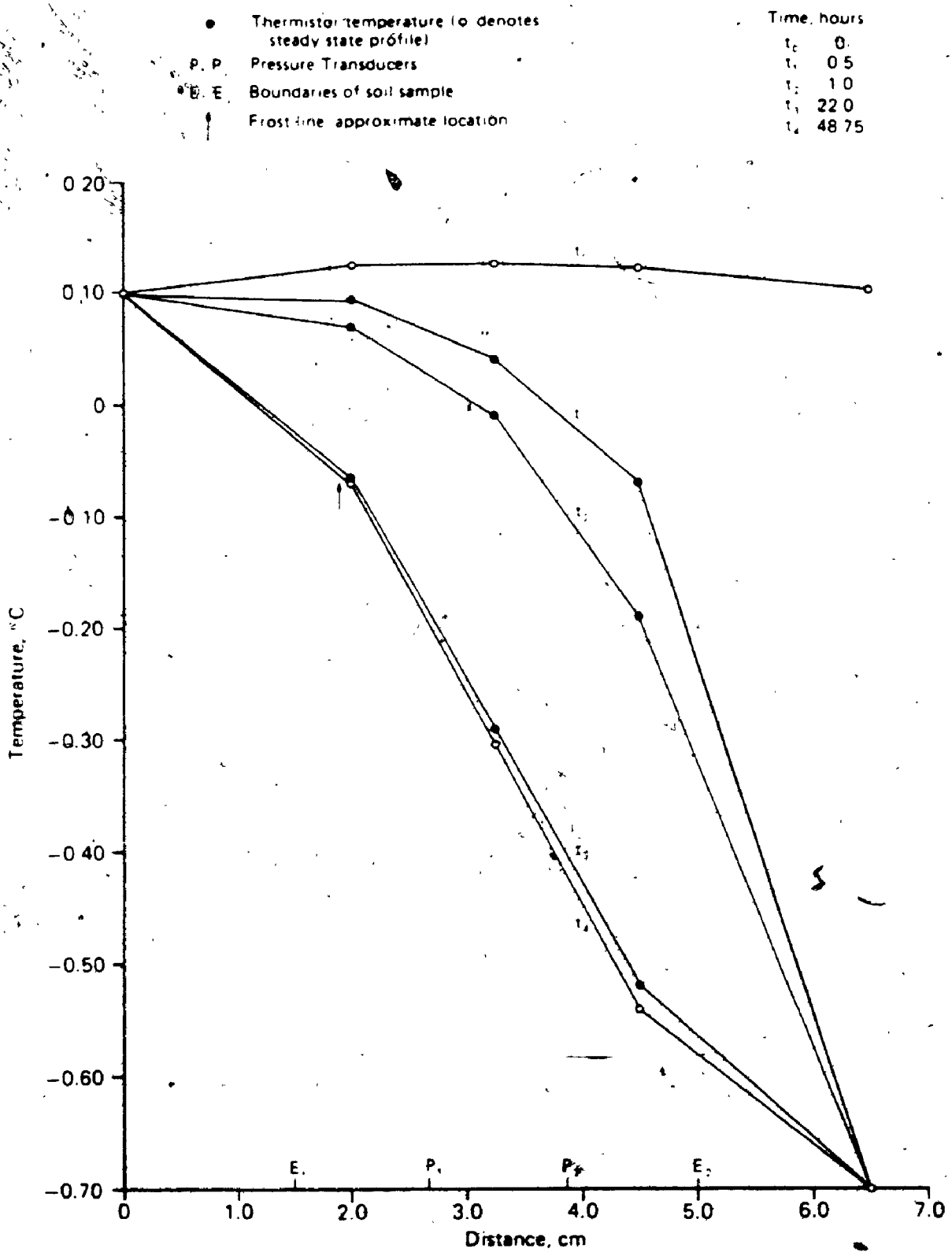

APPENDIX I

PROCEDURE FOR MEASURING WALL FRICTION

The static wall friction is the force per unit wall area required to extract a frozen soil specimen from the frost pressure cell. To measure this the copper tubing was first removed from the walls of the cell and the holes were filled with epoxy resin. A saturated soil specimen (Caen silt) was prepared and frozen inside the cell to a temperature of about -3°C. The cell was then placed on a small support stand located inside the incubator (temperature stability ±0.1°C). A very accurate, linear displacement, dial gauge (resolution 0.01 mm) was positioned beneath the soil specimen. (Test set-up, Plate L.1). The load was applied by means of weights stacked on a platform which pushed against a small ceramic disc resting on the soil surface. Prior to applying the load, the soil was warmed up to about -0.5°C for about 24 hours. Weights were added for a few minutes until displacement began to occur. The displacement accelerated rapidly for about a minute and then failure occurred abruptly. The wall friction is expressed in units of stress, kPa, where the force kN = applied load kg × gravitational constant 9.81 m s^{-2} and the surface area of the inner cell wall = 0.005938 m^2. At -0.5°C, the measured wall friction for the Caen silt was about 10 kPa.

PLATE L.1

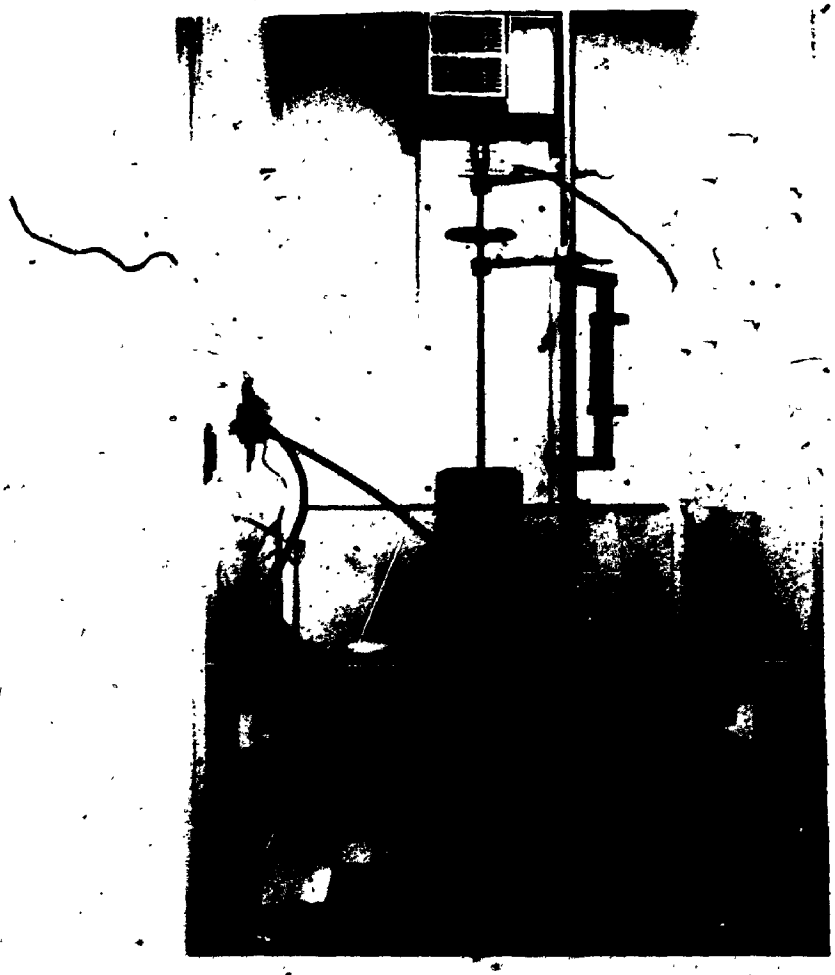

Test Set-Up For Measuring Wall Friction

END

20-06-88

FIN